



**DOTTORATO DI RICERCA IN ELETTRONICA APPLICATA**

# Metals and Organic Materials in the Cultural Heritage Field: an Approach Through Secondary Ion Mass Spectrometry

Paola Biocca

XXX Ciclo della formazione Dottorale

Docente-guida

Prof. Giovanni Sotgiu



The work described in this Ph.D. thesis was partially performed at ISCR (Istituto Superiore per la Conservazione e Restauro) labs in Rome and at LASS (Laboratorio Analisi di Superfici)-Roma Tre University.

# Abstract of thesis

During this work of thesis, the features of low energy ion beam analysis technique were exploited to perform the chemical characterization of samples belonging to the cultural heritage field.

The research was focused on the study of the chemical interactions between metals and organic compounds, which often coexist side by side in artifacts. Thanks to the high mass resolution, selectivity and the excellent lateral resolution of secondary ion mass spectrometry technique is possible the identification and the interpretation of mass spectral data, and localize of these characteristic fragments in the samples studied.

In particular, the research has developed the case of reaction of metallic foils and/or inorganic metallic pigments in contact with oil-resinous compounds, commonly present in pictorial binders. One of the most diffused examples of metallic-organic compound interaction in cultural heritage studies is represented by the gilding decoration technique, transversely applied to wall paintings, sculpture, paintings on wood metallic objects, and widely practiced over the centuries.

In general, the application of a metallic leaf (gold or silver) on a support by means of an adhesive compound is the practice defined as gilding technique. In some cases, the noble leaf is deposited on other metallic foil less noble, as a tin lamina, usually used to smooth the surface of the artwork to decorate. This last case, called *composite lamina*, was investigated through an experimental design in which *ad hoc* samples were performed and artificially aged with the aim to simulate the real state of conservation conditions. The study of the interactions between metallic foil and organic compounds has revealed the production of tin metal soaps due to the interaction among tin leaf with fatty acid presence in adhesive mixture.

At the same time, mass fraction and chemometric studies of the major terpenic molecules that characterize the resinous part of the adhesive mixture in Art and Archaeology, were also performed. Successively, the SIMS analytical technique was adopted for real case studies in order to validate the previous results. Wall paintings cross sections of Giotto and a Giotto's apprentice, characterized by the presence of *composite lamina* technique, were investigated. Moreover, the investigation was extended to the study of a silvered and painted leather artifact and an Etruscan cinerary urn decorated with gold lamina. Their investigation has made possible the knowledge of the various metal foils decoration techniques on different types of artefacts through the centuries.

In addition, cross sections belonging to a wooden triptych painted by the Flemish painter Jheronymous Bosch were also analyzed in order to identify and localize the chemical interaction and degradation products occurred among different materials, paying particular attention on the reactivity of metal-based pigments in the layers of paints.

The use of secondary ion mass spectrometry and imaging were used to detected and map characteristics fragments of oil-resinous medium, metal leave, metal-based pigments, varnishes and their interactions products, with high spatial resolution. Furthermore, all the other materials composing the samples were also characterized, providing a complete overview of artworks.

Finally, the ToF-SIMS dynamic operation mode was exploited to the investigation of metallic gilded artifact, obtaining a tridimensional distribution and localizing diffusion effects from the surface to the bulk of the sample. The ToF-SIMS results were supported by and in agreement with the results obtained with, FTIR in the experimental section and with optical microscopy, SEM-EDS, FTIR and XPS in all case studies investigated.

ToF-SIMS ability coupled to the analytical data obtained with the traditional complementary techniques may constitute a new means for the diagnostics of conservation science, and to extend the knowledge of materials and the state of conservation of the artworks.

## Abstract

## Table of contents

|       |  |    |
|-------|--|----|
| 1     | Introduction .....   | 3  |
| 1.1   | Mass spectrometry techniques in cultural heritage field .....  | 3  |
| 1.2   | Time-of-flight mass secondary ion mass spectrometry (ToF-SIMS) .....   | 5  |
| 1.2.1 | Physical principle and apparatus.....  | 5  |
| 1.2.2 | Static SIMS and Dynamic SIMS.....  | 9  |
| 1.3   | Chemometrics applied to ToF-SIMS mass spectra and imaging .....  | 11 |
| 1.4   | ToF-SIMS in cultural heritage .....  | 13 |
| 2     | High-mass-resolution mass spectrometry and Chemometrics.....   | 22 |
| 2.1   | Tin metal soap .....   | 22 |
| 2.1.1 | Introduction .....   | 22 |
| 2.1.2 | Experimental design.....   | 24 |
| 2.1.3 | Results and discussion .....   | 25 |
| 2.1.4 | Conclusion .....   | 35 |
| 2.2   | Oleanolic and ursolic acid in dammar and mastic resin: isomer discrimination by using ToF-SIMS and multivariate statistics. .... | 36 |
| 2.2.1 | Introduction .....   | 36 |
| 2.2.2 | Materials and methods.....   | 37 |
| 2.2.3 | Results and discussion .....   | 37 |
| 2.2.4 | Conclusions.....   | 42 |
| 2.3   | ToF-SIMS study of pentacyclic triterpenic molecules in birch bark pitch .....  | 43 |
| 2.3.1 | Introduction .....   | 43 |
| 2.3.2 | Materials and methods.....   | 44 |
| 2.3.3 | Result and discussion .....  | 44 |
| 2.3.4 | Conclusion .....   | 48 |
| 3     | Sub-micron molecular imaging .....   | 49 |
| 3.1   | Gilding decoration on wall painting and related organic binding media .....  | 51 |
| 3.1.1 | Fresco Vela della Castità, San Francesco Basilic in Assisi .....   | 51 |
| 3.1.2 | Giotto “ <i>Universal Judgement</i> ”, Scrovegni Chapel in Padua. ....   | 57 |
| 3.2   | Gild and painted leather.....  | 63 |
| 3.2.1 | Introduction .....   | 63 |
| 3.2.2 | Materials and methods.....   | 63 |
| 3.2.3 | Results and discussion .....   | 64 |
| 3.2.4 | Conclusions.....   | 68 |
| 3.3   | Gilding decoration on stone: the case of Etruscan cinerary urn.....  | 69 |
| 3.3.1 | Introduction .....   | 69 |

|       |   |     |
|-------|---|-----|
| 3.3.2 | Materials and methods .....                             | 70  |
| 3.3.3 | Results and discussion .....                            | 70  |
| 3.3.4 | Conclusion .....  | 73  |
| 3.4   | Saint Wilgefortis Triptych by Jherononymous Bosch ..... | 74  |
| 3.4.1 | Introduction .....                                      | 74  |
| 3.4.2 | Materials and methods .....                             | 74  |
| 3.4.3 | Results and discussion .....                            | 76  |
| 3.4.4 | Conclusion .....  | 84  |
| 4     | Depth profiling and 3D imaging .....                    | 85  |
| 4.1   | Gilding technique on copper-based buckle .....          | 85  |
| 4.1.1 | Introduction .....                                      | 85  |
| 4.1.2 | Materials and methods .....                             | 86  |
| 4.1.3 | Results and discussion .....                            | 87  |
| 4.1.4 | Conclusion .....  | 95  |
| 5     | Conclusion .....  | 96  |
|       | Reference .....   | 99  |
|       | Appendix .....  | 110 |

# 1 Introduction

## 1.1 Mass spectrometry techniques in cultural heritage field

Early applications of chemical and physical analytical methods in studies on art materials and archaeological objects demonstrated that scientific investigation is an essential tool for acquiring information on the materials that make up an artwork and for assessing their decay, in order to plan restoration approaches. Chemical diagnosis, together with the investigation carried out by historians, archaeologists and art experts, are valuable contribution to help identify the materials in paintings and ancient artefacts, as well as their state of conservation. The development of scientific procedures that are able to use few micrograms of samples together with the increased availability of advanced analytical instrumentation, have led to great interest in the chemical study of materials used in cultural heritage. This has given rise to a sharp increase in research studies at the interface between art, archaeology, chemistry, and the material science. Especially challenging is the study of organic compounds in artworks that can be identified both as the main constituents of artistic object, and as secondary components, mixed with inorganic compounds. Organic materials can be found in the finish or decoration of the surfaces, or as residues of commodities, such as in ceramic or glass vessels. Moreover, the majority of restoration products applied as consolidants, adhesives, restoration paints, and varnishes are of organic nature. Investigation into this wide range of substances is crucial for conservation since organic constituents are more prone to degradation due to the effects of light, temperature, moisture, biological agents, and environmental oxidizing conditions. Their degradation pathways are thus often crucial in determining the overall decay of an object. Furthermore, the aging effect can origin the degradation of the all compounds linked with the organic species. In the perspective of conservation science, fundamental research is required specifically for understanding the behaviour under natural ageing of new synthetic materials used both for restoration and for art purposes [1].

Over the past decade, particular attention has been focused on the characterization of organic materials occurring, for example, as the residues of food [2-4], medicines and balms in archaeology [5-7], as adhesives [8-11] and as binders in paints [12-15]. The mixture of many materials in ancient recipes and technologies, and the chemical changes induced by ageing make it even more difficult to study these samples [16-18]. In this respect, research relies heavily on structural information at a molecular level, and thus the application of mass spectrometry plays a prominent role. This is mainly due to its ability to obtain detailed compositional information of complex mixtures. In addition, the possibility of coupling mass spectrometry with chromatographic techniques, such as gas chromatography and high-performance liquid chromatography, has made mass spectrometry one of most powerful tool to investigate the complex and aged mixtures of organic molecules that are currently encountered as constituents of artistic, historic and archaeological objects [16,19-20].

The wide variety of features offered by mass spectrometry makes the range of organic materials that can be studied very broad: it includes small volatile molecules such as monoterpenes in essential oils as well as macromolecules and proteins [21-22]. Mass spectrometric based techniques are used for the accurate quantitative analysis of specific, well known species, and also for the identification of unknown, unexpected compounds such as degradation products on the basis of the mass spectra. Furthermore, mass spectrometry studies have recognized specific markers for material identification, and degradation mechanisms, giving an identification of natural and synthetic resins [23-26], proteinaceous binders [27-28], plant gums [29-30], organic dyes [31-33], vegetable oils and waxes [34-37]. Most materials from cultural heritage are composed of complex mixtures of different molecules having a wide range of chemo-physical properties. Most of

them are at trace level, while others are in high amounts. The study and characterization of these molecules can yield information on the use and function of the material, as well as on the customs of the people who used it, their way of life and other useful information invaluable to reconstruct the historical, cultural and social background of a given period in a given geographical area. To obtain reliable information it is necessary to identify and characterize each component in the material. To fulfil this aim, methodologies characterized by high selectivity, specificity and sensitivity are required. Mass spectrometry (MS) is one of the most powerful methodologies for identifying, structurally characterizing, and quantitating wide classes of molecules, ranging from small to very big species. Traditional MS techniques are based on the production of gas phase ions and on their separation according to their mass-to-charge ( $m/z$ ) ratios. Owing to technological innovation and advances in instrumentation, mass spectrometers became more and more sophisticated and versatile tools for different applications in chemistry. The introduction of soft ionization techniques, such as plasma desorption (PD) [38], field desorption (FD) [39], and fast atom bombardment (FAB) [40], marked the beginning of a new era for MS. The growing interest for the identification and characterization of polar and large compounds caused the development and the introduction of new ionization techniques, such as electrospray ionization (ESI) [41], and matrix assisted laser desorption ionization (MALDI) [42], and their more recent improvements, thus establishing new MS based approaches for studying large molecules, polymers and biopolymers, such as proteins and carbohydrates. Parallel to the development of mass spectrometric instrumentation and methodologies, the improvements of separation techniques, such as gas chromatography (GC), high performance liquid chromatography (HPLC) and of their coupling with MS allowed the study of complex mixtures, that are generally encountered in most studies. Nowadays, MS plays an important role in many fields of scientific and technological research for identification, structural characterization and quantitative determination of wide classes of compounds. Its unique capabilities, such as high sensitivity, high selectivity, accuracy in molecular weight determination, and ability to analyse complex mixtures, give this methodology great importance in the solution of problems not easily handled by other techniques. The above-mentioned techniques provide dissolution, derivatization and phase transformation of the sample, involving the total loss of the sample during the analysis, even if only a few micrograms of samples are needed for the analytes identification (the scrapings are usually of 10-100 mg) [43-48]. This could represent a limitation for the analysis of cultural heritage samples. Furthermore, the disadvantage of analysing a scraping is the loss of the information concerning the spatial distribution of the organic constituents in the multi-layered paint systems, as well as the inevitable sacrifice of a valuable paint sample.

In the conservation science view, all the chemical-physical investigations carried out on the artworks should preserve matter and not cause further destruction or degradation. Even when sampling is permitted, is preferable to study the fragments collected with non-destructive analyses, so that to preserve their integrity and allow the investigation of the same samples with others complementary analytical technique. The development of MS technique offers the opportunity to overcome this problem. Thanks to the innovative applications in this field, techniques with high surface sensitivity such as secondary ion mass spectrometry (SIMS) allow the mapping of organic and inorganic compounds in cross-sections and as *it is* samples during a single run analysis, preserving the entire of the sample. The chemical-physical principles of the ToF-SIMS technique in the cultural heritage field are explained below.

## 1.2 Time-of-flight mass secondary ion mass spectrometry (ToF-SIMS)

Secondary ion mass spectrometry (SIMS) is a widespread analytical technique for the study of surfaces in materials science. This technique allows investigating of the first monolayers of the sample. Mostly used for elemental, molecular analyses and depth profiling, it is particularly relevant for many different fields of research including cultural heritage studies. At the begins the SIMS studies on cultural heritage samples were focused on the investigation of ancient glasses or metal artefacts [49-54] but as only elemental information was obtained, these studies are limited to inorganic materials. Nevertheless, the introduction of time-of-flight (ToF) analysers for SIMS analyses, as well as the continue development of liquid ion sources delivering cluster projectiles permit the analysis of organic materials with high sensitivity and selectivity. Moreover, thanks to its excellent lateral resolution (in the order of micro-metres), and its minimal sample preparation, ToF-SIMS has become the reference technique for chemical imaging by mass spectrometry. Beside numerous applications for biological samples [55], studies of organic materials from cultural heritage artefacts have been developed, thanks also the application of new acquisition modality in the ion extraction.

### 1.2.1 Physical principle and apparatus

SIMS experiments involve bombarding a material surface with a primary ion beam, with an energy in order of keV range. The ion impact with the surface induces the so-called 'collision cascade' sputtering process, where the energy of the primary ions is transferred to the surface through nuclear collisions. The direct collisions between the primary ions and the atoms in the sample are highly energetic compared to bond energies [56]. This energy produces the desorption of neutral molecules, positive or negative ions and atoms from the surface when the energy is sufficient to overcome the binding energy [57]. Close to the impact point, the transferred energy is higher than the bond energy of the molecules, leading to bond breaking near the collision site, producing essentially only the emission of atomic particles. In contrast, far from the collision site, this energy decreases, leading to desorption of larger molecular fragments and even of complete molecular species. As the collision cascade moves away from the collision site, the collisions become less energetic. This results in less fragmentation and bond breaking, producing the emission of molecular fragments. Particles produced in approximately the top 2–3 monolayers of the sample have sufficient energy to overcome the surface binding energy and leave the sample. These sputtered particles are ejected as neutral atoms and molecules, electrons, and ions. Only a small fraction of them are charged and their positive or negative state depends on their electron configuration. The entities desorbed are called secondary ions and are charged positively or negatively (Fig.1.1). The mass to charge ratio ( $m/z$ ) of the species are analyzed and yield positive and negative secondary ion mass spectra consisting of the ion  $m/z$  versus the number of ions detected at each  $m/z$ .

Fig. 1.2 shows the schematic representation of a typical ToF-SIMS device. All the system is placed under ultra-high vacuum (UHV typically  $10^{-9}$  Torr) to avoid interactions between ions and air molecules. Primary ions are produced by a liquid metal ion gun and then focused on the sample to a spot with a typical size of less than 1 mm. After they impinge the surface, secondary ions are extracted and analysed by the Time of Flight (ToF) analyzer [58].

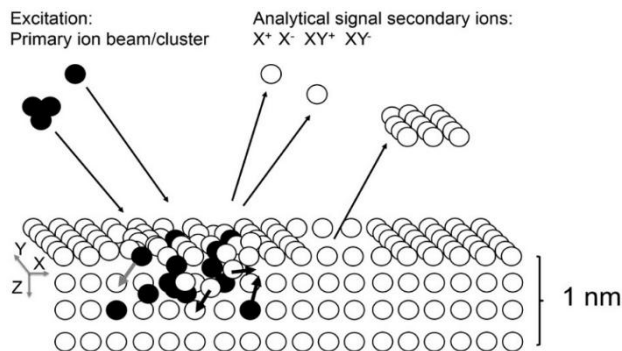


**Figure 1.1.** A schematic drawing of the secondary ion emission process initiated by the impact of a primary ion. Extensive fragmentation occurs near the collision site producing mainly atomic particles. Away from the point of impact collisions become less energetic resulting in the emission of larger molecular fragments

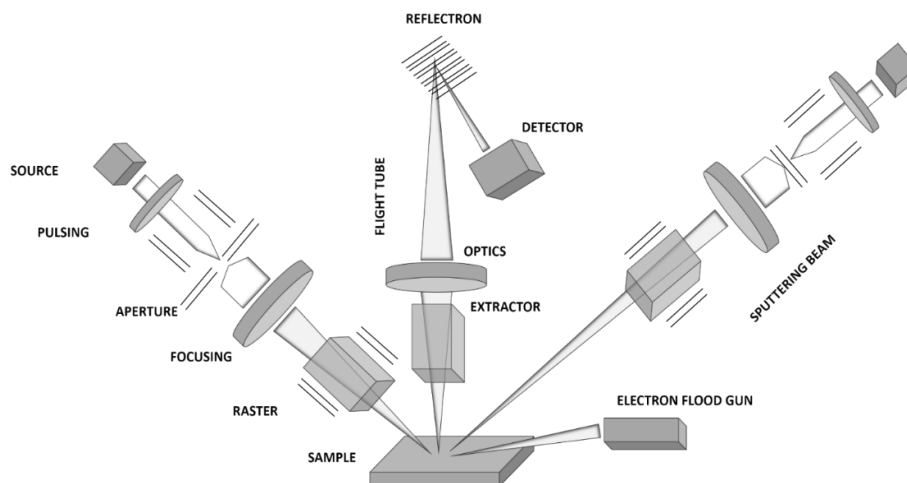


**Figure 1.2.** Schematic drawing of a SIMS instrument with a TOF analyzer. The primary ion source, sample, and flight tube are kept under UHV. The mass of the detected ions is determined by the flight time of the ion between the extractor and the detector. The reflectron helps compensate for energy and angular dispersion that can occur during the emission process.

ToF analyzer is favorite to the others analyzers for its high transmission and parallel detection of ions of all masses, facilitating analysis of the small yield of ions inherent in the SIMS method (Fig. 1.3). Excellent mass resolution (defined as  $m/\Delta m$ ) can also be achieved (often-exceeding 10,000) with the TOF analyzer that separates secondary ions according to  $m/z$  (mass/charge). The mass ( $m$ ), of the ions is determined according to the time it takes them to travel through the length ( $L$ ), of the field-free flight tube, after they have been accelerated in an extraction field to a common energy ( $E$ ).

The relationship between  $E$  and flight time ( $t$ ), is straightforward (where  $v$  is velocity):

$$E = mv^2 / 2 = mL^2 = 2zt^2$$

Since flight time is proportional to the square root of the mass of the secondary ion, the lighter ions travel at a faster velocity and arrive at the detector earlier than the heavier ions:

$$t = L(m/2zE)^{1/2}$$

The best separation of ions, or mass resolution, is obtained when ion energy is constant. The primary ion source must be pulsed with short pulse widths (sub nanosecond) to yield secondary ions with minimal time dispersion, and there by minimal energy spread. A fixed voltage then accelerates the secondary ions into the ToF analyzer, with its polarity determining whether positive or negative secondary ions are analyzed. After separation in the ToF analyzer, the secondary ions are focused onto the detector by an ion lens. A post-acceleration voltage of up to 15 kV is applied to the ions to improve the detection efficiency of the high-mass ions because they travel at slower velocities. The ions strike the detection unit, which is typically composed of a photo converter electrode, channel plate, scintillator, photomultiplier and a counter, in series [58].

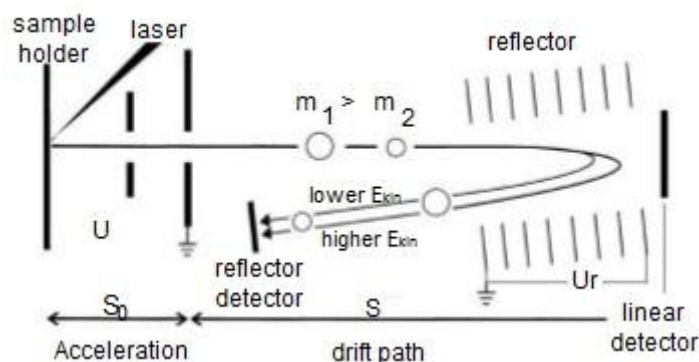


**Figure 1.3.** Schematic representation of time of flight (ToF) analyzer. The accelerated molecular ions leave the sample holder with the same kinetic energy and travel along the linear flight tube with different velocities according to their  $m/z$ . In a reflectron TOF analyzer the ion separation resolution is improved. The spread of flight times of the ions with the same  $m/z$ , caused by spread in kinetic energy of these ions, is diminished.

To synchronize the ToF analyser, the primary ion beam must be in pulsed mode. One of the specificities of ToF-SIMS is the possibility to switch easily from positive to negative ion mode by reversing the extraction potential. This feature allows to analyze species that ionize in different polarity. As far as preparation for the sample is concerned, ToF-SIMS is one of the only mass spectrometric techniques that allow solid samples to be analysed without any extraction of compounds or matrix addition. Generally, no specific preparation technique is required, and solid samples can directly be analysed if they are small enough to be fixed on the sample holder. In most cases, this means that the sample size must not be more than 1 cm. Very flat samples are required to avoid problems of depth of field. Even if this is common to every imaging technique, it is in this case coupled with surface pollution problems. Sample preparation must then lead to flat surfaces without surface pollution.

Part of the samples analysed with ToF-SIMS are composed by organic and insulator materials and they can accumulate charge on their surface during the analysis. This charge build-up can lead to reduce or totally eliminate the secondary ion signal. Sample charging occurs during the sputtering

process, from bombardment of the surface by the positively charged primary ions and the simultaneous loss of secondary electrons. Unless the sample has sufficient electrical conductivity to transport electrons to the sputtered region, this region acquires a net positive charge. To neutralize the charge build-up during ToF-SIMS analysis, the surface is flooded with pulses of low energy electrons between pulses of the primary ions, by a so-called 'flood gun' in pulsed mode.

From the spectra acquired in a ToF-SIMS experiment, information about the chemical structure and composition of the surface can be obtained. Typical mass spectra contain an immense number of peaks. By evaluating the masses of the signals, peaks often can be identified from the molecular ion of the analyte, fragments of the molecular ion, and ions of any other components that maybe in the samples.

The molecular structure can often be identified through the fragmentation pattern and knowledge of the fragmentation pathway. Fragmentation rules that apply for electron impact mass spectrometry (alpha and beta cleavages, rearrangement processes) are useful in elucidating fragmentation processes [59]. ToF-SIMS mass spectra are generally obtained for  $m/z$  ratio from 1 to 1000 or 2000  $m/z$ . However, due to a high fragmentation process, ToF-SIMS mass spectra are generally very complex and the ionization processes are very different compared with other mass spectrometric techniques. Mass spectra interpretation can be very difficult, especially in the case of a complex sample, so the possibility of chemical imaging can help reduce the complexity of the technique. Indeed, instead of using the spectra of the whole sample, specific mass spectra can be recalculated from a precise area giving more specific information. From the global spectrum, peaks that seem interesting are selected and their spatial distribution is drawn. If some of these peaks give a specific spatial distribution with areas of important concentration, spectra from these areas are recalculated [60]. As the primary ion beam can be focused to less than 1 mm, ToF-SIMS is well suited to chemical imaging. For this purpose, the beam is rastered by electrostatic fields all over the surface, and a spectrum is recorded for each point, in a mode referred to as microprobe imaging. This allows the distribution of a specific ion all over the analysed surface to be mapped, and also to access a mass spectrum characteristic of an area by summing the spectra of each pixel of this region (Fig.1.4).

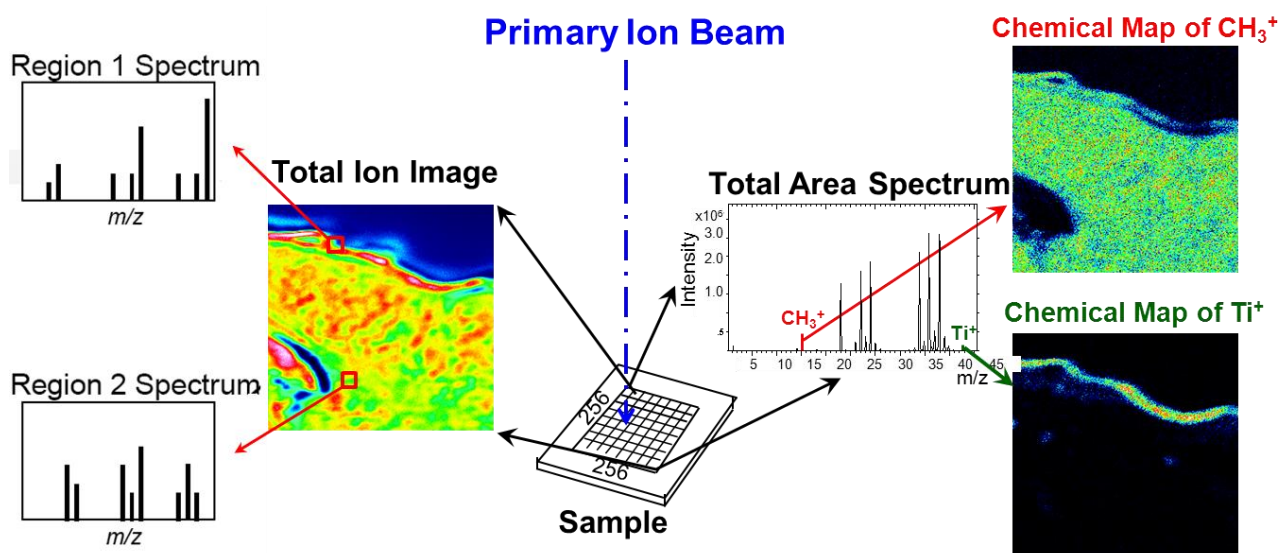


**Figure 1.4.** Principles and schematic representation of Time-of-Flight Secondary Ion Mass Spectrometry.

Using a liquid metal ion gun, the primary beam can be focused to 100 nm, allowing images to be generated with the same lateral resolution. The small beam diameter reduces the amount of substance available per pixel (image point) in the uppermost monolayer. This limits the number of secondary ions that can be generated and lessens the sensitivity and dynamic range for each point. After data acquisition, a specific ion or a combination of ions can be selected and their surface distribution mapped. Also with SIMS imaging, a region of interest from the total ion image can be identified and the mass spectra from the pixels in that region can be summed, allowing spectral evaluation with restored sensitivity and dynamic range. To generate a topographic map of the surface, the ion induced secondary electrons (similar to scanning electron microscopy) or the total secondary ion emission can be used [60].

## 1.2.2 Static SIMS and Dynamic SIMS

SIMS can be divided into two different techniques: static SIMS (SSIMS), which is a surface specific mass spectrometry tool offering organic and inorganic fingerprinting as well as atomic compositional analysis in a bidimensional system (area decrypted by x, y axes), and dynamic SIMS that is capable to offer the same features in depth profiling and bulk analysis. Dynamic SIMS is a useful tool for the study of those objects in which micro-destruction is permitted, obtained as well a profile of chemical characterization long the z axis. In Dynamic SIMS, a sputter gun (generally Cs<sup>+</sup>, Ga<sup>+</sup> Bi<sup>+</sup>, Ar<sup>+</sup>) erodes the surface of the sample, and simultaneously the secondary ions generate from the sample surface are analyzed by the primary gun. By digitally scanning the primary ion analysis beam, high spatial resolution ion images of all secondary ions from the sample surface are produced. By sputtering the sample surface simultaneously images from increasing depth are obtained and hence three-dimensional data are collected. The raw data file contains each point of analysis of the digitally scanned beam with its X, Y, and Z coordinates and a mass spectrum, allowing the creation of 3D images (Fig. 1.5).

Both branches of the technique are capable of trace analysis below 0.1% atomic. In the case of static SIMS this is combined with virtually non-destructive sampling of the top one or two atomic layers only. In some publications, ToF-SIMS is also called Static-SIMS (S-SIMS) because ToF-SIMS analyses are performed in static conditions. In this mode, the damage of the surface is very low and is nominally defined as non-invasive operation mode. Indeed, the primary ion flux is set so that the collisions sites do not overlap with each other. A limit of 10<sup>12</sup> atoms cm<sup>-2</sup> is generally allowed [55]. Under these conditions, secondary ions are emitted from the very extreme surface, from the first few nanometres, and therefore ToF-SIMS is truly a technique for the study of the ultrasurface. The secondary ion yield depends both on the energy and the nature of the primary ions. It has been demonstrated that the use of clusters instead of monoatomic ions improves the secondary yield [61]. Classical primary ions, like Ga<sup>+</sup> and Cs<sup>+</sup>, are increasingly replaced by Au<sub>3</sub><sup>+</sup>, Bi<sub>3</sub><sup>+</sup> or C<sub>60</sub><sup>+</sup> until the new generation of Ar<sup>+</sup> and H<sub>2</sub>O guns which has permitted great progress in organic ToF-SIMS studies [62- 63].

For dynamic SIMS, typically ppm sensitivities can be achieved across the periodic table for the consumption of <10<sup>-13</sup> cm<sup>3</sup> of sample per data point. Both static and dynamic SIMS can be used to generate chemical images with lateral resolution approaching 10 nm using a liquid metal ion gun. Primarily because of the low sampled volume per pixel in the image at the extreme resolution in the former case, sensitivity will be reduced to ~10% atomic at best.

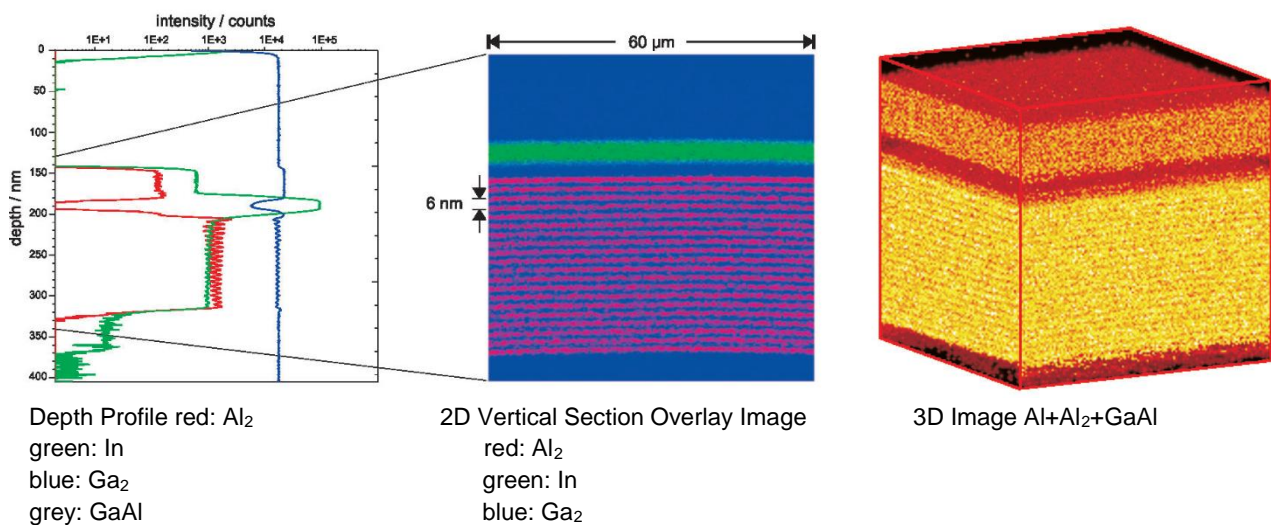


**Figure 1.5.** Example of reconstruction possibilities from raw data. The sample is a GaAs/AlGaAs superlattice. A volume of  $60 \times 60 \mu\text{m}^2$  (surface area)  $\times$  400 nm (depth) was analysed. The 2D section and the 3D image are reconstructed from depths of 130 nm to 340 nm ([www.iontof.com](http://www.iontof.com)).

At the energies used in most SIMS experiments, the area of surface damaged by each ion impact has linear dimensions  $\sim 10$  nm. The criterion for static SIMS is that the probability of sputtering from a pre-existing impact site must be low. This constrains the total primary ion dose per experiment to  $\ll 10^{13}$  ions  $\text{cm}^2$ . For dynamic SIMS it is necessary for the primary beam to create average steady state conditions at the sample surface. The regime of dynamic SIMS lies beyond ion doses of  $10^{16}$ – $10^{17}$  ions  $\text{cm}^2$  therefore. Such steady state conditions may, however, be impossible to achieve, especially if the sample surface is rough, or becomes rough under ion bombardment, or if the bulk sample chemistry changes significantly on a depth scale comparable with the SIMS depth resolution. Under these circumstances, changes in secondary ion intensity may be wholly or partially unconnected with changes in concentration of the analyte. In S-SIMS primary species such as inert gas ions (general purpose) and metal ions  $\text{Ga}^+$ ,  $\text{In}^+$  are used. Recently, there has been much interest in the use of cluster ions,  $\text{Bi}_n^+$ ,  $\text{Au}_n^+$ ,  $\text{C}_{60}^+$ , to promote cluster ion emission for high molecular weight fingerprinting. In dynamic SIMS, inert and metal ion species are used too, but the most common primary ions in use are  $\text{O}_2^+$ ,  $\text{O}^-$  and  $\text{Cs}^+$ . These reactive species are used primarily to control the chemical properties of the altered layer which forms at the surface of the sample if and when equilibrium bombardment conditions are achieved. Caesium promotes negative ion emission both through its effect on reducing the work function and in the increased electron availability in a caesiated surface. It is also useful in positive ion analysis when using  $\text{MCs}^+$  and  $\text{MCs}_2^+$  secondary ions can greatly reduce the matrix effect in analysing for atomic species [64-65].

## 1.3 Chemometrics applied to ToF-SIMS mass spectra and imaging

Chemometric pattern recognition techniques have been widely used in other mass spectrometry techniques and can be equally useful in ToF-SIMS analysis. Chemometric pattern recognition methods involve clustering the samples into groups that are related based on their locations in multivariate space [66].

A typical ToF-SIMS spectrum can contain hundreds of peaks, the intensity of which can vary due to the composition, structure, order, and orientation of the surface species [67]. ToF-SIMS data are inherently multivariate since the relative intensities of many of the peaks within a given spectrum are related, due to the fact that they often originate from the same surface species [68]. The challenge is to determine which peaks are related to each other, and how they relate to the chemical differences present on the surface. This problem is then exacerbated by the fact that a given data set typically contains multiple spectra from multiple samples, which can result in a large data matrix to be analyzed. This data overload is even more prominent in ToF-SIMS imaging where a single 256 x 256 pixel image contains 65536 spectra. This complexity, combined with the enormous amount of data produced in a ToF-SIMS experiment, has led to a marked increase in the use of multivariate analysis (MVA) methods in the processing of ToF-SIMS images and spectra [69]. These methods include, but are not limited to principal components analysis (PCA), discriminant analysis (DA), partial least squares (PLS), multivariate curve resolution (MCR), and maximum autocorrelation factors (MAF). These MVA methods are one of many tools available that can aid in the interpretation of ToF-SIMS images and spectra. These methods are statistically based, and to be used properly require good experimental plans and controls. The use of MVA does not preclude the need for a sound understanding of ToF-SIMS, or for using complementary surface analysis methods in order to interpret the data and understand the surfaces being.

The method that remains preferred for the ToF-SIMS data processing is certainly PCA. Principal component analysis tries to find the directions of greatest variation in the multivariate space defined by the data set. These directions define a new set of axes that explain how the samples and variables relate to each other. Herein a data set is defined as a matrix where the rows contain samples and the columns contain variables. For ToF-SIMS data the samples are spectra and the variables are measured intensities of individual mass channels or integrated peak areas from selected or binned regions. PCA is calculated from the covariance matrix of this original data set [70]. Geometrically, PCA is an axis rotation that aligns a new set of axes, called principal components (PC), with the maximal directions of variance within a data set. PCA generates three new matrices containing the scores, the loadings, and the residuals. The scores show the relationship between the samples (spectra) and are a projection of the original data points onto a given PC axis. The loadings show which variables (peaks) are responsible for the separation seen in the scores plot. The loadings are the direction cosines between the original axes and the new PC axes [71]. Samples that are widely separated along these new axes are not as similar as samples that are grouped close together along these axes. The residuals represent random noise that is presumed to not contain any useful information about the samples [72]. Together the scores and loadings represent a concise summary of the original data that in most cases can aid in interpreting the data being analyzed. The scores and loadings must be interpreted together and have little meaning alone. In general peaks with high loadings on one side of a given PC axis will show a higher relative intensity for samples with high scores on the same side of the given PC axis.

Since all MVA methods are statistically based, it is important to make sure that one collects sufficient data to have statistically relevant results. Care should also be taken to minimize, and

ideally avoid, detector saturation during data collection. Saturated peaks can result in the production of extra factors that describe the non-linear intensity variations of saturated peaks. Furthermore, since ToF-SIMS is so surface sensitive one must be especially careful to avoid the presence of surface contaminants since they can compromise the PCA results. This can be partially remedied through preprocessing of the data before carrying out the multivariate analysis. Due to the large number of peaks typically seen at each nominal mass in ToF-SIMS spectra from organic and inorganic surfaces, manual peak selection is recommended. Data binning is quick, but it loses the high mass resolution information present in the original spectra. Manual peak selection is time consuming, but allows the user to utilize all of the spectral peaks and to check the peak integration limits to assure they are placed properly across all samples. The assumptions made when selecting peaks for ToF-SIMS MVA have been reviewed previously [70]. Before selecting peaks it is important to make sure that all of the spectra are properly mass calibrated, and that the same calibration set is used for all spectra within a given sample set. The same peak list must be used for all samples within a given set.

The results produced by many MVA methods depend strongly on the data matrix preprocessing. Data preprocessing includes normalization, mean centering, scaling and transformation. Spectral pre-processing has not been standardized for ToF-SIMS analysis, but is necessary to remove variations in the instrument over time and the presence of contaminants [73]. One must then decide on a scaling method to use. For multivariate analysis, the most typical choice is between mean centering and autoscaling of the data. In mean centering, the data in each column is centered around a mean of zero. This removes the effects of scale from the data. Autoscaling first mean centers the data and then scales it to unit variance. This gives equal weight to all variables in the matrix. For ToF-SIMS data it is most common to mean center the data. Autoscaling tends to give too much weight to high-mass peaks that typically are of low intensity and contain more random noise [74].

The goal of data preprocessing is to remove variance from the matrix that is not due to chemical differences between the samples. This could include variation due to the instrumentation, differences in the absolute intensity of peaks within a spectrum, differences due to topography or other factors. Normalization is done by dividing each variable (peak) in the matrix by a scalar value. Normalization is necessary to remove variance in the data that is due to differences such as sample charging, instrumental conditions or topography. There are many different ways to scale and transform a data set. It is recommended that one selects a scaling and transformation method based on the experimental uncertainty of each peak. Regardless of the preprocessing methods used, one should understand the assumptions made [70] when applying a given method and choose a method based on what they are trying to learn from the data and not what gives the best looking results.

Once the data set has been processed using MVA the user must interpret what, if anything, the results mean. This is particularly important when using scale dependent methods such as PCA since the results obtained will be affected by the assumptions made when preprocessing the data. Though there are no quantitative measures of the validity for a given result. Multivariate analysis is simply a tool available to help understand large data sets. As with any results, one should always ask if the results obtained make sense. When MVA is used one should also ask if the assumptions made during data pre-processing make sense, and are based off of valid assumptions about the data. Also, since no one surface analytical method can provide all the information needed to understand a surface, it is important to collect complementary data on the samples within a given set. The user can then validate the ToF-SIMS data with respect to the information obtained from the other methods. Another important aspect to keep in mind is that unsupervised MVA methods such as PCA are designed to find the greatest directions of variance within a data set regardless of

their source. That means that if one sample within a data set is contaminated, the first few PCs will most likely separate out the contaminated sample from the other samples. Thus, any variance that is due to the designed surface chemistry may be suppressed by the large variance due to the contamination. However, it is important to note that being able to discover contamination within a sample set can be a valuable piece of information that can help troubleshoot sample preparation and handling protocols. This information can then be fed back into the sample procedures and experimental design so differences in the surface chemistry of interest can be studied [69].

## 1.4 ToF-SIMS in cultural heritage

ToF-SIMS technique was applied to study many artworks made with different materials, mainly focused on the detection of organic molecules. Moreover, as ToF-SIMS is a surface analytical technique, it is well suited to the study of surface interaction between a material and its environment or between a material and products applied to it. The surface modifications can then be studied, making it possible to establish links with degradation processes inherent in cultural heritage objects. Moreover, the chemical imaging feature of SIMS allowed to localized exactly where these reactions have come. The fields of application of this technique in art field include the large example of materials, from textiles to the cross-sections of paintings were investigated along with other analytical techniques, in order to chemical characterize and understanding the sequential events on the materials of art.

Different studies were conducted for the analyses of tapestry fibres. The main aim was to study the surface evolution of these fibres, wool and silk, during light ageing or cleaning procedures. Carr et al. studied the incidence of different cleaning procedures on wool. ToF-SIMS analyses performed on the commercially scoured wool showed the presence of 18-methyleicosanoic acid thioester species, attributed to the presence of 18-methyleicosanoic acid (18-MEA) which is normally the predominant compound of the surface layer of wool. After artificial sunlight exposure, analyses showed that 18-MEA was disappeared from the surface. Different cleaning procedures were tested and the results were compared with the ageing tests. Has been observed that the amount of remaining surfactant was greater after artificial ageing [75]. A similar study was performed on silk [76]. The ToF-SIMS positive ions fingerprint of silk exhibits the presence of different amino acid fragments. In contrast to wool, the effect of artificial ageing was not obvious and no modification appears in the ToF-SIMS spectra. Nevertheless, the study of the cleaning procedures led to the same conclusion as that in the case of wool. The amount of remaining surfactant increased with artificial ageing.

Batcheller et al. also discussed the influence of the dyeing process on the composition of the fiber's surface. They noted that high alkalinity/acidity and extended processing time result in loss of surface lipid [77]. Nevertheless, the dyeing process was limited influence on the ageing process due to light exposure.

The identification of dyes is of great interest in textile studies. The classical procedure requires a hydrolysis step and other extraction techniques, followed by identification of the individual compounds present after separation by a chromatographic technique, e.g. high- performance liquid chromatography [78-79]. However, ToF-SIMS could be an alternative method, avoiding the phase of extraction which is always a time consuming and delicate step because of the possible destruction of the molecular structure of the sample [80]. A specific study of anthraquinone dye (alizarin, purpurin and quinizarin) and their respective lakes (manufactured with aluminium sulfate) was performed. For the lakes, aluminium clusters were also observed in the case of alizarin and

quinizarin. For the alizarin complex,  $[(A-H)_2Al]^+$  ( $m/z$  505) was detected in positive ion mode and  $[A_2Al]^-$  ( $m/z$  503) in negative ion mode. These ions derived from the complexation of aluminium ions. Complexation sites were ceto-phenolates in positive ion mode and ceto-phenolates or diphenolates for negative ions. In the case of quinizarin, only ceto-phenolate complexes were observed [81].

In another study, Lee et al. [82] demonstrated the possibility of identifying dyes on textile fibres. The different studied dyes were curcumin (tumeric), crocin (gardenia), carthamin (safflower), purpurin (madder), alizarin (madder), brazilin (sappanwood), shikonin (gromwell) and indigo. Analyses in positive ion mode of pure pigments showed that molecular ions were detected. Moreover, in each case specific fragments were identified. Lee et al. then proved that this detection is also possible in the case of dyed textile. The different dyes were applied on silk and samples were analysed by ToF-SIMS. Metal ions from mordants (aluminium, tin or copper) could be also detected in the low mass region of spectra. Finally, two ancient textiles of the sixteenth and seventeenth century were studied. The presence of molecular ion at  $m/z$  263 and fragment ions at  $m/z$  235 and  $m/z$  247 demonstrated that indigo was used. No mordant-related peaks were detected. The author explained that indigo has naturally affinity with the fibres that it could be used without mordant.

In the studies described above, organic matter was the main, and most of the time, the only component of the samples. However, in a lot of cases, analyses must be performed on complex samples, composed of both organic and mineral materials. For this reason, organic compounds are often extracted from samples to be analysed with the ordinary analytical methods. ToF-SIMS allows samples to be worked on without extraction, allowing the simultaneous study of organic and inorganic compounds and the characterization of their interactions. It is especially useful in the characterization of paintings. In the study of painting layers, the identification of both pigments and binding media is advantageous. Keune and Boon [83] presented the application of ToF-SIMS analysis to a paint cross-section. The sample studied was from the panel painting 'The Descent from the Cross' (Museo del Prado, Madrid) by the early Flemish painter Rogier van der Weyden (1399/1400–1464). Scanning electron microscopy with energy dispersive X-ray analysis (SEM-EDX) and infrared microscopy were also used to complete and confirm the results. The aim of the study was to reveal whether or not egg tempera was mixed with oil as binding media. The cross-section was studied in both positive and negative ion modes. Lead white with linseed oil, tripalmitin, stearic acid and lead white with egg tempera were studied as reference samples. In positive ion mode, the characteristic peaks representative of the binding media were fatty acids from lead soaps (of palmitic acid at  $m/z$  461–463 and of stearic acid at  $m/z$  489–491). Other peaks corresponding to mono- and diacylglycerol cations, protonated stearic acid or its acylium ions could be found in the spectra of the reference products but not in the paint sample. The spectrum of lead white egg tempera paint exhibits peaks of phosphocholine ( $m/z$  184) and protonated ketocholesterol ( $m/z$  401). These peaks were not found in the spectrum from the cross-section. In negative ion mode, the spectrum of the oil paint mainly showed deprotonated palmitic and stearic acids. In addition, other peaks attributed to short chain fatty acids (8-, 9- and 10-hydrocarbon chain length) were detected. The presence of characteristic peaks from palmitic and stearic acids was consistent with the hypothesis of the use of oil as binding media. The lack of any characteristic ions issued from egg tempera meant that ToF-SIMS did not allow detection of egg tempera in this sample. However, it could be present but was not detected due to high degradation occurring in very old egg tempera. The presence of short chain fatty acids, which were not detected in the new reference sample, was attributed to oil ageing. The distribution of fatty acid ions in the cross-section was well correlated with the distribution of lead (Fig. 1.6). In addition to these numerous

results, two other points were discussed by the authors: fatty acid speciation and oil identification. These two aspects were developed in another publication written by the same authors [84].

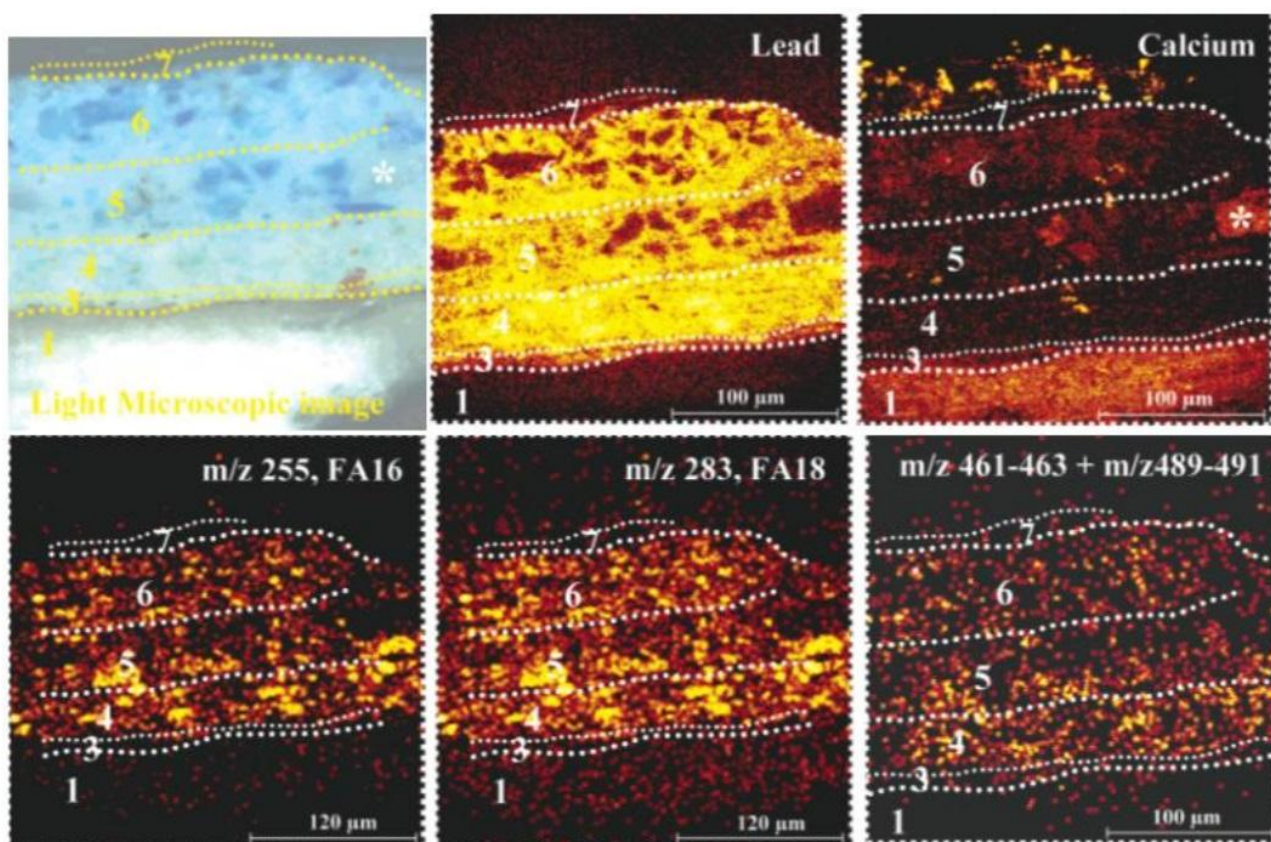


**Figure 1.6.** Microscopic image and ToF-SIMS images of the cross-section from the painting 'The Descent from the Cross' (Museo del Prado, Madrid) by van der Weyden. Images of lead, calcium and lead soaps (m/z 461–463 and 489–491) were acquired in positive ion mode (image size 250x250 mm<sup>2</sup>). Images of palmitic (m/z 255) and stearic (m/z 283) acids were acquired in negative ion mode (image size 300 x300 mm<sup>2</sup>). Yellow represents high intensity and black represents low yields. The numbers on the images refer to the different layers. [Keune et al., 2004]

The fatty acid speciation was based on the positive ion ToF-SIMS analysis and aims to prove if the fatty acids detected existed as free fatty acids, ester bound fatty acids or metal soaps. On account of the study of different standards, it was shown that when free fatty acids were present, the protonated molecular ion and its acylium ( $[M-OH]^+$ ) ion were detected. In cases of ester-bound fatty acid only the acylium ion was detected. Finally, for metal soap, spectra exhibited a peak for the molecular ion of clusters of metal ions and carboxylic fatty acid, and a small peak for the protonated fatty acid whereas the acylium ion was absent. Application of this to the sample of van der Weyden's painting showed that fatty acids were mainly present as metal soaps, which were, in this case, lead soaps because of the use of lead white as chemical drier. This explained the correlation between lead and fatty acids observed previously, even if caution had to be taken when interpreting ToF-SIMS imaging of paint layers containing binders and pigments because the ionization yield of organic species could be influenced by the presence of metals [85]. To identify the kind of oil, Keune et al. used the classical approach based on the palmitic acid/stearic acid (P/S) ratio usually obtained from GC/MS data [84]. Ratios less than 2 corresponded to linseed oil, whereas ratios higher than 5 corresponded to poppy seed oil. Intermediate values can be

attributed to walnut, poppy seed oil or mixtures [86]. The research has shown that ionization efficiency is the same for the two fatty acids in negative ion mode permitting the use of ToF-SIMS for the calculation of the P/S ratio. A test on the oil-paint model system has shown a ratio of 2.0 for linseed oil and 3.6 for poppy seed oil, which could allow the two oils to be differentiated. Nevertheless, it was important to note that the ratio is not constant all over the cross-section.

The same approach was applied to identify the oil used as binding media in the painting 'Plaster Figure of a Female Torso' by Van Gogh [87]. Here the P/S ratios obtained were inconclusive with respect to the type of oil used. To conclude these studies about oil binding media, was demonstrated that an ultrathin gold coating of the painting cross-sections enhanced positive and negative secondary ion yields of lipids [85]. By coating the samples with a 2-nm thick gold layer, the negative secondary ion yield is multiplied by three whereas in positive ion mode factors of two to four were found. They also showed that the fragmentation of the fatty acid was not affected, whereas the dissociation of mineral clusters seems to be reduced.

In literature, was reported another interesting study regarding the chemical characterization of a Rembrandt painting cross-section. Sanjova et. al. presented a work based on the study of painting materials, using high resolution cluster-TOF-SIMS imaging [88]. In the first step, a moderate spatial resolution (2  $\mu\text{m}$ ) was used to characterize the layer structure and the chemical composition of each layer on account of a high mass resolution. Then, in the second step, and despite a low mass resolution, the cluster primary ion beam was focused well below 1  $\mu\text{m}$  in order to reveal smaller structures in the painting sample. The study confirmed the presence of starch in the second ground layer, which is quite surprising and, at least for Rembrandt paintings, was never reported before. TOF-SIMS indicated the presence of proteins, which, added to the size and shape of lake particles, suggests that it was manufactured from shearing of dyed wool, used as the source of the dyestuff. The analyses also showed various lead carboxylates, being the products of the interaction between lead white and the oil of the binding medium. These findings have considerably contributed to the understanding of Rembrandt's studio practice and thus have demonstrated the importance and potential of cluster-TOF-SIMS imaging in the characterization on a sub-micrometer scale of artist painting materials.

Exploiting possible to acquire sub-micrometer spatial resolution mass spectrometry images at the surface of the sample combine with high mass resolution, ToF-SIMS imaging studies have become more focused on new methodologies for data acquisition and setting of the instrumentation, thanks to the use of a delayed extraction of secondary ions that allows to obtained the best quality of chemical mapping. First example for this new methodology of investigation was the study conducted by Noun et. Al. on a Nicolas Poussin painting cross section [89]. In the study the new potential of delayed extraction were shown, through the obtaining of small regions that identified pigment grains and the drawing of the each painting layers limit.

In general, ToF-SIMS has contributed significantly to the field of analytical techniques for cultural heritage, to carry out analysis directly on the painting section, revealing the contemporary presence of different kind of materials. The ability of ToF-SIMS to simultaneously image inorganic and organic species within a paint cross section at micrometer-level spatial resolution makes it a uniquely qualified analytical technique to aid in further understanding the processes of pigment and binder alteration, as well as pigment binder interactions.

Keune et. al, applied Imaging secondary ion mass spectrometry for the first time to paint cross sections with degraded vermilion (red mercury sulfide) paint to cast new light on the well-known problem of its light-induced darkening [90]. The SIMS data were combined with light microscopic, electron microscopic studies and energy-dispersive X-ray analysis to identify and localize the various reaction products. The research leaded of a new hypothesis on the reaction mechanism of the photodegradation of vermilion where two black and white reaction products were formed

sequentially, thanks to the detection of the spatial distribution of atomic and molecular species in paint cross sections of the native vermilion and its reaction products. Under the influence of light, they observed that some of the vermilion ( $\text{HgS}$ ) was converted into  $\text{Hg}(0)$  and  $\text{S}(0)$ . In this process, the chlorine ions, presented in the native vermilion, act as a catalyst. Their hypothesis was that the  $\text{Hg}(0)$  was deposited on the surface of the remaining  $\text{HgS}$  as elementary mercury nanoparticles, which turned the vermilion black. Chloride, derived from an external source, was accumulating in the black phase. The metallic mercury and the remaining  $\text{HgS}$  reacted away with the excess of chloride. At the end, they described also the formation of two intermediate products and a white end product, mercuric chloride ( $\text{HgCl}_2$ ) (Fig. 1.7).

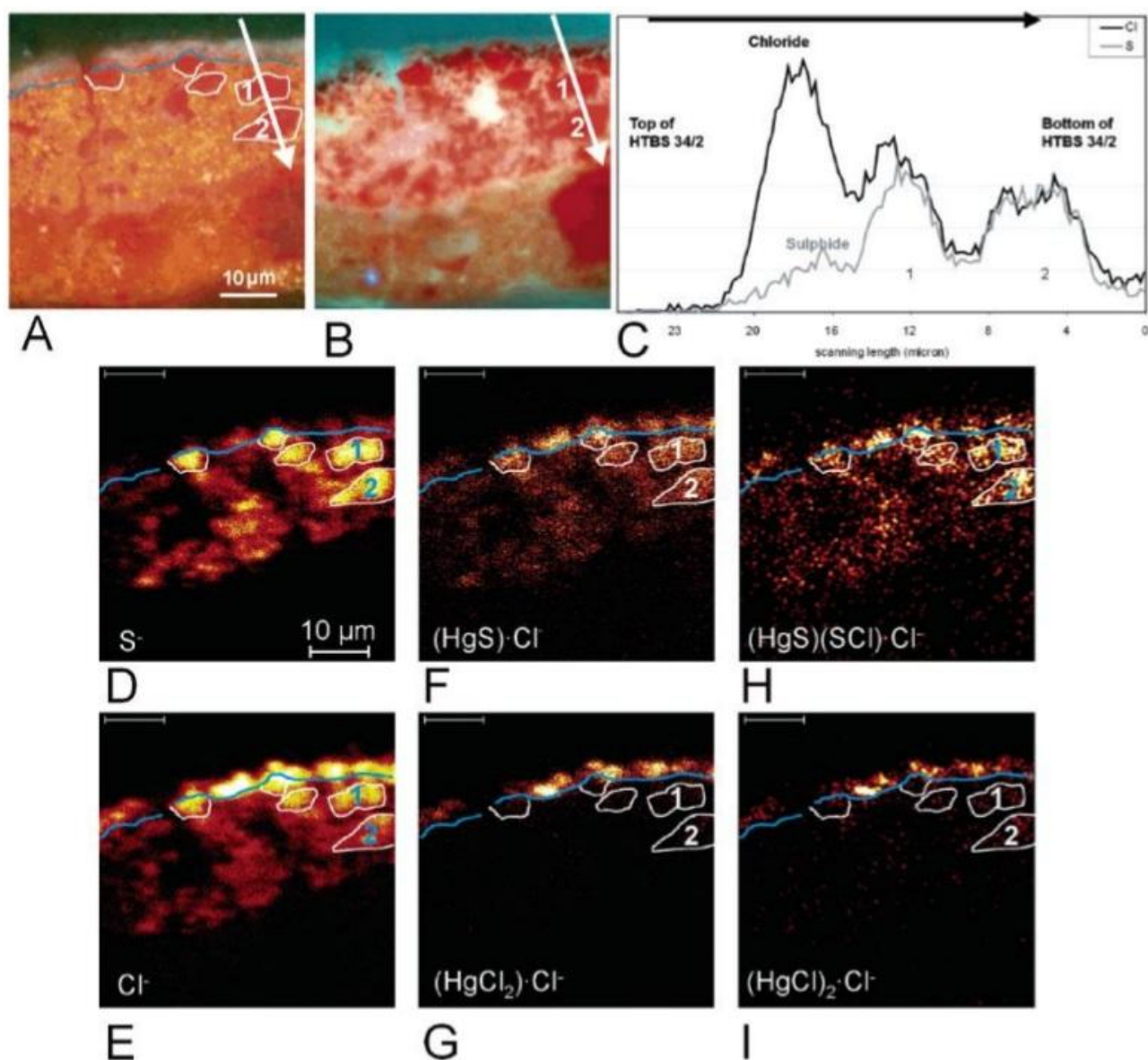


**Figure 1.7.** Distribution of sulfide and chloride and the molecular distribution in a partially degraded vermilion paint. The arrow in the light microscopic image (A) and UV light image (B), which represents the scanned SIMS area, indicates the direction of the line scan (C). The negative SIMS image of mercury-halogen cluster ions elucidates the position of  $\text{S}^-$  (D),  $\text{Cl}^-$  (E),  $(\text{HgS})\text{Cl}^-$  (F),  $(\text{HgCl}_2)\text{Cl}^-$  (G),  $(\text{HgS})(\text{S})\text{Cl}^-$  (H), and  $(\text{HgCl})_2\text{Cl}^-$  (I) in the partially degraded vermilion paint. A contour, based on the light microscopic image and total negative ion image, outlines four red vermilion particles and the boundary between the intact and degraded paint.[Keune et. Al., 2005]

Voras et al., used ToF-SIMS to detect and image both molecular and elemental species related to CdS pigment and binding medium alteration on the painting *Le Bonheur de vivre* (1905–1906, The Barnes Foundation) by Henri Matisse [91]. Three categories of inorganic and organic components were found throughout *Le Bonheur de vivre* and co-localized in cross-sectional samples using high spatial resolution ToF-SIMS analysis: (1) species relating to the preparation and photo-induced oxidation of CdS yellow pigments (2) varying amounts of long-chain fatty acids present in both the paint and primary ground layer and (3) specific amino acid fragments, possibly relating to the painting complex restoration history. ToF-SIMS ability to discern both organic and inorganic species via cross-sectional imaging was used to compare samples collected from *Le Bonheur de vivre* to artificially aged reference paints in an effort to gather mechanistic information relating to alteration processes. The relatively high sensitivity offered by ToF-SIMS imaging coupled to the high spatial resolution has allowed the identification of degradation products. The problem of interaction between binding media and inorganic ions has already been mentioned in the previous case studies. Boon et al., treated the well-known smalt discoloration issue [92]. This blue pigment, which is a ground cobalt glass and was used as a substitute for azurite or ultramarine, is known to undergo discoloration when used with oil binding media. The work was concerned the study of a cross-sections of paint layers with partially or totally discoloured smalt particles. The distribution of different ions in these cross-sections indicated the presence of palmitic acid around smalt particles and levels of potassium were much higher in coloured areas than in discoloured ones (Fig. 1.8). The presence of potassium in the binding media was interpreted as leaching of potassium out of the smalt particle due to the influence of oil organic compounds. This interaction would then be responsible for smalt discoloring.

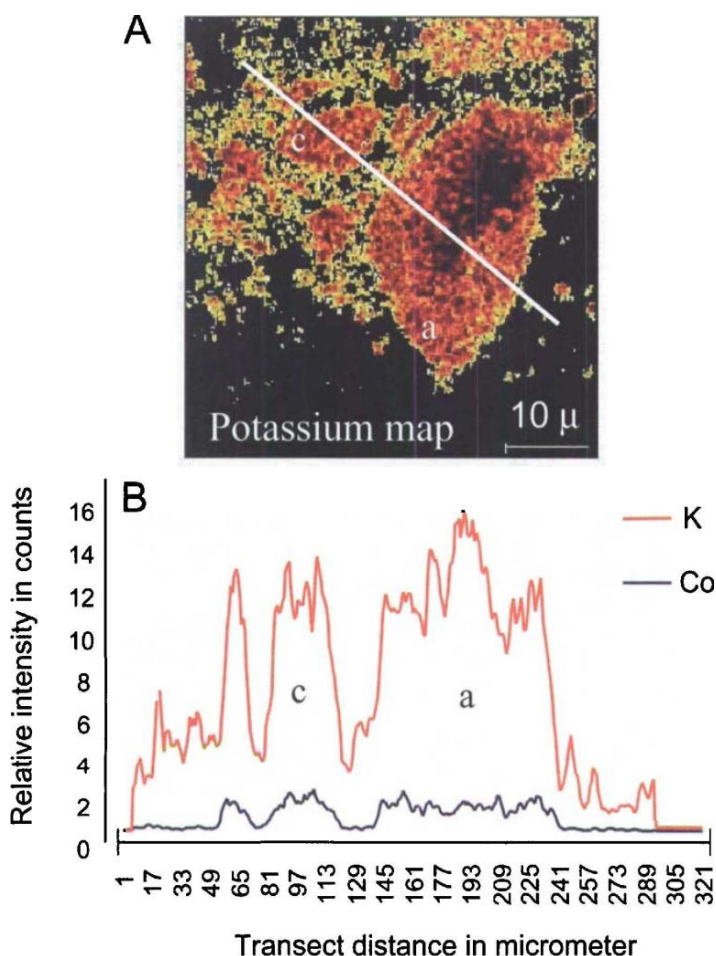


**Figure 1.8.** Line scans of cobalt and potassium along the transect displayed in the potassium imaging SIMS map of particle a in cross-section. The potassium contours ranging from high to low are colour coded from black via red to yellow. Particle c is completely discoloured. Cobalt is confined to the glass particles. The highest K levels from a 'levee' with an average intensity level of 16 in the blue coloured centre of particle a, while the 'banks' coincide with the discoloured rim at an average level of 12. The relatively small difference in K levels between core and rim suggest that the K:Co is close to a critical level. [Boon et. Al.,

Another example of interactions between inorganic ions and the oil component was given the extended study on lead soap formation. Development of such compounds is mainly due to the use of lead white as a drier of oil media but is associated with the ageing process of the paint layer [93]. This phenomenon is also responsible of the development of round protruding masses and white efflorescence crust [94]. The ToF-SIMS study of the cross-section affected by this phenomenon showed that monocarboxylic lead soaps were concentrated in the core, while diacids were detected in the rim of the aggregate (Fig. 1.9). This separation could be related to the formation process of the crystalline lead soap structure. A more detailed description of these phenomena can be found in Boon et al. [95], that treated also the problem of the zinc soaps formation in the painting pigments zinc based.

Zinc soap aggregates were observed in a late 19th century painting by R. Godfrey Rivers by Osmond et. Al. [96] Fourier Transform Infrared Spectroscopy (FTIR) was used to confirm the presence of zinc carboxylates together with ToF-SIMS technique. Moreover, Scanning Electron Microscopy Energy Dispersive X-ray (SEM- EDX) maps and spot analyses were used to examine aggregates in detail. The authors discussed on the variety of factors were likely to influence the formation of soap aggregates in paint films and their potential to cause defects. These include the inherent reactivity of zinc in oil, the quality and source of the zinc, the type and preparation of oil, the combination of components in the paint, and the environmental conditions and treatment interventions the painting might have experienced. The cause of the zinc soaps formation has been related to the high mobility oil molecules used in the painting and the preparation of the pigments themselves, together with the high environmental moisture present in contact with painting. Furthermore, others causes, as additives and modern formulation were decrypted.

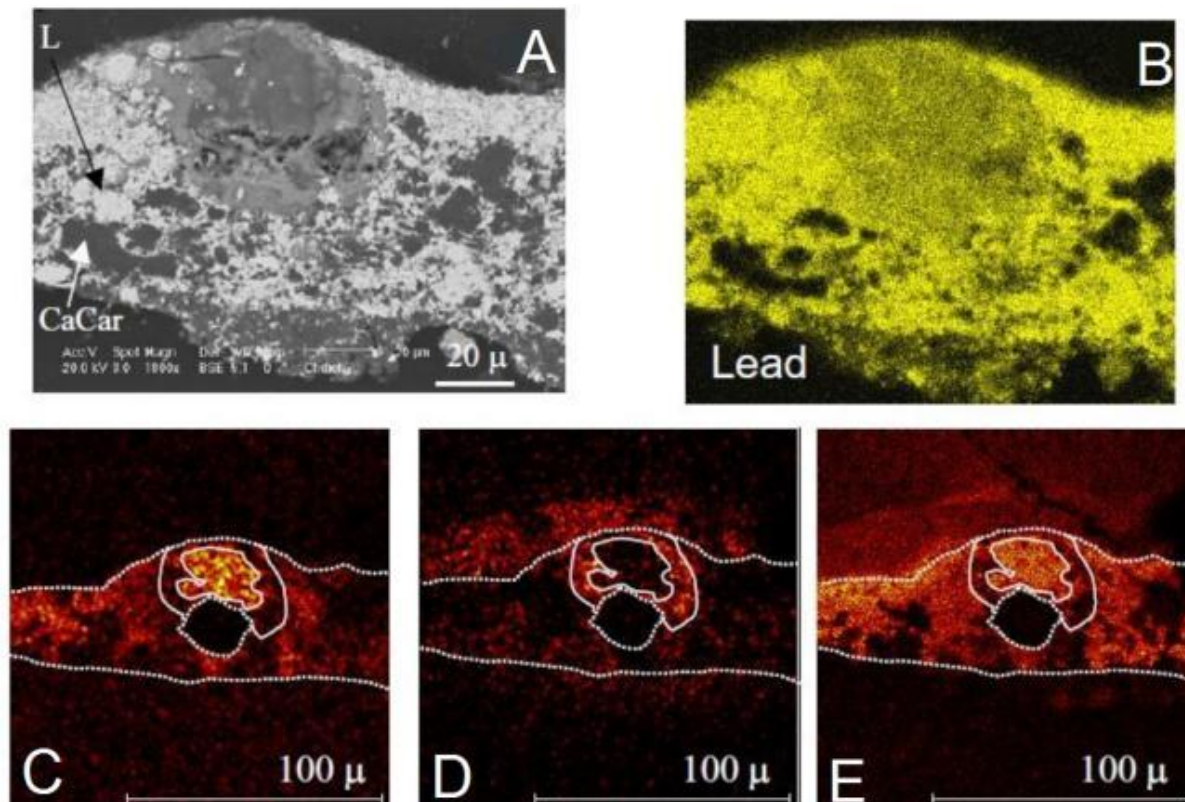


**Figure 1.9.** Cross-section of a sample from a painting from the Hudson River School presenting a round protruding mass. (A) SEM image and EDX images of (B) lead, (C) lead soaps, (D) azelaic acid and (E) stearic acid. [Boon et al., 2005]

Though paintings represent the most varied cases in the field of cultural heritage samples, the potentialities of ToF-SIMS technique were employed in the investigation of Archaeological findings. The main problem with organic analyses from archaeological remains is their state of conservation. Many authors have proven that in certain conditions, preservation is possible [97-98]. In the case of preservation of organic materials, ToF-SIMS is well suited for such a study, because samples are very small and precious, and no sample preparation is required and it is a nondestructive technique for the sample. In the study of the bones of an exceptionally well-preserved *Tyrannosaurus rex*, Schweitzer et al. try to determine the remains of original tissues through the presence of preserved proteins from the original collagen [99]. Demineralized samples were submitted to ToF-SIMS analyses. Analysis of proteins by ToF-SIMS has been described in several articles, and leads, in positive ion mode, to short fragments of amino acids [100-102]. Using high mass resolution, low mass species could be attributed without ambiguity. Glycine ( $m/z$  30) and alanine ( $m/z$  44) were the main amino acids detected with a relative ratio of 2.6:1. This was comparable with the specific collagen  $\alpha 1$  type 1 from chicken in which the ratio is 2.5:1. Proline ( $m/z$  70), lysine ( $m/z$  84) and leucine/isoleucine ( $m/z$  86) were also detected. These results proved the presence of well conserved proteins in the dinosaur bones.

Another example of ToF-SIMS investigation on archaeological findings concern the study conducted on the African art objects. Mazel et al. investigated the organic compounds detected on ritual African statues, in which blood and proteins were also detected along with balms and waxes used from the population as a traditional practice during rituals [103-105].

Indeed, many African art objects are in fact related to ritual ceremonies and are covered with a thick patina formed by materials spread on their surface during ceremonies where sacrifices may have taken place. In Mali, Dogon wooden statuettes from Bamana culture, are good examples of this practice. The identification of blood is generally performed using immunological tests. However, ToF-SIMS can also be used, with a different approach [103]. For this study, a microsample of patina was removed from the surface, and cross-sections were prepared by ultramicrotomy. Two-dimensional images of all protein low molecular weights fragments were drawn and compared. Correlation between the different images confirmed the presence of proteins. Furthermore, the positive ion mode was used to investigate haem, an iron porphyrin which is a blood marker. Spectra taken of the haem reference showed that it could be detected due to  $[M]^+$  and  $[M+H]^+$  ions (respectively, at  $m/z$  616.2 and 617.2), and also due to a large distribution of fragment at lower molecular weights. The same spectrum was also obtained for haemoglobin leading to the conclusion that the presence of protein did not disturb the detection of haem. From comparison with the spectrum of the reference, it was possible to locate the haem signal in Bamana sculptures.

Blood is the most often reported component of the patina from African ritual statuettes but other materials were also used. The patina is generally a quite complex mixture of different products from various chemical families. In the study of such complex mixtures, ToF-SIMS could detect in a unique analysis a great number of different compounds. In the investigation of Dogon statuette, Mazel et al. coupled ToF-SIMS with infrared micro spectrometry and SEM in order to characterize the compounds presence in the patina [105]. Along with proteins fragments, polysaccharide, recognized in positive polarity, lipid as deprotonated stearic, palmitic and arachidic acid were detected in negative ion mode. All these lipids showed the same distribution all over the sample with a predominance of stearic acid. This could be consistent with the use of shea butter or karite in the recipe of the patina, products commonly used in West Africa. This result represented a surprise and was less common in a cultural heritage study.

All the studies reported show the large range of possible applications of ToF-SIMS in the cultural heritage field. It can be used for the characterization of different kinds of materials such as textiles, painting materials or biological samples, and any other material could be considered. ToF-SIMS presents two main advantages. First, it permits the analysis of solid samples with minimal sample preparation. This avoids the necessity of extractions, and therefore, it can be very useful for small and precious samples. The second advantage is the possibility of performing chemical imaging analyses, with the best spatial resolution performance. ToF-SIMS results are sometimes difficult to interpret, but they often allow complementary results to be obtained using different techniques.

## 2 High-mass-resolution mass spectrometry and Chemometrics

A time-of-flight mass spectrometry is especially suitable for the analysis of secondary ions because of its high transmission, high mass resolution, and ability to detect ions of different masses simultaneously. Its peculiarities have been exploited to study isotopic fragmentation and to analyze molecules with high molecular weight, without derivatization or vaporization of the sample. Two studies were conducted by using ToF-SIMS technique, in parallel.

Initially, was conducted a study of the possible saponification reaction between metallic compounds and organic binders in wall decorations paintings. Representative samples were produced and artificially aged. The resultant alteration products were recognized through a systematic study of mass fragmentations and molecular vibrations detected also with the employ of FTIR spectroscopy.

Simultaneously, mass-fragmentation study of tri-terpene standards molecules were performed. These compounds are generally known in mass spectrometry literature as markers within natural resins used as varnishes, binders or glues since the Neolithic Age. In addition, mass-fragmentation studies of reference dammar and mastic resins, and birch bark tar were also carried out. The mass fragmentation of all these compounds were studied applying methods of multivariate statistics analysis, particular useful in the treatment of large amount of data, as is the case of those generate from ToF-SIMS measurements. The use of chemometric, on the one hand has allowed to identify the discriminating fragments for the recognition of natural resins within a real case study, and on the other hand, has proved to be a valuable tool for the discrimination of structural isomers present within these natural compounds.

### 2.1 Tin metal soap

#### 2.1.1 Introduction

In artworks, the presence of metal soaps is often related to various types of oil paint degradation. In general, metal soaps have been identified in efflorescence deposits, paint layers that have become transparent and in large aggregates that appear within the paint system [106]. It is now well established that the soaps contain mainly stearate and palmitate, and that the metals lead and zinc are predominant. So far, the synthesis of metal soaps for conservation studies was focused on so-called 'neutral' soaps (following the general formula  $Mn+FA_n$ , with M = metal and FA = fatty acid) and their characterization was obtained by the commonly techniques used in conservation science laboratories [107].

Usually, saponification phenomena in the cultural heritage samples are processes by which heavy metals (usually present in pigments) react with fatty acids, producing glycerol and a fatty acid salt, called 'soap'. Lipids containing fatty acid ester linkages can undergo hydrolysis. This represents the case of oil paintings. The reaction starts in the deep layers of the painting and works toward the surface. At present, there is no way to stop the reaction and the only effective restoration method is retouching.

More in general, metal soaps are low-water-insoluble compounds containing alkaline earth or heavy metals combined with monobasic carboxylic acids of 7–22 carbon atoms. The most

important group of metal soaps detected in artwork samples consists of driers that promote or accelerate the drying, curing or hardening of oxidizable coating vehicles such as paints, like cobalt naphthenate in the modern paintings. [108-109]. For example, Bell observed loss of gloss in alkyd gloss paints containing zinc white and found it to be due to the appearance of protuberances resulting from the formation of zinc soaps; the hazing effect being worst in the case of alkyd resins with high saturated and oleic acid ester content [110]. Bell also noted a reduction in opacity in paint films and suggested that it could be explained by a layer of zinc soaps, close to the zinc white particles, of refractive index intermediate between those of the resin and the pigment [111].

Metal soaps can also form from the reaction of a simple metal salt, present as a drier or pigment, with an organic medium. While such reaction may reinforce the physical properties of the film and can also play a role in the development of anti-corrosive properties, metal soaps can also have detrimental effects on paint films. The formation of metal soaps is not only limited in the paintings system, but they can also result from the reaction of oil used as protective coating or lubricant with a metal surface to which it was applied, or from the interaction of a metal support or metal leaf with drying oil in a painted artwork. For example, copper soaps formed on the brass wire wrapped around the socket part of African iron spears that had been coated with animal fat [112], in paintings on copper [113], and in paintings where brass leaf had been used instead of gold leaf [114]. Such uncontrolled, in situ reactions may often be detrimental to the artifact or work of art, as shown in the case of Benin copper-alloy objects where application of oil as a protective coating resulted in discolored and corroded surfaces [115-116]. The negative impact of copper soaps that formed on the surface of bronzes was described by Burmester and Koller [117].

The identification of metal soaps is often difficult, especially in mixtures. In theory, gas chromatography would be the ideal method. However, since fatty acid salts are usually converted to methyl ester derivatives in order to be analyzed, it is difficult to specify whether they were originally present as metal soaps, as free fatty acids, or as glycerides. Metal soaps, which form as degradation products on the surface of metal artifacts are often crystalline, could be analyzed with X-ray powder diffraction or with Fourier transform infrared spectroscopy (FTIR) in non-crystalline system, where the sampling is allowed. On the contrary, the imaging obtained through the ToF-SIMS technology allows, in the case of cross-section, to localize degradation products along the layers of the stratigraphy or in a specific area of the sample surface. Furthermore, the feature to combine the detection of the organic and inorganic compounds in a single run analysis allows to detect metal-organic adducts, as metal soaps. Considering the occurrence of saponification reactions, this experimentation was focused to the possible metal soap formation in the composite lamina decoration technique, largely diffused in wall paintings since XI century.

The term “*composite lamina*” is referred to a specific decoration technique, characterized by the overlapping of different metal foils (usually a noble foil, gold or silver lamina, superimposed on a less noble base, tin or copper) by means of an oil-resinous adhesive mixture on a support. Many examples of this decoration practice were found in frescos and paintings on wood [118]. The pattern of a classic gilding on tin foil is shown in Fig. 2.1. The contact between the metallic sheet and the organic oil-resin compound can result in a series of chemical interactions and reactions, also favored by specific moisture condition for a prolonged period of time. Furthermore, temperature variations may also play a role in the kinetics and thermodynamics of soap formation. In particular, the experimental design has been focused on the possible formation of metallic soaps between systems consisting of metal tin foil in contact with the fatty acids present in the adhesive

mixture. In addition, experiments could help to understand and pinpoint the possible aesthetic degradation effects on metal decoration in wall paintings.

To prove the saponification between composite lamina components, samples *ad hoc* prepared have undergone artificial aging cycles. It was possible to observe the progression of the saponification reaction with FTIR spectroscopy and subsequently characterize the mass fragmentation by using ToF-SIMS technique, which allowed the 2D chemical mapping of the inorganic and organic species in the samples. The following paragraphs illustrate the experimental setup and the results obtained for the two types of metal tin used.

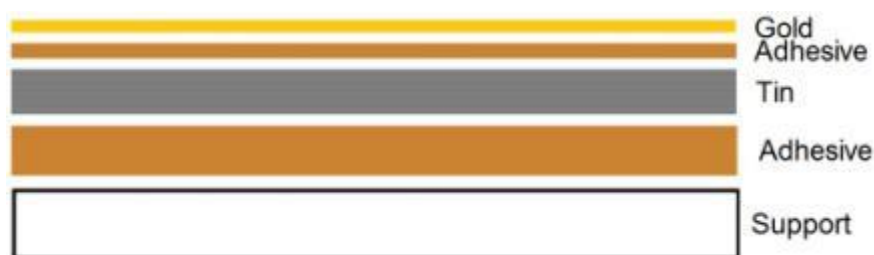


**Figure 2.1.** Schematic representation of the so called *composite lamina* technique. The tin foil is pasted to a support with an adhesive mixture and superimposed by a gold leaf, which is also pasted with the same oil-resinous compound.

## 2.1.2 Experimental design

The experiment was carried out parallel to nanoparticles of metallic tin and tin foil, which were in contact with the main fatty acids present in the siccative oils and resins also used in the glue mixture. Reference standards of tin metal nanoparticles (Sn, 118,71 u.m.a), tin oxide (SnO, 134,71 u.m.a), and tin dioxide (SnO<sub>2</sub>, 150,71 u.m.a) were mixed in a stoichiometric ratio of 1:2 with certified standards of the main fatty acids contained in siccative oils and in resinous compound for artistic use. Furthermore, an oil for artistic use and a resin were also used for the samples preparation. Azelaic acid (C<sub>9</sub>H<sub>16</sub>O<sub>4</sub>, 188.22 u.m.a., dicarboxylic acid), palmitic acid (C<sub>16</sub>H<sub>32</sub>O<sub>2</sub>, 256.42 u.m.a.), stearic acid (C<sub>18</sub>H<sub>36</sub>O<sub>2</sub>, 284.47 u.m.a.), abietic acid (main markers of colophony, C<sub>20</sub>H<sub>30</sub>O<sub>2</sub>, 302.46 u.m.a.) tri-stearyl glycerol (C<sub>57</sub>H<sub>110</sub>O<sub>6</sub>, 891.48 u.m.a.), linseed oil and colophony were used for the experimentation.

The organic samples were dissolved in few microliters of CH<sub>2</sub>Cl<sub>2</sub> and deposited on duplicate slides via spin coating. At the same time, it was also necessary to verify the formation of metal soaps even on tin metal lamina. Metallic tin sheets were cut into squares of the size of 1 cm<sup>2</sup>. Half of the samples were treated with sandpaper to increase the surface area and the resulting contact with the acids and the resins, before the deposition of the single standard acids. Furthermore, a second part was immersed few seconds in hydrochloric acid (1N) to accelerate the formation of tin alteration products (oxides, hydroxides and chlorides). Few milligrams of each standard acid was dissolved in about 200 µl of dichloromethane and dropped by means a spin coater on the lamina samples. The list of the samples is reported in Tab. 1. All samples were placed in a climate chamber for artificial aging, exposed to controlled temperature and humidity conditions. The samples were aged for about 90 days during which the progression of the saponification reaction was monitored by FTIR analysis. A new climatic cycle was set up following each FTIR control

analysis, increasing humidity and temperature values, and thus changing the conditions of the previous cycle to accelerate the kinetics of the saponification reaction. The initial temperature and humidity parameters of 40° C and 90% RH were increased progressively until reaching 98% RH and a temperature of 70° C values. FTIR measurements were performed weekly by a Thermo Scientific Nicolet iN10 FTIR (Thermo Fisher Scientific, Nicolet iS10, Waltham, MA, USA) operating in ATR (Attenuated Total Reflection) mode with germanium crystal using a nitrogen-cooled MCT detector. The IR spectra were obtained from different portions of the samples area. The analyzed areas were of 400x400  $\mu\text{m}^2$ , in the spectral region from 4000 to 650 $\text{cm}^{-1}$  with a resolution of 4 $\text{cm}^{-1}$  and 64 scans for each spectrum. To validate the hypothesis of the saponification reaction, the samples were also analyzed with to ToF-SIMS instrument. ToF-SIMS analyses were performed on a TOF-SIMS V (ION-TOF GmbH, Münster, Germany) equipped with a Bi liquid metal ion gun. A 30 keV  $\text{Bi}_3^{2+}$  ion beam was selected with an incidence angle of 45° operating in the high mass resolution bunched mode. The ion beam was rastered over an area of 500x500 $\mu\text{m}^2$  with an ion dose density below the static limit ( $10^{-12}$  ion/ $\text{cm}^2$ ). Charge neutralization was obtained by using low-energy electrons supplied by a pulsed flood gun. The spectra were acquired in positive polarity, after a superficial surface cleaning by a 30 KeV scan of  $\text{Bi}_3^{++}$ . This operation was necessary to remove from the sample any contamination derived to the climatic chamber.

| SAMPLES                | Azelaic acid | Palmitic acid | Stearic acid | Abietic acid | Glyceril tristearate | Liseed oil | Colophony) |
|------------------------|--------------|---------------|--------------|--------------|----------------------|------------|------------|
| <b>Sn powder</b>       | 1.1          | 1.2           | 1.3          | 1.4          | 1.5                  | 1.6        | 1.7        |
| <b>SnO</b>             | 2.1          | 2.2           | 2.3          | 2.4          | 2.5                  | 2.6        | 2.7        |
| <b>SnO<sub>2</sub></b> | 3.1          | 3.2           | 3.3          | 3.4          | 3.5                  | 3.6        | 3.7        |
| <b>Sn foil</b>         | 4.1          | 4.2           | 4.3          | 4.4          | 4.5                  | 4.6        | 4.7        |
| <b>Sn s.</b>           | 4.1N         | 4.2N          | 4.3N         | 4.4N         | 4.5N                 | 4.6N       | 4.7N       |
| <b>Sn HCl</b>          | 4.1HCl       | 4.2HCl        | 4.3HCl       | 4.4HCl       | 4.5HCl               | 4.6HCl     | 4.7HCl     |

**Table 2.1.** List of the samples. The samples named with the “N” letter, and the suffix HCl, were prepared with sandpaper and hydrochloric acid, respectively. The chemicals used in the experiment were provided by sigma Aldrich. Technical specifications of the reagents are listed in Table A1 present in Appendix.

### 2.1.3 Results and discussion

FTIR analysis were carried out with particular attention to the region of the spectrum around 1550  $\text{cm}^{-1}$  typically the wavelength of the carboxyl stretch vibration, indicators of the formation of metallic soaps by fatty acids. After a few weeks since the beginning of aging, a slight double peak in the region between 1580 and 1540  $\text{cm}^{-1}$  was observed in some samples, that represent the peaks of the formation of tin metallic carboxylates.

Double peaks appeared in samples of tin nano-powder (Sn, SnO and SnO<sub>2</sub>) and tin treated foil (series 4N) in combination with azelaic, palmitic, stearic acid, and glyceril tristearate. Furthermore,

only two samples of tin sheet treated with HCl gave rise to saponification reaction (4.3HCl and 4.5HCl). No metal tin soaps were detected in Sn foil series (samples 4.1-7). Although all the samples were subjected to the same temperature and humidity variations, at the end of the artificial aging treatment the totality of the systems formed by tin, tin oxides and laminas with colophony and linseed oil had not reacted.

Due to the huge amount of data collected during the experiment, the most significant samples in which the saponification reaction took place are presented. In Figs. 2.2 and 2.3 are shown the FTIR spectra recorded in different time, per tin powders (samples 1.3, 2.1, 2.2) and tin foils abraded samples with azelaic, palmitic and stearic acids (samples 4.1N, 4.2N, 4.3N), respectively.

The infrared absorptions of fatty acids and the tin azelate, palmitate and stearate formed on tin powders and foils are listed in Tabs. 2.2 and 2.3, respectively. As can be expected, the infrared spectra of palmitic and stearic acids are very similar, while differing from that of azelaic acid, being this latter a dicarboxylic acid. These spectra can be observed in all samples at initial time  $T_0$ , in the Figs. 2.2 and 2.3.

The main difference between the infrared spectra of palmitic and stearic acid is that there are seven bands between about  $1310$  and  $1185\text{ cm}^{-1}$  in the spectrum of palmitic acid, while there are eight in the spectrum of stearic acid. These multiple bands are due to  $\text{CH}_2$  wagging modes coupled with carboxyl vibrations. The spectrum of azelaic acid has a different profile in the region between  $2930$  and  $2660\text{ cm}^{-1}$ , and the vibration of carbonyl group below at  $1700\text{ cm}^{-1}$ .

The formation of soaps is marked, in some case, by the attenuation of the very strong bands of  $\text{C}=\text{O}$  and  $\text{C}-\text{O}$  stretching around  $1700$  and  $1300\text{ cm}^{-1}$ , with the bands attributed to the  $\text{COO}^-$  asymmetric and symmetric stretching around  $1570$  and  $1400\text{ cm}^{-1}$ , respectively. In the specific case of tin soaps, the  $\text{COO}^-$  asymmetric stretching consists in a doublet around at  $1573$  and  $1539\text{ cm}^{-1}$ , for all the sample in which the reaction were recorded. So the type of fatty acid, seems did not influence the wavelength. The tin carboxylates, compared with the literature values of  $\text{COO}^-$  group asymmetric stretch band contained in copper ( $1590\text{ cm}^{-1}$ ), zinc ( $1540\text{ cm}^{-1}$ ) and lead soaps (doublet at  $1540$ - $1510\text{ cm}^{-1}$ ), are located in the center of this region, confirming that the shifting absorbing depends on the metal cation involved in the saponification process [107].

However, in all the samples analyzed, the band belonging to the  $\text{COO}^-$  symmetric stretch is covered by the bending vibration of  $\text{CH}_2$  groups, of fatty acids signals that did not reacted. as also testified of the carbonyl vibration group present at  $1700\text{ cm}^{-1}$ , (Figs. 2.2c and 2.3a). This could be ascribed to the method of deposition used. In fact, although for all nano particles samples the same deposition method has been adopted, it may be possible that spin coater use has in some cases produced a powdery dispersion.

Consequently, part of the tin nanoparticles calculated to comply the stoichiometric ratio did not contribute to the saponification reaction, leaving the reaction to an intermediate stage in which only part of the deposited tin powders has reacted. It is therefore plausible that the surface of the samples presents an excess of fatty acid which interfered in the interpretation and detection of the  $\text{COO}^-$  symmetrical stretch band at  $1400\text{ cm}^{-1}$ .

| Azelaic acid | Palmitic acid | Stearic acid | Tin azelate | Tin palmitate | Tin stearate | Attribution                          |
|--------------|---------------|--------------|-------------|---------------|--------------|--------------------------------------|
| 3300-2500 br | 3300-2500 br  | 3300-2500 br |             |               |              | $\nu$ OH                             |
| 2932 m       | 2954 m        | 2954 m       | 2953 m      | 2950 m        | 2954 m       | $\nu_{as}$ CH <sub>3</sub>           |
| 2912 vs      | 2917 vs       | 2917 vs      | 2910 vs     | 2914 vs       | 2916 vs      | $\nu_{as}$ CH <sub>2</sub>           |
| 2870 m       | 2871 vs       | 2871 m       |             |               |              | $\nu_s$ CH <sub>3</sub>              |
| 2853 m, br   | 2849 vs       | 2850 vs      | 2854 m      | 2847 vs       | 2850 vs      | $\nu_s$ CH <sub>2</sub>              |
| 2658 vs      | 2677 m, br    | 2676 m, br   |             |               |              | $\nu$ OH                             |
| 1692 vs      | 1703 vs       | 1703 vs      | 1692 vs     | 1703 vs       | -            | $\nu$ C=O                            |
|              |               |              | 1573-1539 w | 1573-1539 m   | 1573-1539 s  | $\nu_{as}$ COO                       |
| 1468 m       | 1471 m        | 1472 s       | 1472 s      | 1469 s        | 1473 s       | $\delta$ CH <sub>2</sub>             |
| 1445 m       | 1463 m        | 1463 m       |             |               | 1462 m       | $\delta$ CH <sub>2</sub>             |
|              |               |              |             |               |              | $\delta$ CH <sub>2</sub>             |
| 1433 m       | 1432 m        | 1432 m       | 1434 m      | 1429 m        | 1434 m       | $\delta$ CH <sub>2</sub>             |
|              |               |              |             |               |              | $\nu$ COO                            |
| 1409 m       | 1410 m        | 1411 m       | 1408 m      | 1412 m        | 1411 m       | $\nu$ CH <sub>2</sub>                |
| 1358 vw      | 1372 vw       | 1372 vw      | 1378 vw     | 1376 vw       | 1380 vw      | $\nu$ CH <sub>3</sub>                |
| 1345 vw      | 1348 vw       | 1347 vw      | 1359 w      | 1350 w        | 1330 w       |                                      |
| 1321 w       | 1329 w        | 1331 w       |             |               |              |                                      |
| 1311 m       | 1311 m        | 1313 m       | 1314 m      | 1309 m        | 1315 m       |                                      |
| 1297 m       | 1296 m        | 1298 s       |             | 1291w         | 1299 m       | $\delta$ CH <sub>2</sub>             |
| 1278 m       | 1272 m        | 1279 m       | 1279 w      | 1271 w        | 1280 w       |                                      |
|              |               | 1260 m       | 1251 m      | 1250 m        | 1261 m       |                                      |
| 1259 m       | 1250 m        |              |             |               |              |                                      |
|              |               | 1241 m       |             |               | 1242         |                                      |
| 1227 m       | 1228 m        | 1223 m       | 1225 m      | 1228 m        | 1222 m       |                                      |
| 1205 m       | 1207 m        | 1204 m       | 1208 m      | 1202 m        | 1203 m       |                                      |
| 1196 m       | 1188 m        | 1187 m       | 1195 m      | 1182 m        | 1188 m       |                                      |
|              |               |              | 1129 w      |               |              |                                      |
| 1097 w       | 1099 w        | 1103 w       | 1097 m      | 1098 m        | 1103 m       | $\nu$ C-C + $\delta$ C-C-C           |
|              |               |              | 1039 w      | 1046 w        |              | $\nu$ C-C + $\delta$ C-C-C           |
|              |               |              | 1002 w      | 1005 w        |              | $\nu$ C-C + $\delta$ C-C-C           |
| 982 m        | 942 m         | 942 m        | 978 m       | 942 m         | 941m         | $\delta$ CH <sub>2</sub>             |
| 916 w        | 911 w         | 913 w        | 914 w       | 886 w         | 891 w        |                                      |
| 849 w        | 891 w         | 892 w        |             |               |              | $\nu$ C-C (carboxyl)                 |
|              |               |              |             |               |              | $\delta$ CH <sub>3</sub> + $\nu$ C-C |
|              |               | 811 vw       | 822 vw      | 845 vw        | 810 vw       |                                      |
| 775 w        | 782 w         |              |             |               |              |                                      |
|              |               | 762 vw       | 772 vw      | 780 vw        | 759 vw       |                                      |
| 725 m        | 720 m         | 719 m        | 723 m       | 724 m         | 721 m        |                                      |
| 682 w        | 688 w         | 688 w        | 682 w       | 689 w         | 690 w        | $\delta$ COO                         |

**Table 2.2.** Infrared wave number (cm<sup>-1</sup>) for azelaic, palmitic and stearic acid and tin soaps on metal nanoparticles. The values of the metal soaps refer to the last acquisition.  
*vs=very strong, s=strong, m=medium, w=weak, vw=very weak, sh=shoulder, br=broad,  $\nu$ =stretching,  $\delta$ =bending*

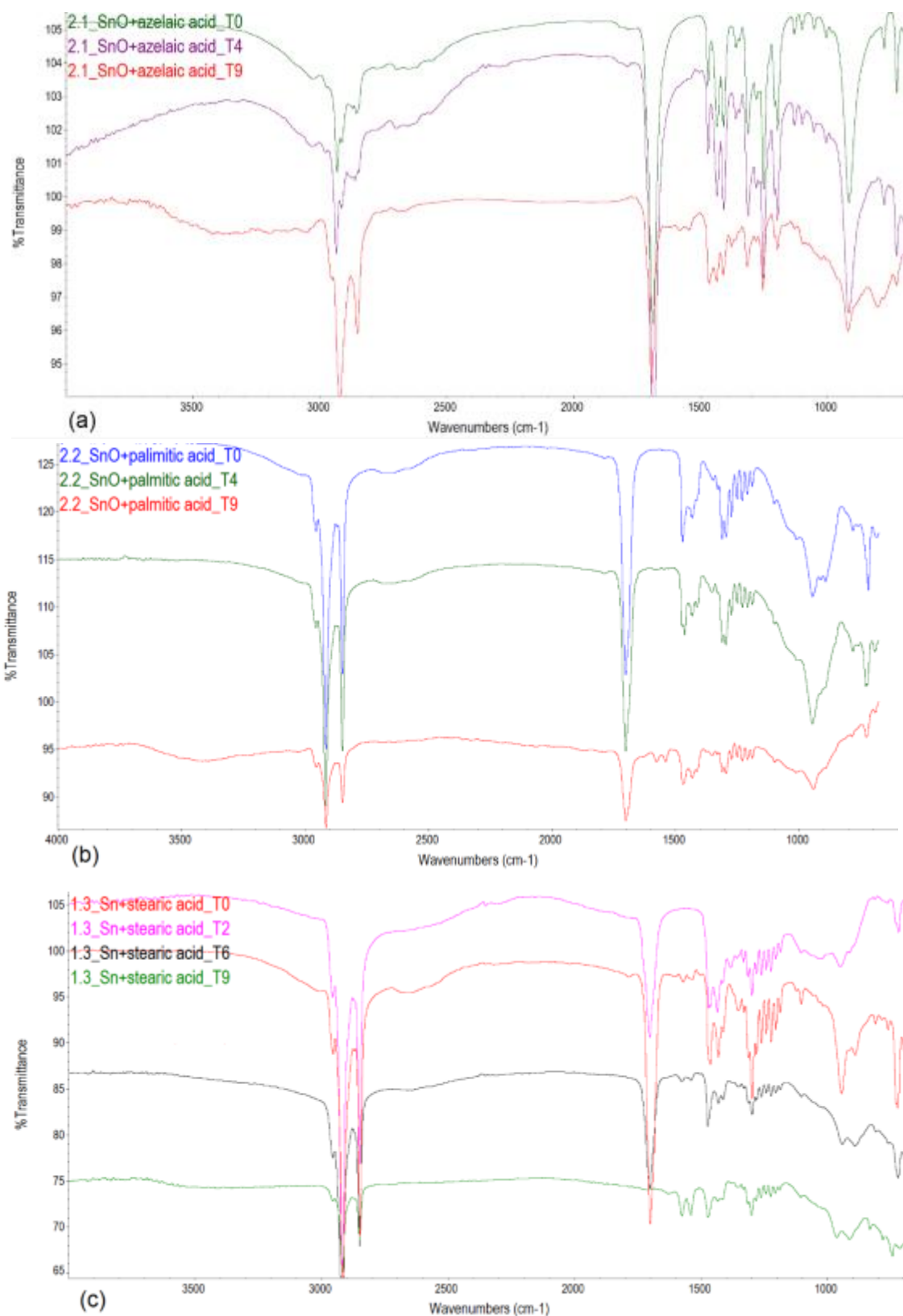


**Figure 2.2.** FTIR spectra of tin azelate sample 2.1 (a), tin palmitate sample 2.2 (b), and tin stearate sample 1.3 (c).

| Azelaic acid | Palmitic acid | Stearic acid | Tin azelate | Tin palmitate | Tin stearate | Attribution                     |
|--------------|---------------|--------------|-------------|---------------|--------------|---------------------------------|
| 3300-2500 br | 3300-2500 br  | 3300-2500 br |             |               |              | v OH                            |
| 2932 m       | 2954 m        | 2954 m       | 2957m       | 2954 m        | 2954 m       | v <sub>as</sub> CH <sub>3</sub> |
| 2912 vs      | 2917 vs       | 2917 vs      | 2923 vs     | 2916 vs       | 2916 vs      | v <sub>as</sub> CH <sub>2</sub> |
| 2870 m       | 2871 vs       | 2871 m       |             |               |              | v <sub>s</sub> CH <sub>3</sub>  |
| 2853 m, br   | 2849 vs       | 2850 vs      | 2854 m      | 2846 vs       | 2850 vs      | v <sub>s</sub> CH <sub>2</sub>  |
| 2658 vs      | 2677 m, br    | 2676 m, br   |             |               |              | v OH                            |
| 1692 vs      | 1703 vs       | 1703 vs      | -           | 1703 m        | 1703 s       | v C=O                           |
|              |               |              | 1573-1539 s | 1573-1539 m   | 1573-1539 m  | v <sub>as</sub> COO             |
| 1468 m       | 1471 m        | 1472 s       |             |               |              | δ CH <sub>2</sub>               |
| 1445 m       | 1463 m        | 1463 m       | 1469 m      | 1469 m        | 1469 m       | δ CH <sub>2</sub>               |
|              |               |              |             |               |              | δ CH <sub>2</sub>               |
| 1433 m       | 1432 m        | 1432 m       | 1434 m      | 1429 m        | 1431 m       | δ CH <sub>2</sub>               |
|              |               |              | -           | -             | -            | v COO                           |
| 1409 m       | 1410 m        | 1411 m       | 1407 m      | 1412 m        | 1411 m       | v CH <sub>2</sub>               |
| 1358 vw      | 1372 vw       | 1372 vw      | 1377 vw     | 1374 vw       |              | v CH <sub>3</sub>               |
| 1345 vw      | 1348 vw       | 1347 vw      | 1342 m      | 1350 m        | 1353 m       |                                 |
| 1321 w       | 1329 w        | 1331 w       |             | 1329 w        | 1330 w       |                                 |
| 1311 m       | 1311 m        | 1313 m       | 1315 m      | 1313 m        | 1311m        |                                 |
| 1297 m       | 1296 m        | 1298 s       | 1284 s      | 1291 s        | 1296 s       | δ CH <sub>2</sub>               |
| 1278 m       | 1272 m        | 1279 m       |             | 1271 m        | 1261 m       |                                 |
|              |               | 1260 m       | 1249 m      | 1249 m        | 1242 m       |                                 |
| 1259 m       | 1250 m        |              |             |               |              |                                 |
|              |               | 1241 m       |             |               |              |                                 |
| 1227 m       | 1228 m        | 1223 m       |             | 1226 m        | 1222 m       |                                 |
| 1205 m       | 1207 m        | 1204 m       |             | 1207 m        | 1203 m       |                                 |
| 1196 m       | 1188 m        | 1187 m       | 1193 m      | 1188 m        | 1188 m       |                                 |
| 1097 w       | 1099 w        | 1103 w       |             | 1099 w        | 1103 w       | v C-C + δ C-C-C                 |
|              |               |              |             |               |              | v C-C + δ C-C-C                 |
|              |               |              |             |               |              | v C-C + δ C-C-C                 |
| 982 m        | 942 m         | 942 m        |             | 937 m         | 941 m        | δ CH <sub>2</sub>               |
| 916 w        | 911 w         | 913 w        |             |               |              | v C-C (carboxyl)                |
| 849 w        | 891 w         | 892 w        |             | 891 w         | 891 w        | δ CH <sub>3</sub> + v C-C       |
|              |               | 811 vw       |             | 848 vw        | 810 vw       |                                 |
| 775 w        | 782 w         |              |             | 810 vw        | 759 vw       |                                 |
|              |               | 762 vw       |             |               |              |                                 |
| 725 m        | 720 m         | 719 m        |             | 725 m         | 721 m        |                                 |
| 682 w        | 688 w         | 688 w        |             | 686 w         | 690 w        | δ COO                           |

**Table 2.3.** Infrared wave number (cm<sup>-1</sup>) for azelaic, palmitic and stearic acid and tin soaps on metal foil.

The values of the metal soaps refer to the last acquisition.

vs=very strong, s=strong, m=medium, w=weak, vw=very weak, sh=shoulder, br=broad, v=stretching, δ=bending

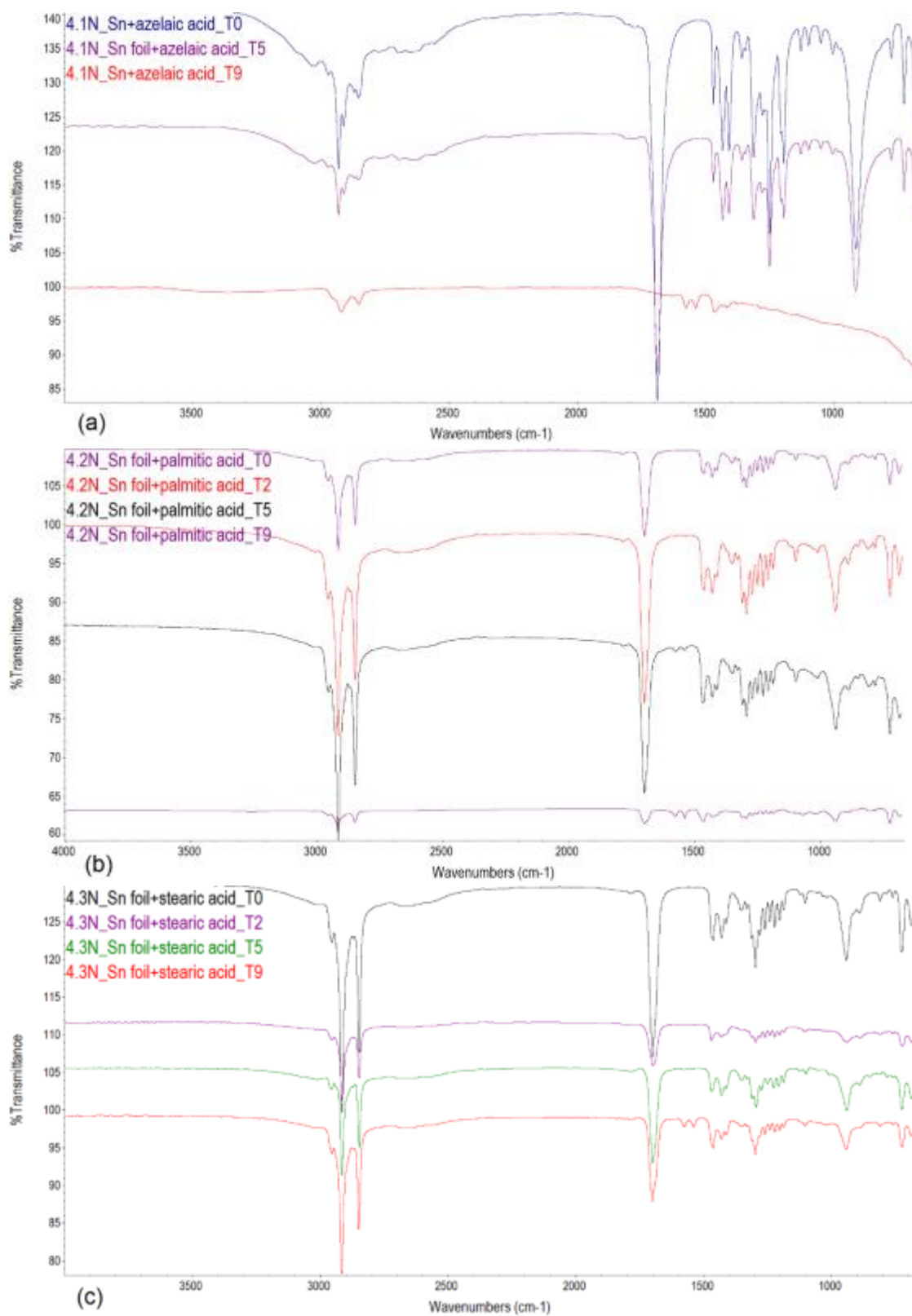


**Figure 2.3.** FTIR spectra of tin azelate (a) tin palmitate (b) and tin stearate (c), deriving from tin abraded foil.

To confirm the FTIR results, ToF-SIMS analyses were performed on the same sample presented before, with the aim to find the fragmentation pathway of metallic carboxylates hypothetically formed, and confirm the saponification. The acquisition of the spectra is occurred in positive polarity. This choice was due to the better ionization of soaps species in this polarity [119]. Furthermore, preliminary investigation in negative mode were acquired, identifying the characteristic fragments of fatty acid chains and tin oxides, present in the start sample or that formed during the ageing process (spectra not shown). The positive and negative characteristic fragments of the main fatty acids involved in the saponification process were identified by previous FTIR analyzes are listed in Tab. 2.4.

| m/z (+) | Assignment          | FA                    | m/z (-) | Assignment          | FA                    |
|---------|---------------------|-----------------------|---------|---------------------|-----------------------|
| 27      | $C_2H_3^+$          | A, P, S               | 38      | $C_3H_2^-$          | A, P, S               |
| 29      | $C_2H_5^+$          | A, P, S               | 39      | $C_2O^-$            | A, P, S               |
| 41      | $C_3H_5^+$          | A, P, S               | 41      | $C_2HO^-$           | A, P, S               |
| 43      | $C_3H_7^+$          | A, P, S               | 43      | $C_2H_3O^-$         | A, P, S               |
| 55      | $C_4H_7^+$          | A, P, S               | 58      | $C_2H_2O_2^-$       | A, P, S               |
| 57      | $C_4H_9^+$          | A, P, S               | 59      | $C_2H_3O_2^-$       | A, P, S               |
| 69      | $C_5H_9^+$          | A, P, S               | 71      | $C_3H_3O_2^-$       | A, P, S               |
| 95      | $C_7H_{11}^+$       | A, P, S               | 113     | $C_6H_9O_2^-$       | A, P, S               |
| 109     | $C_8H_{13}^+$       | A, P, S               | 127     | $C_7H_{11}O_2^-$    | A, P, S               |
| 239     | $C_{16}H_{31}O^+$   | P                     | 141     | $C_8H_{13}O_2^-$    | A, P, S               |
| 257     | $C_{16}H_{33}O_2^+$ | P (M+H <sup>+</sup> ) | 155     | $C_8H_{15}O_2^-$    | A, P, S               |
| 267     | $C_{18}H_{35}O^+$   | S                     | 169     | $C_{10}H_{17}O_2^-$ | A, P, S               |
| 285     | $C_{18}H_{37}O_2^+$ | S (M+H <sup>+</sup> ) | 183     | $C_{11}H_{19}O_2^-$ | P, S                  |
|         |                     |                       | 187     | $C_9H_{15}O_4^-$    | A (M-H <sup>+</sup> ) |
|         |                     |                       | 197     | $C_{12}H_{21}O_2^-$ | P, S                  |
|         |                     |                       | 211     | $C_{13}H_{23}O_2^-$ | P, S                  |
|         |                     |                       | 225     | $C_{14}H_{25}O_2^-$ | P, S                  |
|         |                     |                       | 237     | $C_{16}H_{29}O^-$   | P                     |
|         |                     |                       | 255     | $C_{16}H_{31}O_2^-$ | P (M-H <sup>+</sup> ) |
|         |                     |                       | 265     | $C_{18}H_{33}O^-$   | S                     |
|         |                     |                       | 283     | $C_{18}H_{35}O_2^-$ | S (M-H <sup>+</sup> ) |

**Table 2.4.** Characteristic positive and negative secondary fragment ions of azelaic (A), palmitic (P) and stearic (S) acid, analysed with SIMS.

In Fig. 2.4 are shown mass spectra relative to the sample 2.1, composed by tin oxide (SnO) and azelaic acid ( $C_9H_{16}O_4$ ). The window region between m/z 280 and m/z 350 shows the relative fragmentation of metallic adducts with azelaic acid (Fig. 2.4b). Two cluster of weak peaks in the range at m/z 284-289 and m/z 303-306 could be belong to tin azelate. The peaks at m/z 306 and m/z 289 can be attributed to tin azelate  $C_9H_{15}O_4Sn^+$  and tin azelate with the loss of a hydroxylic group  $C_9H_{14}O_3Sn^+$ . These signals have mapped on the spectrum in order to localize them on the SIMS image. In the Fig. 2.5 are shown the map of tin azelate distribution and the ion maps of  $Sn^+$  and  $Sn_xO_y$  clusters, compare to the total positive ion image. All three species are distributed over the same area, confirming the formation of azelate tin soap. In the same way, the experiments conducted on the sample 2.2, tin oxide (SnO) and palmitic acid ( $C_{16}H_{32}O_2$ ), show the fragmentation of two cluster of peaks in the range at m/z 353-357 and m/z 370-374, likely belonging to tin palmitate (Fig. 2.6). Even if the recorded signals are very weak, the compresence of palmitic acid and tin oxide could confirm the formation of tin palmitate soaps.

Thus, the peaks at m/z 374 and 353 can be attributed to tin palmitate  $C_{16}H_{31}SnO_2^+$  and tin palmitate with the loss of a hydroxylic group  $C_{16}H_{30}SnO^+$ , respectively. In the secondary ion images

of the sample, these signals are mapped with tin and tin oxides, supporting the hypothesis of the metallic carboxylates formation in this case too (Fig. 2.5).

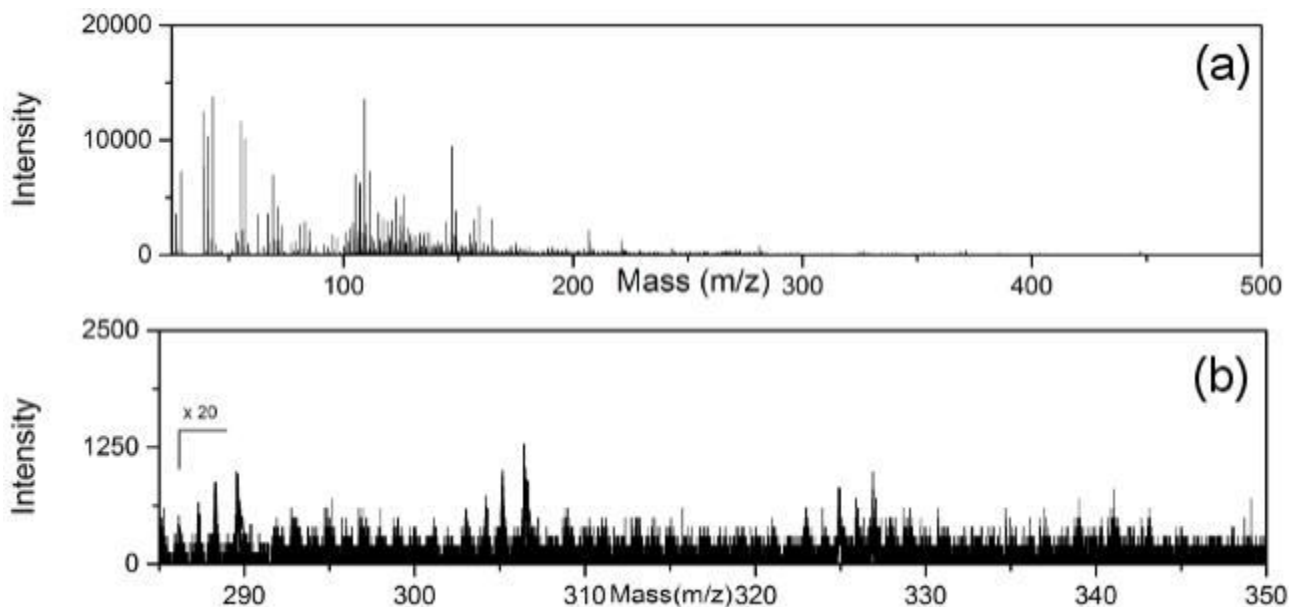


**Figure 2.4.** Positive mass spectra of sample 2.1. The window region shows the cluster belonging to tin azelate (b).

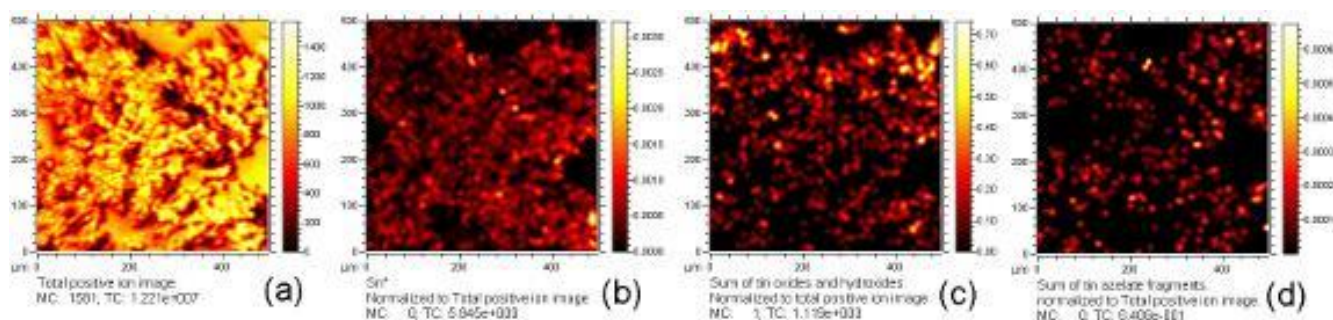


**Figure 2.5.** ToF-SIMS positive ion maps of sample 2.1. Total positive ion (a),  $\text{Sn}^+$  signal (b), tin oxides cluster (c) and tin azelate (d) were normalized to the total ion image and filtered to avoid topographical effects.

The last sample compared with ToF-SIMS investigation was the sample 1.3, constituted by metallic tin powder ( $\text{Sn}^+$ ) and stearic acid ( $\text{C}_{18}\text{H}_{36}\text{O}_2$ ) (Fig. 2.8). The enlarge region shown in Fig. 2.8b presents two clusters of peaks in the positive mass spectra in the range at  $m/z$  384–392 and  $m/z$  401–409. The most intense of these peaks were observed at  $m/z$  386 and 402, respectively. These distribution pattern could suggest the possible formation of tin soaps. The peaks at  $m/z$  402 and 386 can be attributed to tin stearate  $\text{C}_{18}\text{H}_{35}\text{SnO}_2^+$  and tin stearate with the loss of a hydroxylic group  $\text{C}_{18}\text{H}_{34}\text{SnO}^+$ . The sum of the signals of tin stearates arise from the same area of tin and tin oxides distribution, confirming the soaps formation (Fig. 2.9). For all the samples analyzed the soaps assignment were confirmed by a comparison with the theoretical isotope pattern. The isotopic pattern and the mass accuracy observed for the clusters of peaks provide strong evidence for the correct assignment of these signals.

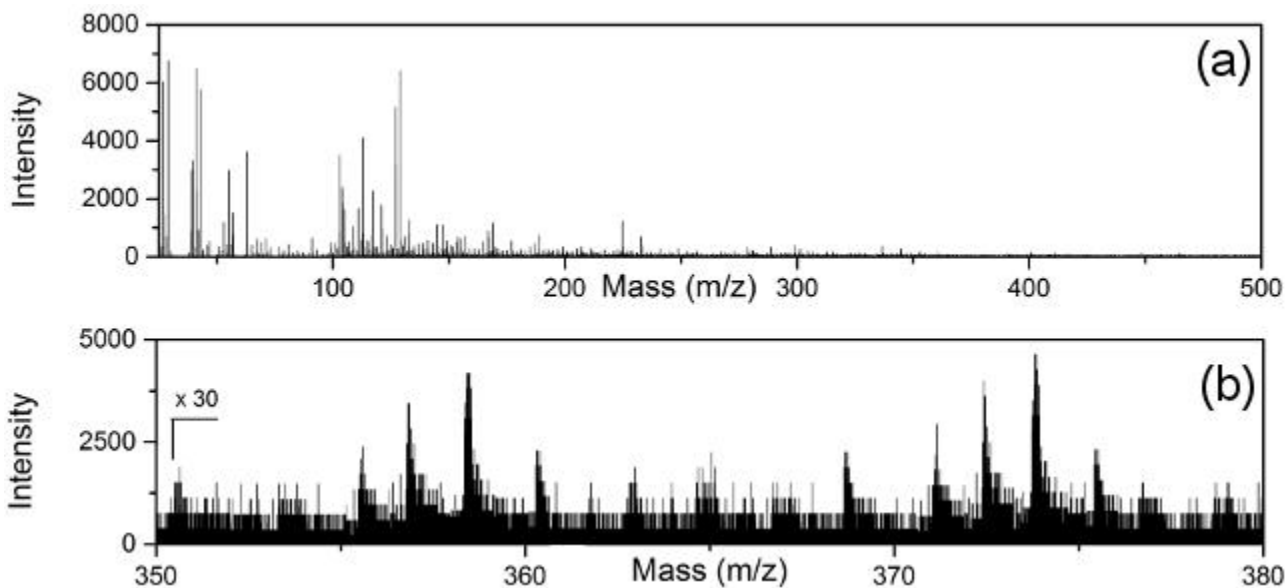


**Figure 2.6.** Positive mass spectra of sample 2.2. The window region shows the cluster belonging to tin palmitate (b).

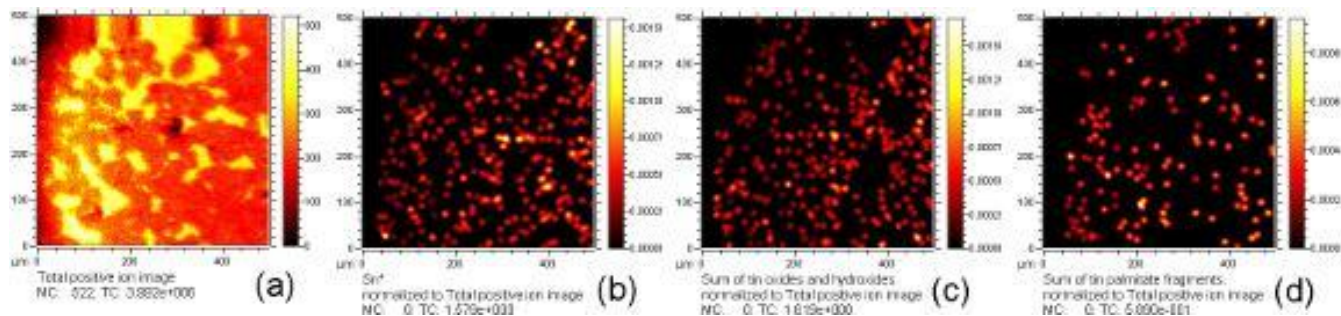


**Figure 2.7.** ToF-SIMS positive ion maps of sample 2.2. Total positive ion (a),  $\text{Sn}^+$  signal (b), tin oxides cluster (c) and tin palmitate (d) were normalized to the total ion image and filtered to avoid topographical effects.

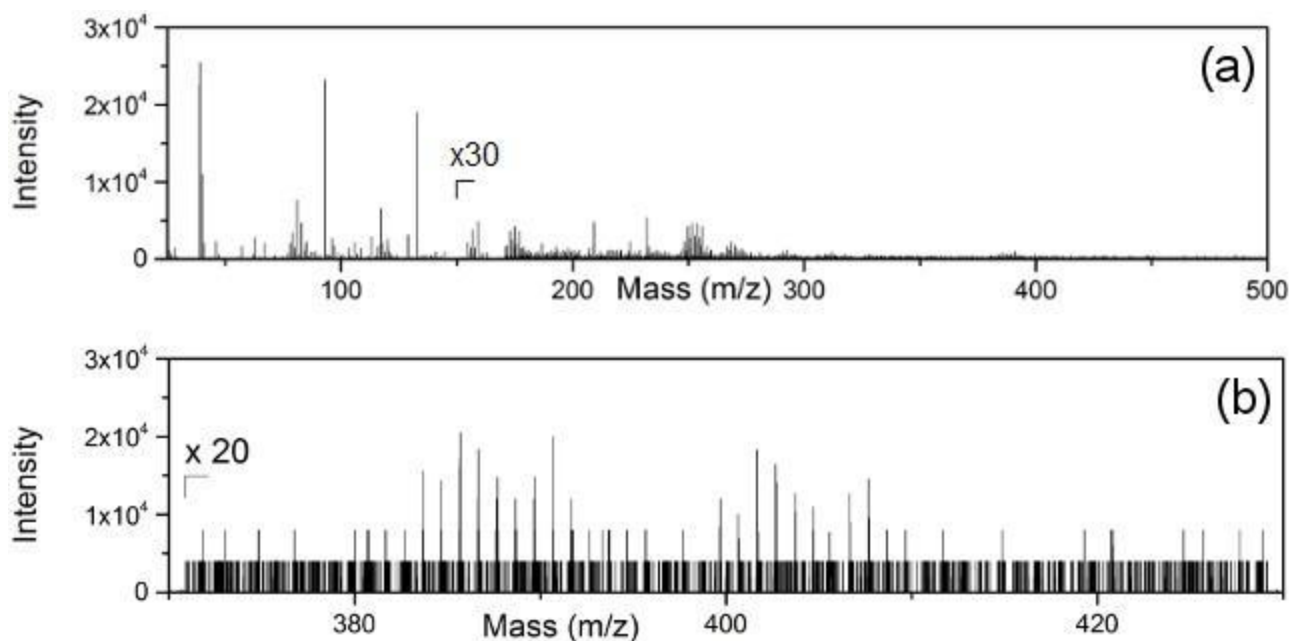


**Figure 2.8.** Positive mass spectra of sample 1.3. The window region shows the cluster belonging to tin stearate (b).

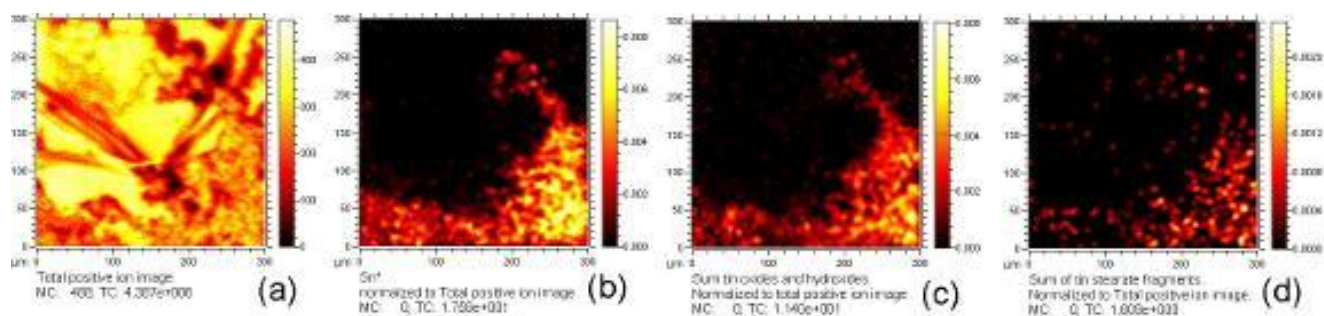


**Figure 2.9.** ToF-SIMS positive ion maps of sample 2.2. Total positive ion (a),  $\text{Sn}^+$  signal (b), tin oxides cluster (c) and tin stearate (d) were normalized to the total ion image and filtered to avoid topographical effects.

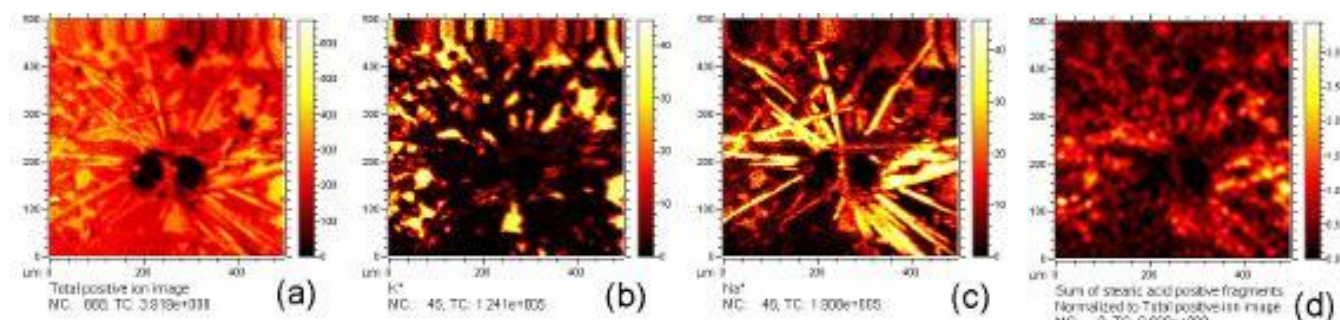


**Figure 2.10.** ToF-SIMS positive ion maps of a tin foil sample. Total positive ion image (a), map of  $\text{K}^+$  (b), map of  $\text{Na}^+$  (c) and sum of fatty acid positive ion fragments (d). All the images were normalized to total ion image and filtered to avoid topographical effects.

ToF-SIMS analyzes were limited to investigate the samples where metal powders were dispersed in fatty acids. The preliminary superficial operation cleaning with scan of bismuth, made necessary to remove from the sample the possible interferers derived from the aging chamber, was not sufficient to decontaminate the samples of tin foils and fatty acids. In all of these samples were recorded contaminating substances. In some cases, the positive ion secondary image showed the crystallization of fatty acids with sodium and potassium salts on the surface of the sample, which hindered the investigation of the underlying area (Fig. 2.10).

Since the ToF-SIMS technique is, by definition, a surface analysis technique that is limited to the first monolayer investigation, it is evident that the presence of these deposited products, hampers the study of the fragmentations of metallic carboxylates.

Nevertheless, tin soaps were previously recognized on 4N samples by FTIR measurements using ATR tip. The tip, exerts a pressure on the sample and collects the signal even from the layers below the superficial acid film. It is plausible to assume that these metal degradation products have formed at the interface between the metal foil and the fatty acids, and cannot be detected by the ToF-SIMS technique, as they are prepared. The investigation of these samples requires the study of a separation method at the interface which allows to analyze also the morphology of metal foil alteration. Indeed, the preventive operation of surface cleaning with continuous  $\text{Bi}^{++}$  beam did not decontaminate these samples. It was chosen to not continue with the ablation of the surface in order to preserve the extractor and the cleaning of the main chamber in the instrumentation.

Forward, longer aging times are needed for all those samples that have not undergone saponification reaction since the temperature and humidity conditions had already been brought to the limit. Moreover, a specific consideration could be made to justify non-reaction in samples with abietic acid. Since the acidic dissociation constant of the abietic acid is lower than that of the

aliphatic acids, it can be assumed that its lower acidity may have influenced the occurrence of the reaction. In addition, its hydrophobicity feature may prevent the reaction of hydrolysis and the dissociation of OH<sup>-</sup> and H<sup>+</sup> [120].

In Tab. 2.5 are summarized the sample in which saponification reaction were recorded.

| SAMPLES                | Azelaic acid | Palmitic acid | Stearic acid | Abietic acid | Glyceril tristearate | Liseed oil | Colophony) |
|------------------------|--------------|---------------|--------------|--------------|----------------------|------------|------------|
| <b>Sn powder</b>       | 1.1          | 1.2           | 1.3          | 1.4          | 1.5                  | 1.6        | 1.7        |
| <b>SnO</b>             | 2.1          | 2.2           | 2.3          | 2.4          | 2.5                  | 2.6        | 2.7        |
| <b>SnO<sub>2</sub></b> | 3.1          | 3.2           | 3.3          | 3.4          | 3.5                  | 3.6        | 3.7        |
| <b>Sn foil</b>         | 4.1          | 4.2           | 4.3          | 4.4          | 4.5                  | 4.6        | 4.7        |
| <b>Sn s.</b>           | 4.1N         | 4.2N          | 4.3N         | 4.5N         | 4.5N                 | 4.6N       | 4.7N       |
| <b>Sn HCl</b>          | 4.1HCl       | 4.2HCl        | 4.3HCl       | 4.4HCl       | 4.5HCl               | 4.6HCl     | 4.7HCl     |

**Table 2.5.** Samples marked in black are the samples in which the saponification reaction were recorded. The sample marked in red need more time than 90 days of aging chamber, to activate the reaction process.

## 2.1.4 Conclusion

In conclusion, the results showed that the fragmentation of tin azelate, palmitate and stearate has been identified with difficulty. In spite of precautionary operation cleaning of the samples surfaces, they were still highly contaminated and the holding signal was affected by the matrix effect of fatty acids that contained tin nanoparticles. However, although the signals recognized as metallic carboxylates were very weak, they were selected and mapped into the secondary ion image. The fragmentation sum of tin soaps is associated with the tin ion and tin oxides clusters for all the samples analyzed, confirming the hypothesis of saponification products as suggested by the FTIR preliminary results.

The study here presented has confirmed the actual formation of tin degradation products in decorative systems model where the tin foil is associated to an oil-resin adhesive medium. The finding obtained with this experiment potentially allows the investigation of real case studies in which a *composite lamina* is present.

## 2.2 Oleanolic and ursolic acid in dammar and mastic resin: isomer discrimination by using ToF-SIMS and multivariate statistics.

### 2.2.1 Introduction

Dammar and mastic are triterpenoid resins widely used in the past during the production of art works. Plant resins such as dammar and mastic are exudates usually present on the surface of different kinds of trees. From a chemical point of view, natural resins are mostly constituted by low volatile and non-volatile terpenoid compounds. In particular, both dammar and mastic are composed of triterpenoid molecules and a variable fraction of polymeric material.

These organic constituents confer to the natural resins aesthetic and protective functions when these are adopted in works of art. For this reason, they are extensively used in paintings and artwork as coatings, waterproofing materials, varnishes and paint binders by both artists and restorers. As aforementioned, varnishes not only have an important aesthetic function but also represent a barrier against deteriorating agents of the environment. This physical barrier deteriorates in the course of time, leading to yellowing and brittleness. Thus, it is important to understand the chemical processes occurring during ageing of natural resins [1]. In the cultural heritage field, the study of ageing process effects on organic content can reveal information about the adopted painting technique or suggest a restoration approach. From, diagnostic point of view addition the analysis of resins remains a big challenge because of their intrinsic complexity due to the enormous number of isomers present in the terpenoid class. Furthermore, the processes of oxidation and polymerization during the ageing contribute to increase the complexity of characterization.

Recently, time-of-flight secondary ion mass spectrometry (ToF-SIMS) technique has been included among the analytical techniques applied to the cultural heritage studies. The data obtained from ToF-SIMS are complex and intrinsically multivariate; therefore, to aid spectral assignment, multivariate analysis (MVA) methods are increasingly being used, especially for organic and biological samples [68]. Principal component analysis (PCA) is the most widely applied method to reduce the size of ToF-SIMS large datasets with a minimal loss of information. This is accomplished by analysing the variance of each mass channel across the dataset, where the combination of mass channels containing the most variance is defined as the first principal component (PC1). Therefore, a set of peak loadings and sample scores are calculated for each PC. Sample scores show how individual mass spectrum is correlated with other mass spectra in the dataset. On the other hand, peak loadings indicate the main peaks responsible for the sample differences. With regard to the study of resins, this approach has been recently adopted to differentiate diterpene resin acids and assess the geochemistry of amber [121]. In this work, the high reproducibility and selectivity of ToF-SIMS technique have been exploited to study two of the main components of the dammar resin: oleanolic acid and ursolic acid. Oleanolic and ursolic acid share the same molecular formula and consequently the same fragment ions in the mass spectra, but each isomer shows its characteristic relative abundance of fragment ions. The isomer discrimination is an interesting challenge for mass spectrometry techniques. However, they can be well distinguished by gas chromatography techniques coupled with electron impact mass spectrometry detection systems [122-124]. Although this powerful method provides detailed structural information, a derivatization procedure for such compounds is often required. Through high mass-resolution ToF-SIMS, we have investigated structural isomers without modifying their functionality. Furthermore, PCA has been used to reveal the differences between each spectrum

and correlate them back to the differences in the fragmentation pattern of the isomers spectra. Early work is present in literature where PCA has been successfully applied to ToF-SIMS data in order to distinguish between stereo isomers and structural isomers of biologically relevant monosaccharides [125]. ToF-SIMS has also been used to characterize dammar and mastic. As described previously, both resins contain several different triterpenoid acids and a fraction of polymeric material. In particular, dammar resin contains both structural isomers; on the other hand, mastic resin contains just oleanolic acid. The list of characteristic peaks obtained from ToF-SIMS analysis of oleanolic and ursolic acids has been used for PCA in order to differentiate the dammar spectrum from the mastic spectrum.

## 2.2.2 Materials and methods

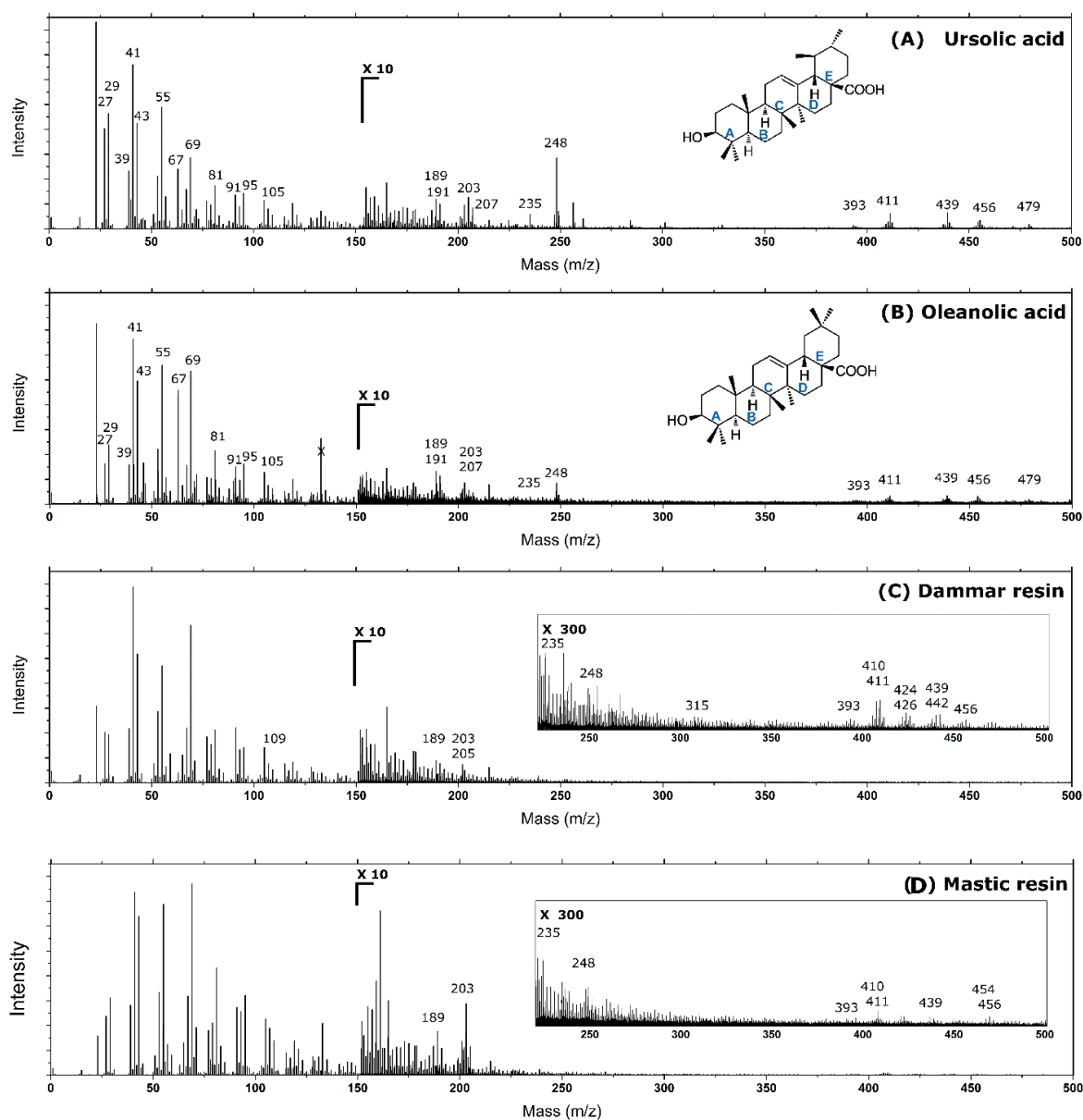
Oleanolic and ursolic acids were purchased from Extrasynthèse, Genay, France (>95% purity). Mastic resin was purchased from Sigma-Aldrich (>97% purity). Dammar resin was purchased from Ditta Zecchi, Florence, Italy. The dammar and mastic resins analysed in this work were stored in darkness at room condition and have an age of over 10 years. Samples were diluted in CH<sub>2</sub>Cl<sub>2</sub> to a concentration of ≈1mg/ml. Aliquots of solution were deposited on silicon wafer by spin coating technique. The wafer was attached to a spin coater (Spin-1200 T, MIDAS Co. Ltd, Daejeon, Korea) rotating at 1000 rpm. Aliquots were allowed to spin for 30 s. The samples were analysed using a TOF-SIMS5 instrument (ION-TOF GmbH, Munster, Germany) equipped with a 30 keV bismuth (Bi<sub>3</sub><sup>++</sup>) liquid metal cluster primary ion source in high mass resolution bunched mode. The ion beam was rastered over an area of 500 × 500 μm<sup>2</sup> for 120 s in order to remain below the static limits. Charge neutralization was obtained by using low energy (20 eV) electrons supplied by the instrument's pulsed electron flood gun. Secondary ions were extracted with 2 keV voltages and were post-accelerated to 10 keV kinetic energy. Cycling time of instrument was set to 300 μs, allowing the acquisition of spectra in a mass range from 1 to 1200 m/z. The dimensionality of raw ToF-SIMS data was reduced by PCA performed using MATLAB v.R2013a (MathWorks, Inc., Natick, MA, USA). PCA was used to identify similarities and differences in ToF-SIMS spectra. The peaks in each spectrum were normalized to the sum of the selected areas. The data were mean-centered before PCA.

## 2.2.3 Results and discussion

In Fig. 2.11, positive ToF-SIMS spectra (m/z 1 – 500) of ursolic (Fig. 2.11A) and oleanolic acid (Fig. 2.11B) are shown. Representative mass spectra in positive ion mode of dammar resin (Fig. 2.11C) and mastic resin (Fig. 2.11D) are reported; an expanded view (m/z 225–500) is shown in Fig. 2.11C inset and Fig. 2.11D inset. Each mass spectrum displayed in Fig. 2.11 is obtained from an average of nine representative mass spectra of both triterpenic acids and resins that are spotted on three different silicon substrates. Averages of mass spectra are needed to avoid topography effects due to the formation of a solid reticulated film with a slightly irregular surface. Ursolic and oleanolic acid possess highly similar mass spectra. In the positive ion mass spectra (Figs. 2.14A and B), the intense peaks in the lower part of the mass range (m/z<100) are due to aliphatic hydrocarbon fragments (C<sub>n</sub>H<sub>n</sub>, C<sub>n</sub>H<sub>2n+1</sub>, C<sub>n</sub>H<sub>2n+2</sub>, C<sub>n</sub>H<sub>2n-1</sub>, C<sub>n</sub>H<sub>2n-2</sub>). Both spectra contain a series of fragment ions that are descriptive of the hydroxyl and carboxyl end groups (C<sub>n</sub>H<sub>2n</sub>O, C<sub>n</sub>H<sub>2n+1</sub>O, C<sub>n</sub>H<sub>2n-1</sub>O). In the higher part of the mass range, there are clusters of peaks from 800 to

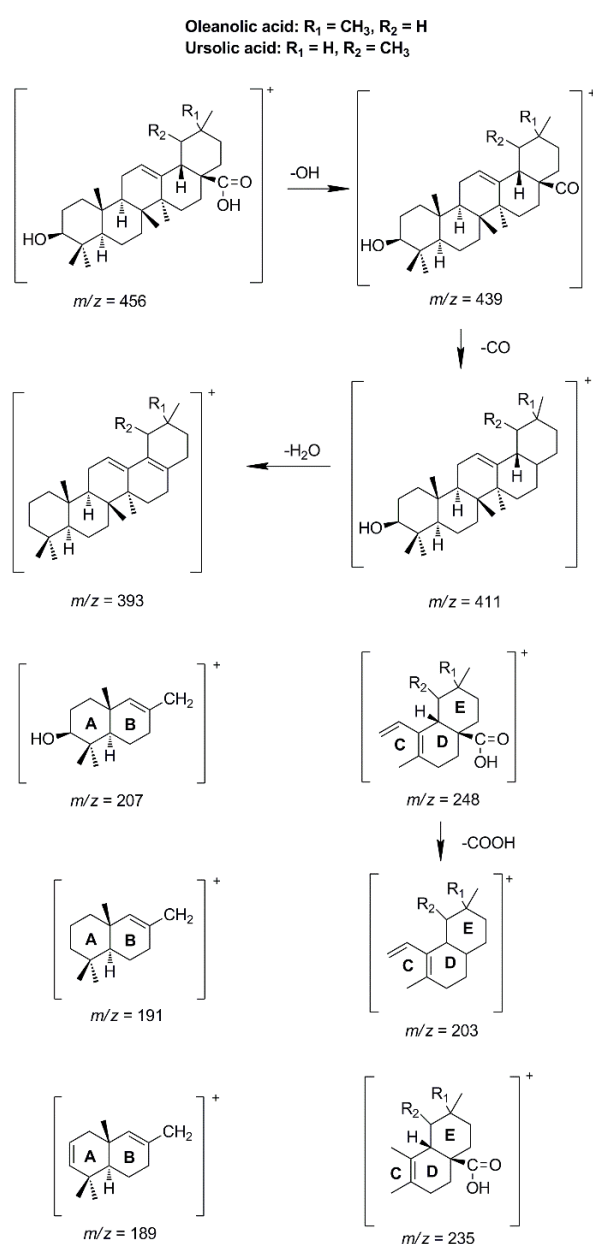
1050 m/z, and in the most relevant cluster (m/z 911.68–915.68), the peaks could belong to triterpenoid dimers (Figs. A1–A2 in Appendix). The molecular ion peak at m/z 456.34 ( $C_{30}H_{48}O_3^+$ ) with a mass resolution of 9500m/ $\Delta m$  is clearly visible. The presence in both triterpenic acid mass spectra of an intense sodium peak at m/z 22.98 and the corresponding  $[M+Na]^+$  peak at m/z 479.36 is appreciable.

Figure 2.12 illustrates the main fragment ions of oleanolic and ursolic acid obtained under bombardment with positive primary ions during ToF-SIMS experiments. The fragmentation pathways of position isomers, such as oleanolic acid and ursolic acid, have been well described by GC-MS methods [122-123]. In this case, characteristic fragment ions obtained from high-mass-resolution-ToF-SIMS mass spectra have been assigned, taking into account the mass spectral fragmentation pattern of the corresponding trimethylsilylated triterpenic acids obtained under electron impact conditions. The main fragment ion signals are present at m/z 456.34 (molecular ion), 439.34, 411.35, 393.35, 248.17, 235.16, 207.16, 203.17, 191.18, 189.16 (Figs. A1–A2 in Appendix).



**Figure 2.11.** Positive time-of-flight secondary ion mass spectrometry spectra (m/z 1-500) of ursolic acid (A) oleanolic acid (B) dammar (C) and mastic resins (D).

The proposed scheme for the fragmentation pathway, presented in Fig. 2.12, shows that the peak at  $m/z$  439.34 ( $C_{30}H_{47}O_2^+$ ) could be due to a hydroxyl group loss. Subsequently, a neutral CO can be also lost producing an ion at  $m/z$  411.35 ( $C_{29}H_{47}O^+$ ) of about the same intensity of  $[M - OH]^+$ . Fig. 2 also shows an additional fragmentation by loss of water from the alcohol functional group. This loss results in the fragment ion at  $m/z$  393. Upon electron impact, these triterpenic acids usually undergo a retro-Diels Alder reaction [122]. In this important mode of fragmentation, a cleavage of the C ring occurs, and this leads to species ranging from 200 to 300  $m/z$ . These species consist of ABC-rings and CDE-rings where C-ring is partial. In the positive ToF-SIMS spectra, fragment ions at  $m/z$  248.17 ( $C_{16}H_{24}O_2^+$ ), 235.16 ( $C_{15}H_{23}O_2^+$ ), 207.16 ( $C_{14}H_{23}O^+$ ), 203.17 ( $C_{15}H_{23}^+$ ), 191.18 ( $C_{14}H_{23}^+$ ), 189.16 ( $C_{14}H_{21}^+$ ) are assigned to fragments containing A, B rings or D, E rings with partial C ring. However, GC-MS analyses support these proposed fragmentations [123]. Figs. 2.11C and D shows the positive ToF-SIMS spectra of dammar and mastic resin, respectively.



**Figure 2.12.** Fragmentation pathway of ursolic acid and oleanolic acid leading to the characteristic fragment ions during time-of-flight secondary ionmass spectrometry experiments

The presence in both resins of elevated concentrations of sodium results in adducts formation of sodiated molecular ions from organic components of resin. In Figs. 2.11C and Fig. A3 (Appendix), positive ion mass spectrum of dammar resin is visible. According to the literature, the molecular ion peak at  $m/z$  456.34 ( $C_{30}H_{48}O_3^+$ ), representing oleanolic and ursolic acid, has been found in the positive ion mass spectrum of dammar resin [1]. Furthermore, the peak at  $m/z$  442.37 ( $C_{30}H_{50}O_2^+$ ) could be attributed to the molecular ion of hydroxydammarone and the peaks at  $m/z$  424.37 ( $C_{30}H_{48}O^+$ ),  $m/z$  315.27 ( $C_{22}H_{35}O^+$ ),  $m/z$  205.16 ( $C_{14}H_{21}O^+$ ), and  $m/z$  109.10 ( $C_8H_{13}^+$ ) could arise from its fragmentation.[19,20] The spectrum shows peaks at  $m/z$  426.37 ( $C_{30}H_{50}O^+$ ) and  $m/z$  424.37 ( $C_{30}H_{48}O^+$ ) attributable to dammaradienol and dammaradienone, respectively [129-132]. Another fragment of dammarane-type molecules, likely belonging to noramyrene, is observed at  $m/z$  410.36 ( $C_{29}H_{46}O^+$ ). In Figs. 2.11D and Fig. A4 (Appendix), the positive ion mass spectrum of mastic resin is reported. Low-intensity peaks of triterpenoid molecular ions have been detected in the mass range between  $m/z$  400 and 500 during ToF-SIMS measurements.

Unlike the attribution in the dammar resin, in this case, the peak at  $m/z$  456.34 ( $C_{30}H_{48}O_3^+$ ) can represent oleanolic acid, masticadienolic acid and isomasticadienolic acid. Furthermore, peaks of moronic acid at  $m/z$  454.34 ( $C_{30}H_{46}O_3^+$ ) and noramyrene  $m/z$  410.36 ( $C_{29}H_{46}O^+$ ) are also appreciable [25]. All ions assigned to dammar and mastic resins are shown in Tables A2 and S2 (Supporting Information). Ions arising from the fragmentation of oleanane-type molecules at  $m/z$  439.34, 411.35, 393.35, 248.17, 235.16, 203.17 and 189.16 are present in mass spectra of both dammar and mastic resins, and their structure are shown in Fig. 2.12 and Tables A2 and A3 (Appendix)[126-128].

Other fragment ions are revealed at low masses ( $m/z < 100$ ). Both dammar and mastic consist of dammarane and oleanane compounds. As reported in literature, the comparison of relative intensities of mass peaks attributed to dammarane and oleanane compounds permits to distinguish fresh dammar from mastic by using GC-MS and direct temperature-resolved mass spectrometry (DTMS) [133]. Several marker compounds have been proposed to discriminate dammar from mastic such as moronic acid [132] and (iso)masticadienoic acid [134]. Some components of the dammar are the same as those components found in mastic such as oleanolic acid. On the contrary, ursolic acid is present exclusively in the dammar resin, thus emerging as a potential marker. The great similarity between the mass spectra of oleanolic and ursolic acid makes the differentiation of these isomeric triterpenic acids quite difficult. In fact, the problem is that because the structural isomers have the same molecular formula, they produce the same dataset of ToF SIMS peaks. Nevertheless, statistical analysis such as PCA appears to be able to summarize the differences in the ursolic and oleanolic acid datasets (Fig. 2.13A) and to report the peaks responsible for these differences (Fig. 2.13B).

In order to guarantee the reproducibility during the statistical analysis, PCA of ursolic and oleanolic acid is performed using just a selection of 61 peaks (Table S3 in Supporting Information). This is required because the data analysis can be dominated by the presence of sodium ( $m/z$  23), potassium ( $m/z$  39) and substrate peaks that have largest values, obscuring the differences in the triterpenic acid isomer peaks. In this case, PCA processing is achieved by an appropriate selection of ions within the lower mass aliphatic hydrocarbon fragments and oxygen-containing related species. Characteristic fragment ions generated by the fragmentation process are also included. Figures 2.13A and B shows the scores and loadings plot from the two structural isomers.

The PCA scores, shown in Fig. 2.13A, display the clustering of ursolic and oleanolic samples and the separation of mass spectra from the two different isomers. The PC1 loadings plot (Fig. 2.13B) shows that peaks with positive loading, corresponding with samples with positive scores in the first principal component (Fig. 2.13A), are due to the greater relative abundance of fragment ions at  $m/$

z 41 and 55 in oleanolic acid. The peaks at  $m/z$  41 and 55 correspond to  $C_3H_5^+$  and  $C_4H_7^+$  fragment ions, respectively.

On the contrary, the peaks with negative loadings correspond to the samples of ursolic acid with negative scores in PC1. The discrimination of ursolic acid is due to the greater relative abundance of peaks at  $m/z$  81 and 91, corresponding to  $C_6H_9^+$  and  $C_7H_7^+$  fragment ions, respectively. Oleanolic acid and ursolic acid are position isomers of the methyl group on the ring E. In particular, oleanolic acid has two methyl groups on the C-20 position, whereas ursolic acid has a methyl group on C-19 and C-20 positions. In this case, the abundance of relatively low molecular weight fragments such as  $C_3H_5^+$ ,  $C_4H_7^+$ ,  $C_6H_9^+$ , and  $C_7H_7^+$  are probably due to the ring E cleavage. The correctness of these assignments cannot be given in this preliminary work, and further investigations are needed. The same peak list has also been applied to dammar and mastic mass spectra. PCA is shown in Figs. 2.13C and D. The PC1 and PC2 capture 69% and 18% amount of information, respectively. For this dataset, we selected the second principal component because this allowed a better sample separation compared with PC1 (data not shown). In fact, as it is shown by loadings plot of PC2 (Fig. 2.13D), the peaks at  $m/z$  41 and  $m/z$  55 are related to oleanolic and mastic samples (Fig. 2.13C).

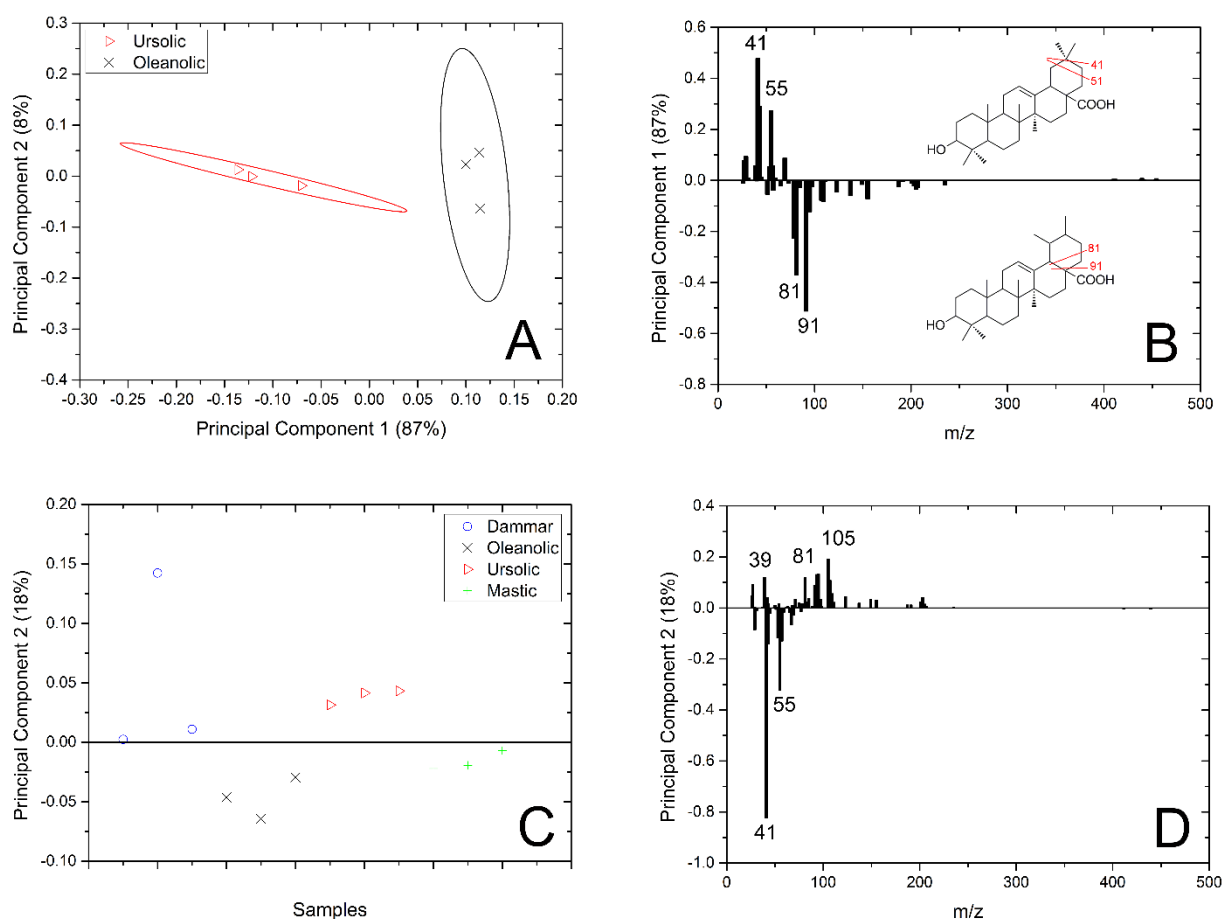


**Figure 2.13.** Results of principal component analysis model obtained from positive time-of-flight secondary ion mass spectrometry ion spectra. Score plot (A) of principal component 1 (PC1) and PC2 grouping the samples as a function of their chemical differences. Ellipses are 95% confidence intervals. PC1 loadings plot (B) shows masses responsible for the separation of ursolic and oleanolic acids. Scores plot (C) of PC2 highlights similarities and differences among the samples. PC2 loadings plot (D) shows peaks responsible for the separation of acids and resins.

On the other hand, positive loadings at  $m/z$  81 ( $C_8H_9^+$ ) and 105 ( $C_8H_9^+$ ) are associated with dammar and ursolic acid (Figs. 2.13C and D). The variance among the data of dammar samples is probably due to the surface roughness originated by the polymerization cross-linking process of resin deposited onto the silicon wafer. A not excellent separation among the scores can be related to the presence of fragmentation peaks coming from other triterpenic acids and polymeric material.

## 2.2.4 Conclusions

Within this paper oleanolic acid, ursolic acid, dammar resin and mastic resin are characterized by using high- mass resolution ToF-SIMS. In particular, a fragmentation mechanism for ursolic and oleanolic acid under ion bombardment conditions has been proposed. Furthermore, ToF-SIMS and PCA have permitted to discriminate between these underivatized structural isomers of triterpenic acids. Multivariate statistical analysis has also been adopted to identify ursolic and oleanolic acid in mastic and dammar. These preliminary results confirm the potentialities of combining ToF-SIMS and multivariate statistical analysis as a powerful tool to study triterpenic resin such as dammar and mastic, frequently used in the field of conservation and restoration of art.

## 2.3 ToF-SIMS study of pentacyclic triterpenic molecules in birch bark pitch

### 2.3.1 Introduction

The use of pitch from Betulaceae bark as an adhesive on arrowheads or flint tools from prehistoric ages has been highlighted [135-139]. In particular, a gas chromatography/mass spectrometry (GC/MS) chemical study of two amorphous pieces recovered at Konigsau (Germany) associated with flint artefacts 38 revealed that birch bark pitch was already being produced in the Middle-Palaeolithic period. The detection of birch bark pitch has also been reported in ceramic artefacts and its function has been identified as an adhesive in order to seal, repair or to coat the inner surfaces of vessels [10-11,135,140-142]. Betulin and lupeol together with low amounts of lupenone, betulone and betulinic acid are known to be characteristic of birch bark [143-147]. The technique that has been used to obtain the majority of results in the identification of terpenic resinous materials in archaeological samples is GC/MS. This technique has been extremely useful for characterising archaeological resinous substances, by the identification of specific molecular markers [148-152]. However, it often requires time-consuming sample pre-treatment, which can entail extraction, purification, hydrolysis and derivatisation reactions before the sample is analyzed. For these reasons, attention has recently focused on other techniques based on direct mass spectrometry that can reduce sample manipulation. In particular, ToF-SIMS technique has been applied in the characterisation of dammar resin, mastic resin and triterpenoid standard in paint varnishes [153].

This work discusses the application of ToF-SIMS technique for the characterisation of triterpenic molecules and birch bark pitch, and their identification in archaeological finding. To discrimination of these materials, pattern analysis of ToF-SIMS mass spectral data was performed by principal component analysis (PCA). For this purpose, a systematic study of standard triterpenic molecules contained in birch bark pitch and of raw tar of a known origin was carried out by ToF-SIMS in order to define the most significant fragment ions for the identification of the resinous material in real case. Finally, the analytical protocol was applied to an archaeological sample (Fig. 2.14) collected during an archaeological excavation in the palafittic site of Lucone di Polpenazze (Brescia, Italy).



**Figure 2.14.** The object of the study: the wooden sickle found during the dig of archaeological area of Lucone di Polpenazze

### 2.3.2 Materials and methods

Betulin (lup-20(29)-en-3b,28-diol, purity >98%), and betulinic acid (3-hydroxy-lup-20(29)-en-28-oic acid, purity >90%) were supplied by Sigma (St. Louis, MO, USA). Oleanolic acid (3-hydroxy-olean-12-en-28-oic acid), lupeol (lup-20(29)-en-3b-ol) and lupenone (lup-20(29)-en-3-one) were supplied by Extrasynthese (Genay, France), all with a purity >99%. Furthermore a pitch derived from wood of *Betula* spp. was kindly provided by Prof. B. Holmbom (Åbo Akademi University, Turku/Åbo, Finland). The archaeological sample was collected from a wooden sickle, found during the archeological dig on Garda Lake (Brescia, Italy). The sickle, with flint blade and a “mandible” type structure was dated to the Early Bronze age. The analyzed sample collected from the finding is constituted by a little black lump of amorphous organic material (1-3mg) present between the wooden handle and the flint tip. All the Samples were diluted in few microliter of dichloromethane and deposited on silicon wafer by spin coating. The mass fragmentation study of the samples were performed by using a TOF-SIMS5 instrument (ION-TOF GmbH, Munster, Germany) equipped with a 30 keV bismuth ( $\text{Bi}^{3++}$ ) liquid metal cluster primary ion source in high mass resolution bunched mode. The ion beam was rastered over an area of  $100 \times 100 \mu\text{m}^2$  for 120 s in order to remain below the static limits. Charge neutralization was obtained by using low energy (20 eV) electrons supplied by the instrument's pulsed electron flood gun. Secondary ions were extracted with 2 keV voltages and were post-accelerated to 10 keV kinetic energy. Cycling time of instrument was set to 120  $\mu\text{s}$ , allowing the acquisition of spectra in a mass range from  $m/z$  1 to 800. Ten measurement for each sample were collected. The dimensionality of raw ToF-SIMS data was reduced by PCA performed using MATLAB v.R2013a (MathWorks, Inc., Natick, MA, USA). PCA was used to identify similarities and differences in ToF-SIMS spectra. Furthermore the data analysis was used to discriminate the contribution of each markers in the birch bark tar reference and in the samples representing the real cases. The peaks in each spectrum were normalized to the sum of the selected areas. The data were mean-centered before PCA.

### 2.3.3 Result and discussion

Due to the complexity of triterpenic resinous materials and of the mass spectra arising from ToF-SIMS analysis, the results of the standard triterpenes are reported and discussed first. The results of the birch bark reference are reported next, followed by that for the sample collected from the archaeological object. ToF-SIMS positive ion mass spectra of oleanolic acid (MW 456), betulinic acid (MW 456), betulin (MW 442), lupeol (MW 426), and lupenone (MW 424) are shown in Fig. 2.15. Oleanolic acid (3-hydroxyolean-12-en-28-oic acid) was considered as representative of triterpenes with oleanane structures. In the mass spectrum of Oleanolic acid, the abundant ions at  $m/z$  189, 203 and 218 can be related to the typical fragmentation pathway of both oleanane- and ursane-type molecules with a double bond in position 12 [122]. In particular, the ion at  $m/z$  218 is due to a classical retro-Diels-Alder fission of ring C and ions at  $m/z$  189 and 203 arise from fragmentation rearrangements of the radical ion at  $m/z$  218 [122, 154-155]. The mass spectrum of oleanolic acid, which has a carboxylic acid group in position 17 of ring E, has a molecular ion at  $m/z$  456 and it is characterised by the presence of a fragment ion at  $m/z$  248 due to a retro-Diels-Alder fragmentation of the ring C53 analogous to that reported for the formation of the ion at  $m/z$  218. Fragment ions at  $m/z$  438 and 410 are also evident due to the loss from the molecular ion of  $\text{H}_2\text{O}$ ,  $\text{CO}_2\text{H}$  radical, and  $\text{HCO}_2\text{H}$  from ring E, respectively. The loss of a methyl radical and of  $\text{H}_2\text{O}$  leads to the formation of  $m/z$  423. Betulin, lupeol, betulinic acid and lupenone were considered as

representative of triterpenes with a lupane structure, their ToF-SIMS mass spectra are all shown in Fig.2.15.

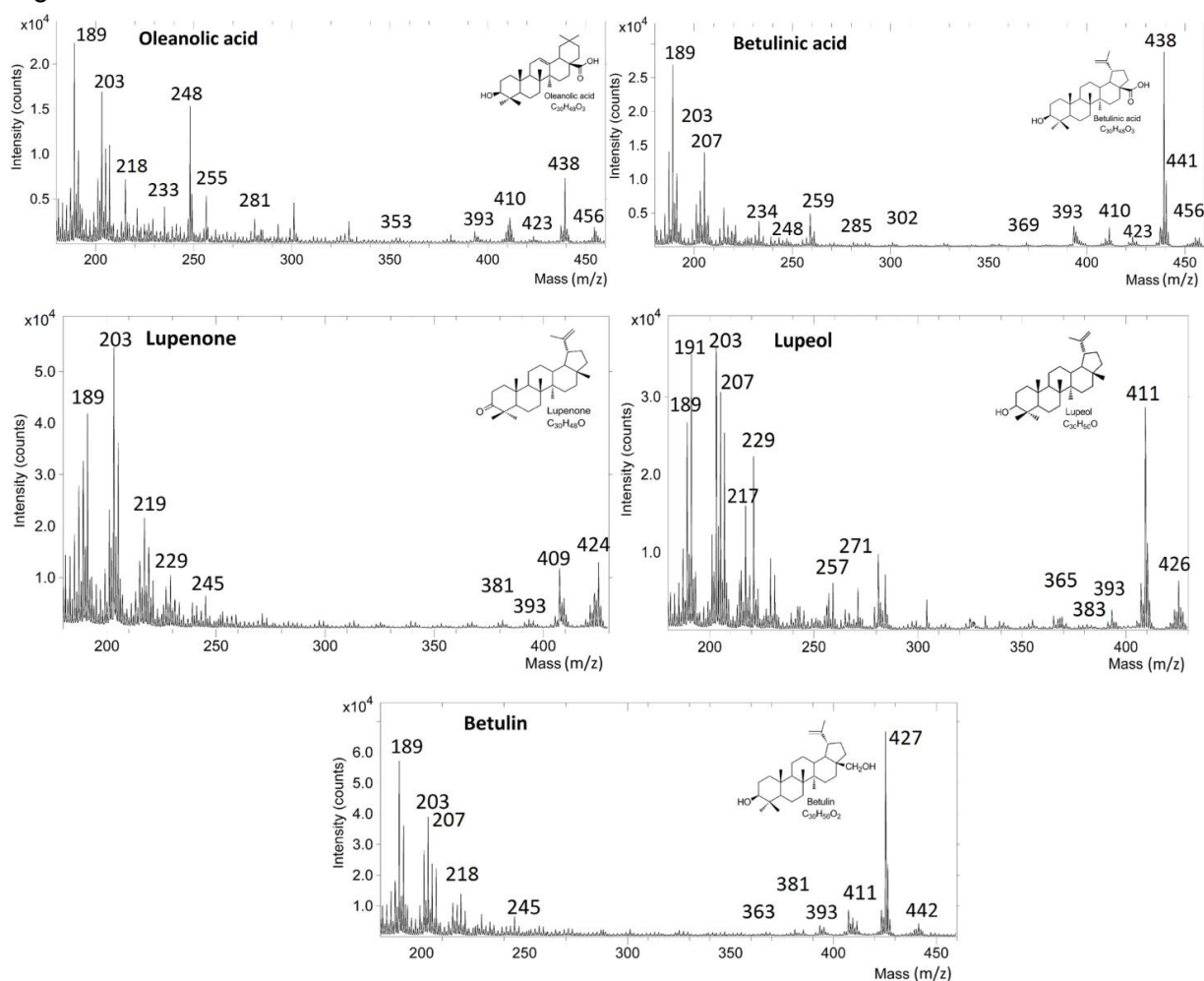


**Figure 2.15.** ToF-SIMS positive mass spectra of oleanolic acid, betulinic acid, lupenone, lupeol, and betulin.

The mass spectra of betulin, lupeol and betulinic acid exhibit a base peak at m/z 189, which is considered characteristic for the fragmentation of triterpenoid molecules with a lupane skeleton bearing a hydroxy group in position 3. This ion arises from the fragmentation of the C ring system by cleavage of the 9–11 and 8–14 bonds followed by the loss of a molecule of  $H_2O$  [122,156]. Other abundant fragment ions are at m/z 203 and 207: the first can be related to the retention of an additional methylene group from the C ring with respect to the fragment ion at m/z 189, and the second represents the fragment obtained from the fragmentation of the C ring before the dehydration reaction leads to the formation of the ion at m/z 189 [122, 156]. In the mass spectrum of betulin, the molecular ion is present at m/z 442. Loss of a water molecule, a  $CH_2OH$  radical and of both leads to the formation of the ions at m/z 424, 411 and 393, respectively. The loss of water and of a methyl radical gives rise to the ion at m/z 409. In the mass spectrum of lupeol, the molecular ion is at m/z 426, and the ions at m/z 411 and 393 are formed by the loss of a methyl group, and by the subsequent loss of a water molecule. The mass spectrum of betulinic acid, in which the molecular ion is at m/z 456, has fragment ions at m/z 441, 438 and 423 formed by the loss of a methyl radical, a molecule of  $H_2O$  and of both. The loss of  $HCO_2H$  gives rise to the ion at m/z 410, while the loss of the  $CO_2H$  radical leads to the ion at m/z 411. Finally, in the mass spectrum of lupenone, the base peak occurs at m/z 205, followed in abundance by the ion at m/z

189. The pathway that leads to formation of the ion at  $m/z$  205 is analogous to that reported for lupine-type molecules with a hydroxyl group in position 3, except that lupenone has a keto group, rather than a hydroxy group, at position 3. The molecular ion at  $m/z$  424 and that at  $m/z$  409 formed by loss of a methyl radical are also present in quite high abundance [140]. All the molecular fragments structures of these triterpenes are reported in figures shown in Appendix (A5-A9).

The ToF-SIMS positive mass spectrum of the birch bark pitch reference is shown in Fig. 2.16a. It is qualitatively comparable with that reported in the literature [10]. It contains abundant ions at  $m/z$  189 and 203, arising from the fragmentation of triterpenoid molecules. The ion at  $m/z$  189 can be related to the presence of triterpenes with a lupane skeleton with a hydroxy group at position 3, as obtained for the reference standards: betulin, lupeol, betulinic acid and lupenone. By comparison with the spectra obtained for the standards, the fragment ions at  $m/z$  363, 381, 393, 409, 411, 424 and 442 can be directly related to the occurrence of betulin, lupeol and lupenone, which are typical constituents of birch bark pitch [11,135-136,141].

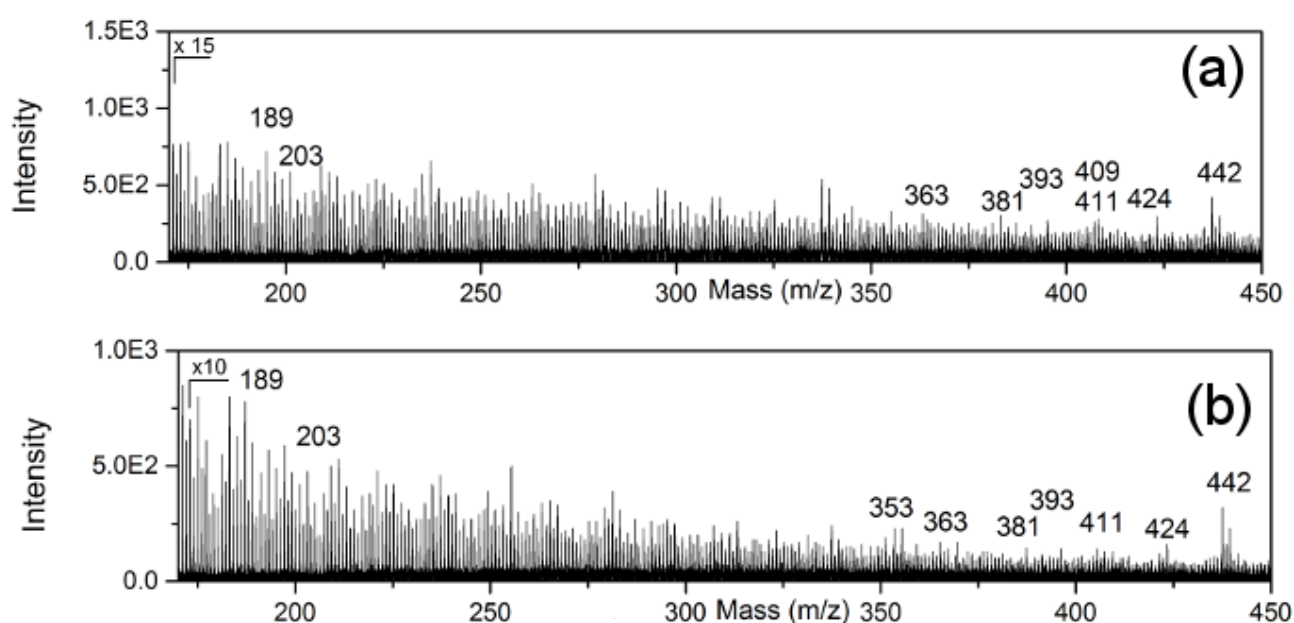


**Figure 2.16.** ToF-SIMS Positive mass spectra (range  $m/z$  170-450) of reference pitch derived from bark of a *Betula* spp. (a) and archaeological blackish sample collected from the sickle (b).

Betulin and lupeol together with small amounts of lupenone and betulone are known to be characteristic of birch bark [141, 143-147]. The other observed compounds are not present in birch bark, but most of them are known to be formed by dehydration mechanisms when the bark is thermally treated to obtain tar [135]. During the heating process, betulin is partially transformed into lup-2,20(29)-dien-28-ol whereas heating of lupeol leads to the formation of a triterpenoid hydrocarbon identified as lup-2,20(29)-diene. These two constituents are thus indicative of a human operated heating treatment. Depending on the duration and the intensity of the hard-heating treatment, the proportions of the different constituents change: the amount of lupenone and betulone, naturally present in fresh birch bark only in very small amounts, may increase during tar production by oxidation of lupeol and betulin, respectively [127]. The ToF-SIMS positive mass spectrum of the sample collected from archaeological sickle is shown in Fig. 2.16b.

The spectrum has abundant ions at  $m/z$  189 and 203 that are characteristic of the fragmentation of triterpenoid molecules and, in particular, the ion at  $m/z$  189 may be related to the occurrence of triterpenes with a lupane skeleton and a hydroxyl group at position 3. The presence of fragment ions at  $m/z$  363, 381, 393, 409, 411, 424 and 442 may be related to the occurrence of betulin and lupeol as the main constituents. This data could hypothesize the nature of the adhesive as birch bark tar. PCA analysis present in Fig. 2.17a shows that the reference pitch is highly correlated to betulin in both PC1 and PC2. Furthermore, the sample is also correlated to the betulinic and oleanolic acid, generally present in fresh tar. This may provide a relative indication of the freshness degree of the resin, inasmuch hydroxyl groups present in the acid molecules have not yet undergone oxidation reactions [127]. Finally, the PCA analysis confirms the nature of the archaeological pitch as birch bark tar (Fig. 2.17b). The biplot in Fig. 2.17b shows the very good fit between the reference birch bark pitch and the archaeological sample, highlighting the occurrence of a pure material. Finally, the pitch samples are very correlated to betulin, the most abundant marker present in this materials according to the literature.

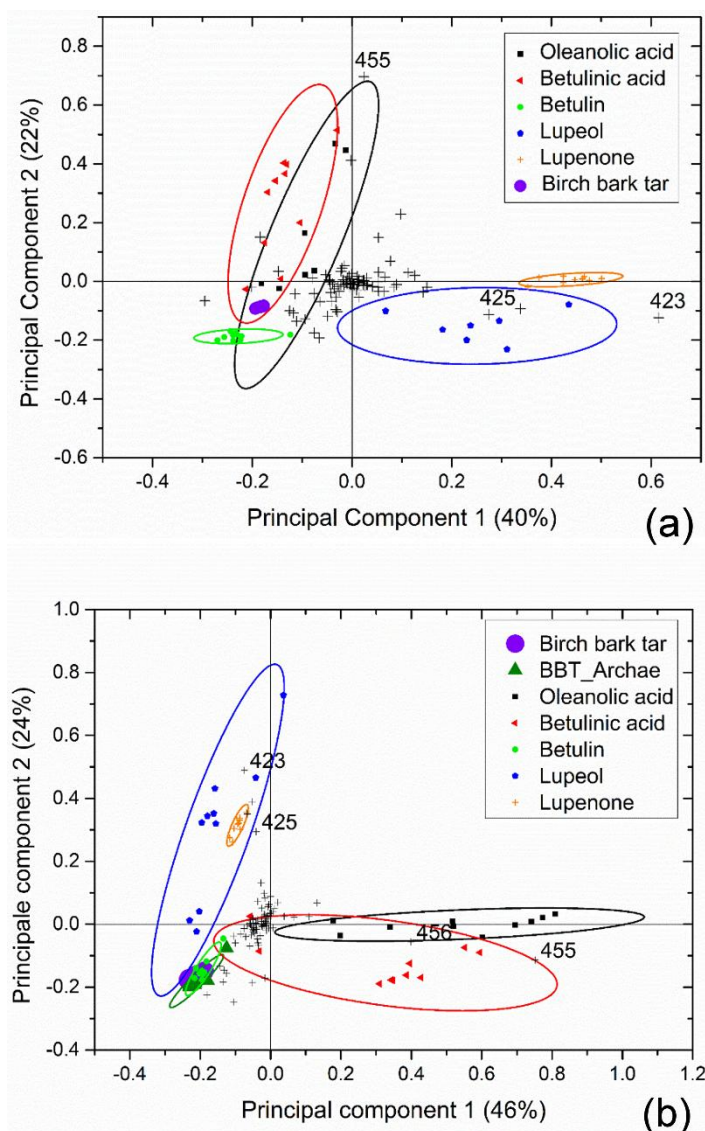


**Figure 2.17.** Biplot of oleanolic acid, betulinic acid, betulin, lupeol, lupenone and birch bark tar birch (a). The birch bark tar reference sample is high correlate to betulin and the oleanolic and betulinic acid. PCA analysis confirms the nature of the archaeological pitch as birch bark tar (b).

### 2.3.4 Conclusion

The analytical procedures proposed in this work are efficient for the characterization of triterpenoid molecules. Due to its high sensitivity, selectivity, and minimum sample requirement, ToF-SIMS technique is suitable for identifying such materials in samples from archaeological findings. In particular, it enables us to distinguish between very similar triterpenic molecules such as oleanolic acid, betulinic acid, betulin, lupenone and lupeolo. Moreover, the fragmentation study allowed to find their characteristic fragments in real reference sample.

The application of principal component analysis on spectral data recorded by ToF-SIMS at selected mass ranges, corresponding to the fragmentation of triterpenoid molecules, enabled us to correlate the freshness of newer birch bark tar to the characteristic fragments described in literature in the fresh tar and in the same time, confirm the nature of archaeological sample.

### 3 Sub-micron molecular imaging

In this chapter the TOF-SIMS analytical capabilities for imaging applications are illustrated by real case studies. The ability of ToF-SIMS to detect inorganic and organic compounds in a single run analysis proves to be the best feature to identify all the compounds composing the multi-layer matter of artworks.

An approach for a better understanding of such complex painting materials and techniques is to study their cross sections. This approach allows not only the study of the multilayer structure but also the detection of the chemical interaction between the layers and their alteration products. Furthermore, the high sensitivity, selectivity and the excellent lateral resolution of secondary ion mass spectrometry imaging allows the chemical characterization and localization of the compounds along the cross-section matrix. Moreover, the use of ToF-SIMS in static mode allows further complementary analyses on the same sample.

Thanks to the collaborations with the different research groups within the Roma Tre University and the Istituto Superiore per la Conservazione ed il Restauro (ISCR), it was possible to obtain samples from previous artworks restorations, to be characterized with ToF-SIMS technique. These collaborations have provided samples from inestimable cultural and fact-finding value, giving the opportunity to study many different materials.

The ISCR has kindly provided all the cross-sections in which a metal leaf decoration was present. In order to validate the results obtained from the previous tin soaps experiment, real case studies that presented “composite lamina” formed by tin and gold leaves, were selected first. The use of metal leaves in painting is frequent and reported in medieval painting treatises, especially in wall paintings [157]. Pictorial mural cycles depicted between XIII and XV centuries document the presence of several types of metal leaves: silver, gold, copper, tin and the so-called “*composite lamina*” consisting of overlapping leaves of different metal composition [158]. The lack of scientific literature regarding the gilding techniques on walls is often due to the complexity of the study of a large number of thin layers [159]. Furthermore, the aging process and the resulting alteration of organic and inorganic compositions contribute to increase the difficulty of the chemical characterization.

The first sample characterized by ToF-SIMS technique has been the cross-section of a fresco present in the Basilica of San Francesco in Assisi, likely painted by a Giotto’s apprentice. The second investigated sample belong to the pictorial cycle painted by Giotto in the Scrovegni Chapel in Padua. Both samples represent the case of a wall gilding decoration. The carried out investigations were aimed at the chemical characterization of the cross- sections, identifying the presence of alteration products in the adhesive-lamina system, and finding confirm to the hypothesis of tin soaps formation in composite lamina decoration. In addition, where the lamina had an exterior red lake decoration, it was also characterized providing useful information in the recognition of organic dyes that remain for many analytical techniques difficult to identify.

Subsequently, was extend the research to the typology of gilding case studies on different support, keeping the focus on the interactions between the metal materials and the organic compounds present in the artwork. The case of a gilt and painted leather artifact and a golden decoration applied on stone were investigated.

The leather artifact under investigation was an altar frontal, coming from the church of San Domenico in Orvieto (Italy), represent a false gilding technique case in which a silver leaf was decorated with a varnish to reproduce golden effect. Moreover, The metal decoration was painted

with inorganic and organic pigments, increasing the value of the artwork and the interest from an analytical point of view.

In addition, was investigated a cross section representing a golden decoration applied on stone. The sample was taken from an archaeological excavation concerning the finding of an Etruscan hypogeum in the territory of Perugia province (Italy) and belong to a cinerary urn that was richly decorated with paintings and gold leaves in antiquity.

The extension of the study to different type of golden artifacts has highlighted the procedure methods and the various gilding techniques adopted, and has expanded the knowledge of the variety of materials employed over the centuries and the various possible interactions between metal and organic materials.

Finally, the last case study concerned the investigation of a painting on wood, kept at the Gallerie dell'Accademia in Venice. The study of the samples taken from the Saint Wilgefortis Triptych, painted by Bosch, was made possible thanks to the collaboration with the research group operating in the Department of Science of Roma Tre University in cultural heritage field. This latter case does not represent a gilding lamina decoration. Nonetheless, the potentialities of ToF-SIMS technology have been exploited in the discrimination between various superimposed organic compounds and for reveal the presence of different metal soaps within a pictorial system rather than on a metal lamina.

## 3.1 Gilding decoration on wall painting and related organic binding media

### 3.1.1 Fresco Vela della Castità, San Francesco Basilic in Assisi

#### 3.1.1.1 Introduction

The first case study of lamina composite analyzed in this thesis represents the case of a gold leaf decoration, superimposed onto a tin leaf with an adhesive mixture and painted by a red lake. The sample was collected to the fresco Vela della Castità (Fig. 3.1a) at the San Francesco Lower Basilica in Assisi. This wall painting is present in the cycle of Franciscan allegories. The depicted scenes are attributed to a Giotto's apprentice and dated to the first half of 14th century. The study of gilding decoration technique in wall painting cross section has been already carried out using imaging and mapping micro-FTIR techniques [160]. This approach allowed a preliminary classification of the chemical compounds. The data shown here are only concern the ToF-SIMS evidence and potentiality that have been exploited to locate inorganic and organic compounds along a cross section in a single run.

#### 3.1.1.2 Materials and methods

The investigation was carried out on two fragments taken from a soldier's golden shield decoration in the fresco Vela della Castità (Fig.3.1a) located in San Francesco Lower Basilica, Assisi. Samples were taken away from the fresco with a scalpel during a restoration operation in the 1970s. A fragment was embedded in polyester resin in order to perform analysis on the cross section (Fig. 3.1c). A second fragment was analyzed as it is. The samples were observed with an optical microscope under visible and ultraviolet light (Olympus AX70 equipped with Hg short arc HBO lamp, Olympus, Tokyo, Japan). Samples were glued onto a SEM stub immediately before introducing it into ToF-SIMS load lock. Analyses were performed on a TOF-SIMS V (ION-TOF GmbH, Münster, Germany) equipped with a Bi liquid metal ion gun. A 30 keV Bi<sub>3</sub><sup>2+</sup> ion beam was selected with an incidence angle of 45° operating in the high mass resolution bunched mode. The ion beam was rastered over an area from 250×250 μm<sup>2</sup> to 150×150 μm<sup>2</sup> with an ion dose density below the static limit (10<sup>-12</sup> ion/cm<sup>2</sup>). Charge neutralization was obtained by using low-energy electrons supplied by a pulsed flood gun. Both positive and negative polarity spectra and images (256×256 pixels) of elements and molecular fragment distribution were recorded. All SIMS images were normalized to the total ion image and filtered with an averaging filter in order to remove topographical effects, and salt-and-pepper noise. Both samples were earlier analyzed by SEM-EDS and FTIR, respectively. Scanning electron microscopy with X-ray micro analysis measurements were performed using a Zeiss EVO 60 (ZEISS EVO 60, Carl ZEISS SMT, Germany), an environmental scanning electron microscope, equipped with an INCAX-sight dispersive X-ray spectrometer (Detector 7636 Energy EDS, Oxford Instruments, PaloAlto, CA) for elemental characterization of the samples. The analyses were carried out at pressure of 100 Pascal without a conductive coating. FTIR micro spectroscopy measurements were performed by a Thermo Scientific Nicolet iN10 FTIR (Thermo Fisher Scientific, Nicolet iS10, Waltham, MA, USA) operating in transmission mode on diamond cell using a nitrogen-cooled MCT detector. The IR spectra were obtained from different portions of the non-embedded sample. The analyzed area ranged from 20×20 to 50×50 μm<sup>2</sup>, in the spectral region from 4000 to 650 cm<sup>-1</sup> with a resolution of 4cm<sup>-1</sup> and 64 scans for each spectrum

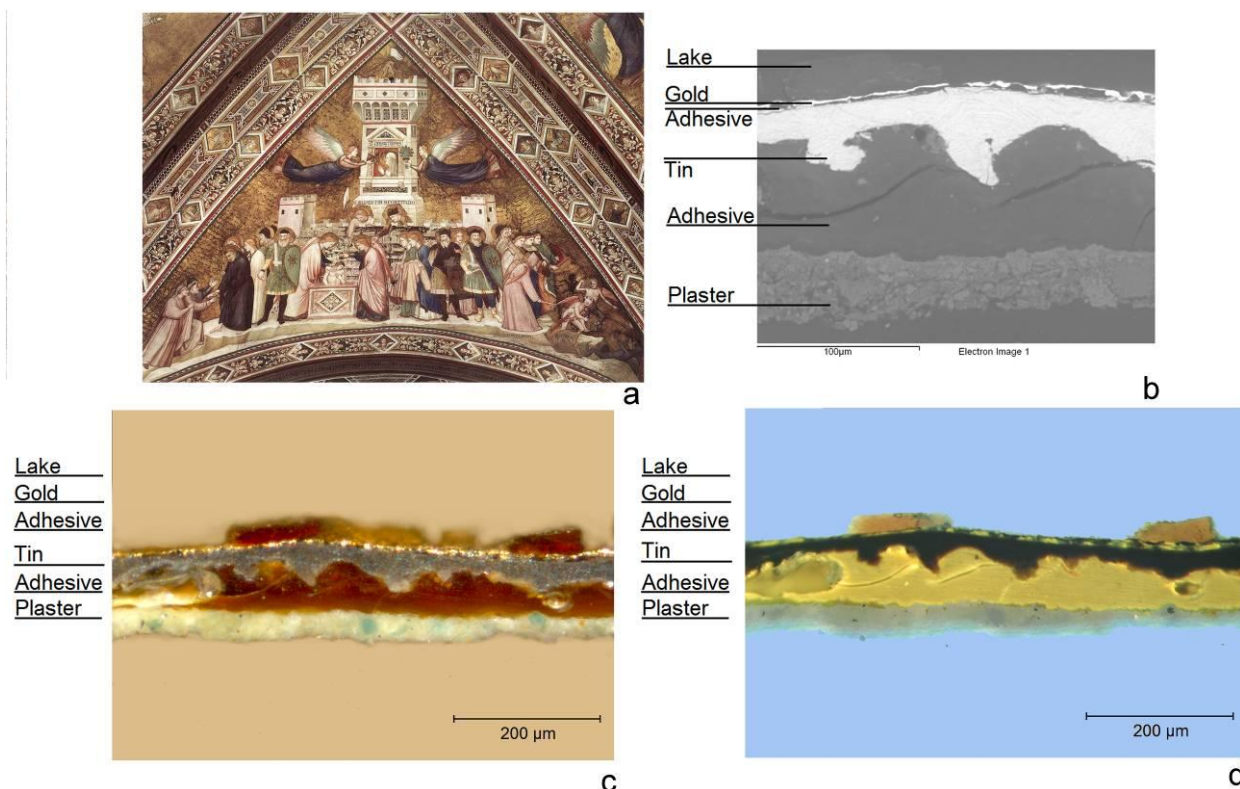


**Figure 3.1.** (a) Fresco Vela della Castità, (b) back scattered electron image with the legend of layers, (c) visible light optical cross-sectional image, and (d) ultraviolet light optical cross section image.

### 3.1.1.3 Results and discussion

Results obtained from cross section and untreated sample analyses were compared to confirm the data obtained from the other analytical techniques. The observation of both samples by a UV/Vis source highlights (Fig. 3.1c and d) the presence of six layers in the cross section with different composition and thickness as also shown in SEM image (Fig. 3.1b). Starting from the bottom, the image of cross section showed the first inorganic layer belonging to the plaster with some particles of mineral pigments: azurite, green earth, and ochre (Fig. 3.1c). These pigments were also detected through polarization microscopy (images not shown). The second layer with a variable thickness ranging from 40 to 70 µm showed the typical yellow fluorescence of oily and resinous substances (Fig. 3.1d) [161]. This layer represents the adhesive between the plaster and the tin leaf. The third layer is represented by a tin leaf that has very irregular thickness ranging from 20 to 40µm. On the top of this metal leaf, a fourth layer is present. It consists of a smaller thin film of adhesive that provides the same fluorescence of the previous adhesive layer (Fig. 3.1d). The fifth layer is represented by a thin gold leaf that completes the so-called composite lamina technique and it is decorated with a red lake (sixth layer).

The plaster layer is mostly composed of calcium carbonate as shown in the ToF-SIMS spectrum with the signal at  $m/z$  40 ( $\text{Ca}^+$ ) and SEM-EDS mapping (Figs 3.2a and 3.3a). The presence of calcite was verified by FTIR analysis (Fig. 3.3d) conducted on micro particles from untreated sample. The bands at  $725$ ,  $1067\text{ cm}^{-1}$  and  $780$ ,  $1450\text{ cm}^{-1}$  correspond to symmetric and asymmetric stretching vibrations of  $\text{CO}_3$  group, respectively (Fig. 2d). ToF-SIMS and SEM-EDS analyses on cross section confirmed the presence of inhomogeneous grain size of inorganic pigments (Fig.

3.3a). Peaks of  $Mg^+$  ( $m/z$  24),  $Al^+$  ( $m/z$  27),  $Si^+$  ( $m/z$  28),  $K^+$  ( $m/z$  39),  $Fe^+$  ( $m/z$  55), and  $Cu^+$  ( $m/z$  63) in ToF-SIMS positive mass spectra suggest the use of green earth, ochre and azurite, respectively (Fig. 3.2a).

Negative ToF-SIMS spectrum relative to the adhesive layer (Fig. 3.2b), showed the peaks of deprotonated molecular ions of azelaic, palmitic and stearic acids ( $m/z$  187, 254, and 283). The presence of azelaic acid could be due to the curing process of drying oils such as linseed or walnut oil. In fact, during the curing process of liquid drying oils, oxidation and cross-linking reactions can occur, leading to the formation of solid film. On the contrary, the presence of saturated palmitic and stearic acids represents the fraction of the oil, which had not been cured [162]. Fragment ions of fatty acids ( $m/z$  227, 211, 197, 169, 155, 127, 113, 99, 85, and 71) were also detected in the second and fourth layers (Fig.3.3c) [46]. A positive ToF-SIMS spectrum (Fig. 3.2a) of the same layers showed protonated molecular ion of azelaic, palmitic, and stearic acids ( $m/z$  189, 256, and 285) and acyl ions of palmitic and stearic acid ( $m/z$  239 and 267) [163]. In general, negative and positive ToF-SIMS spectra of mordant mixture (second and fourth layers) showed the characteristic fragments of fatty acids chain with  $C_2H_3(CH_2)_xCOO$  formula. This attribution was formulated considering the characteristic peaks in positive ( $m/z$  189, 239, 256, 267, and 285) and negative polarity ( $m/z$  71, 85, 99, 113, 127, 155, 169, 187, 197, 211, 227, 254, and 283). Mass spectra in positive ion mode revealed also some weak signals at  $m/z$  253, 269, 300, 315, 317, and 331, from both layers, suggesting the presence of diterpenoid acids belonging to the adhesive mixture used for the metal leaves. Current state of the art reports numerous studies on the characterization of natural terpenic resins with different analytical techniques and their detection in several case studies [164-165]. The peak at  $m/z$  300 could belong to a molecular ion of dehydroabietic acid (DHA) oxidation product of abietane acid in aged resin, recognized as one of colophony markers [10]. The colophony, pine resin also known as rosin, is a diterpenoid resin that mainly consists in abietane and pimarane acids. Ancient recipes suggest that colophony-drying oil mixtures have been frequently used [166]. Other oxidation products of the aged colophony were detected at  $m/z$  315 (7-oxo-DHA+ $H^+$ ),  $m/z$  317 (15-hydroxy-DHA acid+ $H^+$ ), and  $m/z$  331 (7-hydroxy-DHA + $H_+$  and/or 7-oxo-15-hydroxy-DHA acid+ $H^+$ ) as also reported by Scalarone et al [129]. Furthermore, the peaks detected at  $m/z$  253 ( $C_{19}H_{25}^+$ ) and 269 ( $C_{19}H_{25}O^+$ ) could represent a loss process of carboxyl group from C20 chain. As shown in Fig. 3.3b, ToF-SIMS imaging confirmed the simultaneous presence of oil binder and resin over and under the gold and tin leaves.

The peak at  $m/z$  208 belongs to  $Pb^+$ , detected in the same layer with oil binder and rosin. Its identification, presumably as main component of an inorganic pigment used as a siccative for the drying oil, is better discussed in FT-IR analysis later. ToF-SIMS data collected on mordant layers were partially confirmed by FTIR analyses conducted on single grains from the untreated sample. The FTIR spectrum (Fig. 3.3d) of the adhesive mixture for the metal leaves records the vibration of ester bond in enlarged band between  $1740$  and  $1690\text{cm}^{-1}$  that includes vibration of  $C=O$  coming from oil and from rosin. Stretch vibrations of CH bonds were recorded at  $2940$  and  $2860\text{cm}^{-1}$  and their asymmetric bending vibration at  $1460\text{cm}^{-1}$ . Lead white pigment  $PbCO_3Pb(OH)_2$  was detected thanks to the identification of carbon- ate group around  $1430\text{cm}^{-1}$  and the stretching band of hydroxylic group at  $3440$ ,  $1048$ ,  $776$ , and  $681\text{cm}^{-1}$  (data not shown). A little shoulder around  $1547\text{cm}^{-1}$  could suggest the presence of lead soap, due to the hydrolysis of the oil binder by the basic lead compound.

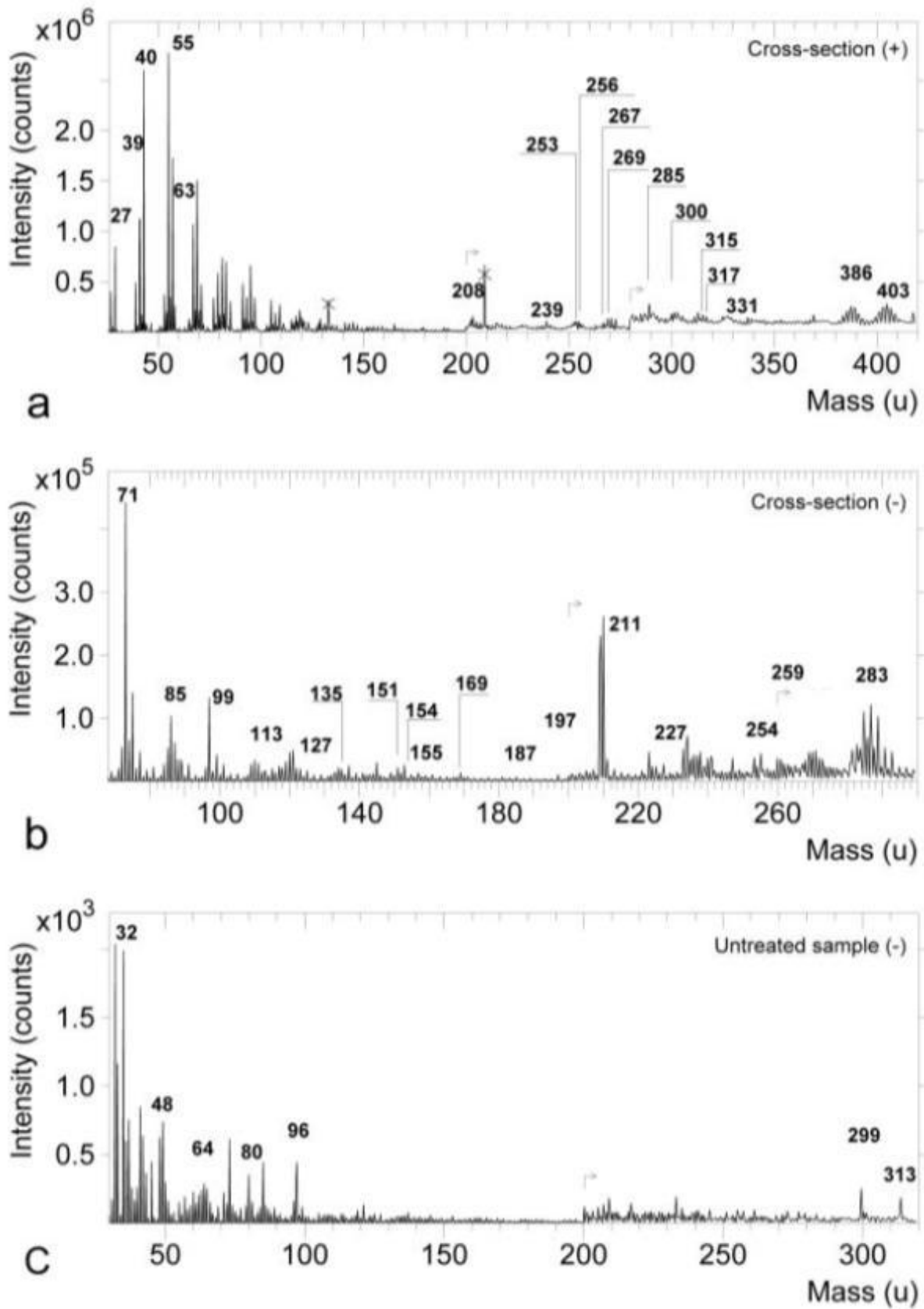


**Figure 3.2.** Relevant time of flight secondary ion mass spectrometry spectra of fresco cross section: (a) positive ion mode, (b) negative ion mode, and (c) negative ion mode of red lake area (untreated sample).

Time of flight secondary ion mass spectrometry results obtained from both the cross section and the untreated sample demonstrate the state of degradation of metal tin leaves. Tin leaf has been partially replaced by its oxides and chlorides. The negative ion spectrum shows the peaks at  $m/z$  135 and 151 corresponding to tin oxides  $\text{SnO}^+$  and  $\text{SnO}_2^+$  (romarchite and cassiterite), respectively (Fig. 3.2b). These minerals have been often observed on tin leaves by X-ray powder diffraction analysis [167]. Furthermore, negative mass spectra show chlorine ion at  $m/z$  35 and chlorinated compounds at  $m/z$  154 and 259 ( $\text{SnCl}^-$  and  $\text{SnCl}_4^-$ , respectively) localized on the tin area as shown in Fig. 3.3c. The presence of pigments altered by chlorine compounds has been already reported for the wall paintings present in the upper and the lower parts of the same Basilica. In the high mass range, the positive ToF-SIMS spectrum (Fig.3.2a) presents two clusters of peaks in the range at  $m/z$  384–392 and  $m/z$  401–409. The most intense of these peaks were observed at  $m/z$  386 and 402, respectively. The co presence of stearic acid and tin oxides in the metal leaf area suggests the possible formation of tin soaps (Fig. 3.3b).

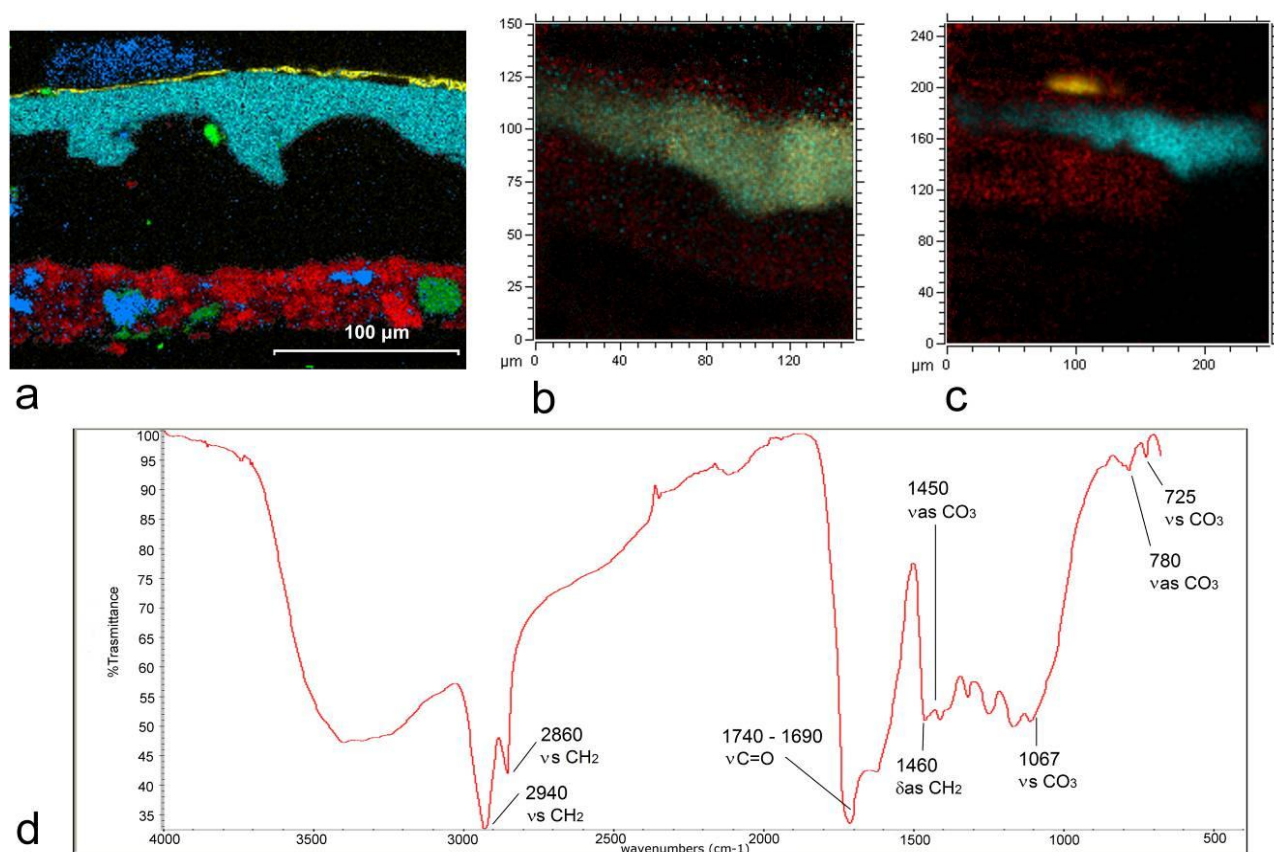


**Figure 3.3.** (a) Scanning electron microscopy with X-ray microanalysis mapping image of aluminum (blue), gold (yellow), tin (pale blue), calcium (red) and silicon (green). Time of flight secondary ion mass spectrometry ion image overlay of the fresco cross section: (b) positive ion image of colophony and oil signals (red) (sum of  $m/z$  253, 269 300, 315, 317 331 and 189,239, 256, 267, 285, respectively) and tin leaf and tin soap ions (yellow and pale blue) (sum of  $m/z$  119, 120, 124, 239, 255, 384 386, 387, 388, 389, 390, 392, 402 403, 404, 405, 406, 407, and 408); (c) negative ion image of gold ions (yellow) (sum of  $m/z$  197, 223, 394, 427, and 591), alteration products of tin leaf (pale blue) (sum of  $m/z$  17, 35, 120, 135, 136, 151, 152, 153, 154, 155, 167, and 259) and fatty acid fragments (red) (sum of  $m/z$  71, 85, 99, 113, 127, 155, 169, 187, 197, 211, 227, 254, and 283). (d) Micro-Fourier transform infrared spectrum.

Thus, the peaks at  $m/z$  402 and 386 can be attributed to tin stearate  $C_{18}H_{35}SnO_2^+$  (mass deviation, 70ppm) and tin stearate with the loss of a hydroxylic group  $C_{18}H_{34}SnO^+$  (mass deviation, 84ppm), respectively. Their assignment was confirmed by a comparison with the theoretical isotope pattern. The isotopic pattern and the mass accuracy observed for the two clusters of peaks provide strong evidence for the correct assignment of these peaks. Furthermore, in the negative ToF-SIMS spectra, characteristic peaks of the lipid chain fragmentation at  $m/z$  71, 85, 99, 113, 127, 155, 169, 183, 211, and 227 were detected on the untreated sample where the red lake was lost. Deprotonated molecular ions of azelaic acid ( $m/z$  187), palmitic acid ( $m/z$  254), and stearic acid ( $m/z$  283) were also detected, as a residual presence of the oil binder used for the red lake. Au peaks that identify the gold leaf were seen at  $m/z$  197 ( $Au^-$ ), 394 ( $Au_2^-$ ), and 590 ( $Au_3^-$ ) (Figs 3.2a and 3.3c).

Time of flight secondary ion mass spectrometry surface analysis in positive polarity an untreated sample from the red lake portion showed the presence of  $Na^+$  ( $m/z$  23),  $Mg^+$  ( $m/z$  24),  $Al^+$  ( $m/z$  27),  $Si^+$  ( $m/z$  28),  $K^+$  ( $m/z$  39), and  $Ca^+$  ( $m/z$  40) belonging to inorganic compounds on which the red dye is adsorbed. Furthermore, the positive mass spectra present peaks at  $m/z$  208 ( $Pb^+$ ), 432 ( $Pb_2O^+$ ), and 449 ( $Pb_2O_2H^+$ ). In addition, a signal attributed to palmitic lead soap at  $m/z$  463 was recorded. These peaks suggest the presence of lead white as drying agent for the oil binder with the consequent production of lead soaps [168]. In negative spectra  $S^-$  ( $m/z$  32),  $SO^-$  ( $m/z$  48),  $SO_2^-$  ( $m/z$  64),  $SO_3^-$  ( $m/z$  80), and  $SO_4^-$  ( $m/z$  96) were detected (Fig. 3.2c). These data confirm the use of potash alum as inorganic substrate during the lake preparation [168]. Negative spectra of the red lake surface did not show characteristic peaks of oil binder but evidences two small peaks at  $m/z$  299 and  $m/z$  313 that could most likely be attributed to the loss of  $CH_2OH$  and hydroxylic group from kermesic acid (Fig. 3.2c). Kermesic acid is one of cochineal compounds used as a dyestuff since the Roman ages [169]. Nevertheless, the molecular peak of kermesic acid was not found (at  $m/z$  330). Neither the molecular ion nor fragmentation of carminic acid ( $m/z$  492) that is the main component of the cochineal red dye was detected. In view of these data, it is not possible to give a certain assignment of cochineal for the red lake

### 3.1.1.4 Conclusion

The painting technique of 'composite lamina' adopted in the execution of wall painting was characterized by ToF-SIMS. The components of each layer were identified and mapped. The inorganic components found mostly belong to the layer of lime plaster in which grains of mineral pigments are sprinkled. The individual components of the mordant used for the adhesion of metallic leaves were identified. Typical fragmentation of azelaic, palmitic, and stearic acids belonging to drying oils, such as linseed or walnut oils, and colophony were found. In the same mixture, the signals of lead white used as a drying agent were recognized. The tin leaf presents alteration products, as oxides and chlorides. Furthermore, in this work, for the first time, the presence of tin soaps was reported. In fact, peaks likely to belong to the tin stearate were found in a real case of artworks. In the cultural heritage field, the presence of tin soaps was never revealed neither with ToF-SIMS analyses nor with others analytical techniques. Lastly, two peaks attributable to kermesic acid suggested the presence of cochineal as dye used to prepare the lake applied on gold leaf. To the best of our knowledge, this paper represents a starting point to better understand the Giotto's school studio practice in gilding technique.

## 3.1.2 Giotto “*Universal Judgement*”, Scrovegni Chapel in Padua.

### 3.1.2.1 Introduction

A sample belonging to the Giotto's pictorial cycle present in the Scrovegni Chapel in Padua was characterized by using ToF-SIMS technique, in order to recognize the degradation products in the tin golden decoration. The sample, represented by a cross section (named 3L), was collected from the fresco “*Universal Judgement*” (1305 A.D.) in correspondence of an angel's golden halo (Fig. 3.4) and represent another case of composite lamina with tin and gold foils, adhered each other with an oil-resinous glue. Results obtained from cross section analyses were compared to the data obtained from the other analytical techniques, conducted in the past study on the same sample [160]. In fact, the inorganic elemental distribution on cross-section layers was investigated by SEM-EDS analysis, as well as the mineral crystal habit alterations were observed *in situ* using the XRD analysis. Moreover, the 3L sample was also object of the application of linear imaging FTIR microscopy, in which the nature of the adhesive was not completely defined. The FTIR analyses identified the organic origin of the glue, but not the type of resin used in the blend. The ToF-SIMS features to detect mass fragmentation in high mass and spatial resolution allows to recognize and localize the organic species along the cross-section layers. The analyses were focus with the aim to recognize the species involved in the adhesive mixture and the alteration products present on the tin lamina that could be formed as result of saponification reaction.

### 3.1.2.2 Materials and methods

The cross section 3L was analyzed by using TOF-SIMS V (ION-TOF GmbH, Münster, Germany) equipped with a Bi liquid metal ion gun. A 30 keV  $\text{Bi}_3^{2+}$  ion beam was selected with an incidence angle of  $45^\circ$  operating in the high mass resolution bunched mode. The ion beam was rastered over an area of  $300 \times 300 \mu\text{m}^2$  with an ion dose density below the static limit ( $10^{-12}$  ion/ $\text{cm}^2$ ). Charge neutralization was obtained by using low-energy electrons supplied by a pulsed flood gun. Both positive and negative polarity spectra and images ( $256 \times 256$  pixels) of elements and molecular fragment distribution were recorded. All SIMS images were normalized to the total ion image and filtered with an averaging filter in order to remove topographical effects, and salt-and-pepper noise. In order to characterize only the metal layers and the organic adhesive mixture, the analyses were carried out on the external left side of the cross-section (marked with a red box in Fig. 3.4c), excluding the inorganic plaster layer and the consequence matrix effect. The information concerning the composition of the preparatory layer was discussed on the base of previous study [160], no secondary ion mass spectrometry measurements were carried out on it.

### 3.1.2.3 Results and discussion

The 3L cross section was previously observed under optical microscope, in order to identify the layers sequence. The visible and UV light observations, confirmed that a golden tin was adopted (Figs. 3.4d-e). Giotto made use in this case of a fine real gold leaf superimposed to a tin foil instead of a tin foil tinted with a golden varnish which represented in the ancient techniques a cheap substitute for gold. A gold leaf has been applied over a tin leaf by the use of a thin mordant gilding (3–5  $\mu\text{m}$  thick) which fluoresces bright yellow when observed under UV light (Fig. 3.4e).

This feature is generally considered as a first indication of the presence of an oily substance. The tin foil itself was fixed to the wall by means of another mordant layer, (15–50  $\mu\text{m}$  thick), which also shows a bright yellow fluorescence under UV illumination.

ToF-SIMS analyses of the Giotto cross section have recorded the mass fragmentation of an oil-resinous mordant, confirming the use of this type of compounds as supposed by the UV observation and past FTIR analyses. The positive ion mass spectrum shows the protonated molecular ion peaks of palmitic ( $m/z$  257) and stearic acid ( $m/z$  285) (Fig. 3.5a). Furthermore the presence of oily compound is also recognized in the fragmentation of fatty acid chain present in negative ion spectrum. In the Fig. 3.5d are marked the peaks belonging to the aliphatic chain fragment ion with a mass increment of 14 amu ( $m/z$  71, 85, 99, 113, 127, 141, 155, 169, 183, 197, 211, 225, 239). These negatively charged fragments were already assignment to the type  $\text{C}_2\text{H}_3(\text{CH}_2)_x\text{COO}^-$  fragmentation pathway found in fatty acids references [119]. Furthermore the peaks likely belonging to deprotonated palmitic ( $m/z$  255) and stearic acid ( $m/z$  283) were also identify (Fig. 3.5d).

Moreover, the data collected suggests the presence of a terpenic resin inside the adhesive layers. In the lower yield of positive ion mass spectrum were recognized characteristic signals that are in common in the terpenic resins mass fragmentation. The peaks at  $m/z$  185, 197, 211, 253 and 299 could derived to the molecular fragmentation of diterpenoic compounds like abietane molecules recognized as markers of pine resin (Fig. 3.5a) [1, 26]. In the spectrum shown in Fig. 3.5b, were identified two peaks, which could indicate the presence of an aged diterpenoid varnish. The peaks at  $m/z$  330 and 314 were assigned to the 15-hydroxy-7-oxo-dehydroabietic acid (15-OH-7-oxo-DHA) and 7-oxo-dehydroabietic acid (7-oxo-DHA), respectively. Both compounds are known as main oxidation products of abietic acid, present in colophony [25]. Moreover, in the negative mass spectrum was detected a peak at 329  $m/z$  that could represent the deprotonated 15-OH-7-oxo-DHA (Fig. 3.5e). This result, could complete the identification provided by the previous FTIR analysis that identify a resinous compound in the mordant layer, but not the class of belonging. The sum of the fragments identified as the two component of the adhesive mixture, oil and resin, are shown in the secondary ion imaging represent in Figs. 3.6 and 3.7 respectively. These images show that the trend in the signal distribution follows the deposition of the tin and the gold leaves, and results interposed among them (Figs. 3.6b and 3.6f). In the Fig. 3.8 is described the fragmentation pathway of 7-oxo-dehydroabietic acid recognized in the positive ion mass spectrum. However, the adhesive mixture seems to have been absorbed by the tin foil, seeing as how part of the mordant signal is located within the same area where  $\text{Sn}^+$  ion ( $m/z$  119) is recorded. In addition, oxidation products of tin metallic lamina were recognized on the tin layer. The XRD analysis conducted on the sample during the past study, have given specific mineral attribution to the tin oxides, identifying the presence of romarchite and cassiterite. The positive ToF-SIMS spectrum and image show the signals and the maps of romarchite,  $\text{SnO}$  ( $m/z$  135) and, cassiterite  $\text{SnO}_2$  ( $m/z$  151) in the Figs 3.5a and 3.6c, respectively.

Finally, in the positive ion mass spectrum were also recorded the signals likely belonging to the tin carboxylates. Two cluster of peaks in the range at  $m/z$  384–392 and  $m/z$  401–409 appear on the spectrum shown in Fig. 3.5c. The contact between the oily material and the tin leaf, can have started the reaction of saponification. The co presence of stearic acid and tin oxides in the metal leaf area strengthens the hypothesis of tin soaps formation. Thus, the most intense peaks at  $m/z$  402 and 386 can be attributed to tin stearate  $\text{C}_{18}\text{H}_{35}\text{SnO}_2^+$  and tin stearate with the loss of a hydroxylic group  $\text{C}_{18}\text{H}_{34}\text{SnO}^+$ , respectively. Their isotopic fragmentation were summed and mapped in Fig. 3.6d. This data confirms the possible occurrence of carboxylation processes on metallic tin leaf.



**Figure 3.4.** Giotto's "*Universal Judgement*" frescoes located in the Scrovegni Chapel (a). Angel's gilded halo (b) from which the sample 3L was collected in order to perform a cross-section (c). Cross-section under visible (d) and UV light investigation (e).

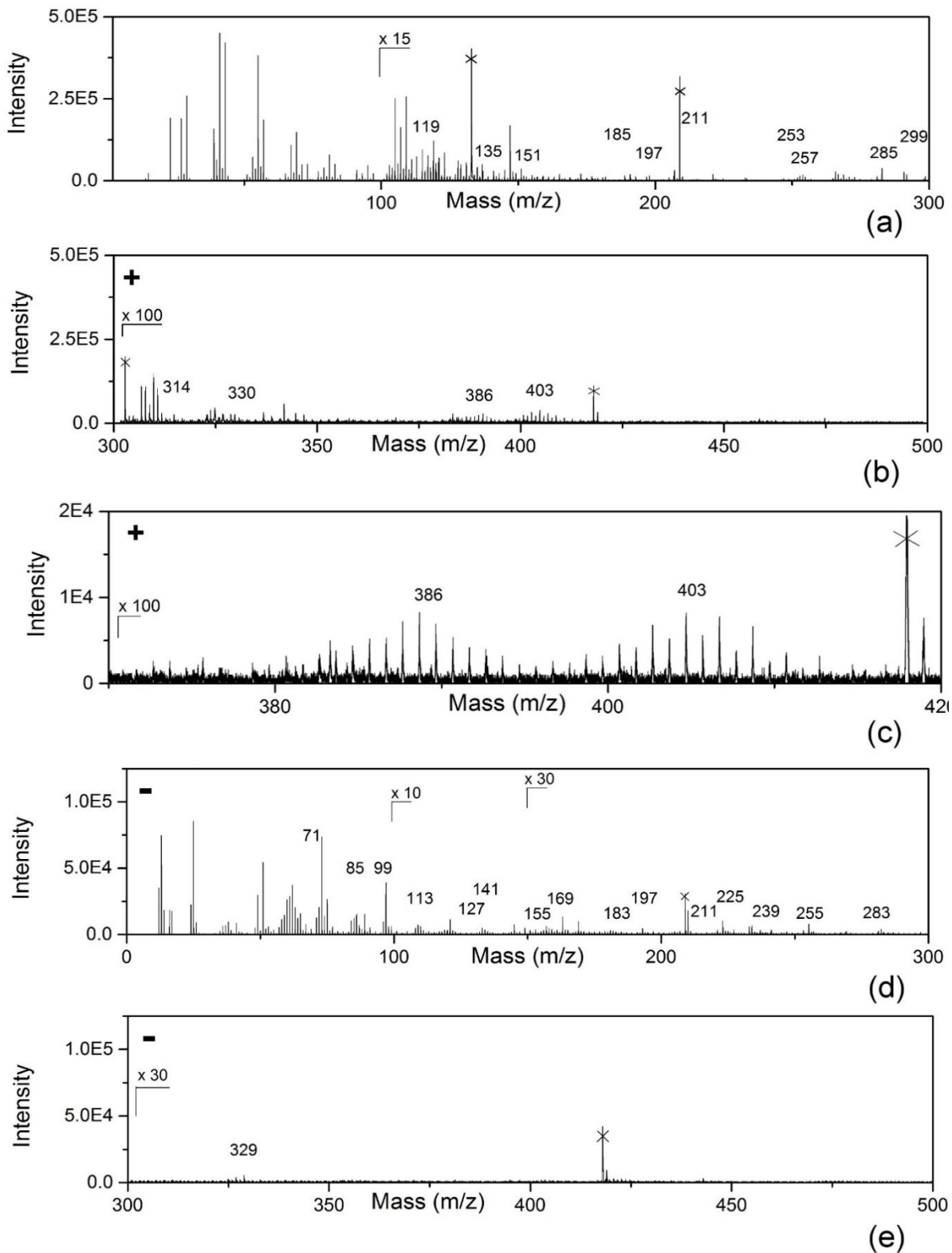


**Figure 3.5.** ToF-SIMS mass spectra. In the positive map spectrum shown in Fig. 3.5a, are marked the signals of tin ( $m/z$  119) tin oxide ( $m/z$  135, 151) the fragmentation of natural resin ( $m/z$  185, 197, 211, 253, 299) and the molecular protonated ion of palmitic and stearic acid ( $m/z$  257, 285). Fig. 3.5b shows the positive ion of 15-OH-7-oxo-DHA and 7-oxo-DHA ( $m/z$  330 and 314) and the peaks belonging to tin stearate ( $m/z$  386 and 403). The positive pattern distribution of tin carboxylates is shown in Fig. 3.5c. The negative mass spectrum shown in Fig. 3.5d present the fragmentation of fatty acid chain ( $m/z$  71, 85, 99, 113, 127, 141, 155, 169, 183, 197, 211, 225, 255, 283) and molecular deprotonated ion of palmitic and stearic acid ( $m/z$  255 and 283). Finally deprotonated 15-OH-7-oxo-DHA ( $m/z$  329) is shown in negative spectrum illustrated in Fig. 3.5e).

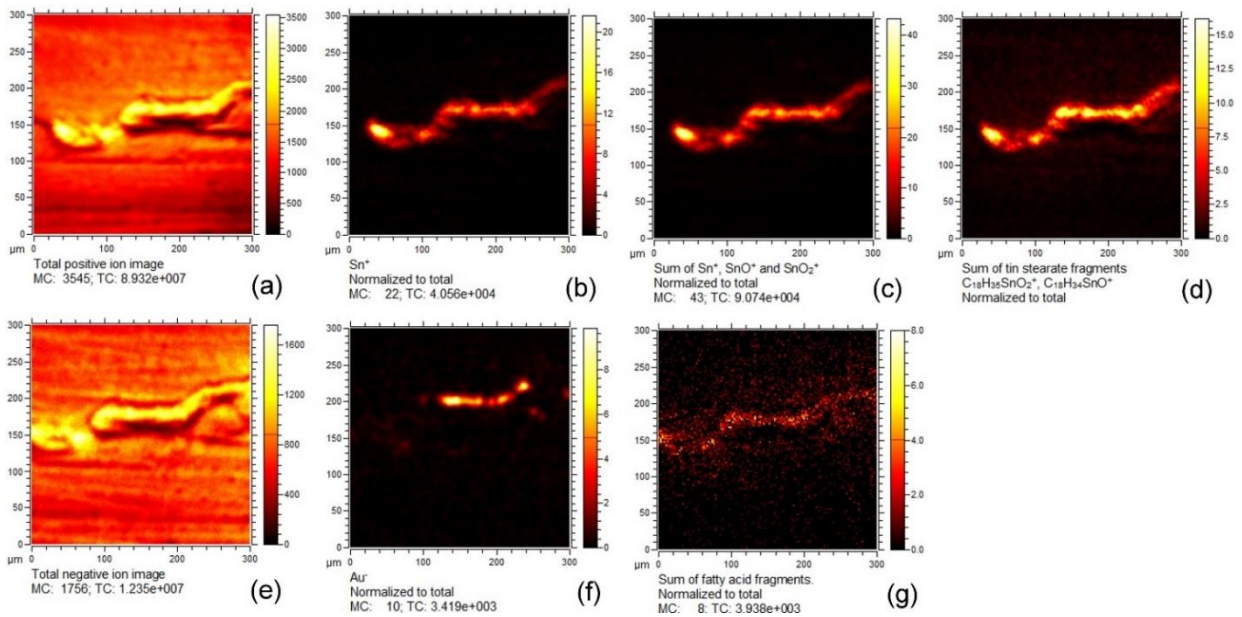


**Figure 3.6.** Imaging panel of cross section 3L. In the positive ion imaging (a), were detected the presence of tin (b), tin oxides, cassiterite and romarchite (c) and in the same area the fragmentation pattern of tin stearate (d). The negative ion images (e) shows the presence of gold leaf (f) and the fatty acid fragments distribution in the area below it, in correspondence of tin foil (g).

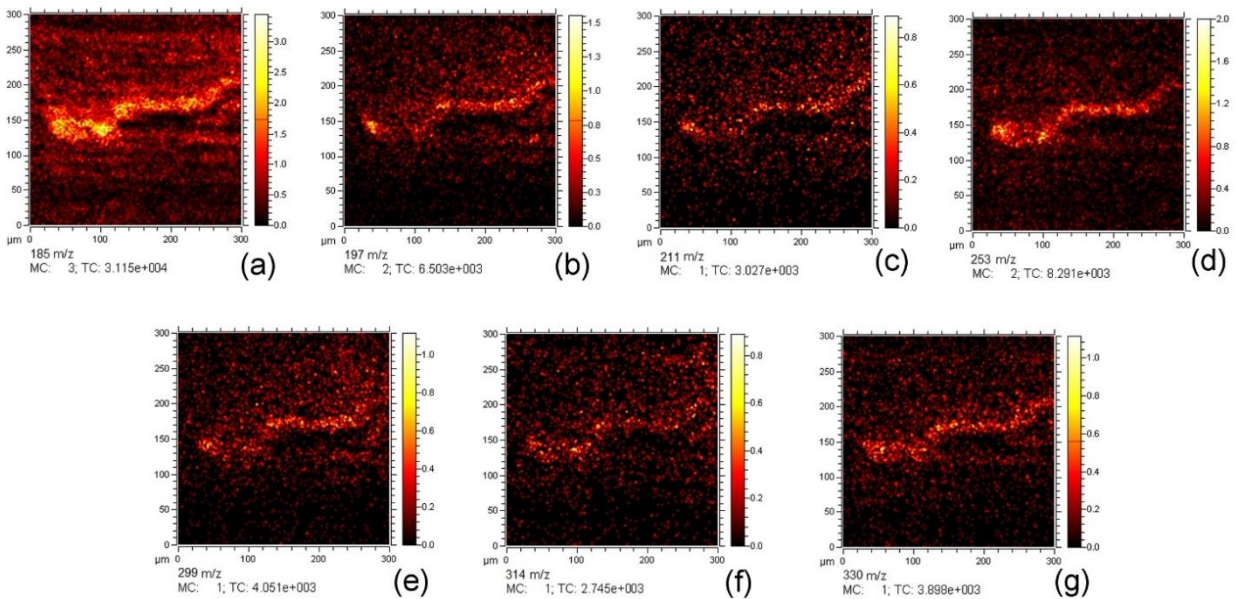


**Figure 3.7.** Positive ion imaging panel of fragments attributed at the natural resin detected in the cross-section.

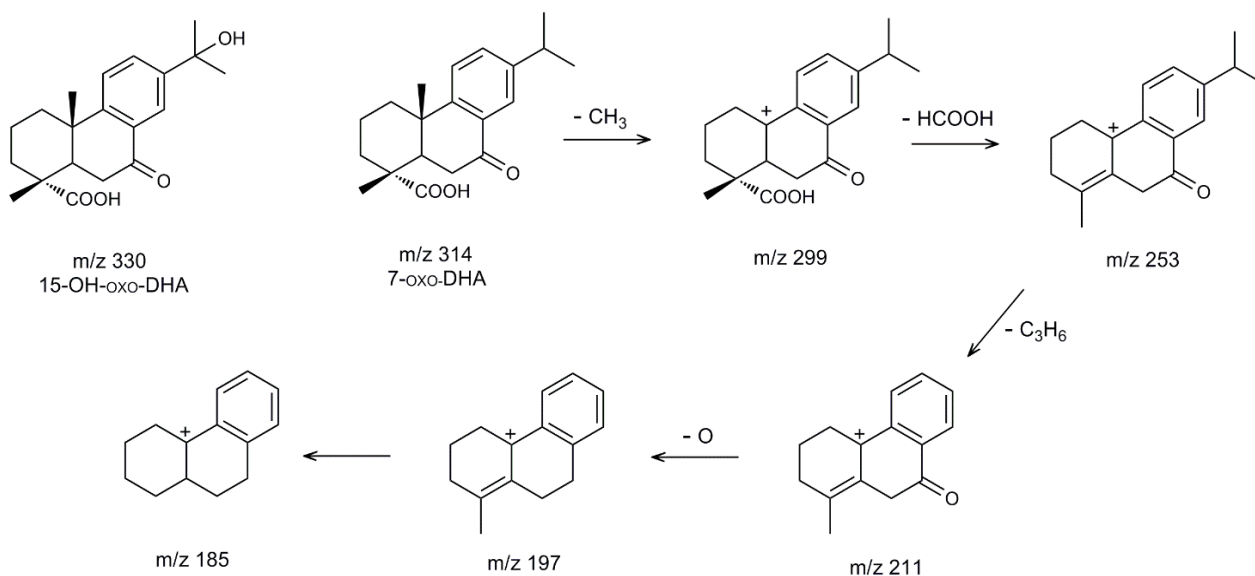


**Figure 3.8.** Fragmentation pathway of dehydroabietic acid oxidation products.

### 3.1.2.4 Conclusion

ToF-SIMS investigation carried out on the Giotto's cross section have highlighted and localized each element composing the *composite lamina* technique, and detected the degradation products formed on tin metal foil. Oxidation products as cassiterite and romarchite were recognized coupled with the stearic tin soaps produced from the interaction with the free fatty acids present in the adhesive mixture. Furthermore, were identified mass fragmentation peaks likely belonging to the oxidation products of abietic acid, that leave hypothesize the presence of colophony as diterpenic resinous component of the mixture. These results identify the compounds in adhesive mixture, clarifying the methods of gilding technique in wall painting and confirm the previous study on the tin soaps formation. Nevertheless, no specific signals were recognized in the layer between the tin foil and gold lamina belonging to the adhesive. In conclusion, specific study on the state of conservation of these samples could provide elements for the restoration interventions on the artworks in which composite lamina decoration technique is present.

## 3.2 Gild and painted leather

### 3.2.1 Introduction

In this case study, we describe a study of painting technique of a gilt and painted leather artifact, paying particular attention to the organic materials contained in the gold varnish and in the paint layer. Gilt and painted leather was used in the past for interior decoration such as wall hangings, altar frontals, paintings and other furnishings. The tanned skin was covered by a silver leaf, which was then burnished and covered by an oil-resinous varnish, containing yellow pigments giving to the leaf the gold appearance. A paint layer was then applied for decorations. The object under investigation here is an altar frontal, coming from the church of San Domenico in Orvieto (Fig. 3.9a), which can be dated by style and iconography to the mid-17<sup>th</sup> century. During the conservation treatment at the ISCR, various scientific analyses were employed (optical microscopy, XRF, SEM-EDX, micro-FTIR and micro Raman), which allowed the identification of most constitutive materials; an interesting result was the detection of indigo for depiction of petals of the blue flowers.[170] More difficult was the identification of the components of gold varnish, in particular to recognize the type of resin. The procedures for preparing gold varnishes are described in ancient recipes, which often give imprecise names to the components. We have thus considered it a good challenge to use ToF-SIMS technique, to complete the characterization of painting materials and to compare results with those obtained by other analytical techniques. To the best of our knowledge, this is the first application of ToF-SIMS to the study of gilt and painted leather artifacts.

### 3.2.2 Materials and methods

ToF-SIMS investigation of standard samples of siccative oils (raw linseed oil, stand oil and walnut oil) and natural resins (colophony, shellac, gamboge, sandarac, arabic gum and dammar) was performed (data not shown) in order to compare results with those obtained from samples taken from the artifact. Standards were dissolved in a small volume of chloroform or ethanol and placed on a glass slide. ToF-SIMS investigation of gilt and painted leather presented in this work was carried out on two scraped fragments: sample 1 (Fig. 3.9b) is a portion of a flower painted with various shades of a blue pigment, which has undergone extensive darkening, and sample 2 (Fig. 3.9c) was taken from a portion of gold varnish background close to a white flower; the sample contains white pigment paint brushes (Fig. 3.9, area A). Samples were adhered to standard SEM stub immediately prior to introducing it into ToF-SIMS load lock; no further sample preparation was performed. Analyses were performed on a TOF.SIMS V (ION-TOF GmbH, Münster, Germany) equipped with a Bi liquid metal ion gun. A 30-keV Bi<sub>3</sub> ion beam was selected with an incidence angle of 45° operating in the high mass resolution bunched mode.[56] The ion beam was rastered over an area of 500 × 500 μm<sup>2</sup> for 120s in order to remain below the static limits. Charge neutralization was obtained by using low energy electrons supplied by the instrument's pulsed electron flood gun. Secondary ions were extracted with 2 keV voltages and were post accelerated to 10 keV kinetic energy. Both positive and negative polarity spectra and images of the distribution of elements and molecular fragments were recorded. Infrared analyses of the same samples were performed by a Thermo Scientific Nicolet iN10 FTIR Microscope. Analysis was performed by operating in transmission mode using a diamond cell and by micro-ATR using a Germanium slide-On Micro-Tip ATR accessory. Spectra were collected in the 4000 to 650 cm<sup>-1</sup> spectral range, using a Nitrogen cooled MCT detector.

### 3.2.3 Results and discussion

A fragment of gilt and painted leather sampled from a blue flower was embedded in polyester resin in order to perform a cross section analysis, while a second fragment was left untreated. Contaminations from sample handling and abundant presence of resin over the cross section surface have made it difficult to characterize the embedded sample by ToF-SIMS.

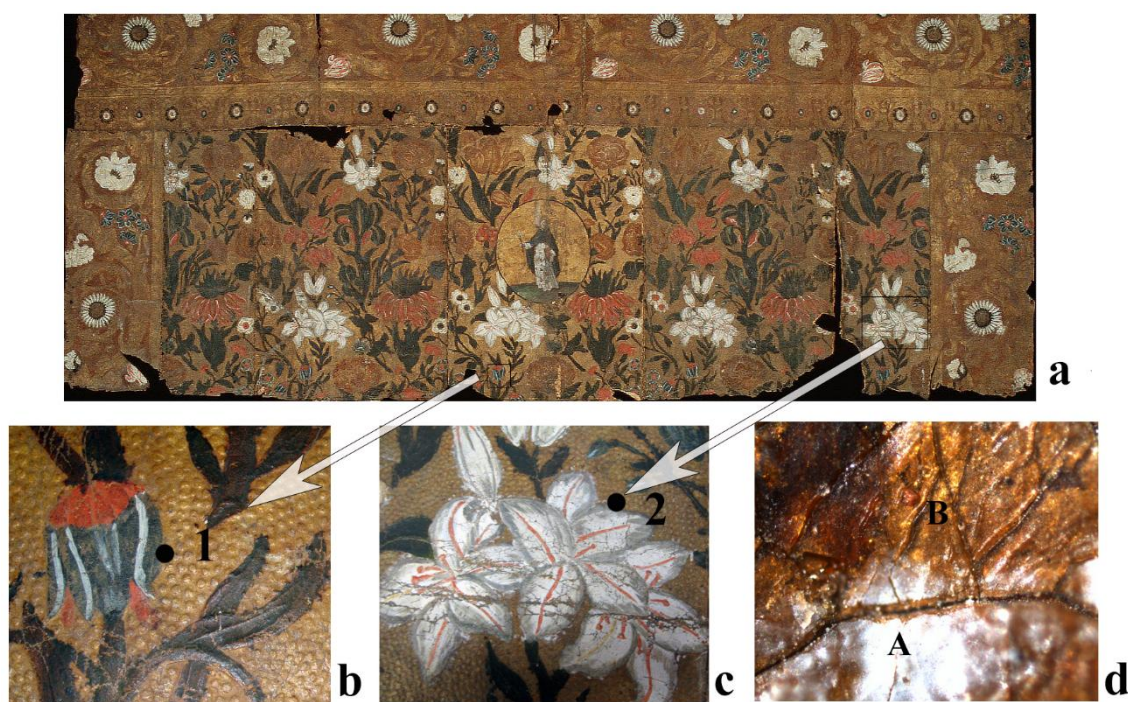


**Figure 3.9.** Gilt and painted leather artifact examined. (a) San Domenico altar frontal general view; (b) detail of sampling area 1; (c) detail of sampling area 2; (d) microscope image of sample 2 showing white (A) and gold varnish portion (B).

However, cross section was analyzed with optical microscopy and SEM-EDX; results have been discussed in a previous publication. [12] On the other hand, SIMS studies of the not embedded fragments were performed. Figs. 3.10a-3.10c show positive ion SIMS spectra of the blue area in sample 1. Peaks of sodium ( $m/z$  23), aluminum ( $m/z$  27), titanium ( $m/z$  48), iron ( $m/z$  56), copper ( $m/z$  63) and calcium ions ( $\text{Ca}^+$ ,  $m/z$  40;  $\text{CaOH}^+$ ,  $m/z$  57;  $\text{Ca}_2\text{OH}^+$ ,  $m/z$  97;  $(\text{CaO})_2\text{H}^+$ ,  $m/z$  113;  $(\text{CaO})_3\text{H}^+$ ,  $m/z$  169) were detected. Cluster of lead ( $m/z$  208, 416, 624 and 832), lead oxides ( $\text{PbO}^+$ ,  $m/z$  225;  $\text{Pb}_2\text{O}^+$ ,  $m/z$  432;  $\text{Pb}_3\text{O}_2^+$ ,  $m/z$  656 and  $\text{Pb}_3\text{O}_3^+$ ,  $m/z$  672) and lead hydroxides [ $(\text{PbO})_2\text{H}^+$ ,  $m/z$  449;  $\text{Pb}_2\text{O}_3\text{H}_3^+$ ,  $m/z$  467 and  $\text{Pb}_3\text{O}_4\text{H}^+$ ,  $m/z$  689] were localized in correspondence of round protruding masses and white efflorescent crusts present onto paint surface as also reported by Bonn et al.[94] The region of the spectrum ranging from  $m/z$  200 to 400 (Fig. 3.10b) is the most important for the determination of organic pigments, binding media and varnishes. Positive mode revealed the presence of indigotin due to the detection of peaks relative to the molecular ion ( $[\text{M} + \text{H}]^+$ ) at  $m/z$  263 ( $\text{C}_{16}\text{H}_{11}\text{N}_2\text{O}_2$ ) and to the characteristic fragmentation of the molecule at  $m/z$  247 ( $\text{C}_{16}\text{H}_{11}\text{N}_2\text{O}$ ). These results are consistent with the ToF-SIMS studies of the indigotin used on ancient textile performed by Lee and coworkers [82] even though the

experimental conditions and dye sample were different. In the altar, frontal indigo is present in the dark blue petals of some flowers. Here, the pigment is used in an oil binder applied directly in a very thin layer over the gold varnish and is mixed with lead white added in varying proportions to obtain shadows, highlights and half tones. Due to the thinness of the blue paint layer, showing isolated cracking, the gold varnish underneath is also visible by surface analysis, and the molecular signature from the presence of an old resin has been proved by cluster SIMS as well as by infrared spectroscopy (FTIR). Natural resins were the most common component of gold varnish and can be divided into those produced by conifers and those from non-cone-bearing trees. Conifers produce oleoresins containing at least one of five primary diterpenoid acids, all of which isomerize to abietic acid upon aging. Several studies focused on art, and archeological artifacts have characterized the oxidative products found in varnishes subjected to accelerated photo-aging processes or analytic studies on naturally aged resins.[163,171-172] In the positive ion SIMS spectra of sample 1, ion peak at  $m/z$  299 ( $C_{20}H_{27}O_2$ ) (Fig. 3.10b) suggests the presence of diterpenoid acids and in particular this signal could be attributable to  $\Delta^6$ -dehydroabietic acid and the peak at  $m/z$  282 ( $C_{20}H_{26}O$ ) representing hydroxyl group loss from this molecule.

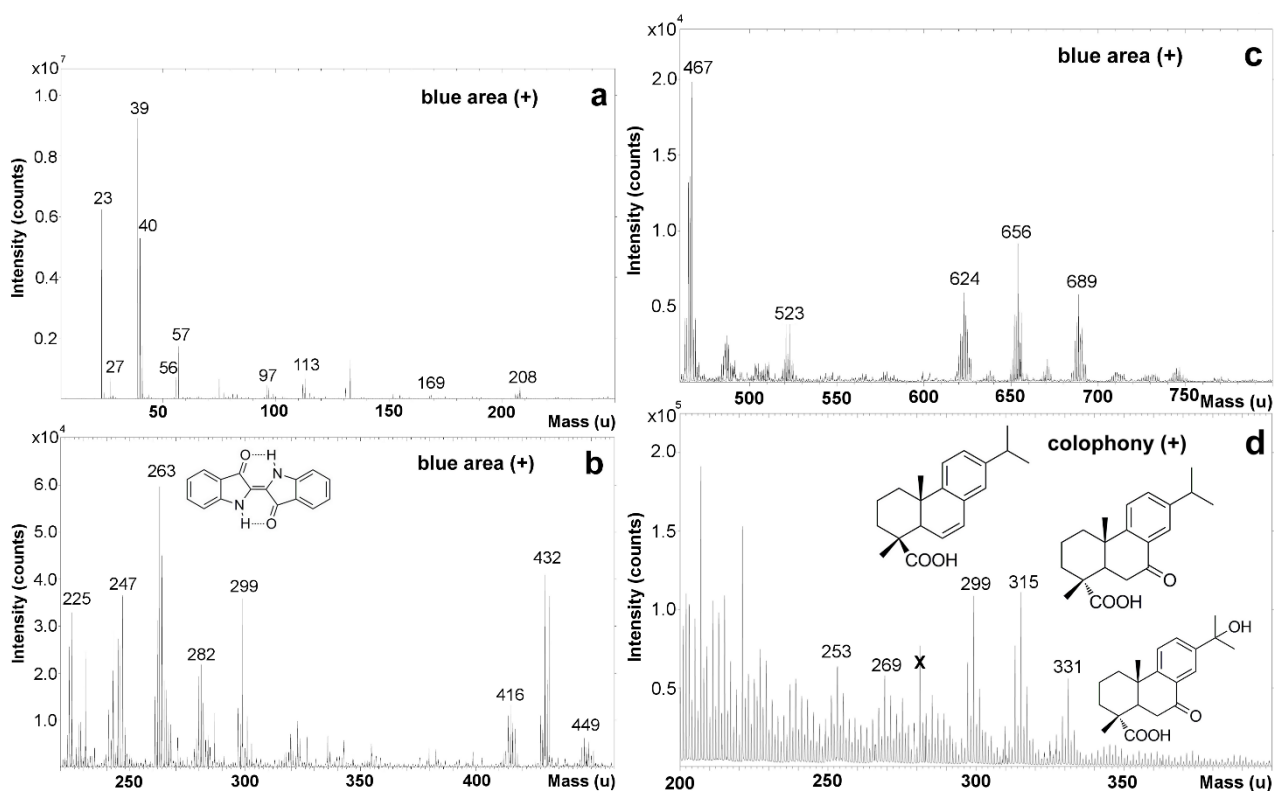


**Figure 3.10.** ToF-SIMS spectra in positive mode of sample 1 (a,b,c) and fresh colophony reference sample (d).

Additional characteristic peaks of fresh colophony reference sample are shown in Fig. 3.10d.  $[M + H^+]$  ions at  $m/z$  299 ( $C_{20}H_{27}O_2$ ),  $m/z$  315 ( $C_{20}H_{27}O_3$ ) and  $m/z$  331 ( $C_{20}H_{27}O_4$ ), each differing from the next by a single oxygen atom, indicate the presence of oxidation products of abietic acid. In particular, the molecular formula of  $C_{20}H_{27}O_4$  of the  $m/z$  331 peak was expected to be 15-hydroxy-7-oxo-dehydroabietic acid, oxidation product of 7-oxo-dehydroabietic acid ( $m/z$  315). Therefore, the molecular formula of  $C_{20}H_{27}O_4$  of the  $m/z$  299 peak indicates the lack of the oxo group and the presence of an additional double bond with respect to 7-oxo-dehydroabietic acid.

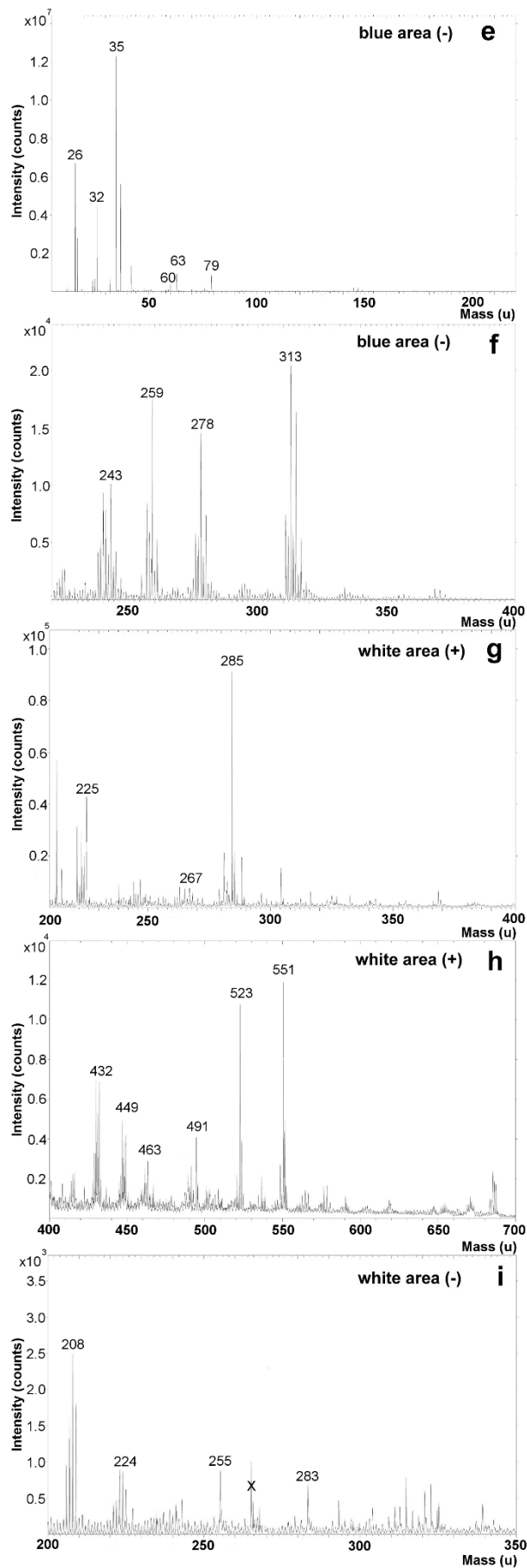


**Figure 3.11.** Negative secondary ion spectra of sample 1 (e,f) and sample 2 (i). ToF-SIMS spectra in positive mode of sample 2 (g,h).

This molecular formula was attributed to  $\Delta^6$ -dehydroabietic acid, dehydration product of 7-oxo-dehydroabietic acid, by Proefke and Rinehart during their studies voted to determine, by using fast atom bombardment mass spectrometry (FAB/MS), the composition of the resinous material recovered from the wrappings of an Egyptian mummy. [164] In addition, two peaks at masses  $m/z$  269 ( $C_{19}H_{25}O$ ) and  $m/z$  253 ( $C_{19}H_{25}$ ) represent a part of the gradual loss process of carboxylic group from the C20 peaks. The negative ion spectrum of sample 1 in the mass range of 0–400  $m/z$  is reported in Figs 3.11e and 3.11f. In the negative ToF-SIMS spectrum ions indicative of elements and fragments, such as phosphorus ( $m/z$  31), sulfur ( $m/z$  32), chlorine ( $m/z$  35), carbonate ( $m/z$  60), cluster of lead oxides and hydroxides ( $m/z$  224, 240, 463 and 687) were observed, together with ions indicative of proteinaceous components and phosphate-containing compounds at  $m/z$  26 ( $CN^-$ ),  $m/z$  63 ( $PO_2^-$ ) and 79 ( $PO_3^-$ ).

The  $m/z$  200–400 region of negative ion ToF-SIMS spectrum shown in Fig. 3.11f is dominated by the peaks at  $m/z$  313, 278, 259 and 243. In the negative ion mode, the 20 carbons of diterpenoids could be represented by the peak at  $m/z$  313 in the molecular formula of  $[M-H]^-$ , corresponding to 7-oxo-dehydroabietic acid. The constant mass loss in these compounds suggests a fragmentation or rearrangement process leading to the additional peaks at  $m/z$  278, 259 and 243. Sodhi et al.[121] considered ambers and standards (abietic acid) ToF-SIMS spectra, obtained in negative polarity mode, more interpretable in terms of identifying major peaks. On the contrary, in the present study, the colophony deposited onto glass surface does not provide in this mass range satisfactory negative secondary ion spectra. Signals consistent with the presence of colophony (data not shown) were observed also in the positive ion SIMS spectra from the gold varnish portion of sample 2 (Fig. 3.9d, area B). A more detailed ToF-SIMS characterization of natural diterpenic resins will be presented elsewhere. The other point of analysis corresponds to a lead white portion over the gold varnish area of sample 2 (Fig. 3.9d, area A). Fatty acids, fatty acid soaps and ions from aliphatic chains of fatty acid moieties were observed (Figs 3.11g and 3.11h) as well described by Boon.[83] Spectra obtained by using cluster SIMS in positive mode still show the peaks of lead, lead oxides and lead hydroxides.

In addition in areas where varnish cracks have left the silver surface unprotected, thus more exposed to oxidation damage, cluster of silver ( $m/z$  107, 214, 321, 428 and 535), silver oxides ( $m/z$  355 and 573) and silver chlorides ( $m/z$  250 and 395) was detected (data not shown). In the lead white area, characteristic positive ion peaks representative of the binding media were observed. Protonated stearic acid ( $m/z$  285), its acylium ion ( $m/z$  267) and lead soaps of palmitic ( $m/z$  463) and stearic acids ( $m/z$  491) were detected (Figs 3.11g and 3.11h). Furthermore, characteristic peaks of oil paint in this sample are represented by diacylglycerols of palmitic acid ( $m/z$  523 and 551). In the negative SIMS spectrum of the white area of sample 2, the presence of free fatty acid was confirmed by the signals of deprotonated palmitic ( $m/z$  255) and stearic ( $m/z$  283) acids (Fig. 3.11i). The FTIR study performed on samples 1 and 2 confirmed results obtained by ToF-SIMS. In particular, FTIR analysis of the white portion of sample 2 (Fig.3.9d, area A) shows characteristic bands of lead white ( $3536$ ,  $1400$ ,  $1045$  and  $681\text{ cm}^{-1}$ ), oil ( $2920$ ,  $2852$ ,  $1730\text{ cm}^{-1}$ ) and fatty acid lead soaps (carboxylate band at  $1530\text{ cm}^{-1}$ ) (Fig. 3.14, spectrum A). On the varnish portion (Fig. 3.9d, area B), a FTIR spectrum was obtained (Fig. 3.14, spectrum B) very similar to the reference colophony. More pronounced C–H bands at  $2920$  and  $2852\text{ cm}^{-1}$  indicate the presence of oil.

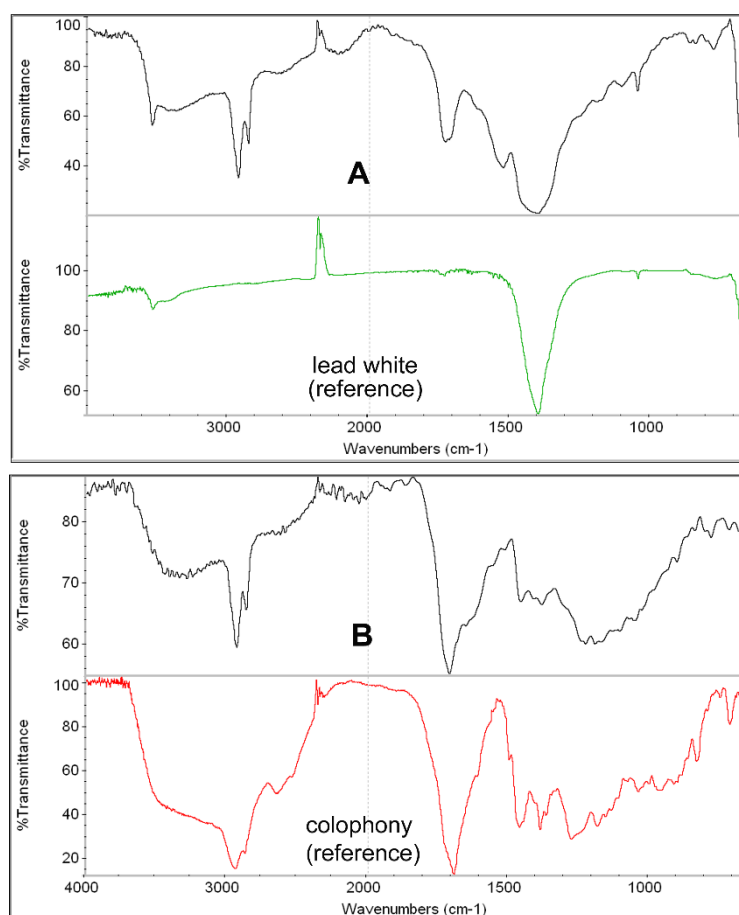


**Figure 3.1.** Micro-FTIR spectra of sample 2 compared to reference spectra. (A) White portion: reference lead white and (B) gold varnish portion: reference colophony

### 3.2.4 Conclusions

This work confirms the potential of cluster SIMS as an analytical tool to study paint sample containing oil, dyes and resins. This was applied to the characterization of two scraped fragments of a gilt and painted leather artifact. ToF-SIMS analyses proved the presence of indigo to depict blue petals of the flowers. Lead white in an oil binder was employed to depict white areas as resulted by the presence of palmitic and stearic acids signals with their diacylglycerols, lead soaps, lead oxides and hydroxides. The comparison of positive ion spectra of indigo paint and gold varnish sample areas with those taken from standard samples of natural resins suggested the presence of colophony. Additionally, a more exhaustive interpretation of colophony ToF-SIMS results was reported. Silver chlorides, oxides and sulfides were detected where the silver leaf was not covered by the gold varnish. Results obtained by ToF-SIMS integrate and complete data obtained by other analytical techniques. Work is still in progress to complete the characterization of the painting materials.

### 3.3 Gilding decoration on stone: the case of Etruscan cinerary urn

#### 3.3.1 Introduction

A sample coming from an Etruscan cinerary urn belonging to the funerary hypogeum complex of Cacni family of Perugia (Italy) [173], was investigated. The precious findings are dated from III to I century before Christ. The entire complex is constituted by more than twenty exemplars and represent the employ of different execution techniques: from the aged and simplest boxes, finished with stucco, to urns decorated with high-low reliefs and paintings. Almost all urns have an inscription with the name of the deceased, which has allowed to rebuild the Cacni's family tree. The cinerary urn object of this study, is built of travertine blocks and decorated with low and high reliefs. The artwork was enriched with colors and gildings, whose residues are still present on the artifact surface (Fig. 3.13). The cross section obtained from the inclusion of the sample in polymeric resin, represents a portion of gilding. The sample initially observed at the optical microscope, was then analyzed by using SEM-EDS and ToF-SIMS techniques.

Preliminary SEM-EDS analysis was performed on cross-section in order to discriminate the layers composing the stratigraphy. ToF-SIMS was used to detect and map both molecular and elemental species related to the gilded decoration. In particular, the study was focused to identify the adhesive medium of the gold leaf, finding the evidence to define the procedure adopted in ancient time for the gilding of stone artworks. The results obtained could shed light on the use of organic compounds as adhesive since Etruscan time.

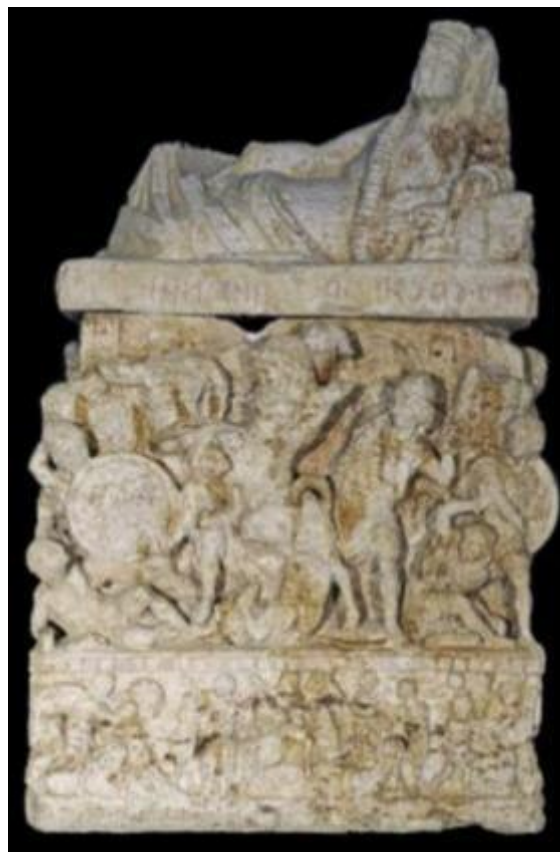


**Figure 3.13.** Etruscan cinerary urn from which the sample studied was collected.

### 3.3.2 Materials and methods

The investigation was carried out on a cross section taken from the gilded portion of the urn during a restoration operation. The sample is made up only of the gold foil and the gilding preparation layer. The sample was observed with an optical microscope under visible and ultraviolet light (Olympus AX70 equipped with Hg short arc HBO lamp, Olympus, Tokyo, Japan) and at a later time was glued onto a SEM stub immediately before introducing it into ToF-SIMS load lock. Scanning electron microscopy with X-ray micro analysis measurements were performed using a Zeiss EVO 60 (ZEISS EVO 60, Carl ZEISS SMT, Germany), an environmental scanning electron microscope, equipped with an INCAX-sight dispersive X-ray spectrometer (Detector 7636 Energy EDS, Oxford Instruments, Palo Alto, CA) for elemental characterization of the samples. The analyses were carried out at pressure of 100 Pascal without a conductive coating. Secondary ion mass spectrometry analyses were performed with TOF-SIMS V (ION-TOF GmbH, Münster, Germany) equipped with a Bi liquid metal ion gun. A 30 keV  $\text{Bi}_3^{2+}$  ion beam was selected with an incidence angle of  $45^\circ$  operating in the high mass resolution bunched mode. The ion beam was rastered over an area of  $200 \times 200 \mu\text{m}$  with an ion dose density below the static limit ( $10^{-12}$  ion/ $\text{cm}^2$ ). Charge neutralization was obtained by using low-energy electrons supplied by a pulsed flood gun. Both positive and negative polarity spectra and images ( $1024 \times 1024$  pixels) of elements and molecular fragment distribution were recorded. All secondary ion images were normalized to the total ion image and filtered with an averaging filter in order to remove topographical effects, and salt-and-pepper noise.

### 3.3.3 Results and discussion

In the visible light image of cross section are clearly identify the layer of gold leaf and the preparation layer (Fig 3.14a). In the sample observed under UV light, no fluorescence was observed (image not shown). This evidence could represent an indicator of the absence of an oily compound in the binding media used for the gold lamina. SEM-EDS analysis confirm the presence of a pure gold leaf on the top of the cross section. In addition, EDS maps of Al, Si, and Fe suggests that gold leaf was deposited over a ochreish layer. Furthermore, the presence of calcium below the ochre layer hypothesises the use of a white lime-based preparative layer (Fig. 3.14). The detection of inorganic elements in SEM-EDS analysis, have found confirm in the results obtained from ToF-SIMS measurements. In the Fig. 3.15, are shown the positive ion maps of the element composing the ochre. The distribution of aluminium ( $m/z$  27), silicon ( $m/z$  28) and iron ( $m/z$  56) ions was mapped in correspondence of the gilding preparation layer. Furthermore, the positive ion mass spectra showed the distribution of aliphatic chain fragments  $[\text{C}_n\text{H}_{2n-1}]^+$  ( $1 \leq n \leq 5$ ) (Fig. 3.15c). Their signals are distributed on the total analyzed area, but more concentrated in correspondence of gilding preparation layer. These data along with the detection of a weak signal of  $\text{NH}_4^+$  ( $m/z$  18) in the same area, could belong to a proteinaceous compound used as binding media (Fig. 3.15b). To reinforce this hypothesis, in the negative ion spectrum were recognized the fragments of  $\text{CN}^-$  ( $m/z$  26),  $\text{CNO}^-$  ( $m/z$  42),  $\text{S}^-$  ( $m/z$  32) and  $\text{HS}^-$  ( $m/z$  33) that could be representative for the presence of protein derived from a glue, commonly used in the past practice [12]. Moreover, in the negative ion spectrum was also detected and mapped the gold ion,  $\text{Au}^-$  ( $m/z$  197). All the negative secondary ion images of molecular fragments and ions are shown in Fig. 3.16.

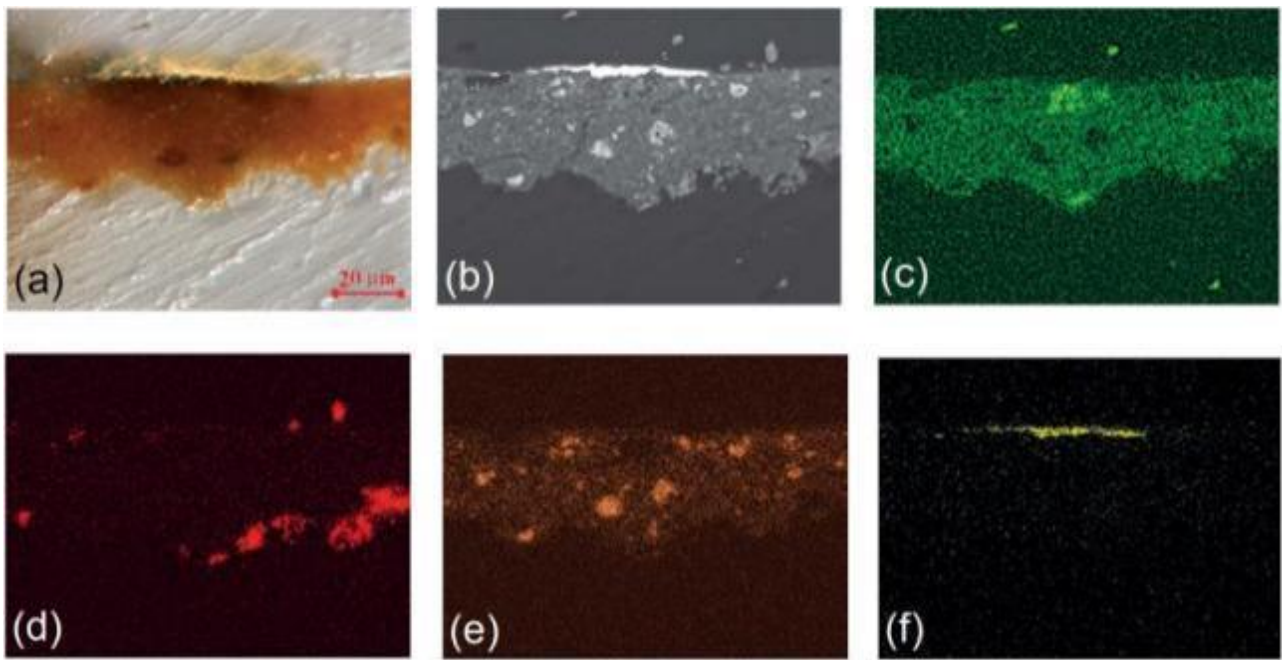


**Figure 3.14.** SEM mapping of main elements found in cross-section. Visible light optical image (a) and back scattered electron image of cross-section (b). X ray maps of silicon (c), calcium (d), iron (e) and gold (f).

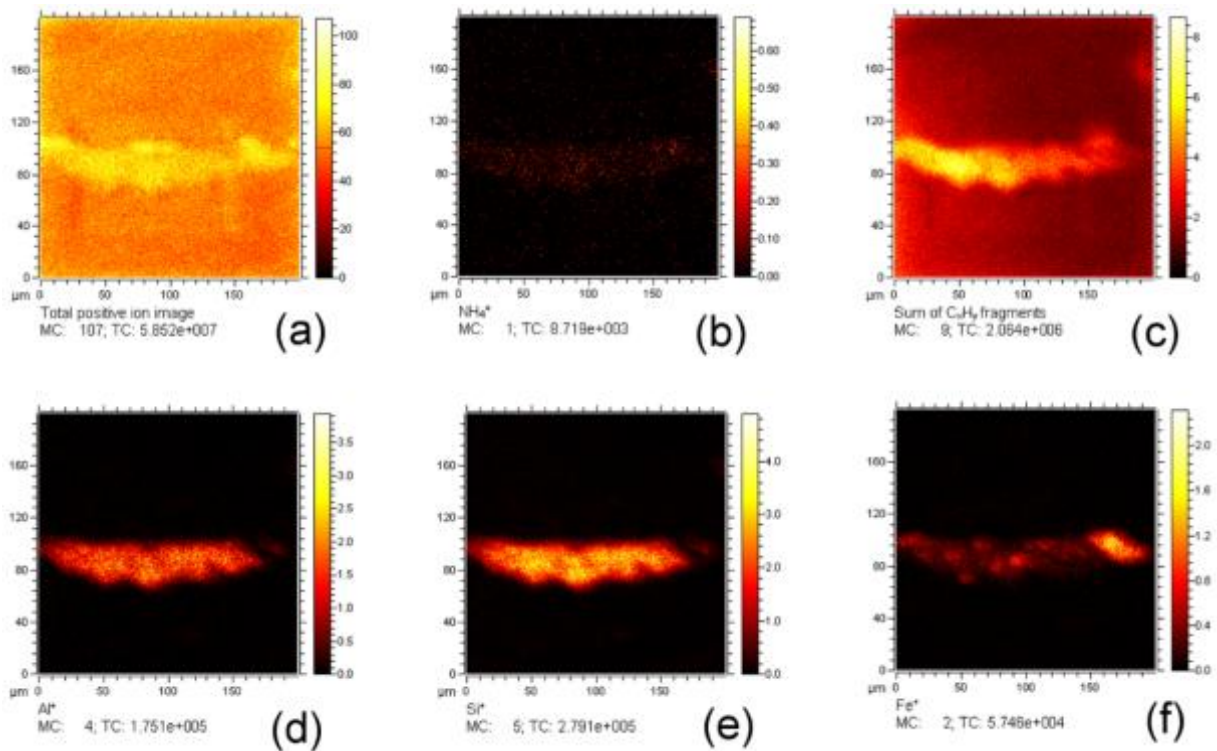


**Figure 3.15.** Main positive ion images detected in the cross section. Total positive ion image (a). The detection of  $\text{NH}_4^+$  (b) and the sum of  $\text{C}_n\text{H}_{2n-1}^+$  fragments (c) identify the presence of a proteinaceous compound in the preparation layer. Aluminium (d) silicon (e) and iron (f) identify the ochre.

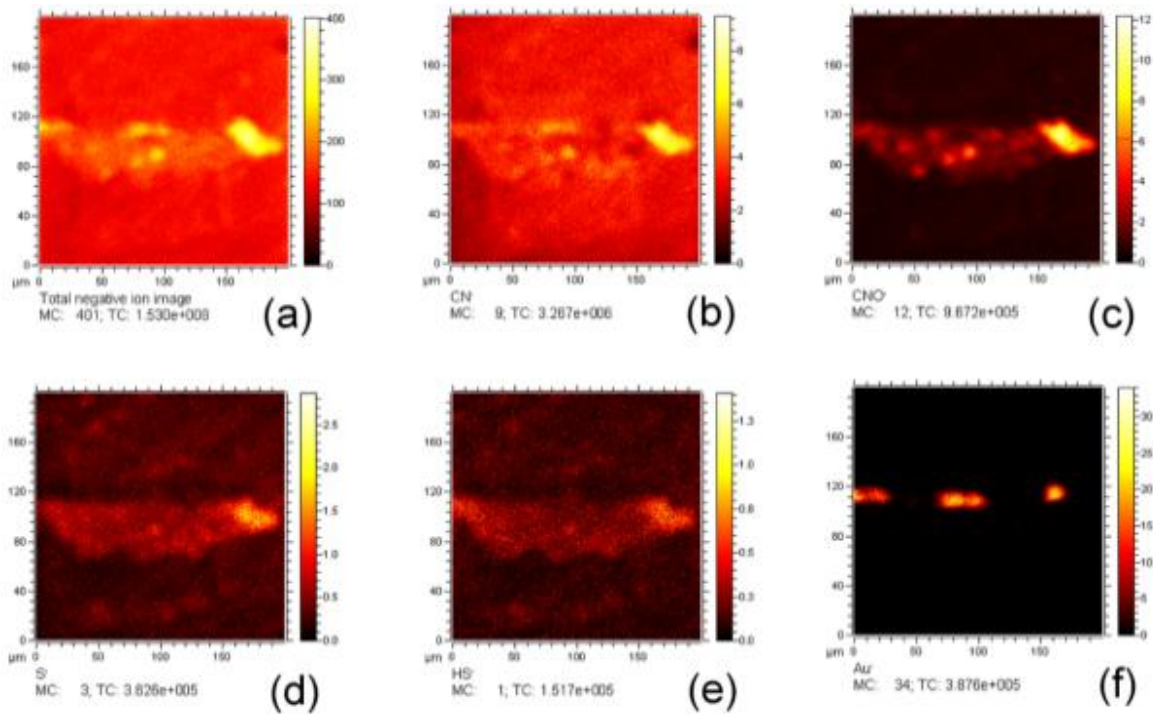


**Figure 3.16.** Main negative ion images detected in the cross-section. Total negative ion image (a). Maps of  $\text{CN}^-$  (b),  $\text{CNO}^-$  (c),  $\text{S}^-$  (d) and  $\text{HS}^-$  (e) could indicate the presence of a proteinaceous compound in the ochreys layer as binding media. The gold leaf was detected on the top of the sample (f).

Furthermore, the detection of a proteinaceous compound could be indirectly identify to the presence of calcium oxalate, a degradation product of calcite in correspondence of calcium distribution in the plaster layer. The calcium ion was mapped in the cross section as residue belonging to the plaster localized between the travertine and the ochreish layer (Fig. 3.17a).

The sum of calcium oxalate molecular ion  $\text{CaC}_2\text{O}_4$  ( $m/z$  128) and calcium oxalate fragments  $\text{CaC}_2\text{O}_3^+$  ( $m/z$  112),  $\text{CaC}_2\text{O}_2^+$  ( $m/z$  100),  $\text{CaC}_2\text{O}^+$  ( $m/z$  88),  $\text{CaC}_2$  ( $m/z$  64)  $\text{CaC}^+$  ( $m/z$  52) is mapped in positive secondary ion imaging and shown in Fig. 3.17 along with the positive ion map of calcium ion ( $\text{Ca}^+$ ,  $m/z$  40). This product could be formed by the reaction of degradation of proteinaceous compound mixed in ochre layer in contact with the calcium carbonate underlying. Furthermore, the presence of calcium compounds fragments could also likely belong to calcium containing adhesive, as casein, but its identification has not been proven. In addition, no entire molecules to justify the presence of animal glue were found. Thus, considering the aging of the artwork is plausible hypothesize the degradation of proteins structure, which does not make an identification unambiguous of entire molecule.

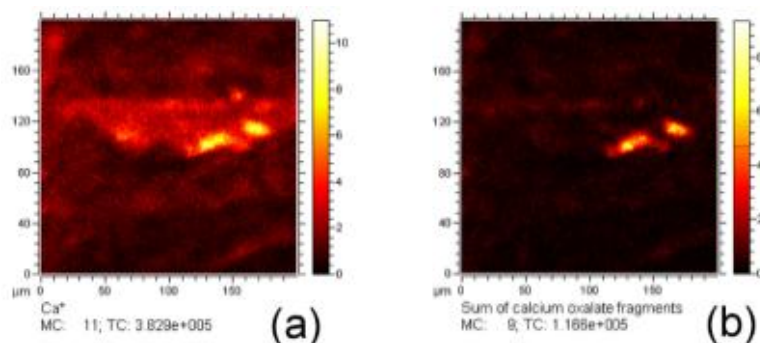


**Figure 3.17.** Positive ion maps of calcium (a) and calcium oxalate detected in the same area (b).

### 3.3.4 Conclusion

The Etruscan urn was studied coupling SEM-EDS and ToF-SIMS analysis. The peculiarity of ToF-SIMS technique to detect and map inorganic and organic compounds in the same run of analysis, was exploited to chemically characterize the sample collected from the archaeological finding. The results have confirmed the elemental distribution of inorganic compounds long the preparatory layer and the gilding preparation. The ochreish layer was applied to prepare the stone to the decoration with the gold leaf. The choice of this type of material and colour was generally adopted to give a warm effect below the decoration. The binding media in the ochre mixture was recognized as a proteinaceous based adhesive, probably derived from animal glue. The detection of amide group in the layer below the gold decoration, along with the alteration of the calcite layer in calcium oxalate, suggest the use of a proteic glue as binder. A specific recognition of type of proteins in the adhesive mixture has not been possible. Due the antiquity of the artifact, it seems plausible not to find these organic molecules perfectly preserved.

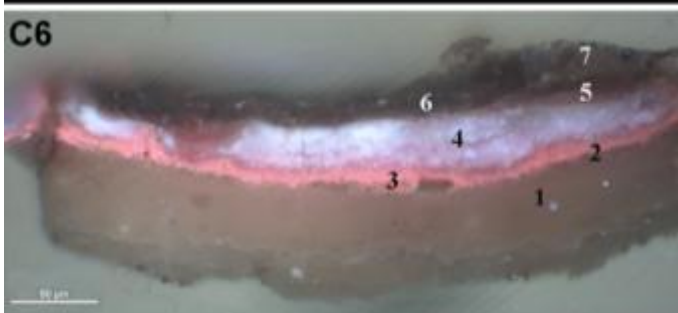
## 3.4 Saint Wilgefortis Triptych by Jheronimus Bosch

### 3.4.1 Introduction

As described until now, ToF SIMS is a valuable tool for cultural heritage studies, especially when used in conjunction with established analytical techniques in the field. Potentiality of chemical imaging of the 2D distribution of molecules in the same region of mass spectra acquisition represents a powerful feature in the domain of cultural heritage materials for also the better understanding the artistic procedure of the painters. The recent restauration of Jheronimus Bosch's masterpieces in occasion of *Bosch Research and Conservation Project* has permitted the knowledge of Flemish master technique and the state of conservation of his paintings [174]. In particular, the investigated artwork in this study represents an extraordinary example of paint on wood. The analyses were performed on the triptych entitle *Saint Wilgefortis Triptych*, exhibited at Gallerie dell'Accademia in Venice and described as an oil on oak. The analyses were realized on two cross-sections coming from the red dresses of two male figures (samples C6 and C7). Preliminary investigation with optical microscopy under visible and ultraviolet light, SEM-EDX and micro-Raman spectroscopy were conducted on the samples in occasion of the restoration phase, but the data will not shown in this thesis, these data are to be published. ToF-SIMS analyses were performed operating in delayed extraction of secondary ions, that permit to combine sub-micrometer spatial resolution mass spectrometry images at the surface of the sample together with high mass resolution in the same acquisition run. The potential of delayed extraction mode in order to discriminate very small region in a painting cross-section was recently employed, providing precise chemical information on the spatial distribution of the different compounds and to detection of metal soaps [175].

### 3.4.2 Materials and methods

The artwork of *Saint Wilgefortis Triptych* is composed of three oak panels. During a past restoration, some micro samples were collected in order to perform cross-sections. All the painting samples were embedded in a polyester resin. Two of them (samples C6 and C7) were the samples investigated here and both were collected from red areas, nearness of lacunas. The sample C6 was obtained from the red dress of male figure in foreground to the right on the central panel. The second cross-section, sample C7, was collected from the red sleeve of the soldier depicted on the right wing of the triptych (Fig. 3.18a). The main chemical characterization study of the samples presented in this work was carried out with time of flight secondary ion mass spectrometry. The ToF-SIMS experiments were performed with a TOF-SIMS V mass spectrometer (ION-TOF GmbH, Munster, Germany) equipped with a bismuth liquid metal ion gun. A 30 keV  $\text{Bi}_3^{++}$  ion beam was selected with an incidence angle of  $45^\circ$ . The emitted secondary ions were accelerated to a kinetic energy of 2 keV toward field-free region. Secondary ion were post-accelerate to a kinetic energy of 10 keV before hitting the detector composed of a micro-channel plate, a scintillator and a photomultiplier. Charge neutralization was obtained by using low-energy electrons supplied by a pulsed flood gun. The extraction voltage was set to 1 kV and the delay time was 1.1  $\mu\text{s}$ , operating in high mass resolution bunched mode. Delayed extraction acquisition mode was successfully employed to characterize artwork samples [89]. The consequences mass and spatial resolutions of  $\text{Pb}^+$  ion peak were 3,5 and 0,5  $\mu\text{m}$  respectively. The ion beam was rastered over an area of  $200 \times 200 \mu\text{m}^2$  with an ion dose density below the static limit ( $10^{-12}$  ion/ $\text{cm}^2$ ). Both positive and negative polarity spectra and images (512 x 512 pixels) of elements and molecular fragments distributions were recorded.



- Grayish layer - 7
- Trace of red lake - 5
- Cinnabar - 3
- 6 - Varnish
- 4 - Lead white and red lake
- 2 - Trace of black pigment in an organic media
- 1 - Preparation layer



- Degradation product - 6
- Varnish - 4
- Lead white layer - 2
- 7 - Retouch
- 5 - Red layer with cinnabar
- 3 - Black layer with lead white
- 1 - Preparation layer

**Figure 3.18.** Bosch's Saint Wilgefortis Triptych with sampling areas of samples C6, C7, (a). Figs. b and c show the optical microscopy images of cross section under UV light and the graphic outline of samples C6 and C7, respectively.

All secondary ion images shown were normalized to the total ion image and filtered with an averaging filter in order to remove topographical effects, and salt and pepper noise. Mass spectra were internally calibrated using  $C^+$ ,  $CH^+$ ,  $CH_2^+$ ,  $CH_3^+$ ,  $C_2H_2^+$ ,  $C_2H_3^+$ ,  $C_2H_5^+$ ,  $C_3H_5^+$  in positive ion mode and  $C^-$ ,  $O^-$ ,  $OH^-$ ,  $C_2H^-$ ,  $C_3^-$ ,  $C_3H^-$  in negative mode, respectively. The data were acquired and processed using the SurfaceLab 6.4 software (ION-TOF GmbH, Munster, Germany). Initially, for each cross-section will be summarized the preliminary results obtained with the other analytical techniques during the restoration phase, but only the data concerned the ToF-SIMS analysis will be shown.

### 3.4.3 Results and discussion

#### *Cross-section C6 preliminary results*

The preliminary UV and VIS optical microscopy observations of the sample C6 have identify the presence of seven layers (Fig. 3.18b). SEM-EDS and micro-Raman analyses have supplied specific information regarding the elemental distribution and the class of organic compounds present in the stratigraphy as well as the presence of different degradation products. As shown in the graphic outline present in Fig. 3.18b, starting from the bottom the sample presents the first preparatory layer in which calcium carbonate and protein-based glue were recognized. Moreover, Raman-spectroscopy have also identify the presence of weddellite ( $CaC_2O_4 \cdot 2H_2O$ ) a common degradation product of protein. The remaining six layers of the pictorial layer are constituted of a very thin oil-based isolating layer (second layer) and a succession of reddish and pinkish layers covered by a varnish layer, presumably. The first red layer (third layer) was identify as cinnabar and the pinkish superimposed layer (fourth layer) was recognized as lead white in which some red lake particles are dispersed. The last reddish layer (fifth layer) probably appears to be made of a red lake hint. In the sixth and seventh layers were recognized a varnish and a grey alteration, respectively. The nature of the varnish and the binding media of the painting have not been clearly identified with the analytical techniques cited, except to the protein in the ground layer. In particular, the presence of lead soap detected with Raman spectroscopy in the lead white layer hypothesize an oily binder (data not shown). Afterwards the ToF SIMS results will be illustrated clarifying the present of organic compounds in the cross section.

#### *Cross section C6 ToF-SIMS results*

ToF-SIMS analyses of the C6 cross section have confirmed the compounds of preparatory first layer based on proteinaceous binder and calcite. In order to characterize the preparation in the sample, calcium containing ions were tracked in the positive and negative mass spectra (Figs. 3.19a and 3.19f). The presence of  $CaCO_3$  was confirmed in positive ion mode with the detection of  $Ca^+$ , calcium oxides  $Ca_xO^{x-1}$ ,  $(CaO)_nH^+$  and  $Ca_2O_{n-2}H^+$  with  $2 \leq n \leq 14$  (Fig. 3.19b) and calcium carbonate fragments  $CaC^+$ ,  $CaCO^+$ ,  $CaCO_2^+$  and  $CaCO_3^+$  (Fig. 3.19c). Furthermore, calcium oxide ( $CaO^-$ ) and carbonate group ( $CaCO_3^-$  and  $CO_2^-$ ) were recorded in negative ion mode (Fig. 3.19h). The characterization of proteinaceous binder was possible to the identification of  $NH_4^+$  fragment in positive ion mode (Fig. 3.19e) and the detection of  $CN^-$ ,  $CNO^-$  and the trace of  $HS^-$  ions in negative polarity (Fig. 3.19g). No fragments belonging to the amino acids characterizing the animal glues were recorded in the positive ion mass spectrum, expect for the  $NH_4^+$  ion [176]. This could be due to the degradation of the protein molecules over the time. In addition, the presence of weddellite recognized with the Raman spectroscopy (spectrum not shown) is confirmed with the identification

of calcium oxalate fragments,  $\text{CaC}_2\text{O}_4^+$  and  $\text{CaC}_2\text{O}_3^+$ ,  $\text{CaC}_2\text{O}_2^+$  in the positive ion mass spectrum (Fig. 3.19d). The calcium oxalate is generally observed in artworks as a possible transformation of organic materials, usually proteinaceous compounds [12].

According to the detection of calcite and organic components, the thickness of the ground layer estimated to be between 80-100  $\mu\text{m}$ . The map distribution of calcium and organic signals is co-localized not only in the first layer, as was expected to be, but there is also a weak distribution of  $\text{Ca}^+$  and a marked presence of  $\text{CN}^-$  and  $\text{CNO}^-$  groups in correspondence of one of two external painting layers (sixth layer). This evidence could suggest also the use of calcium caseinate, largely diffused in the past restoration practice, but further investigation are needed.

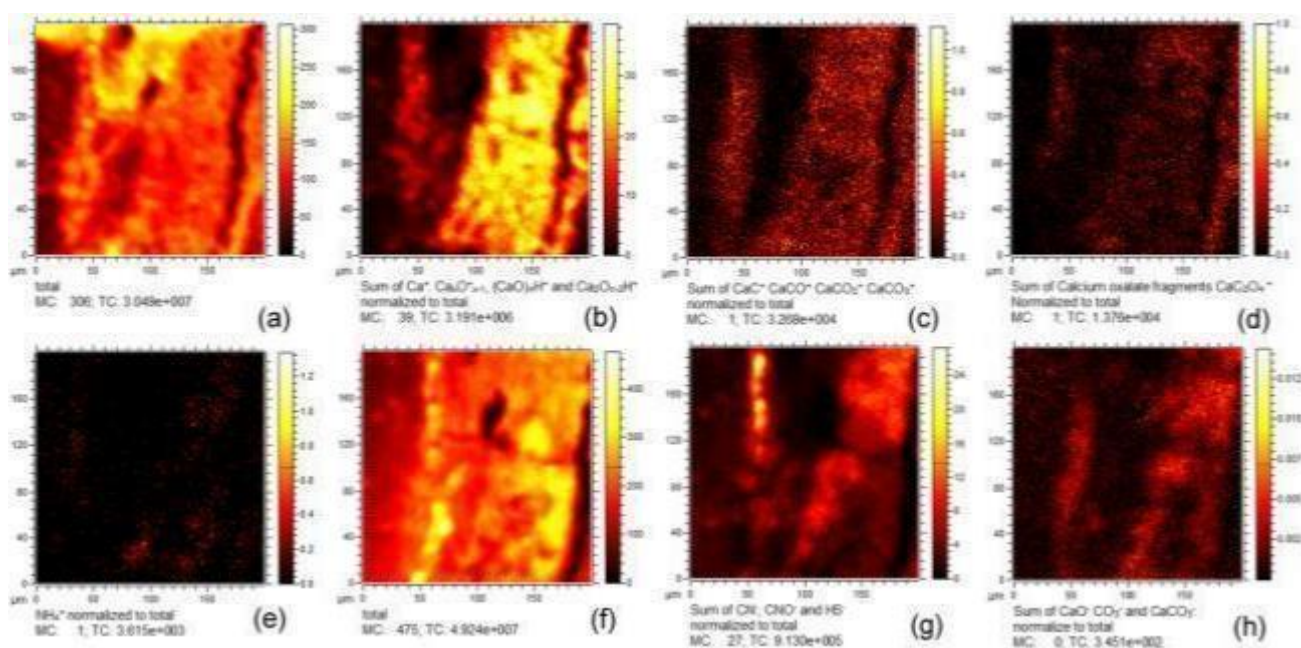


**Figure 3.19.** ToF SIMS results on C6 preparation layer. In Figs. a and f, are shown the total distribution of positive and negative ion maps. Calcium oxides (b), carbonates (c, h) and oxalate (d) confirm the presence of calcite in preparatory layer along with a proteinaceous compound signals mapped in secondary positive (e) and negative ion maps (g).

The characterization of the successive painting layers with ToF-SIMS technique has permitted to confirm origin of inorganic pigment and their degradation products, to identify the organic binder, as well as the recognition of modern polymer. Fig. 3.20 shows the positive and negative secondary ion maps of the main inorganic compounds detected in the pictorial layer. ToF-SIMS analyses carried out on the second cross-section layer did not provide a comprehensive answer to the identification of the black pigment, previously observed by optical microscopic. The distribution of  $\text{C}^+$ , albeit homogeneous throughout the analyzed area, may suggest the use of a charcoal-black (data not shown).

In the third layer the presence of cinnabar ( $\text{HgS}$ ) is confirmed by the distribution of sulfur ions in the red area (Fig. 3.20a). The detection of Hg ion has not been possible due to the degas effect of this element under UHV condition. The thickness of cinnabar layer was measured approximately 10-15  $\mu\text{m}$ .

The fourth layer was previously recognized as lead white. Lead ions, lead oxide cluster ions detected as  $\text{Pb}_n^+$  ( $1 \leq n \leq 6$ ),  $(\text{PbO})_n^+$  ( $1 \leq n \leq 6$ ),  $\text{Pb}_n\text{O}^+$  ( $n=2,3$  and  $4$ ),  $\text{Pb}_n\text{O}_{n+1}^+$  ( $1 \leq n \leq 6$ ),  $\text{Pb}_n\text{O}_{n+1}^-$

( $1 \leq n \leq 6$ ),  $(\text{PbO}_2)_n^-$  ( $n=1$  and  $2$ ) and  $\text{Pb}_n\text{O}_{n+2}^-$  ( $n=3,4,5$  and  $6$ ) confirm this data in positive and negative secondary ion maps, respectively (Figs.3.20b and Fig.3.20d). Furthermore, localized in the same area the presence of lead chloride ions ( $\text{PbCl}^-$ ,  $\text{PbClO}^-$ ,  $\text{PbCl}_2^-$ ,  $\text{PbClH}^-$  and  $\text{PbCl}_2\text{OH}^-$ ) were recorded (Fig. 3.20e). The lead chloride ions detected could belong to the mineral laurionite ( $\text{PbClH}$ ). It occurs as an oxidation product in lead ore deposits, and is also produced on lead-bearing slag by reaction with saline solutions. Besides, the chlorination of lead white could be correlated to the high concentration of chlorides that characterize the atmosphere of the Venetian lagoon. Nevertheless, Noun et al. have recently given an explanation to the chlorine associated with lead white related to a historical method of production of the white pigment, known as *Dutch process* [89].

Could be many reasons to explain the presence of chlorine in painting, so it is not possible to provide a unique answer to this evidence.

In the end, the negative ion map of  $\text{Cl}^-$  is superimposed immediately on of the cinnabar layer (Fig. 3.20f), it could be assumed that part of the chlorine signal was also derived from the alteration of  $\text{HgS}$  in  $\text{Hg}_2\text{Cl}_2$  due to the exposition to a rich chlorides atmosphere [90]. This hypothesis is not supported by the others analytical techniques, that have not revealed the presence of calomelan ( $\text{Hg}_2\text{Cl}_2$ ), but seems the more probable and would justify the presence of chloride ion in lead white layer. The lead-white layer is distributed in the cross-section with a thickness of between 10 and 20  $\mu\text{m}$ .

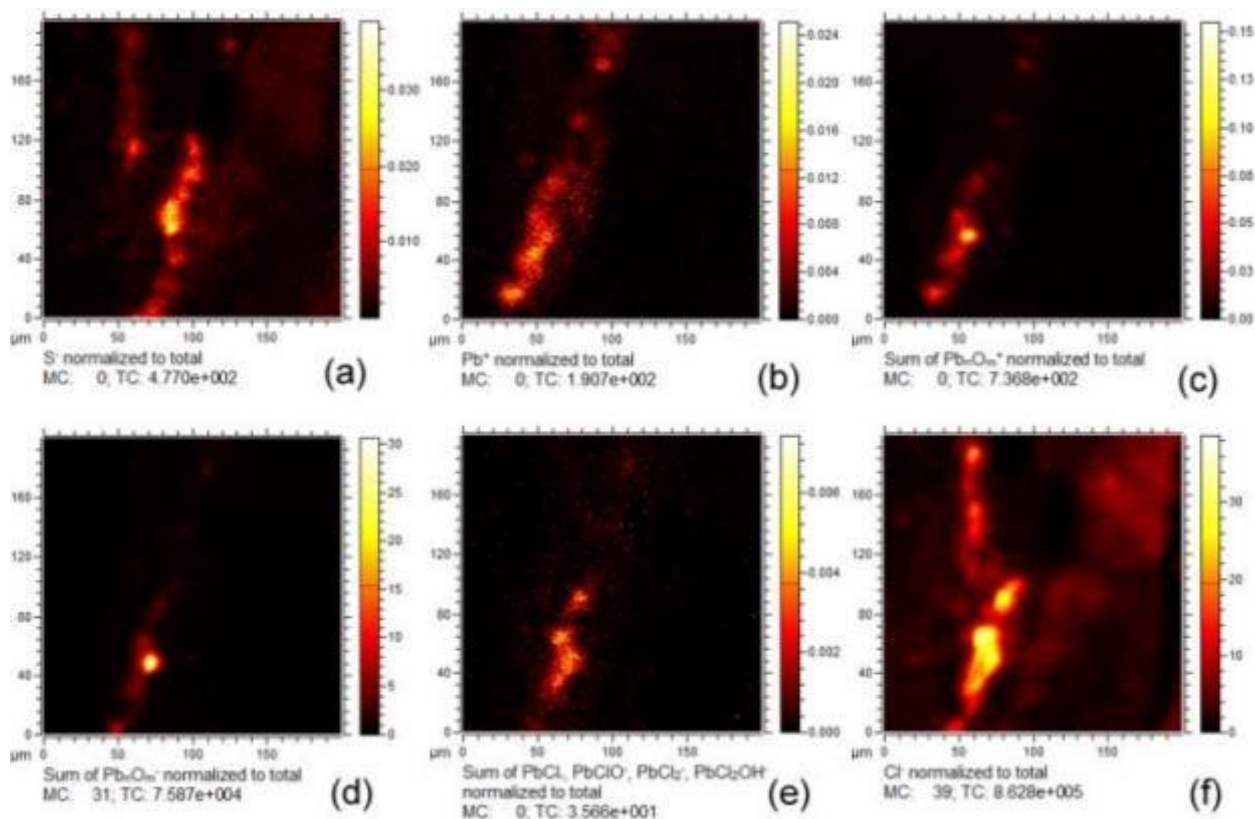


**Figure 3.20.** ToF-SIMS imaging of C6 pictorial layers. Negative maps of sulphur (a) and (f) identify the presence of vermilion ( $\text{HgS}$ ) and its degradation product calomelan ( $\text{Hg}_2\text{Cl}_2$ ) in the third layer, respectively. Positive ion maps of lead (b) and lead oxides (c), along with negative ion maps of lead oxides (d) and lead chlorides (e) identify the lead white layer in the fourth layer.

In the fourth layer of the sample C6, were also detected weak peaks likely belonging to the lead soaps. For verify this signals a region of interest (ROI) was drawn in correspondence of  $\text{Pb}^+$  area,

so as to avoid the matrix effect of the surrounding area and collect the signal coming only from the lead white layer. The Fig. 3.21a shows part of the positive ion mass spectrum of the ROI. In correspondence of  $\text{Pb}^+$  positive ion map (Fig. 3.21b), the sum of positive ion palmitic and stearic lead soaps ( $m/z$  461-463 and 489-491) is recorded (Figs. 3.21c-d). Lead soaps are a buffering problem for the state of conservation of the artworks because they produce cracks, white aggregates and discontinuity on the painting layers, causing aesthetic and chemical damages. Resulting from a long interaction between oil and lead pigments, their revelation identifies the class of binders in which the pigment is dispersed [107-177]. The identification of lead soaps could clarify the type of the oily medium used by Bosch in his masterpiece.

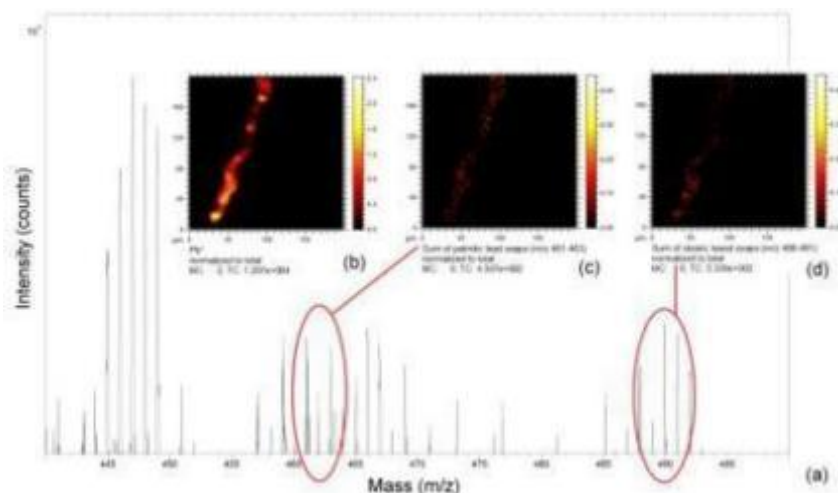


**Figure 3.21.** Lead soaps detection in the fourth layer of C6 cross-section. Positive ion mass spectrum (a) shows two cluster of peaks belonging to palmitate ( $m/z$  461-463) and stearate ( $m/z$  489-491) lead soaps recorded from the ROI drawn on the lead white layer (b). Palmitate (c) and stearate lead soaps (d) fragments correspond on the same area of  $\text{Pb}^+$ .

Fragments ions of fatty acids ( $m/z$  71, 85, 99, 113, 127, 141, 155, 169, 183, 197, 211, 225, 239) were detected and map in all painting layers [84]. This, along with the detection of negative ions of deprotonated myristic ( $m/z$  227), oleic ( $m/z$  281), palmitic ( $m/z$  255) and stearic acids ( $m/z$  283) are indicative of the distribution of the oil binding medium in the paint layers (Fig. 3.22).

The recognition of the type of oil used in the paintings is based on the measurement of the relative amounts of palmitic and stearic acid (P/S). The use of ToF-SIMS technique was successfully adopted for the identification of oil nature in individual layers of paintings cross section [119]. A P/S ratio lower than 2 suggests the presence of linseed oil in the layers. A ratio larger than 5 could identify the use of poppy seed oil in the artwork and the intermediate ratio could suggest the presence of walnut, poppy seed oil or mixtures of them. The P/S ratio calculated for the painting layers, ranging from 1.07 to 1.2, indicating the use of linseed oil. The pictorial medium seems to be the same throughout the cross-section.

ToF-SIMS investigations aimed at the recognition of red lake dispersed in the lead-white layer and in the fifth layer, did not produce a satisfactory result. Some peaks detected in negative ion mass spectrum ( $m/z$  240, 223 and 206) could hypothesize the presence of Alizarin in the cross-section (data not shown). A univocal identification of the dye cannot be certain because in the same layer  $\text{Pb}_n\text{O}_m^-$  negative ions were co-localized. Lead oxides own molecular weights very similar to the possible fragments of alizarin and could cover the weak organic dye signals by matrix effect.

Overlapped to the fifth layer, the sixth layer was identified as an animal glue, possible linked to a past restoration thanks to the distribution of  $\text{Ca}^+$  and  $\text{CN}^-$  and  $\text{CNO}^-$  groups in the positive and negative ion maps (Fig. 3.19). In correspondence of external layer (seventh layer), siloxane compound fragments were observed. The PDMS is known in ToF-SIMS studies as one of the main contaminant species [178]. In this case the distribution of the recorded signals was map along the last layer. Moreover, part of the signals seems apparently penetrate into the early layers of the painting. The sum of these fragments ( $\text{Si}^+$ ,  $\text{SiH}^+$ ,  $\text{SiCO}^+$ ,  $\text{SiCHO}^+$  clusters) is shown in Fig. 3.23. The thickness of polymer layer was measured 10-20  $\mu\text{m}$ , approximatively.

In the 1980s, the use of silicon based products has began to spread as consolidating in stone works [179]. With the aim of preserving works of art, it seems plausible that these products have been experimented or adapted to paintings on wood. The recognition of siloxane compound could derive to a past operation of restauration even if the use of these compounds in paintings is unusual. Given the nature and sequence of the overlapping of the last two layers (sixth and seventh), it is plausible to presume that two distinct conservative interventions have taken place in years apart from each other, or hypotize a rehash of the author on the artwork.

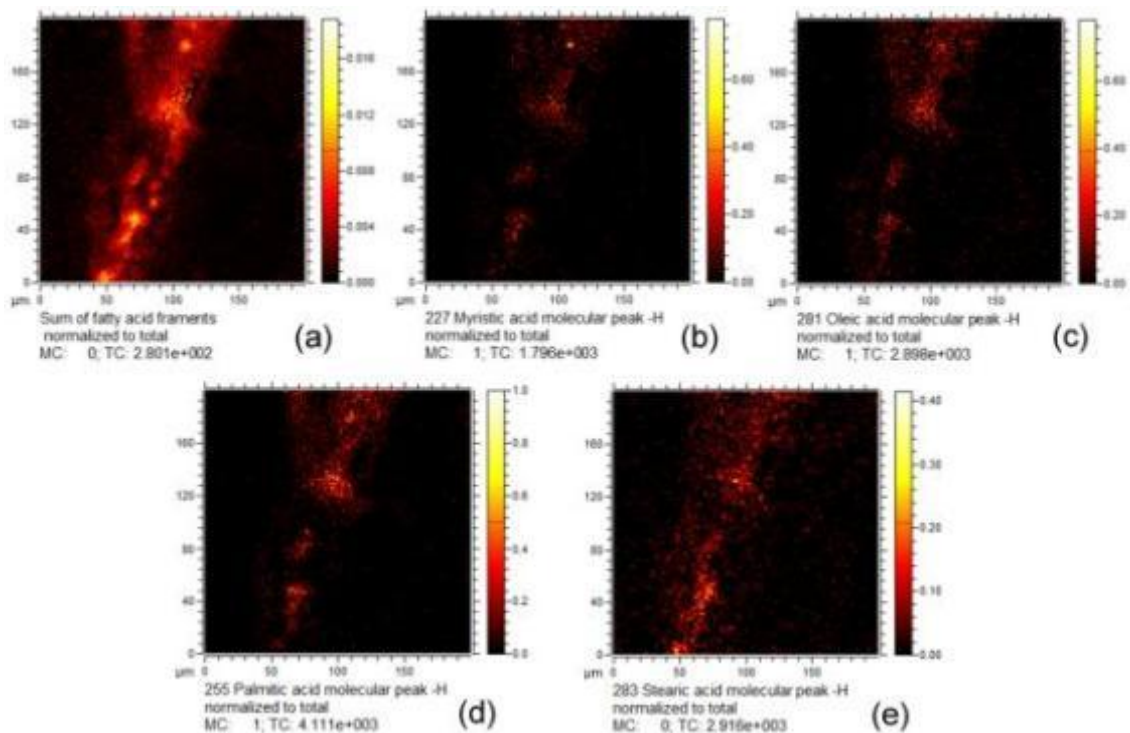


**Figure 3.22.** Negative ion images of fatty acids detected in the C6 cross-section. In figure 5a are summed the deprotonated molecular ion of myristic (b), oleic (c), palmitic (d), and stearic acid (e).

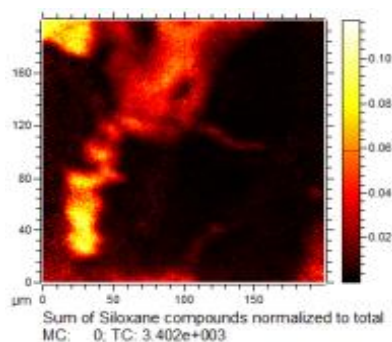


**Figure 3.23.** Positive ion mapping of PDMS fragments detected in C6 cross section.

### *Cross-section C7 preliminary results*

In this sample, have been also identify the presence of seven layers. The graphical scheme of the each layer is shown in Fig 3.18c. As observed in the C6 cross-section, preliminary analyses identify in C7 sample a first layer composed of  $\text{CaCO}_3$  and proteinaceous binder. In the second layer lead white was identified. Moreover, lead white and charcoal-black were detected in the third layer. For both layers, an oily binder was assumed. A layer of varnish appears to constitute the fourth layer, no identification of its nature was provided by the Raman analysis. Red pigment (fifth layer) was identified as cinnabar. Furthermore, the presence of calomelan ( $\text{Hg}_2\text{Cl}_2$ ) was detected in the sixth layer, attributed to the  $\text{HgS}$  chemical alteration. In the final layer (seventh layer) was hypotized the presence of a painting retouch.

### *Cross section C7 ToF-SIMS results*

In the positive mass spectrum of cross-section C7, calcium ion, calcium oxide and hydroxide were detected. Moreover, the presence of  $\text{CN}^-$  and  $\text{CNO}^-$  groups recorded in the negative mass spectrum and mapped in the same area of calcium adducts, has confirmed the use of proteinaceous compound as binder in the preparation layer along with the  $\text{CaCO}_3$  used as inert (Fig. 3.24). According to the detection of calcite and organic components, the thickness of the ground layer was estimated to 100  $\mu\text{m}$ . In the second and third layers, the only presence of lead-white was detected. ToF-SIMS analysis have not found signals attributable to the charcoal-black revealed with the other analytical techniques in the third layer. The distribution of  $\text{Pb}^+$  ion and lead oxide cluster ions  $(\text{PbO})_n^+$  ( $1 \leq n \leq 6$ ),  $\text{Pb}_n\text{O}^+$  ( $n=2,3$  and  $4$ ),  $\text{Pb}_n\text{O}_{n+1}^+$  ( $1 \leq n \leq 6$ ),  $(\text{PbO}_2)_n^-$  ( $n=1$  and  $2$ ) and  $\text{Pb}_n\text{O}_{n+2}^-$  ( $n=3,4,5$  and  $6$ ) are shown in Fig. 3.25, in positive (Figs. 3.25a-b) and negative (Fig. 3.25c) polarity, respectively. Unlike sample C6, in this case no signals belonging to lead metal soaps were found. This could depends to a different ratio between the oil binder and the white pigment in that specific fragment. Furthermore, it is not excluded that the triptych, was dismantled and stored in different location during the past, but further information about the history of its conservation conditions are needed.

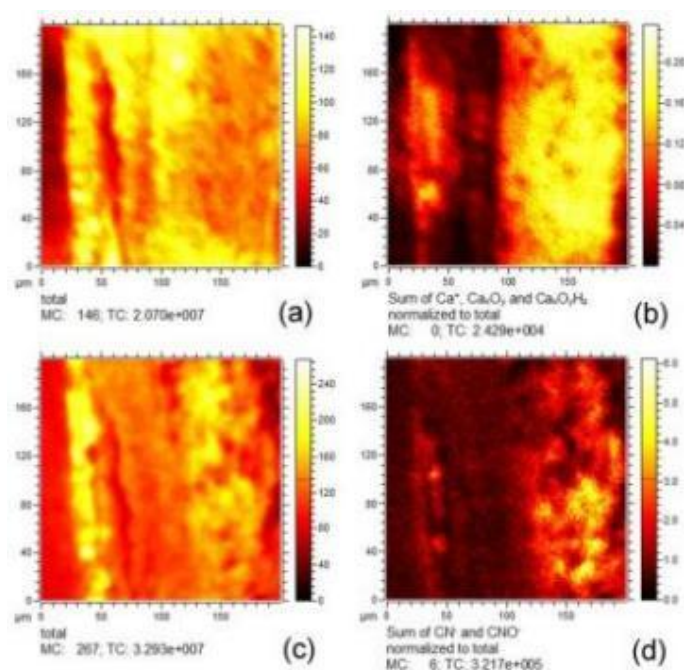


**Figure 3.24.** ToF-SIMS imaging of C7 cross-section. Positive and negative ion maps of the area analyzed (a-c). Calcium oxides (b) and cyanate group (d) characterize the preparatory layer.

The total thickness of second and third layers was calculated to be about 20  $\mu\text{m}$ . Lead oxides clusters were noticed on the surface along with the cinnabar pigment. This could suggest the use of lead white pigment in the mixture. The reddish fifth layer was recognized as cinnabar, thanks the detection of  $\text{S}^-$  ion (Fig. 3.25d). Furthermore, in correspondence of the sixth layer the investigations have recognized chlorine ion (Fig. 3.25e) associated with the sulphur ion. The Fig. 3.25f shows the superimposition of  $\text{Cl}^-$  and  $\text{S}^-$  ions, confirming the presence of calomelan ( $\text{Hg}_2\text{Cl}_2$ ) as degradation product of cinnabar ( $\text{HgS}$ ) as previously assumed by observations to the optical microscope. The thicknesses of cinnabar and calomelan layers were estimated to 20 and 15  $\mu\text{m}$ , respectively. No organic compounds signals belonging to the varnish present on cinnabar layer described in the fourth layer were recognized. The signals belonging to the cross-section embedding resin were detected along these pictorial layers, not allowing to clearly identifying the signals of the organic compounds fragmentation, used as painting medium (data not shown). Nevertheless, weak signals likely belonging to fatty acids molecular ions were recorded in correspondence of central layers. In particular, negative mass spectrum shows the presence of peaks at  $m/z$  227, 255, 281 and 283 that could represent deprotonated myristic, palmitic oleic and stearic acids, respectively. The sum of fatty acid deprotonated ions is shown in Fig. 3.26. The P/S ratio calculated (1,2) identify the nature of oil binder as linseed oil, confirming the use of the same binder in all the samples analyzed.

Finally, ToF-SIMS analysis did not indicate the presence of a seventh layer as observed by optical microscopy investigation. The seventh layer previously described as “retouch” seems to be co-localized on the same area of chlorine ion. Furthermore, the distribution of chlorine ions was mapped in the same region of lead area, as seen in C6 sample. This could suggest that the lead-white pigment was mixed with cinnabar, and the detection of chlorine is imputable to the degradation products of cinnabar in calomenlan ( $\text{Hg}_2\text{Cl}_2$ ). In addition, positive  $\text{Pb}^+$  ion, lead oxides cluster and calcium adducts along with negative proteinaceous fragments ( $\text{CN}^-$  and  $\text{CNO}^-$ ) were also recognized in the same region (Figs. 3.24 and 3.25).

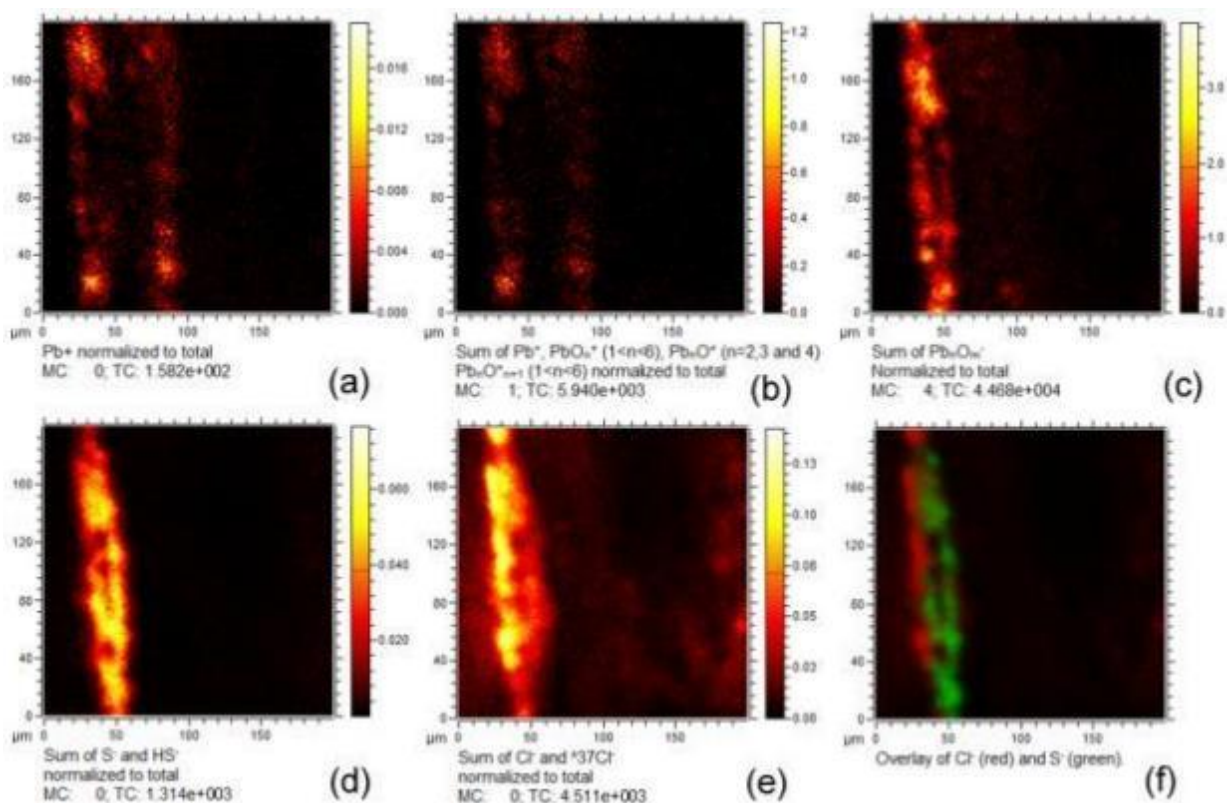


**Figure 3.25.** ToF-SIMS imaging of C7 painting layers. Ion image of  $Pb^+$  (a), positive (b) and negative (c) lead oxides belonging to lead white layer. Sulphur (d) and chloride (e) negative ion maps localize cinnabar and calomelan alteration product. The overlay of these elements is shown in Fig. f.

The detection of calcium and lead ions, could regard the use of pigments composed of these elements blended with cinnabar, in order to compose the reddish shade of the soldier suit. At the same time, the weak detection of protein fragments may belong to a consolidation intervention linked to a past restoration, (as supposed in cross-section C6) or represent the testimony of a glue medium mixed with the inorganic pigments. Nevertheless, it is difficult at the present state of knowledge explain this evidence.

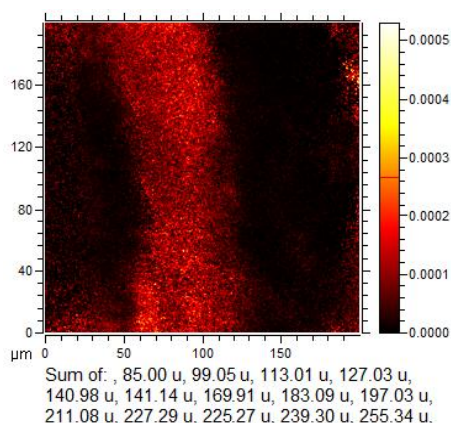


**Figure 3.26.** ToF-SIMS negative imaging sum of fatty acids deprotonated molecular ions, detected in C7 cross-section.

### 3.4.4 Conclusion

The high spatial resolution analysis of a cross-sections from *Saint Wilgefortis Triptych* of Jheronimus Bosch has provided specific chemical information on the spatial distribution of the different components. ToF-SIMS analysis has confirmed preliminary results obtained with the others analytical techniques, like come Scanning Electron Microscopy with Energy Dispersive X-Ray and micro-Raman Spectroscopy for the recognition of mineral pigments and the preparatory layer. Furthermore, the ToF-SIMS feature to analyze in a single run both inorganic and organic compounds in the cross-section, has allowed to identify the nature of oily binder, as well as alterations due to chemical interaction between different compounds in the layers and with surrounding environment. Finally, the investigation has provided evidence of past restorations, likely belonging to two distinct interventions.

## 4 Depth profiling and 3D imaging

ToF-SIMS in dynamic mode is an appropriate analytical technique to study multilayer structures with an accurate depth and lateral resolution. These features were exploited to characterize the nature and the morphology of metallic objects remained under water per centuries, in order to study the chemical interaction between the artifact and surrounding environment in a 3D elements map distribution.

In particular, the case of gilding made with a mercury amalgam on copper metal buckles found during the dredging of Tiber river (Rome) will be presented. In this case, the investigation was conducted by using several analytical investigation techniques, with the aim to obtain a complete overall picture of executive technique, materials, and degradation products. The use of different type of analytical procedures provides useful information for a better understanding the reactions that happened in this systems in which different materials were in contact for century each other in underwater environment. The obtained information were confirmed by the 3D distribution of the elements and compounds found during the excavation investigations.

### 4.1 Gilding technique on copper-based buckle

#### 4.1.1 Introduction

Here, is represented the case of a fire-gilding claps, an antique gilding technique carried out by artists and craftsmen for applying a thin layer of gold onto the surface of different types of metal artefacts by using a mercury amalgam. Different objects such as jewels, statues, works of art, weapons, armours, and ornaments were commonly decorated with these amalgam-based methods. The amalgam was prepared by mixing Au grains with mercury to obtain a paste with roughly the consistency of butter. This was spread uniformly on the clean oxide-free metal substrate as thin as possible in order to save the precious metal. Gentle thermal treatment was then carried out at approximately 250–350 °C, below the boiling point of mercury (357 °C), to remove a large percentage of the original mercury. The thermal process produced a well-bonded layer of gold with a variable amount of residual mercury, whose thickness could range from a few tenths of micron to about one micron. Because of its unevenness and porosity, the final finishing was carried out mechanically by means of a bone or agate burnisher. This delicately compressed and compacted the porous structure of the mercury-enriched Au layer, creating a smooth, shiny surface, similar to that of solid gold [180-181]. The gilded metal artefacts from many years ago, have likely been subjected to different degradation phenomena caused by the interaction with the surrounding environment, either underground or outdoor with acid rainwater interaction or indoor atmosphere, which have almost certainly changed their surface chemical composition and morphology [182-183]. However, many of the ancient gilded artefacts have been buried for periods of several hundred years up to about one or two thousand years before being excavated, or, like many gilded works of art, have been exposed to indoor atmospheres. During the long-term interaction with the surrounding environment, specific corrosion products are formed with peculiar structures that are sometimes different from the degradation compounds grown on archaeological or historical artefacts and generally ascribed to the common degradation pathways [184-186]. In this work is presented the chemical characterization of a gilded pendant copper-based, naturally corroded and dating back to 16th–17th centuries.

The investigated artifact was found during the cleaning operations on the banks of the river Tiber (Rome, Italy) and has interacted for several hundred years with soil constituents. The information that can be obtained could be of a great interest for the study of the long-term corrosion. This is due to the fact that the combined action of different degradation phenomena could have caused relevant chemical and structural modifications over time.

The main chemical investigations of the surface and sub-surface was carried out using X-ray photoelectron spectroscopy (XPS), scanning electron microscopy coupled with energy-dispersive spectroscopy (SEM + EDS) and optical microscopy (OM). Furthermore, for the first time ToF-SIMS in dynamic mode was exploited to study the sub-surface of a small metallic artifacts. The use of ToF-SIMS technique in the study of metallic artworks, could be complementary to other near-surface techniques such as SEM-EDX, XPS and electrochemical methods.

ToF-SIMS depth profiling analysis, allowed to display the 3D distribution of the elements and the corrosion products along z axis, differentiating the corroded area from the unaltered. Furthermore, ToF-SIMS used in dynamic mode can provide very high sensitivity analysis with high spatial resolution, consuming a negligible sample volume that is potentially attractive in the cultural heritage field. The work was focused to investigate chemical changing occurred in this kind of ancient metal artifacts, interpreting a number of aspects of the manufacturing methods, and the degradation mechanisms, clarifying the interactions occurring between metals and their surrounding burial environments.

#### **4.1.2 Materials and methods**

The gold coated buckle was found during the cleaning operations on the banks of the river Tiber (Rome, Italy) and their surface were investigated in as-received state after a cleaning procedure carried out by using distilled water and then, ethyl alcohol to remove carbon contamination. In order to characterize the layered corrosion structures, representative cross-sectioned samples were produced: small fragments were collected, embedded in epoxy resin for 24 h and then micro-sectioned by using a diamond saw in order to preserve the structural and chemical features of the outer layers as much as possible. The sections were then polished with silicon carbide papers until 1200 grit and the final polishing was performed with diamond pastes up to  $\frac{1}{4}$   $\mu\text{m}$  in order to have flat mirror-like surfaces.

Metallurgical and chemical features were observed by means of a scanning electron microscope (SEM) Cambridge Stereoscan360 (Cambridge, UK) and a high brilliance, high spatial resolution LEO Gemini 1530 (Zeiss, Germany) field emission scanning electron (FE-SEM) microscopes. SEM and FE-SEM microscopes are equipped with an INCA 250 and INCA 450 (Oxford Instruments Analytical, UK) energy-dispersive X-ray microanalysis system, respectively and four-sector back-scattered electron (BSE) detectors. SEM micro-graphs images were recorded both in secondary electrons (SE) and BSE modes at an acceleration voltage of 20 kV while the FE-SEM images were recorded at different acceleration voltages from 1 kV to 20 kV in order to better disclose the nano-morphological features of the fire-gilded artefacts as for innovative nano-materials. Before the analysis, the surfaces of the cross-sectioned objects were coated with a thin layer of carbon or chromium in order to avoid charging effects.

Optical microscopy (OM) investigations were performed by using a Leica LAS multi focus stereo, MZFLIII and MEF IV micro-scopes equipped with digital cameras (Leica DFC 320 and 420, Leica Microsystems, Germany).

XPS investigation was performed by using an ESCALAB Mk II (VG Scientific, UK) spectrometer equipped with standard Al K $\alpha$  and Mg K $\alpha$  excitation sources, 1486.6 and 1253.6 eV, respectively. The size of the analyzed area was about 2 mm in diameter. The spectra were collected at 20 eV constant pass energy that corresponds to 1.0 eV energy resolution for Ag 3d<sub>5/2</sub> in Ar<sup>+</sup> cleaned metal and a base pressure in the analysis chamber of 10<sup>-8</sup>Pa. The binding energy (BE) scale was calibrated by measuring the C 1s peak (BE = 285.0 eV) of adventitious carbon due to surface contamination, Au 4f<sub>7/2</sub> peak (BE = 84.0 eV) from sputter-cleaned Au 99.99% foil and Zr 3d<sub>5/2</sub> (182.3 eV) signal from ZrO<sub>2</sub>. The accuracy of the BE scale was  $\pm 0.1$  eV. In order to reduce the sample damage introduced during XPS measurements via dehydration or mercury sublimation or also X-ray induced reduction and decomposition, short acquiring times were selected and a suitable copper sample holder cooled by liquid nitrogen was used.

ToF-SIMS measurements were performed by using a ToF.SIMS 5 (ION-TOF Munster, GmbH, Germany) secondary ion mass spectrometer, equipped with bismuth liquid metal ion gun (LMIG) and cesium ion sputter gun. The analysis was not performed on the cross-section. The entire sample was first analyzed in bunched mode using Bi<sup>+</sup> at 30 keV as primary beam with dose density below the static limit ( $< 10^{12}$  ions/cm<sup>2</sup>) in order to distinguish deteriorated areas from the unaltered. A low energy electron flood gun (20 eV) was utilized to investigate the non-conductive blackish degraded areas. ToF-SIMS depth profiles were acquired in dual beam mode using Bi<sup>+</sup> (30 keV and pulse width: 15.6 ns) as primary ions and Cs<sup>+</sup> (2 keV) gun as erosion beam operated in interlaced mode. Cesium ion dose density was calculated as  $\approx 10^{18}$  ion/cm<sup>2</sup>. The analysis area (100 x 100  $\mu\text{m}^2$ ) was set at the center of the sputter region (300 x 300  $\mu\text{m}^2$  and 500 x 500  $\mu\text{m}^2$ ). All images were collected at a pixel density of 128 x 128 pixels and with a lateral resolution of 3  $\mu\text{m}$ , approximately. Secondary ions were extracted at 2 KeV voltage and traveled through the ToF analyzer for a time of 100  $\mu\text{s}$  per cycle allowing to obtain a mass range from m/z 1 to 800. Mass spectra were acquired in both positive and negative ion mode. All SIMS images shown, were normalized to the total ion image and filtered with an averaging filter in order to remove topographical effects, and salt-and-pepper noise. All the data presented in this case study are shown in negative polarity, even for elements that are usually easier to detect in positive polarity.

### 4.1.3 Results and discussion

The presented case study was investigated to identify degradation phenomena occurring in gilded objects during the long-term burial and to gain further insight into the ancient coating techniques. The case study was focused on the micro and nano-chemical and morphological features of the surface of a gilded clasp for bridles. SEM and OM images combined with XPS and EDS spectra and taken on the areas where gold is still partially present are shown in Figs. 4.1-4.3. Furthermore, ToF-SIMS mass spectrum of golden area analyzed is reported in Fig. 4.4. In addition, the elements and compounds detected during the ToF-SIMS depth profile acquisition mode were rendered in 3D images to better understand the distribution of all the species revealed (Fig.4.5). The obtained results highlight the complex morphology and surface chemical composition of the plated artefact.

EDS investigation reveals the presence of a noticeable amount of mercury in the gilded layer, ranging from 7.4 weight percent (hereafter wt%) to about 9.1 wt%, demonstrating that an amalgam was used to coat the clasp. The co-presence of Hg (m/z 200.02) and Au (m/z 196.96) is confirmed also in ToF-SIMS investigation (Figs. 4.4-4.5). These elements appear coupled and deposited on the substrate of copper. In particular, the signal of Au is overlapped to the signal of Cu in ToF-SIMS 3D images. The 3D distribution of the mercury appears in low amount, as expected according to the heating procedure of the amalgam (Fig.4.5).

In addition, SEM and OM images showed that the long-term corrosion has remarkably modified both the surface and the interface between the copper substrate and the thin gold layer. As a result, indeed, in some areas only a small amount of the plating remains in situ. The interaction between the soil components and the clasp has given rise to the formation of different corrosion products whose nature has been remarkably affected by the character of the soil and of the artefact. Specifically, plated artefacts, constituted by metals with different electrochemical potentials, exhibit a peculiar corrosive behavior, which is also influenced by the electrical connection between the different metals and the water. The latter contains soluble soil components and thus acts as an electrolyte. The contact enhances the oxidation of the less noble metal, i.e. copper, which becomes anodic and increases the degradation of the substrate.

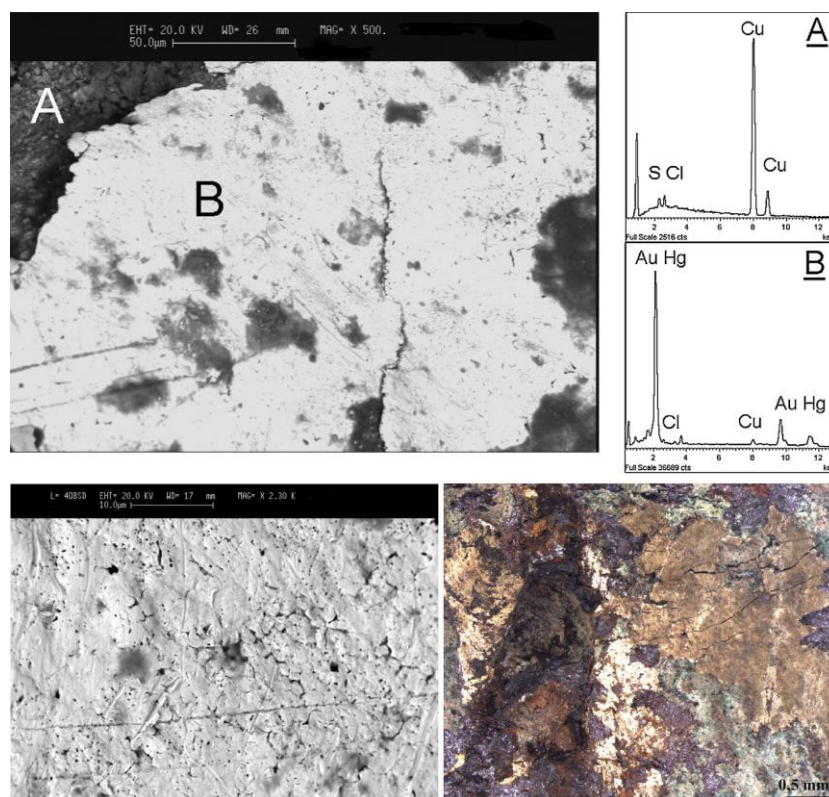


**Figure 4.1.** BSE images and EDS spectra of a gilded clasp for bridles. The results reveal that the plating is composed of small rounded and flattened grains of gold with a low amount of mercury. The diameter of the grains range from 1  $\mu\text{m}$  to 3  $\mu\text{m}$ . OM micro-graph shows the presence of erupting cuprite ( $\text{Cu}_2\text{O}$ ) that has caused the partial removal of the plating.

The amount of current that flows and, therefore, the extent of corrosion depends on many variables. Some of these parameters are of major importance: the chemico-physical parameters of the burial environment (chemical composition, pH, resistivity etc.) the difference in the electrochemical potential of the metals, the presence and nature of the electrolyte and the micro-chemical structure and the metallurgical features of the metallic substrate and of the noble metal layer. These factors can cause different chemical and structural transformations in the artefact

giving rise to the formation of a wide range of possible mineral species [184-185,187-189]. The BSE image of Fig. 4.2 shows that the thickness of the gilded layer is less than 10  $\mu\text{m}$ , as often observed by other authors in Roman and Barbarians artefacts [180, 190-191] and EDS analyses do not detect the presence of Au and Hg in the substrate under the gilded layer thus excluding the occurrence of an Au-Cu inter-diffusion phenomenon, which has been observed by other authors [192].

BSE and OM images also show that a granular structure is visible somewhere in the plating, with porous areas and flattened rounded grains whose diameter ranges from about 1 up to 3  $\mu\text{m}$ . Furthermore, BSE investigation has revealed that the gold layer is characterized by cracks likely attributable to micro-defects of manufacturing. These details indicate that the plating layer was only partially compacted by the craftsmen the grains not being perfectly burnished.

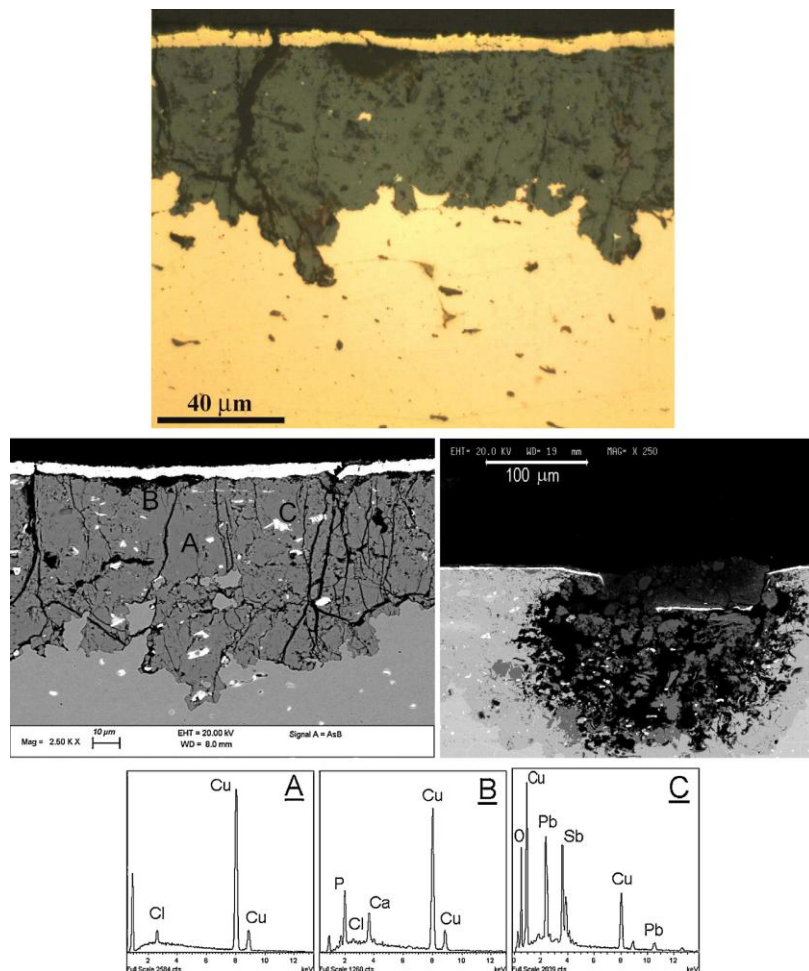


**Figure 4.2.** Micro-chemical structure of the gilded clasp for bridles. The BSE and OM images with the EDS spectra reveal that the thickness of the gold layer is about 6 $\mu\text{m}$  and that the copper substrate has been largely corroded and transformed in cuprite ( $\text{Cu}_2\text{O}$ ), with chlorine and phosphorous species also present. EDS spectra show the local chemical composition, and reveals that small Pb–Sb islands (spectrum C) are randomly scattered in the nearly pure copper matrix of the substrate

It is worth noting that these defects play a detrimental role during burial because both the intergranular spaces and the pits act as reactive areas and channels where the aggressive soil species (Cl, S, O, P) dissolved in water come into contact with the less noble underlying copper substrate. As a result, galvanic areas are formed and corrosion occurs [180,183,193]. These chemical and metallurgical features induce dramatic corrosion phenomena as shown in Figs. 4.1 and 4.2 in some representative images. The presence of  $S^-$  (m/z 32.06),  $P^-$  (m/z 30.97) and  $Cl^-$  (m/z 34.45) ions were detected in negative ToF-SIMS mass spectrum and mapped in 3D imaging (Figs.4.4-4.5).

It is also noteworthy that the distribution of S and P ions, starts from the surface of the object to arrive in the core, following the conic trend of the gilding fracture and filling the same area. Chlorine ion is more related to the copper distribution, its presence indicates the consequently formation of degradation products as nantokite ( $CuCl_2$ ) also shown in ToF-SIMS 3D imaging (Fig.4.5). Furthermore, the BSE, EDS and OM results also provide evidence that soil aggressive elements in the soil modified the surface composition of the gilded layer.

In addition, they severely attacked along the nano-and micro-cracks of the gilded layer causing the formation of a corrosion layer under the gold coating (in contact with the metal core) constituted by red cuprous oxide (cuprite,  $Cu_2O$ ) whose expansion and eruption have induced spalling, break-up and detachment of the gold layer in some areas. The detection of copper oxides ( $CuO$  and  $Cu_2O$ ) was also revealed in ToF-SIMS mass spectrum and in the depth profile measurement as shown in Figs. 4.4-4.5. These data confirm the state of conservation of copper core, detected with the others analytical techniques. The role of the cuprite layer in the corrosion phenomena of copper-based alloys has been discussed by Lucey [194] and has been considered to act as an electrolytic membrane allowing the transport of anions such as Cl and  $O_2$  inward and cuprous ions outward. In addition, ToF-SIMS analysis has also revealed the presence of  $O_2$  in correspondence of Cu area (Figs.4.4-4.5).

Copper chlorides in archaeological artefacts is frequently detected and could indicate a notice able transportation of chlorides from the soil through the permeable external layers to the internal zone and remaining Cu-based matrix. The accumulation of chloride ions can be interpreted as an autocatalytic reaction that facilitates the oxidation of copper, also resulting in an accumulation of chloride ions and in the formation of cuprite and cuprous chloride ( $CuCl_2$ , nantokite), as described in details by Robbiola et al. [184]. These findings suggest that particular care must be used during the removal of the encrustations and of the external corrosion products to avoid the loss of the relics of the noble layer often floating or embedded in the corrosion products (see Fig. 4.2). Furthermore, the protective  $Cu_2O$  cuprite layer should not be removed, so as to avoid the harmful exposure of copper chlorides to humidity and oxygen, and therefore to prevent the occurrence of the cyclic copper corrosion, which is roughly defined as “bronze disease” [180,182,186,195].

As regards the chemical composition of the substrate, EDS information revealed that it is constituted by copper with a small amount of Pb and Sb, 1.6 wt% and 1.4 wt%, respectively, which form small randomly scattered micro-metric islands in the nearly pure copper matrix of the substrate as shown in Fig. 4.2 (EDS spectrum C). The BSE image for the cross-sectioned clasp and EDS data for the surface demonstrated that the Pb and Sb are not released through the gold layer during the long-term interactions with the soil but form small mineralised inclusions inside the cuprite layer underlying the gold coating. The detection of these elements in the 3D imaging ToF-SIMS does not appear in specific agglomerates, as decrypted by the BSE image, but are dispersed within the copper matrix in low quantity. This could be explained to the analysis of a different portion of the object and testifies to the heterogeneity of the artifact.

In order to gain further insight into the chemical state of the surface species formed by degradation phenomena, XPS investigations were performed and the spectra were interpreted. The wide scan XPS spectrum shown in Fig. 4.3 (spectrum A) with the identification of the main peaks confirms the surface predominant presence of Au, Hg, Cu, C and O as well as of Cl and S from the burial soil. These two latter elements are present as sulphide and chloride compounds, being the Cl 2p and S 2p signals peaked at 198.6 eV and 162.5 eV, respectively [192] thus revealing the interaction between the soil's aggressive compounds and the artefact. These compounds have been related to the complex interaction between the metal artefact and sulphide anions produced by the sulphur reducing bacteria (SRB) under anaerobic condition, which give rise to the formation of metal sulphides [196-198].

Concerning the chemical state of gold the Au 4f<sub>7/2</sub> photoemission signal is peaked at a binding energy (BE) value of about 84.0 eV, which corresponds to metallic Au. No other components appear in the Au 4f<sub>7/2</sub>-Au 4f<sub>5/2</sub> energy region shown in Fig. 4.3, and therefore, gold is only present in the metallic state, not forming any compound with the corroding species deriving from the surrounding environment. As shown in Fig. 4.3, XPS detected the presence of mercury; the peak fitting of the Hg 4f<sub>7/2</sub>-Hg 4f<sub>5/2</sub> doublet recorded on the surface shows that the peak is characterized by the presence of two components assigned to Hg<sup>0</sup> (BE = 100.1 eV) and to Hg<sup>2+</sup> (BE = 102.0 eV). The higher BE for the Hg 4f<sub>7/2</sub> suggests that mercury is present as in HgCl<sub>2</sub> and/or HgS [199-200]. This result reveals that Hg is subjected to a surface chemical modification induced by the burial environment and could be related to the presence of the chlorides or sulphides revealed by the XPS and EDS information.

ToF-SIMS mass spectrum and 3D maps confirm the co-presence of mercury with S and Cl ions in the same analyzed portion area (Figs. 4.4-4.5). In addition, a signal attributed to HgCl<sub>2</sub> (m/z 270.92) compound was recognized in the mass spectrum and mapped in 3D distribution (Figs.4.4-4.5) Nevertheless, the HgS was not detected by ToF-SIMS analysis.

In some areas of the clasp, EDS and XPS also revealed the presence of a small amount of Si-Al and Si compounds, this latter was identified via X-ray diffraction (XRD) analysis as quartz. In order to better, identify the chemical nature of the silico-aluminum compound. XPS has also revealed the hygroscopic nature of the corrosion products. The line-shape analysis of the O 1 s photoemission peaks (not shown) demonstrated both the presence of anhydrous and hydrated species at the surface; their co-existence is shown by a small component of the O 1 s band peaked at about 529.8 eV, which indicates the presence of O-Metal bonds, a weak component peaked at 533.0 ± 0.2 eV attributed to adsorbed water and O-Si bond and finally by a third weak component assigned to hydroxyl O H groups peaked at 532.0 eV [192-193, 201].

Moreover, the peaks attributed to AlO (m/z 42.97) and Si (m/z 28.08) were recognized and 3D rendered in the ToF-SIMS mass spectrum and depth profile images, respectively (Figs. 4.4-4.5). In particular, the Fig. 4.5 shows how these two compounds are perfectly arranged in the same area, assuming the same shape and proving their bond. This evidence confirm the presence of silico-aluminate clay that could be penetrated in the cracks of the object during its deposition on the burial soil. The signals of Si and AlO are shown also in 2D map images of analyzed area, present in Fig. 4.6. Their signals (Figs. 4.6c-d) are mapped in the same area and fill the lack of copper signals, confirming that the silico-aluminate clay start from the bottom of the surface and penetrate to the cracks present on the golden object.

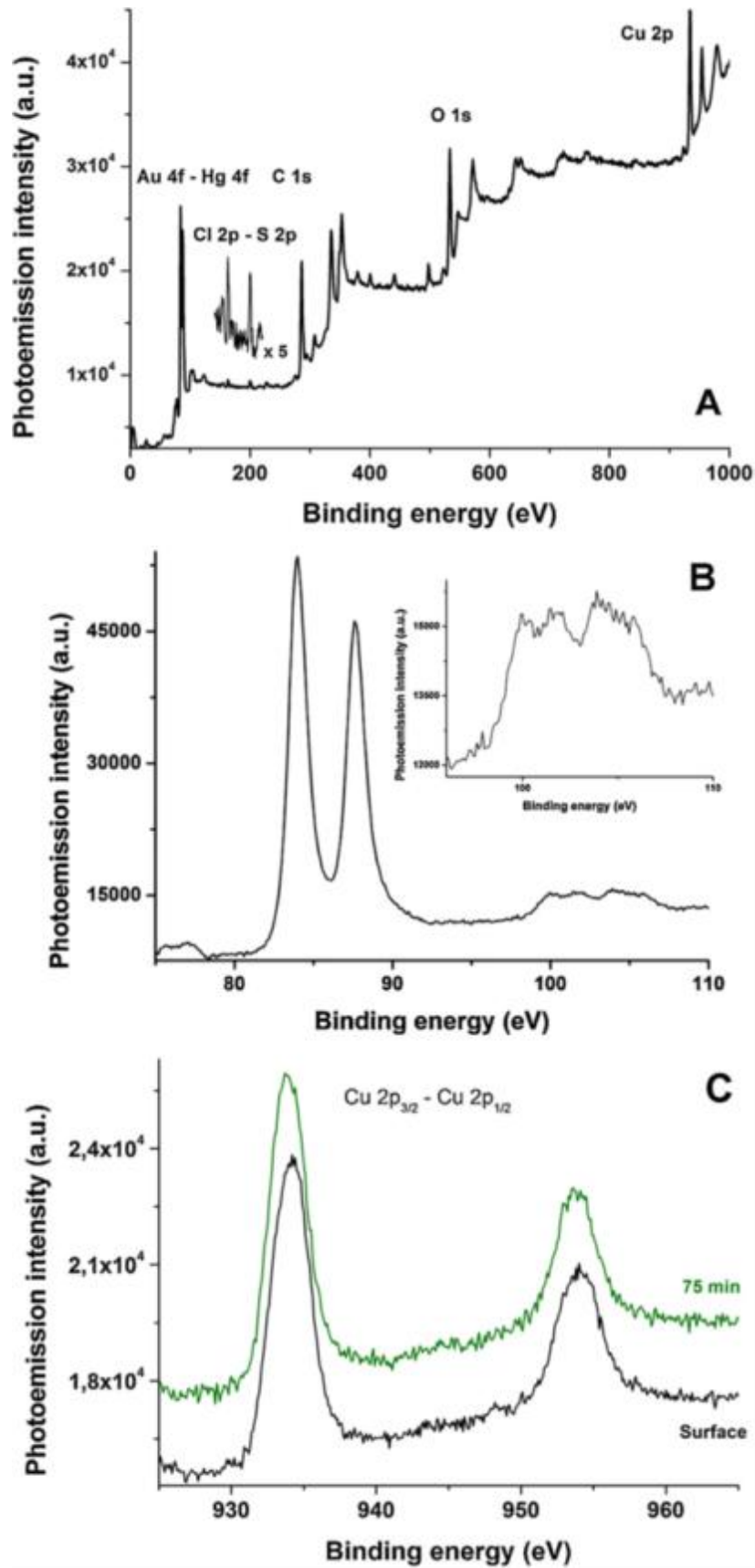


**Figure 4.3.** XPS wide scan of the surface of the gilded clasp with identification of the main peaks of C, O, Cl, S, Cu, Au and Hg; Au 4f<sub>7/2</sub>-Au 4f<sub>5/2</sub> and Hg 4f<sub>7/2</sub>-Hg 4f<sub>5/2</sub> core level spectra; Cu 2p<sub>3/2</sub>-Cu 2p<sub>1/2</sub> core level spectra, A, B and C, respectively.

XPS results for copper (spectra C of Fig. 4.3) reveal that the areas where the precious metal has been removed by the erupting corrosion products are characterized by the predominant presence of cuprite ( $\text{Cu}_2\text{O}$ ). This assignment is supported by the line-shape analysis and the value of the binding energy (BE) of Cu  $2p_{3/2}$  photoemission signal that is peaked at 932.9 eV in the reddish-brown areas [187, 202-203]. The analysis of the Cu 2p photoemission signal recorded in different areas of the clasp sometimes reveals the presence of a second small contribution located at BE of 934.0 eV. This can be assigned to Cu (II) species, according to the low intensity shake-up satellites positioned at BE = 944.4 eV [187, 202-204] and is likely due to a scarce presence of copper carbonates. It is worth noting that the XRD results do not indicate the presence of atacamite [ $\text{CuCl}_2 \cdot 3\text{Cu}(\text{OH})_2$ ]. On the contrary, dynamic SIMS conducted on a different area revealed the presence of  $\text{Cu}_3\text{H}_2\text{O}_2$  ( $m/z$  224.62) recorded along with  $\text{CuCl}_2$  ( $m/z$  134.44) (Figs.4.4-4.5). The co-presence of this two compounds in the same zone could identify the presence of the atacamite [ $\text{CuCl}_2 \cdot 3\text{Cu}(\text{OH})_2$ ] or its polymorphs, which induces the destructive copper cyclic corrosion [195].

Finally, the XPS investigations have confirmed that other metal elements such as tin, lead or zinc are not present on the surface of the clasp or inside the gilded layer neither as oxide nor as in the metallic form [205-206]. On the contrary, ToF-SIMS 2D distribution of elements detected in the first monolayer reveals the weak presence of Pb ( $m/z$  207.2) and Sb ( $m/z$  121.76) on the surface (Figs. 4.6.f-g) along with high amount of chlorine (Fig. 4.6e) deposited on the gold layer (Fig. 4.6a). Furthermore, the ToF-SIMS imaging of the surface shows the distribution of Si and AlO in the same area (Figs. 4.6c-d), perfectly filling the absence of signal in the copper map (Fig. 4.6b).

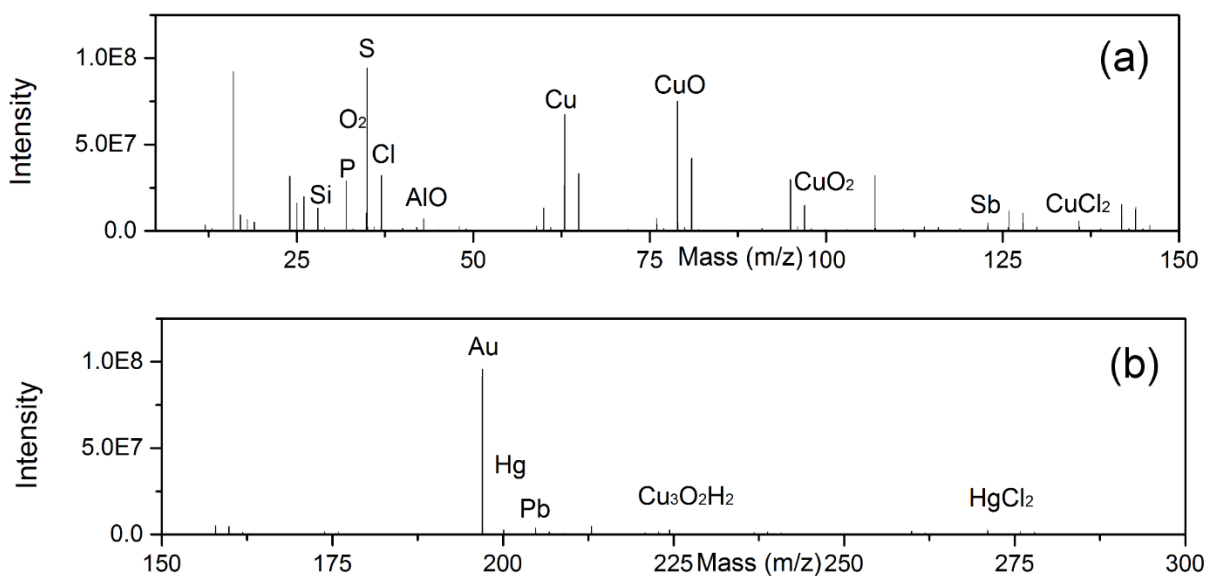


**Figure 4.4.** ToF-SIMS negative ion spectrum of the analyzed area. In Fig. (a) is shown the mass fragmentation range from  $m/z$  5 to 150. In this range are marked the peaks of Si ( $m/z$  28,08), P ( $m/z$  30,97), O<sub>2</sub> ( $m/z$  31,99), S ( $m/z$  32,06) Cl ( $m/z$  35,45), AlO ( $m/z$  42,97), Cu ( $m/z$  63,54), CuO ( $m/z$  79,54), CuO<sub>2</sub> ( $m/z$  95,54), Sb ( $m/z$  121,76) and CuCl<sub>2</sub> ( $m/z$  134,44). Fig. b shows the mass fragmentation range from  $m/z$  150 to 300. In this range is highlighted the presence of Au ( $m/z$  196,96), Hg ( $m/z$  200,02), Pb ( $m/z$  207,2), Cu<sub>3</sub>O<sub>2</sub>H<sub>2</sub> ( $m/z$  224,62) and HgCl<sub>2</sub> ( $m/z$  270,92).

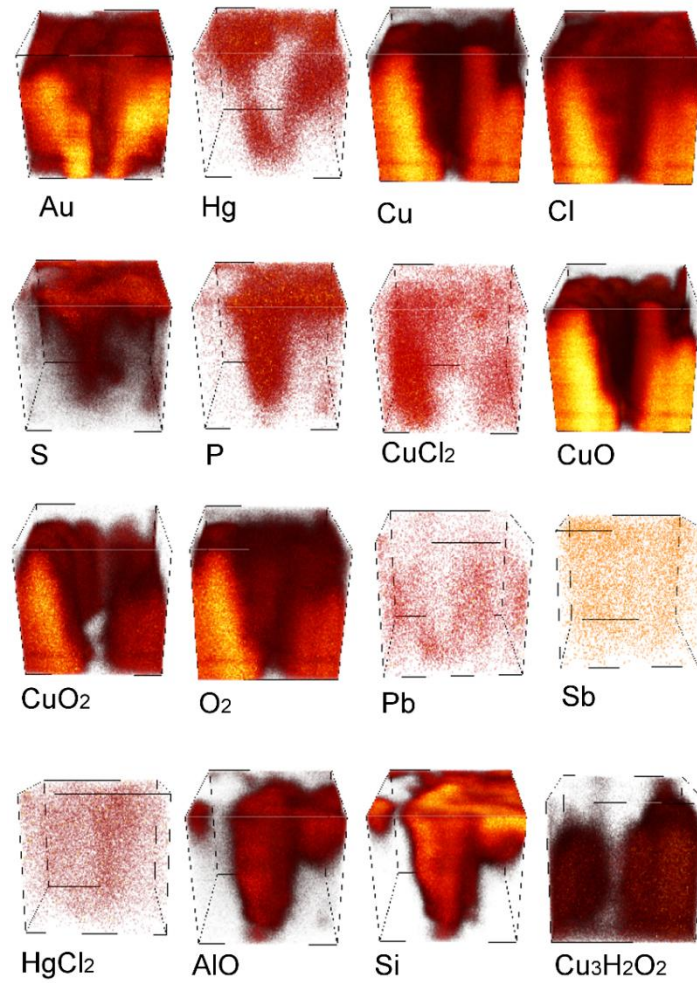


**Figure 4.5.** ToF-SIMS 3D imaging of the main elements and compounds revealed in the artefact.

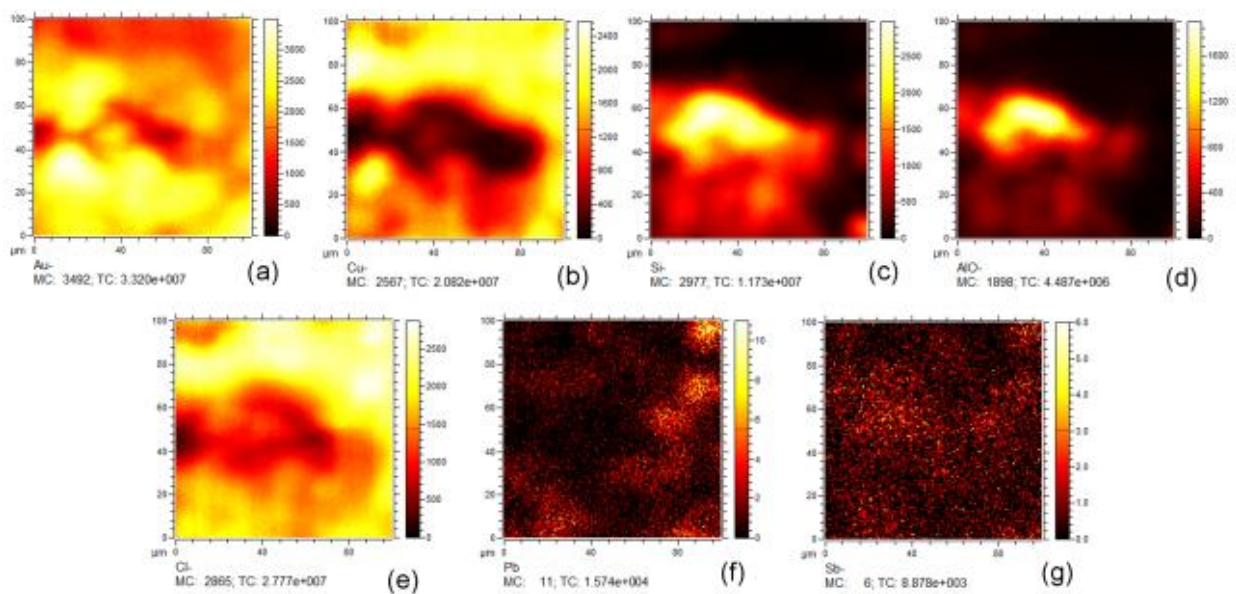


**Figure 4.6.** ToF-SIMS negative ion images of the sample surface.

#### 4.1.4 Conclusion

The combined use of XPS, SEM + EDS, OM and, ToF-SIMS was proved to be very useful for investigating the chemical and structural features of ancient fire-gilded objects buried in a water containing soil and subjected to long-term corrosion phenomena. The results highlighted the relevance of the integrated use of surface spectroscopies and microscopies to allow a significant break through towards the understanding of the complex micro-chemical structures of plated objects, providing evidence of the skills of the ancient metallurgists in manipulating metals on a the micro-scale in order to save expensive metals and to simulate silver or gold surfaces by using low amounts of precious metals. In the light of these analyses, the following main conclusion can be drawn. First, the coating technique was proved to be based on the use of an amalgam to uniformly coat nearly pure copper substrates with a noble metal film. Such works of art have been found to be subjected to different degradation phenomena. Second, the main degrading agents are Cl, S and P species, which derive from the soil and travel along micro-cracks and manufacturing defects present in the thin metal layer of Au. The aggressive species and oxygen attack the substrate and give rise to the formation of a layered structure constituted by remains of the noble metal coating and an internal cuprous oxide ( $\text{Cu}_2\text{O}$ ) layer with soil elements. Substrate corrosion is enhanced by metal galvanic coupling, which makes gilded-metal art-works particularly unstable from a chemico-physical point of view. Moreover, in some artefacts the interaction between Cl and S and the mercury of the gilded layer has also been detected. Moreover, the use of ToF-SIMS depth profiling technique has highlighted the degradation products distribution in the analyzed volume, supporting the results obtained with others analytical techniques and showing the structure that the degrade can assume. Moreover, the high sensitivity and the high spatial resolution features of the technique have allowed to detect degradation products, as oxygen, atacamite, and mercury chloride which did not appear in other areas analyzed by the XPS and SEM-EDS. This study highlights the importance of using more complementary techniques in the same sample that apparently seems to have a homogeneous state of conservation. Finally, the reported results can be useful to improve knowledge of the long-term corrosion phenomena of ancient and historic gilded copper-based artefacts, aiming to design appropriate accelerated degradation tests and tailor safe cleaning and reliable conservation strategies.

## 5 Conclusion

The use of static secondary ion mass spectrometry with time of flight analyzer was successfully employed to study the interaction between metals and organic compounds. The chemical information obtained during ion bombardment experiments coupled to the multivariate statistical analysis were exploited to highlight differences in samples. In particular, the high mass resolution and capability to detect different masses simultaneously, allowed to confirm the actual occurrence of the saponification reaction among tin metal foil and fatty acids, thanks to the identification of isotopic fragmentation pathway of organometallic compounds. Furthermore, the study of mass fragmentation has permitted to recognize the main characteristic fragments of triterpenic resin markers and to find an effective response in real study samples.

In addition, the use of this technique coupled with multivariate statistical analysis methods has proved to be a useful tool for the discrimination of structural isomers that characterize these natural compounds. At the same time, the high sensitivity, selectivity, and the excellent lateral resolution of secondary ion mass spectrometry technique have allowed the chemical characterization and localization of the compounds along all the cross-section presented in abovementioned studies, without causing damage to the samples. This has permitted further investigations of the samples by using other analytical technique, in order to obtain complementary information regarding the state of artwork conservation. In the previously reported case studies, each layer of the cross section was characterized, defining its constituent materials. Inorganic compounds and organic mixtures were detected and localized concurrently with metal soaps, formed in tin metal foils and in pictorial systems. Their detection gives confirm to the possibility of saponification reactions between fatty acid binding media and metal compounds to occur, after the oxidation of the metal compounds (metal foil and metallic pigments). Although the formation and the chemical reactivity of lead soaps on painting system was already largely studied, nothing has yet been verified on the properties of tin soaps, as these studies represent the first investigations carried out on these class of compound, currently in the conservation science literature. The detection of tin metal soaps on "composite lamina" technique, could provide important information to the future restoration operations, opening a series of question on the chemical features of this kind of degradation products, as solubility, acidity or mechanical strength. An expanded study on the chemical reactivity of these compounds could safeguard artworks in which composite lamina gilding technique was adopted, safeguarding the loss of material and the brilliant appearance of the metallic finish, avoiding the detachment between the decoration layers. With the extension of the case studies studied, it was possible to widen the knowledge of the different materials used in the gilding techniques adopted in the course of history, identifying the natural varnish used to recreate the golden effect on the leather artifact and the use of protein-based adhesives since the Etruscan era as a binder between stone supports and gold foil. Finally, ToF-SIMS features in dynamic mode were employed to the characterization of metal artifact. Although it is considered a microdistrictive technique, and not properly adapted to preserving the integrity of the artwork sample, depth profiling analysis has allowed to investigate the degradation degree of an object buried for centuries in an underwater environment, and to map through the 3D distribution the presence of unaltered elements along with those of the degraded, revealing the form they assumed in the object. Lastly, it is important to remember that in all samples analyzed, the ToF-SIMS measurements were sustained by other analytical technique, usually used in the field of conservation science, providing often preliminary information on the chemical characterization of the materials of artwork.

This thesis has shown that the use of ToF-SIMS technology associated with other diagnostic tests can make a greater contribution to the study of complex samples, in which a multitude of different materials coexist in few microns, also highlighting the reactions between these compounds and the surrounding environment conditions. This can help us to understand the history of the artwork from its birth to us, and provide the means for its preservation in the future.



## Reference

- [1] M.P. Colombini, F. Modugno, *Organic Mass Spectrometry in Art and Archaeology*, Wiley, 2009, ISBN: 978-0-470-51703-1.
- [2] P. Cok, B. De Bernard, M.P. Radillo, F. Francescato, *Synoptic Food Composition Tables*, 1986, Edizioni Piccini, Padova.
- [3] US Department of Agriculture, Agricultural Research Service. 2007. USDA National Nutrient Database for Standard Reference, Release 20. Nutrient Data Laboratory Home Page, <http://www.ars.usda.gov/ba/bhnrc/ndl>.
- [4] J.S. Mills, R. White, *The Organic Chemistry of Museum Objects*, 1994, Butterworth Heinemann, Oxford.
- [5] T. Horiguchi, Y. Takase, Y. Arai, H. Ageta, Y. Showa, M. Tokyo, *GC-MS study on ester components of spermaceti*, *Natural Medicines*, 1999, 53, 105–108.
- [6] C. Chemtob, F. Fawaz, F. Puisieux, *Analysis of ointments, oils, and waxes. XX. Chemical composition of waxy lanolin*, *Annales Pharmaceutiques Francaises*, 1975, 33, 243–251.
- [7] M.P. Colombini, F. Modugno, E. Ribechini, *The Egyptian mummies in the 'Museo di Anatomia' of the University of Pisa: a chemical approach for the characterization of balms*, *Science and Technology for Cultural Heritage*, 2004, 13, 83–87.
- [8] J. Connan, O. Kavak, E. Akin, M.N. Yalc, K. Imbus, J. Zumberge, *Identification and origin of bitumen in Neolithic artefacts from Demirkoy Hoyuk (8100 BC): Comparison with oil seeps and crude oils from southeastern Turkey*, *Organic Geochemistry*, 2006, 37, 1752–1767.
- [9] I. Bonaduce, M.P. Colombini, S. Diring, *Identification of garlic in old gildings by gas chromatography-mass spectrometry*, *Journal of Chromatography A*, 2006, 1107, 226–232.
- [10] M. Regert, C. Rolando, *Identification of archaeological adhesives using Direct Inlet Electron Ionization Mass Spectrometry*, *Analytical Chemistry*, 2002, 74, 965–975.
- [11] M. Regert, S. Vacher, C. Moulherat, O. Decavallas, *Adhesive production and pottery function during the Iron Age at the site of GrandAunay (Sarthe, France)*, *Archaeometry*, 2003, 45, 101–120.
- [12] M.P. Colombini, F. Modugno, *Characterisation of proteinaceous binders in artistic paintings by chromatographic techniques*, *Journal of Separation Science*, 2004, 27, 147–160.
- [13] F. Mori, R. Ponti, A. Messina, M. Flieger, V. Havlicek, M. Sinibaldi, *Chemical characterization and AMS radiocarbon dating of the binder of a prehistoric rock pictograph at Tadrart Acacus, Southern West Libya*, *Journal of Cultural Heritage*, 2006, 7, 344–349.
- [14] M.P. Colombini, S. Francesconi, R. Fuoco, F. Modugno, *Characterisation of proteinaceous binders and drying oils in wall painting samples by GC-MS*, *Journal of Chromatography A*, 1999, 846, 101.
- [15] A. Spyros, D. Anglos, *Study of aging in oil paintings by 1D and 2D NMR spectroscopy*, *Analytical Chemistry*, 2004, 76, 4929–4936.
- [16] M.P. Colombini, F. Modugno, R. Fuoco, A. Tognazzi, *A GC-MS study on the deterioration of lipidic paint binders*, *Microchemical Journal*, 2002, 73, 175–185.
- [17] A. Karpowicz, *Ageing and deterioration of proteinaceous media*, *Studies in Conservation*, 1981, 26, 153–160.
- [18] C. Hecht, S. Bieler, C. Griehl, *Liquid chromatographic-mass spectrometric analyses of anaerobe protein degradation products*, *Journal of Chromatography A*, 2005, 1088, 121–125.
- [19] M. Regert, H.A. Bland, S.N. Dudd, P.F. van Bergen, R.P. Evershed, *Free and bound fatty acid oxidation products in archaeological ceramic vessels*, *Proceedings of the Royal Society London B*, 1998, 265, 2027–2032.
- [20] W.J. Muizebelt, M.W.F. Nielen, *Oxidative crosslinking of unsaturated fatty acids studied with mass spectrometry*, *Journal of Mass Spectrometry*, 1996, 31, 545–554.

- [21] M.R. Shilling, H.P. Khanjian, L.A.C. Souza, *Gas chromatographic analysis of amino acids as ethyl chloroformate derivatives. Part 1: compositions of proteins associated with art objects and monuments*, Journal of American Institute for Conservation, 1996, 35, 45–59.
- [22] A. Andreotti, I. Bonaduce, M.P. Colombini, G. Gautier, F. Modugno, E. Ribechini, *Combined GC/MS analytical procedure for the characterization of glycerolipid, waxy, resinous, and proteinaceous materials in a unique paint microsample*, Analytical Chemistry, 2006, 78, 4490–4500.
- [23] M.P. Colombini, F. Modugno, E. Ribechini, *Chemical study of triterpenoid resinous materials in archaeological findings by means of direct exposure electron ionisation mass spectrometry and gas chromatography/mass spectrometry*, Rapid Communications in Mass Spectrometry, 2006, 20, 1787–1800.
- [24] B. Buchele, W. Zugmaier, T. Simmet, *Analysis of pentacyclic triterpenic acids from frankincense gums and related phytopharmaceuticals by high-performance liquid chromatography. Identification of lupeolic acid, a novel pentacyclic triterpene*, Journal of Chromatography B, 2003, 791, 21–30.
- [25] G.A. van der Doelen, K.J. van den Berg, J.J. Boon, N. Shibayama, E.R. de la Rie, W.J.L. Genuit, *Analysis of fresh triterpenoid resins and aged triterpenoid varnishes by high-performance liquid chromatography–atmospheric pressure chemical ionisation (tandem) mass spectrometry*, Journal of Chromatography A, 1998, 809, 21–37.
- [26] K.J. van der Berg, J. van der Horst, J.J. Boon, O.O. Sudmeijer, *Cis-1,4-poly-b-myrcene; the structure of the polymeric fraction of mastic resin (Pistacia lentiscus) elucidated*, Tetrahedron Letters, 1998, 39, 2654–2648.
- [27] R. White, *The characterisation of proteinaceous binders in art objects*, National Gallery Technical Bulletin, 1984, 8, 5–14.
- [28] S. Keck, T. Peters, *Identification of protein-containing paint media by quantitative amino acid analysis*, Studies in Conservation, 1969, 14, 75–82.
- [29] I. Bonaduce, H. Brecoulaki, M.P. Colombini, A. Lluveras, V. Restivo, E. Ribechini, *GC-MS characterization of plant gums in samples from painted works of art*, Journal of Chromatography A, 2007, 1175, 275–282.
- [30] Pitthard, P. Finch, *GC-MS analysis of monosaccharide mixtures as their diethyldithioacetal derivatives: Application to plant gums used in art works*, Chromatographia, 2001, 53, S317–S321.
- [31] J.H. Hofenk de Graaff, *The Colorful Past. Origin, Chemistry and Identification of Natural Dyestuffs*, Abegg-Stiftung, Riggisberg, 2004.
- [32] J. Cannon, M. Cannon, *Dye Plants and Dyeing*, The Herbert Press, London, 1994. 169. E.S.B. Ferreira, A. Quye, H. McNab, A.N. Hulme, *Photo-oxidation products of quercetin and morin as markers for the characterisation of natural flavonoid yellow dyes in ancient textiles*, Dyes in History and Archaeology, 2002, 18, 63–72.
- [33] M.P. Colombini, A. Andreotti, C. Baraldi, I. Degano, J.J. Łucejko, *Colour fading in textiles: A model study on the decomposition of natural dyes*, Microchemical Journal, 2007, 85, 174–182.
- [34] M. Serpico, R. White, *Oil, fat and wax, in Ancient Egyptian Materials and Technology*, P. Nicholson and I. Shaw (Eds), Cambridge University Press, Cambridge, 2000, 390–429
- [35] K. Kimpe, P.A. Jacobs, M. Waelkens, *Analysis of oil used in late Roman oil lamps with different mass spectrometric techniques revealed the presence of predominantly olive oil together with traces of animal fat*, Journal of Chromatography A, 2001, 937, 87–95.
- [36] M.P. Colombini, F. Modugno, E. Ribechini, *Organic mass spectrometry in archaeology: evidence for Brassicaceae seed oil in Egyptian ceramic lamps*, Journal of Mass Spectrometry, 2005, 40, 890–898.

- [37] M. Regert, S. Colinart, L. Degrand, O. Decavallas, *Chemical alteration and use of beeswax through time: accelerated ageing tests and analysis of archaeological samples from various environmental contexts*, *Archaeometry*, 2001, 43, 549–569.
- [38] D. F. Torgerson, R. P. Skowronski and R. D. Macfarlane, *New approach to the mass spectroscopy of non-volatile compounds*, *Biochemical and Biophysical Research Communications*, 1974, 60, 616–621.
- [39] H. D. Beckey, *Field ionization mass spectrometry*, *Res. Dev.*, 1969, 20, 26–31.
- [40] M. Barber, R. S. Bordoli, R. D. Sedgwick and A. N. Tyler, *Fast atom bombardment of solids (F.A.B.): a new ion source for mass spectrometry*, *Journal of the Chemical Society, Chemical Communications*, 1981, 325–327.
- [41] M. Yamashita and J. B. Fenn, *Electrospray ion source. Another variation on the free-jet theme*, *Journal of Physical Chemistry*, 1984, 88, 4451–4459.
- [42] M. Karas and F. Hillenkamp, *Laser desorption ionization of proteins with molecular masses exceeding 10,000 daltons*, *Analytical Chemistry*, 1988, 60, 2299–2301.
- [43] J.S. Mills and R. White, *Analyses of paint media*, *National Gallery Technical Bulletin*, 1980, 4, 65-68.
- [44] J.S. Mills, *The gas chromatography examination of paint media. Part I. fatty acid composition and identification of dried oil films*. *Studies in Conservation*, 1966, 11, 92-108.
- [45] J.D.J. van den Berg, K.J. van den Berg and J.J. Boon, *Determination of the degree of hydrolysis of oil paint samples using a two-step derivatisation method and on-column GC/MS*, *Progress in Organic Coatings*, 2001, 41, 143-155.
- [46] J.J. Boon, *Analytical pyrolysis mass-spectrometry new vistas opened by temperature-resolved in-source py-MS*. *International Journal of Mass Spectrometry and Ion Processes*, 1992, 118, 755-787.
- [47] J.D.J. van den Berg, *Analytical chemical studies on traditional linseed oil paints*. PhD Thesis, University of Amsterdam. 2002 (<http://www.amolf.nl/publications/theses/>).
- [48] G. Spoto, *Secondary ion mass spectrometry in art and archaeology*, *Thermochimica Acta*, 2000, 157-166.
- [49] E. Darque-Ceretti and M. Aucouturier, *Secondary ion mass spectrometry. Application to archaeology and art objects*, in *Non-destructive Analysis of Cultural Heritage Materials*, K. Janssens and R. Van Grieken (eds), *Comprehensive Analytical Chemistry XLII*, Elsevier BV, Amsterdam, 2004, 397–461.
- [50] M. Dowsett and A. Adriaens, *Role of SIMS in cultural heritage studies*, *Nuclear Instruments & Methods in Physics Research Section B-Beam Interactions with Materials and Atoms*, 2004, 226, 38–52.
- [51] A. Adriaens and M. G. Dowsett, *Applications of SIMS to cultural heritage studies*, *Applied Surface Science*, 2006, 252, 7096–7101.
- [52] M. Anderle, M. Bersani, L. Vanzetti and S. Pederzoli, *State of art in the SIMS (secondary ion mass spectrometry) application to archaeometry studies*, *Macromolecular Symposia*, 2006, 238, 11–15.
- [53]. McPhail, *Some applications of SIMS in conservation science, archaeometry and cosmochemistry*, *Applied Surface Science*, 2006, 252, 7107–7112.
- [54] A. M. Belu, D. J. Graham, D. G. Castner, *Time-of-flight secondary ion mass spectrometry techniques and applications for the characterization of biomaterial surfaces*, *Biomaterials*, 2006, 24, 3635-3653.
- [55] A. Brunelle, D. Touboul, O. Lapr evote, *Biological tissue imaging with time-of-flight secondary ion mass spectrometry and cluster ion sources*, *Journal of Mass Spectrometry*, 2005, 40, 985-999.

- [56] R. Sodhi, *Time of flight secondary ion mass spectrometry (ToF-SIMS): versatility in chemical and imaging surface analysis*, *Analyst*, 2004, 129, 483-487.
- [57] B. Hagenhoff, *High resolution Surface Analysis by ToF-SIMS*, *Mikrochimica Acta*, 2000, 132, 259-271.
- [58] E. Niehuis, T. Heller, H. Feld, A. Benninghoven. *Design and performance of a reflectron based time-of-flight secondary ion mass spectrometer with electrodynamic primary ion mass separation*, *Journal of vacuum science and technology*, 1987, 5, 1243-6.
- [59] B. Schueler, *Microscopic imaging by time-of-flight secondary ion mass spectrometry*. *Microscopy Microanalysis Microstructures*, 1992, 3, 119-39.
- [60] McLafferty FW, Turecek F. *Interpretation of mass spectra*, 4th ed. Sausalito, CA: University Science Books, 1993
- [61] N. M. Reed, J. C. Vickerman, *The application of static secondary ion mass spectrometry (SIMS) to the surface analysis of polymer materials*. In: Sabbatini L, Zambonin PG, editors. *Surface characterization of advanced polymers*. Weinheim, Germany: VCH, 1993.
- [62] F. Kollmer, *Cluster primary ion bombardment of organic materials*, *Applied Surface Science*, 2004, 231-232, 153-158.
- [63] D. Touboul, F. Halgand, A. Brunelle, R. Kersting, E. Tallarek, B. Hagenhoff and O. Laprévotte, *Tissue molecular ion imaging by gold cluster ion bombardment*, *Analytical Chemistry*, 2004, 76, 1550-1559.
- [64] Winograd, *The magic of cluster SIMS*, *Analytical Chemistry*, 2005, 77, 143A-149A.
- [65] M. Dowsett, A. Adriaens, *The role of SIMS in cultural heritage studies*, *Nuclear Instrument and Methods in Physics Research section B*, 2004, 226, 38-52.
- [66] D. J. Graham, D. G. Castner, *Multivariate Analysis of ToF-SIMS Data from Multicomponent Systems: The Why, When, and How*, *Bionterphase*, 2012, 7, 49, 1-12.
- [67] R. Michel, D. G. Castner, *Advances in time-of-flight secondary ion mass spectrometry analysis of protein films*, *Surface Interface Analysis*, 2006, 38, 11, 1386-1392.
- [68] D. J. Graham, M. S. Wagner, D. G. Castner, *Information from complexity: Challenges of TOF-SIMS data interpretation*, *Applied Surface Science*, 2006, 252, 19, 6860-6868.
- [69] M. S. Wagner, D. J. Graham, B. D. Ratner, D. G. Castner, *Maximizing information obtained from secondary ion mass spectra of organic thin films using multivariate analysis*, *Surface Science*, 2004, 570, 1-2, 78-97.
- [70] M. Mellinger, *Multivariate data analysis, its method*. *Chemometrics and Intelligent Laboratory Systems*, 1987, 2, 29-36.
- [71] K. R. Beebe, B. R. Kowalski, *An introduction to multivariate calibration and analysis*, *Analytical Chemistry*, 1987, 59, 17, 1007A-1017A.
- [72] S. Wold, K. Esbensen, P. Geladi, *Chemometrics and Intelligent Laboratory Systems*, 1987, 2, 1-3, 37-52.
- [73] J. C. Vickerman, In: J. C. Vickerman, I. S. Gilmore (eds) *Surface analysis-the principal techniques (2nd edn)*. John Wiley & Sons, Chichester, 2009, p. 113-203.
- [74] J. C. Vickerman, D. Briggs, *ToF-SIMS: surface analysis by mass spectrometry*. IM Publications, Chichester, 2001.
- [75] C. M. Carr, R. Mitchell and D. Howell, *Surface chemical investigation into the cleaning procedures of ancient tapestry materials*. Part 1, *Journal of Materials Science*, 2004, 39, 7317-7325.
- [76] D. Howell, R. Mitchell and C. M. Carr, *Surface chemical investigation into the cleaning procedures of historic tapestry materials*. Part 2, *Journal of Materials Science*, 2007, 42, 5452-5457.

- [77] J. Batcheller, A. M. Hacke, R. Mitchell and C. M. Carr, *Investigation into the nature of historical tapestries using time of flight secondary ion mass spectrometry (ToF-SIMS)*, Applied Surface Science, 2006, 252, 7113–7116.
- [78] P. Novotna, V. Pacakova, Z. Bosakova and K. Stulik, *High-performance liquid chromatographic determination of some anthraquinone and naphthoquinone dyes occurring in historical textiles*, Journal of Chromatography, A, 1999, 863, 235–241.
- [79] Szostek, J. Orska-Gawrys, I. Surowiec and M. Trojanowicz, *Investigation of natural dyes occurring in historical Coptic textiles by high-performance liquid chromatography with UV-vis and mass spectrometric detection*, Journal of Chromatography, A, 2003, 1012, 179–192.
- [80] E. S. B. Ferreira, A. Quye, H. McNab and A.N. Hulme, *Photo-oxidation products of quecetin and morin as markers for the characterisation of natural flavonoid yellow*, Dyes in History and Archaeology, 2002, 18, 63–72.
- [81] J. Sanyova, *Contribution à l'étude de la structure et des propriétés de la laque de garance*, PhD Thesis, Brussels, 2001. Downloadable from <http://theses.ulb.ac.be/ETDdb/collection/available/ULBetd-08092006-162429/>.
- [82] Y. Lee, J. Lee, Y. Kim, S. Choi, S.W. Ham and K.-J. Kim, *Investigation of natural dyes and ancient textiles from Korea using ToF-SIMS*, Applied Surface Science, 2008, 255, 1033–1036.
- [83] K. Keune and J. J. Boon, *Imaging secondary ion mass spectrometry of a paint cross-section taken from an early Netherlandish painting by Rogier van der Weyden*, Analytical Chemistry, 2004, 76, 1374–1385.
- [84] K. Keune, E. S. B. Ferreira and J. J. Boon, *Characterization and localization of the oil-binding medium in paint cross-sections using imaging secondary ion mass spectrometry*, Preprints of the 14th Triennial Meeting of ICOM-CC Committee for Conservation, The Hague (Netherlands), 2005, 2, 796–802.
- [85] K. Keune and J. J. Boon, *Enhancement of the static SIMS secondary ion yields of lipid moieties by ultra thin gold coating of aged oil paint surfaces*, Surface and Interface Analysis, 2005, 36, 1620–1628.
- [86] M. R. Schilling and H. P. Khaijan, *Gas chromatographic determination of fatty acid and glycol content of lipids I. The effect of pigments and ageing on the composition of oil paints*, Preprints of the 11th Triennial Meeting of the ICOM Committee for Conservation, Edinburgh, 1996, 1, 211–219.
- [87] B. Marino, J. J. Boon, E. Hendricks, F. Horre ´ard and F. Hillion, *Imaging ToF-SIMS and NANO SIMS studies of barite-celestite particles in grounds from paintings by Van Gogh*, e-Preservation Science, 2006, 3, 41–50.
- [88] J. Sanyova, S. Cersoy, P. Richardin, O. Lapr evote, P. Walter, A. Brunelle, *Unexpected Materials in a Rembrandt Painting Characterized by High Spatial Resolution Cluster-TOF-SIMS Imaging*, Analytical Chemistry, 2011, 83, 753-760.
- [89] M. Noun, E. Van Elslande, D. Touboul, H. Glanville, S. Bucklow, P. Waltera, A. Brunelle, *High mass and spatial resolution mass spectrometry imaging of Nicolas Poussin painting cross section by cluster TOF-SIMS*, Journal of mass spectrometry, 2016, 1196-1210.
- [90] K. Keune, J. J. Boon, *Analytical Imaging Studies Clarifying the Process of the Darkening of Vermilion in Paintings*, Analytical Chemistry, 2005, 77, 4742-4750.
- [91] Z. E. Voras, K. deGhetaldi, M. B. Wiggins, B. Buckley, B. Baade, J. L. Mass, T. P. Beebe Jr, *ToF-SIMS imaging of molecular-level alteration mechanisms in Le Bonheur de vivre by Henri Matisse*, Applied Physics A, 2015, 121, 1015-1030.
- [92] J. J. Boon, K. Keune, J. van der Weerd, M. Geldof and J. de Boer, *Imaging microspectroscopic, secondary ion mass spectrometric and electron microscopic studies on discoloured and partially discoloured smalt in cross-sections of 16th century paintings*, Chimia, 2001, 55, 952–960.

- [93] J. van der Weerd, *Microspectroscopic analysis of traditional oil paint*, PhD Thesis, University of Amsterdam, 2002.
- [94] J. J. Boon, K. Keune and J. Zucker, *Imaging analytical studies of lead soaps aggregating in preprimed canvas used by the Hudson River School painter F. E. Church*, *Microscopy and Microanalysis*, 11(Suppl. 2), 2005, 444–445.
- [95] J. J. Boon, F. Hoogland and K. Keune, Chemical processes in aged oil paints affecting metal soap migration and aggregation, AIC Annual Meeting, Providence, Rhode Island, June 2006, 16–19.
- [96] G. Osmond, K. Keune, J. J. Boon, *A study of zinc soap aggregates in a late 19<sup>th</sup> century painting R. G. Rivers at the Queensland Art Gallery*, *AICCM Bulletin*, 29, 2005.
- [97] R. P. Evershed, C. Heron, S. Charters and L. J. Goad, *The survival of food residues: new methods of analysis, interpretation and application*, in *New Developments in Archaeological Science*, A.M. Pollard (ed.), Proceedings of the British Academy, vol. 77, Oxford University Press, Oxford, 1992, 187–208.
- [98] M. Regert, N. Garnier, O. Decavallas, C. Cren-Olivé and C. Rolando, *Structural characterization of lipid constituents from natural substances preserved in archaeological environments*, *Measurement Science and Technology*, 2003, 14, 1620–1630.
- [99] M. H. Schweitzer, Z. Suo, R. Avci, J. M. Asara, M. A. Allen, F. T. Arce and J. R. Horner, *Analyses of soft tissue from Tyrannosaurus rex suggest the presence of protein*, *Science*, 2007, 316, 277–280.
- [100] J. B. Lhoest, M. S. Wagner, C. D. Tidwell and D. G. Castner, *Characterization of adsorbed protein films by time-of-flight secondary ion mass spectrometry*, *Journal of Biomedical Materials Research*, 2001, 57, 432–440.
- [101] O. D. Sanni, M. S. Wagner, D. G. Briggs, D. G. Castner and J. C. Vickerman, *Classification of adsorbed protein static ToF-SIMS spectra by principal component analysis and neural networks*, *Surface and Interface Analysis*, 2002, 33, 715–728.
- [102] M. S. Wagner and D. G. Castner, *Analysis of adsorbed proteins by static time-of-flight secondary ion mass spectrometry*, *Applied Surface Science*, 2004, 231–232, 366–376.
- [103] V. Mazel, P. Richardin, D. Touboul, A. Brunelle, P. Walter and O. Laprévotte, *Chemical imaging techniques for the analysis of complex mixtures: new application to the characterization of ritual matters on African wooden statuettes*, *Analytica Chimica Acta*, 2006, 570, 34–40.
- [104] V. Mazel, P. Richardin, D. Debois, D. Touboul, M. Cotte, A. Brunelle, P. Walter and O. Laprévotte, *Identification of ritual blood in African artifacts using ToF-SIMS and synchrotron radiation microspectroscopies*, *Analytical Chemistry*, 2007, 79, 9253–9260.
- [105] V. Mazel, P. Richardin, D. Debois, D. Touboul, M. Cotte, A. Brunelle, P. Walter and O. Laprévotte, *The patinas of the Dogon – Tellem statuery: a new vision through physico-chemical analyses*, *Journal of Cultural Heritage*, 2008, 9, 347–353.
- [106] K. Keune, J.J. Boon, *Analytical imaging studies of cross-sections of paintings affected by lead soap aggregate formation*, *Studies in Conservation*, 2007, 52, 161-176,.
- [107] L. Robinet, M.-C. Corbeil, *The characterization of metal soap*, *Studies in Conservation*, 2003, 48, 23-40.
- [108] F.J Licata, 'Some metallic soaps used in the protective coatings industry', *Official Digest* 388 (1957) 485–491.
- [109] J. Rinse, 'Metal soaps', *American Paint Journal* (March 13), 1967, 22–28.
- [110] S.H. Bell, 'Controlling loss of gloss', *Paint and Varnish Production*, 1970, 60, 55–60.
- [111] P. Noble, J. Wadum, K. Groen, R. Heeren, and K.J. van den Berg, 'Aspects of 17<sup>th</sup> century binding medium: inclusions in Rembrandt's *Anatomy Lesson of Dr Nicolaes Tulp*' in *Art et Chimie, la Couleur*, ed. J. Goupy and J.-P. Mohen, CNRS Éditions, Paris, 2000, 126–129.

- [112] D. Tilbrooke, 'The fatty acid corrosion of copper alloys and its treatment', *ICCM Bulletin* 6(3–4), 1980, 46–52.
- [113] I. Horovitz, 'Paintings on copper supports: techniques, deterioration and conservation', *The Conservator* 10, 1986, 44–48.
- [114] M. Gunn, E. Martin, 'Mécanisme d'altération d'un alliage cuivreux en présence d'un liant huileux' in *Art et Chimie, la Couleur*, ed. J. Goupy and J.-P. Mohen, CNRS Éditions, Paris, 2000, 141–145.
- [115] J. L. Schrenk, *Corrosion and past "protective" treatments of the Benin "bronzes" in the National Museum of African Art* in *Materials Issues in Art and Archaeology II*, ed. P.B. Vandiver, J. Druzik and G.S. Wheeler, Materials Research Society, Pittsburgh, 1991, 805–812.
- [116] J. L. Schrenk, 'The royal art of Benin: surfaces, past and present' in *Ancient and Historic Metals: Conservation and Scientific Research*, Getty Conservation Institute, Marina del Rey, 1994, 51–62.
- [117] A. Burmester, J. Koller, 'Known and new corrosion products on bronzes: their identification and assessment, particularly in relation to organic protective coatings' in *Recent Advances in the Conservation and Analysis of Artifacts*, Summer Schools Press, London, 1987, 97–104.
- [118] O. Katsibiri, R. F. Howe, *Microscopic, mass spectrometric and spectroscopic characterisation of the mordants used for gilding on wall paintings from three post-Byzantine monasteries in Thessalia, Greece*, *Microchemical Journal*, 2010, 94, 83–89.
- [119] K. Keune, *Binding medium, pigments and metal soaps characterized and localized in paint cross-sections*, PhD Thesis University of Amsterdam, 2005.
- [120] M. Tsutsui, E. A. Tsutsui, *Diterpenoids*, *Chemical Reviews*, 1959, 56, 1031–1075.
- [121] R. N. S. Sodhi, C. A. Mims, R. E. Goacher, B. McKague, A. P. Wolfe, Differentiating diterpene resin acids using ToF-SIMS and principal component analysis: new tools for assessing the geochemistry of amber, *Surface Interface Analysis*, 2014, 46, 365–371.
- [122] H. Budzikiewicz, J. M. Wilson, C. Djerassi, *Mass Spectrometry in Structural and Stereochemical Problems. XXXII Pentacyclic Triterpenes*, *Journal of American Chemistry Society*. 1963, 85, 3688–3699.
- [123] M. I. Razboršek, D.B.Vončina, V. Doleček, E. Vončina, Determination of oleanolic, betulinic and ursolic acid in Lamiaceae and mass spectral fragmentation of their trimethylsilylated derivatives, *Chromatographia* 2008, 67, 433–440.
- [124] J. Pollier, A. Goossens, *Oleanolic acid*, *Phytochemistry*, 2012, 77, 10–15.
- [125] E. S. F. Berman, K. S. Kulp, M. G. Knize, L.Wu, E. J. Nelson, D. O. Nelson, K. J. Wu, *Distinguishing monosaccharide stereo- and structural isomers with TOF-SIMS and multivariate statistical analysis*, *Analytical Chemistry*, 2006, 78, 6497–6503.
- [126] G. A. van der Doelen, K. J. van der Berg, J. J. Boon, *Comparative chromatographic and mass-spectrometric studies of triterpenoid varnishes: fresh material and aged samples from paintings*, *Studies in Conservation*, 1998, 43, 249–264.
- [127] F. Modugno, E. Ribechini, M. P. Colombini, *Chemical study of triterpenoid resinous materials in archaeological findings by means of direct exposure electron ionisation mass spectrometry and gas chromatography/mass spectrometry*, *Rapid Communication in Mass Spectrometry*, 2006, 20, 1787–1800.
- [128] V. P. Papageorgiou, M. N. Bakola-Christianopoulou, K. K. Apazidou, E. E. Psarro, *Gas chromatographic–mass spectroscopic analysis of the acidic triterpenic fraction of mastic gum*, *Journal of Chromatography A*, 1997, 769, 263–273.
- [129] D. Scalarone, M. C. Duursma, J. J. Boon, O. Chiantore, MALDI-TOF mass spectrometry on cellulosic surfaces of fresh and photo-aged di- and triterpenoid varnish resins, *J. Mass Spectrom.* 2005, 40, 1527–1535.

- [130] S. Vahur, A. Teearu, T. Haljasorg, P. Burk, I. Leito, I. Kaljurand, Analysis of dammar resin with MALDI-FT-ICR-MS and APCI-FT-ICR-MS, *Journal of Mass Spectrometry*, 2012, 47, 392–409.
- [131] P. Dietemann, C. Higgitt, M. Kälin, M. J. Edelman, R. Knochenmuss, R. Zenobi, *Aging and yellowing of triterpenoid resin varnishes e Influence of aging conditions and resin composition*, *Journal of Cultural Heritage*, 2009, 10,30–40.
- [132] P. Dietemann, M. Kälin, S. Zumbuhl, R. Knochenmuss, S. Wulfert, R. Zenobi, *A Mass Spectrometry and Electron Paramagnetic Resonance Study of Photochemical and Thermal Aging of Triterpenoid Varnishes*, *Analytical Chemistry*, 2001, 73, 2087–2096.
- [133] D. Scalapone, J. van der Horst, J. J. Boon, O. Chiantore, *Direct-temperature mass spectrometric detection of volatile terpenoids and natural terpenoid polymers in fresh and artificially aged resins*, *Journal of Mass Spectrometry*, 2003, 38, 607–617.
- [134] D. J. Clifford, P. G. Hatcher, *Structural Transformations of Polylabdanoid Resinites During Maturation*, *Org. Geochem.* 1995, 23, 407-418.
- [135] M. Regert, Investigating the history of prehistoric glues by gas chromatography–mass spectrometry, *Journal of Separation Science*, 2004, 27, 244-254.
- [136] E. W. H. Hayek, P. Krenmayr, H. Lohninger, U. Jordis, F. Sauter, W. Moche, J. Fresenius, *GC/MS and chemometrics in archaeometry*, *Analytical Chemistry*, 1991, 340, 153-156.
- [137] M. Regert, J. Delacotte, M. Menu, P. Petrequin, C. Rolando, *Identification of Neolithic hafting adhesives from two lake dwellings at Chalain (Jura, France)*, *Ancient Biomolecules*, 1998, 2, 81-96.
- [138] J.M. Grünberg, *Middle Palaeolithic birch-bark-pitch*, *Antiquity*, 2002, 76, 15-16.
- [139] K. Evans, C. Heron, *Glue, disinfectant and chewing gum: natural products chemistry in archaeology*, *Chemistry & Industry*, 1993, 12, 446-449.
- [140] S. Charters, R. P. Evershed, L. J. Goad, C. Heron, P. Blinkhorn, *Identification of an adhesive used to repair a Roman jar*, *Archaeometry* 1993, 35, 91-101.
- [141] E. W. H. Hayek, P. Krenmayr, H. Lohninger, U. Jordis, W. Moche, F. Sauter, *Identification of archaeological and recent wood tar pitches using gas chromatography/mass spectrometry and pattern recognition*, *Analytical Chemistry*, 1990, 62, 2038-2043.
- [142] S. N. Dudd, R. P. Evershed, *Unusual triterpenoid fatty acyl ester components of archaeological birch bark tars*, *Tetrahedron Letters*, 1999, 40, 359-362
- [143] R. Ekman, *The Suberin monomers and triterpenoids from the outer Bark of Betula verrucosa Ehrh*, *Holzforschung, International Journal of Biology, Chemistry, Physics and Technology of Wood*, 1983, 37, 205-211.
- [144] Y. Hua, M. D. Bentley, B.J. W. Cole, K. D. Murray, A. R. Alford, *Triterpenes from the Outer Bark of Betula nigra*, *Journal of Wood Chemistry and Technology*, 1991, 11, 503-510.
- [145] B. J. W. Cole, M. D. Bentley, Y. Hua, *Triterpenoid extractives in the outer bark of Betula lenta (black birch)*, *Holzforschung, International Journal of Biology, Chemistry, Physics and Technology of Wood*, 1991, 45, 265-268.
- [146] B. J. W. Cole, M. D. Bentley, Y. Hua, L. Bu, *Triterpenoid Constituents in the Outer Bark of Betula alleghaniensis (Yellow Birch)*, *Journal of Wood Chemistry and Technology*, 1991, 11, 209-223.
- [147] M. M. O'Connell, M. D. Bentley, C. S. Campbell, B. J. W. Cole, *Betulin and lupeol in bark from four white-barked birches*, *Phytochemistry*, 1988, 27, 2175-2176.
- [148] A. M. Pollard, C. Heron, *The Chemistry and Use of Resinous Substances in Archaeological Chemistry*. RSC Paperbacks: Cambridge, 1996, 239.
- [149] N. Robinson, R. P. Evershed, W. J. Higgs, K. Jerman, G. Eglinton, *Proof of a pine wood origin for pitch from Tudor (Mary Rose) and Etruscan shipwrecks: application of analytical organic chemistry in archaeology*, *Analyst*, 1987, 112, 637-644.

- [150] U. Weser, Y. Kaup, H. Etspuler, J. Koller, U. Baumer, *Embalming In The Old Kingdom Of Pharaonic Egypt*, Analytical Chemistry, 1998, 70: 511A-516A.
- [151] M. P. Colombini, G. Giachi, F. Modugno, E. Ribechini, *Characterisation of organic residues in pottery vessels of the Roman age from Antinoe (Egypt)*, Microchemichal Journal, 2005, 79, 83-90.
- [152] R. P. Evershed, *Modern Analytical Methods in Art and Archaeology*, Ciliberto E, Spoto G (eds). Wiley-Interscience: New York, 2000, 177–239.
- [153] L. Tortora, P. Biocca, G. Sotgiu, F. de Notaristefani, M. Urbini, M. Ioele, *Oleanolic and ursolic acid in dammar and mastic resin: isomer discrimination by using ToF-SIMS and multivariate statistics*, Surface Interface Analysis, 2016, 48, 398-403.
- [154] J. Karliner, C. Djerassi, Terpenoids. LVII. Mass Spectral and Nuclear Magnetic Resonance Studies of Pentacyclic Triterpene Hydrocarbons Journal of Organic Chemistry 1966, 31, 1945-1956.
- [155] L. Ogunkoya, *Application of mass spectrometry in structural problems in triterpenes*, Phytochemistry, 1981, 20, 121-126.
- [156] J. Schmidt, S. Huneck, Mass spectroscopy of natural products. V—Mass spectroscopic studies of ring a substituted allobetulane derivatives, Organic Mass Spectrometry, 1979, 14, 646-655.
- [157] C. Cennini, *Il libro dell'arte* (Eds: F. Brunello), Neri Pozza Editore, Vicenza, 1993, 103–109 156-157.
- [158] L. Tintori, *Golden tin in Sienese murals of early trecento*, "The Burlington Magazine", 1982, pp. 124, 947, 94-95.
- [159] O. Katsibiri, J. J. Boon, *Investigation of the gilding technique in two post-Byzantine wall paintings using micro-analytical techniques*, Spectrochimica Acta. Part B 2004, 59, 1593–1599.
- [160] E. S. Prati, G. Sciutto, M. Ioele, P. Santopadre, R. Mazzeo, *Performance evaluation of mapping and linea imaging FTIR microspectroscopy for the characterisation of paint cross-sections*, Analytical Bioanalytical Chemistry, 2010, 396, 89–910.
- [161] E. R. De la Rie, *Fluorescence of paint and varnish layers*, Studies in Conservation. 1982, 27, 62–69.
- [162] A. Casoli, D. Cauzzi, G. Palla, *The study of binding media in polychrome works of art: the drying oil*, OPD Restauro 1999, 11, 111–121.
- [163] D. Scalarone, M. Lazzari, O. Chiantore, *Ageing behaviour and pyrolytic characterisation of diterpenic resins used as art materials: colophony and Venice turpentine*, J. Anal. Appl. Pyrol. 2002, 64, 345–361.
- [164] M. L. Proefke, K. L. Rinehart, Analysis of an Egyptian mummy resin by mass spectrometry, J. Am. Soc. Mass. Spectrom. 1992, 3, 582–589.
- [165] M. V. Russo, P. Avino, *Characterization and Identification of Natural Terpenic Resins employed in "Madonna con Bambino e Angeli" by Antonello da Messina using Gas Chromatography–Mass Spectrometry*, Chemistry Center Journal, 2012, 6, 59.
- [166] K. J. van den Berg, J. J. Boon, I. Pastorova, L. F. M. Spetter, *Mass spectrometric methodology for the analysis of highly oxidized diterpenoid acids in Old Master paintings*, Journal of Mass Spectrometry. 2000, 35, 512–533.
- [167] M. Marabelli, P. Santopadre, M. Ioele, R. Cesareo, A. Castellano, *Giotto nella cappella degli Scrovegni*, Bollettino d'Arte 2005, 17, 121–144.
- [168] J. Kirby, M. Spring, C. Higgitt, *The technology of red lake pigment manufacture*, National Gallery Technical Bulletin 2005, 26, 71–87.
- [169] A. M. Hacke, Investigation into the nature and ageing of tapestry materials, PhD Thesis, University of Manchester, 2006.

- [170] M. Ioele, A. V. Jervis, M. Paris, L. Rissotto, A. Sodo, A. Giovagnoli, T. Poli, *Presence of Indigo in the paint layer of gilt and painted leather artefacts*, ICOMM-CC XVI Triennial Conference, Lisbon, 2011.
- [171] I. Pastorova, K. J. van den Berg, J. J. Boon, J. W. Verhoeven, *Analysis of oxidized diterpenoid acids using thermally assisted methylation with TMAH*, *Journal of Analytical and Applied Pyrolysis*, 1997, 43, 41–57.
- [172] K. J. van de Berg, MOLART Report 10 2003.
- [173] F. Aramini, L. Conti, L. Festa, M. C. Laurenti, P. Santopadre, G. Sidoti, F. Vischetti, *Le urne etrusche dipinte e dorate di Perugia: studio e restauro*, *Bollettino ICR nuova serie*, Firenze, 2015, 31, 39-56.
- [174] M. IJssink, Jos Koldeweij, R. Spronk, L. Hoogstede, R.G. Erdmann, R. K. Gotink, Hanneke Nap, and Daan Veldhuizen, *Hieronymus Bosch, painter and draughtsman*, *Catalogue Raisonné*, Brussels, 2016.
- [175] Q.P. Vanbellingen, N. Elie, M. J. Eller, S. Della-Negra, D. Touboul, A. Brunelle. Time-of-flight secondary ion mass spectrometry imaging of biological samples with delayed extraction for high mass and high spatial resolutions, *Communication in Mass Spectrometry* 2015, 29, 1187-1195.
- [176] Z. E. Voras, K. deGhetaldi, B. Baade, E. Gordon, G. Gates, T. P. Beebe, *Comparison of oil and egg tempera paint systems using time-of-flight secondary ion mass spectrometry*, *Studies in Conservation*, 2016, 61, 4, 222-235.
- [177] C. Higgitt, M. Spring, D. Saundres, *Pigment-medium interaction in oil paint films containing red lead or lead-tin yellow*, *National Gallery Technical Bulletin*, 2003, 24, 75-95.
- [178] F. Reich, *Sample handling for ToF-SIMS*, in: J.C. Vickerman, D. Briggs (Eds.), *ToF-SIMS: Material Analysis by Mass Spectrometry*, IM Publications LLP and SurfaceSpectra Limited, UK, 2<sup>nd</sup> edition, 2013, pp. 397-416.
- [179] E. Doehne, C.A. Price, *Stone conservation. An Overview of current Research*, second edition, Getty Publications, Los Angeles, 2010.
- [180] G.M. Ingo, G. Guida, E. Angelini, G. Di Carlo, A. Mezzi, G. Padeletti, *Ancient mercury-based plating methods: combined use of surface analytical techniques for the study of manufacturing process and degradation phenomena*, *Account of Chemical Research*, 2013, 46, 2365–2375.
- [181] G.M. Ingo, C. Riccucci, M. Lavorgna, M. Salzano de Luna, M. Pascucci, G. Di Carlo, *Surface investigation of naturally corroded gilded copper-based objects*, *Applied Surface Science*, 2016, 387, 244–251.
- [182] D.A. Scott, *Metallography and Microstructure of Ancient and Historic Metals*, The J. Paul Getty Conservation Institute, Malibu U.S.A, 1991, ISBN 0-89236-195-6.
- [183] G.M. Ingo, E. Angelini, T. de Caro, G. Bultrini, I. Calliari, *Combined use of GDOES, SEM + EDS XRD and OM for the microchemical study of the corrosion products on archaeological bronzes*, *Applied Physics A: Materials Science Process*. 2004, 79, 199–203.
- [184] L. Robbiola, J.-M. Blengino, C. Fiaud, *Morphology and mechanisms of formation of natural patinas on archaeological Cu-Sn alloys*, *Corrosion Science*, 1988, 40, 2083–2111.
- [185] D.A. Scott, *Copper and Bronze in Art: Corrosion, Colorants, Conservation*, The J. Paul Getty Conservation Institute, Malibu, U.S.A, 2002, ISBN10 0892366389.
- [186] D.A. Scott, *Ancient & Historic Metals: Conservation and Scientific Research*, The J. Paul Getty Conservation Institute, Malibu, U.S.A, 1995.
- [187] R. Schlesinger, H. Klewe-Nebenius, M. Bruns, *Characterization of artificially produced copper and bronze patina by XPS*, *Surface Interface Analysis* 2000, 30, 135–139.
- [188] F. Ospitali, C. Chiavari, C. Martini, E. Bernardi, F. Passarini, L. Robbiola, *The characterization of Sn-based corrosion products in ancient bronzes: a Raman approach*, *Journal of Raman Spectroscopy*, 2012, 43, 1596–1603.

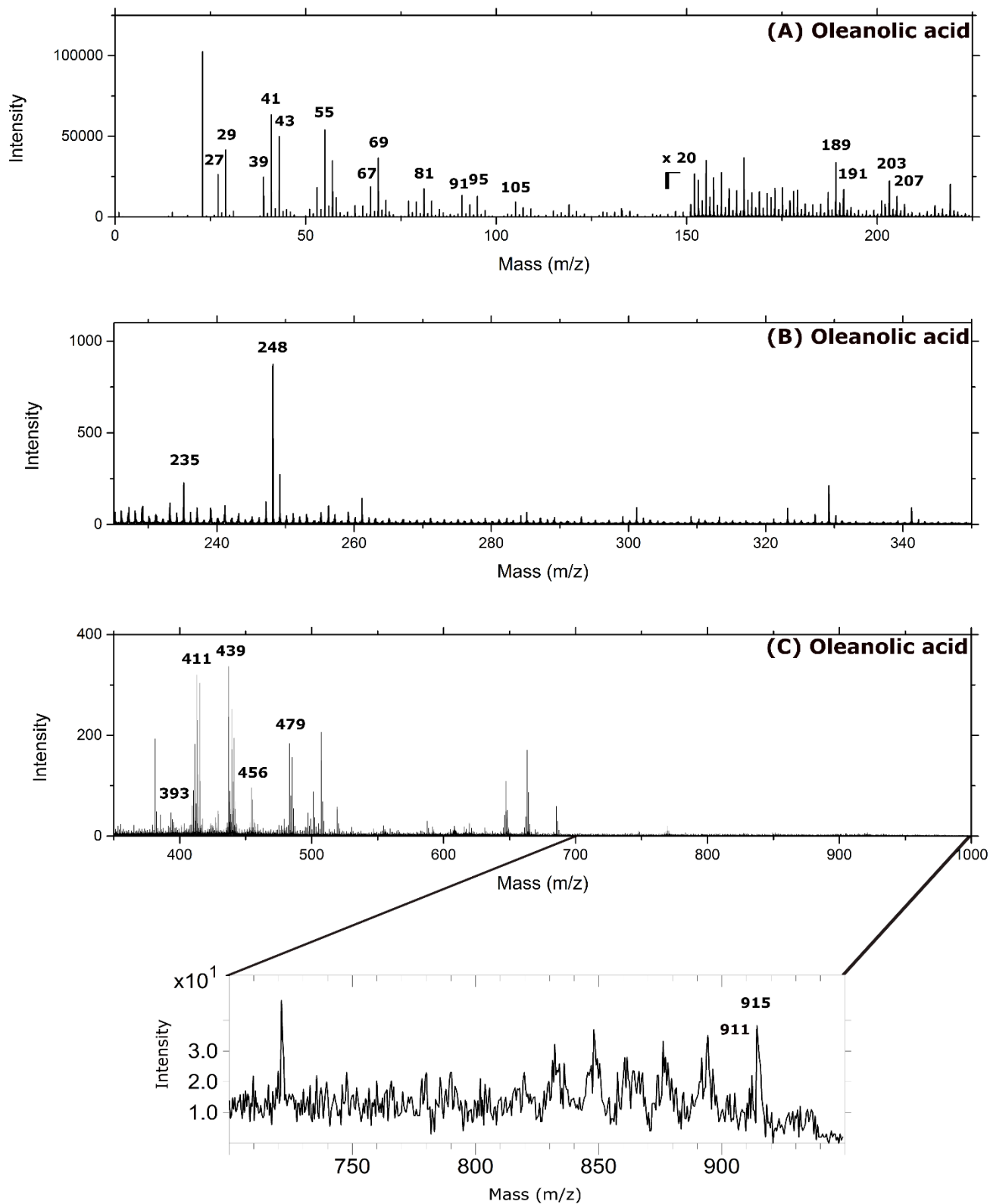
- [189] C. Chiavari, K. Rahmouni, H. Takenouti, S. Joiret, P. Vermaut, L. Robbiola, *Composition and electrochemical properties of natural patinas of outdoor bronze monuments*, *Electrochemical Acta* 2007, 52, 7760–7769.
- [190] W.A. Oddy, *Gilding: an outline of the technological history of the plating of gold on to silver or copper in the old world*, *Endeavour*, 1990, 15, 29–33.
- [191] P.A. Lins, W.A. Oddy, *The origins of mercury gilding*, *Journal of Archaeological Science*, 1975, 2, 365–373.
- [192] H. Peisert, T. Chasse, P. Streubel, A. Meisel, R. Szargan, *Relaxation energy in XPS and XAES of solid compounds*, *Journal Electron Spectroscopy Related Phenomena*, 1994, 68, 321–328.
- [193] D.M. Bastidas, M. Criado, S. Fajardo, V.M. La Iglesia, E. Cano, J.M. Bastidas, *Copper deterioration: causes, diagnosis and risk minimisation*, *International Materials. Reviews*, 2010, 55, 99–127.
- [194] V.F. Lucey, *Developments leading to the present understanding of the mechanisms of pitting corrosion of copper*, *British Corrosion Journal*, 1972, 7, 36–41.
- [195] D.A. Scott, *Bronze disease: a review of some chemical problems and the role of relative humidity*, *Journal of American Institute for Conservation*, 1990, 29, 193–206.
- [196] F. Schweitzer, *Symposium organised by the Paul Getty Museum Proc.*, Edited by J. Podany, B.B. Considine, Paul Getty Museum, Malibu, California, USA, 1994, 1–20.
- [197] D.M. Bastidas, E. Cano, A.G. González, S. Fajardo, R. Lleras-Pérez, E. Campo-Montero, F.J. Belzunce-Varela, J.M. Bastidas, *An XPS study of tarnishing of a gold mask from a pre-Columbian culture*, *Corrosion Science*, 2008, 50, 1785–1788.
- [198] D. Pope, H.R. Gibbens, R.L. Moss, *The tarnishing of silver at naturally occurring H<sub>2</sub>S and SO<sub>2</sub> levels*, *Corrosion Science*, 1968, 8, 883–887.
- [199] E. Talik, R. Babiarz-Zdyb, A. Dziedzic, *Chemical characterization of selected high copper dental amalgams using XPS and XRD techniques*, *Journal of Alloys and Compounds*, 2005, 398, 276–282.
- [200] N.D. Hutson, B.C. Attwood, K.G. Sheckel, *XAS and XPS characterisation of mercury binding on brominated activated carbon*, *Environmental Science & Technology*, 2007, 41, 1747–1752.
- [201] G. Masi, C. Chiavari, J. Avila, J. Esvan, S. Raffo, M.C. Bignozzi, M.C. Asensio, L. Robbiola, C. Martini, *Corrosion investigation of firegilded bronze involving high surface resolution spectroscopic imaging*, *Applied Surface Science*, 2016, 366, 317–327.
- [202] V. Hayez, A. Franquet, A. Hubin, H. Terryn, *XPS study of the atmospheric corrosion of copper alloys of archaeological interest*, *Surface Interface Analysis*. 2004, 36, 876–879.
- [203] M.C. Biesinger, L.W.M. Lau, A.R. Gerson, R.St.C. Smart, *Resolving surface chemical states in XPS analysis of first row transition metals, oxides and hydroxides: sc, Ti, V, Cu and Zn*, *Applied Surface Science*, 2010, 257, 887–898.
- [204] G.M. Ingo, G. Marletta, *Ion beam induced reduction of the metallic cations in yttria-zirconia*, *Nuclear Instruments and Methods in Physics Research section B*, 1996, 116, 440–446.
- [205] G.M. Ingo, L. Giorgi, N. Zacchetti, N. Azzerri, *Electrochemical and XPS studies on lacquer-low tinplated steel adhesion*, *Corrosion Science*, 1992, 33, 361–377.
- [206] E. Paparazzo, G. Fierro, G.M. Ingo, N. Zacchetti, *XPS studies on the surface thermal modifications of tin oxides*, *Surface Interface Analysis*, 1988, 12, 438–439.

## Appendix

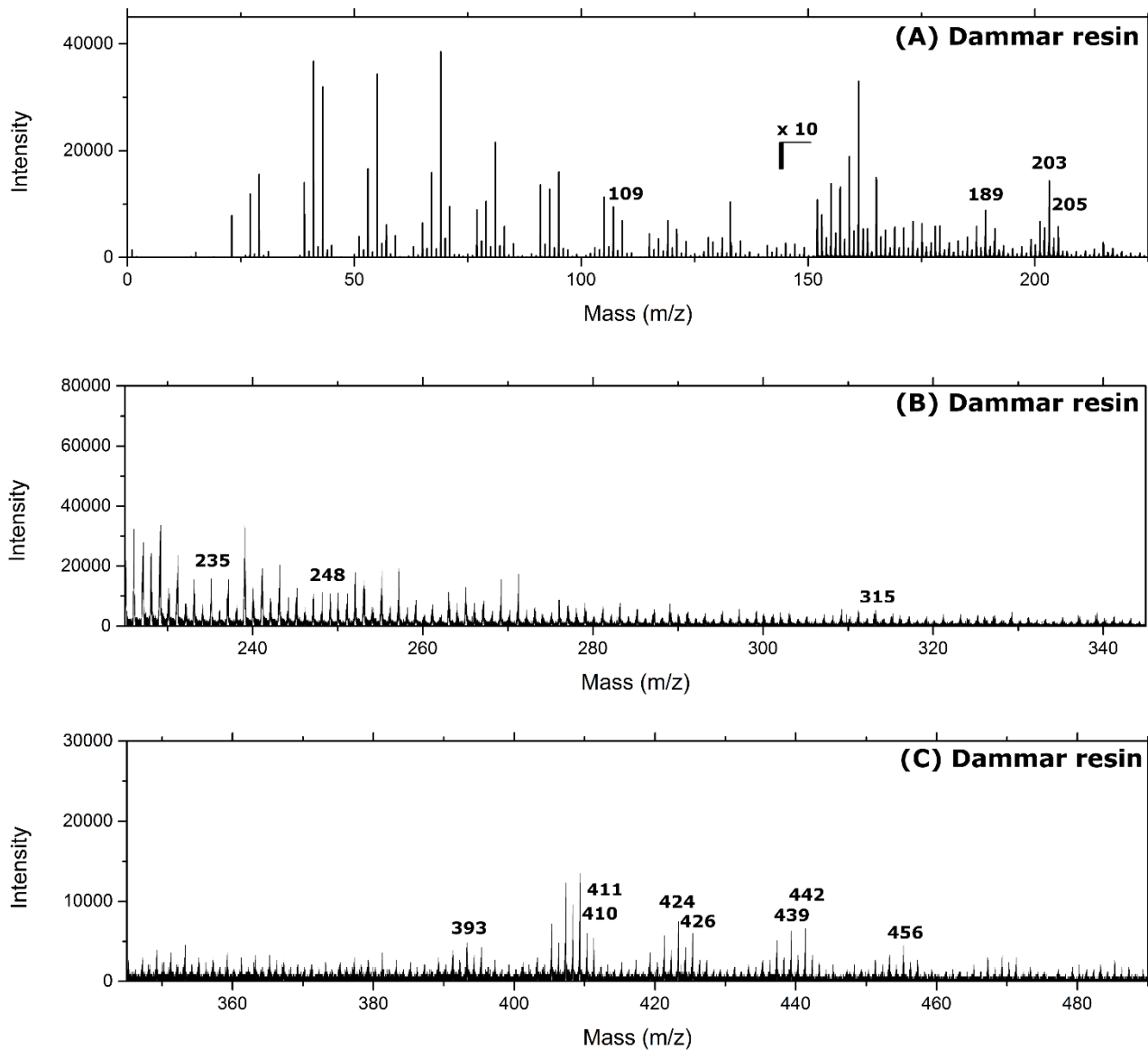
| <b>Reagent</b>              | <b>Cas number</b> | <b>Grade of purity</b> | <b>Provider</b>      |
|-----------------------------|-------------------|------------------------|----------------------|
| <b>Glyceryl tristearate</b> | 69498-250G        | Tecnical Aldrich       | Sigma Aldrich        |
| <b>Tin (II) stearate</b>    | S3752-5G          | >90%                   | Sigma Aldrich        |
| <b>Tin foil</b>             | 356948-20,7G      | 99,9%                  | Sigma Aldrich        |
| <b>SnO</b>                  | 2656325-100G      | 99,8%                  | Sigma Aldrich        |
| <b>SnO<sub>2</sub></b>      | 18282-10-5        | 99,99%                 | Sigma Aldrich        |
| <b>Stearic acid</b>         | 57-11-4           | >95%                   | Sigma Aldrich        |
| <b>Palmitic acid</b>        | 57-10-3           | >99%                   | Sigma Aldrich        |
| <b>Azelaic acid</b>         | 123-99-9          | 98%                    | Sigma Aldrich        |
| <b>Abietic acid</b>         | 514-10-3          | 75%                    | Sigma Aldrich        |
| <b>Linseed oil</b>          | -                 | -                      | Ditta Zecchi Firenze |
| <b>Colophony</b>            | -                 | -                      | Ditta Zecchi Firenze |
| <b>Betulin</b>              | B9757-1G          | >98%                   | Sigma Aldrich        |
| <b>Betulin acid</b>         | 855057-100G       | 90% technical grade    | Sigma Aldrich        |
| <b>Lupeol</b>               | 545-47-1          | ≥99%                   | Extrasynthèse        |
| <b>Lupenon</b>              | 1617-70-5         | ≥95%                   | Extrasynthèse        |
| <b>Dammar resin</b>         | Natural resin     | -                      | Zecchi Firenze       |
| <b>Mastic resin</b>         | Natural resin     | -                      | Zecchi Firenze       |
| <b>Oleanolic acid</b>       | 77-52-1           | ≥98%                   | Extrasynthèse        |
| <b>Ursolic acid</b>         | 508-02-1          | ≥98%                   | Extrasynthèse        |

**Table A1.** List of reagents used in the tin metal soaps experiment.

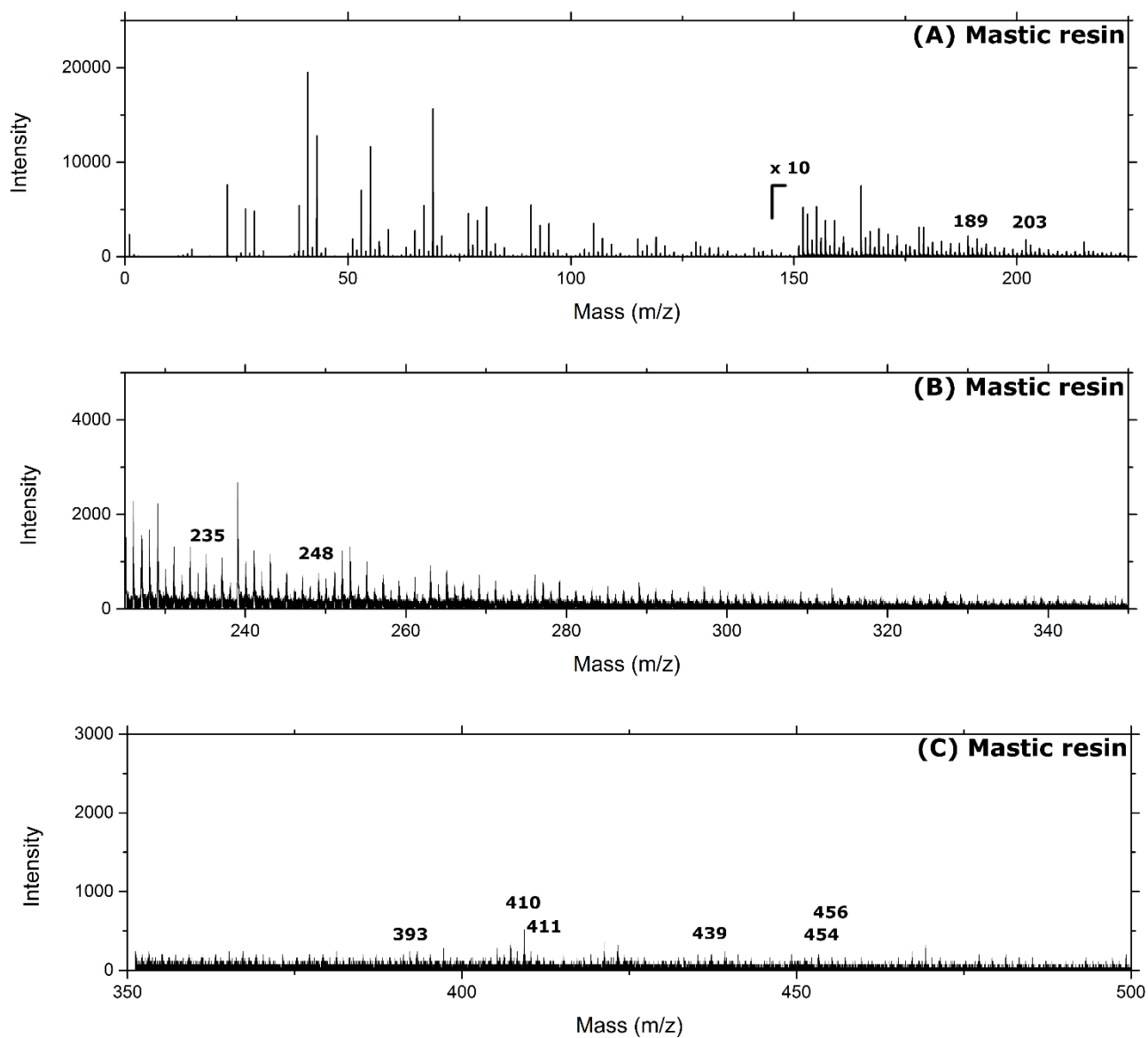
**Figure A1.** Positive ToF-SIMS spectrum of ursolic acid: m/z 1 - 225 (A), m/z 225 – 350 (B) and m/z 350 – 1000 (C).



**Figure A2.** Positive ToF-SIMS spectrum of oleanolic acid: m/z 1 - 225 (A), m/z 225 – 350 (B) and m/z 350 – 1000 (C).

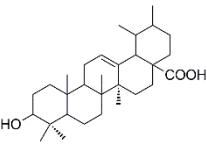
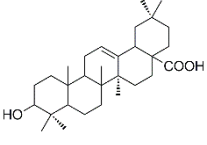
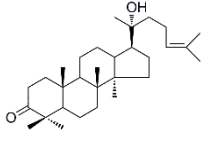
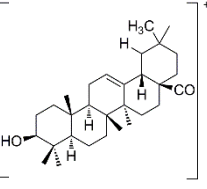
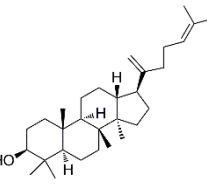
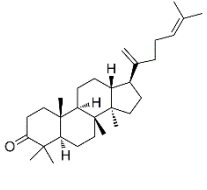
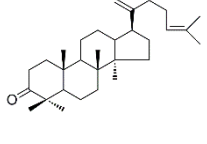
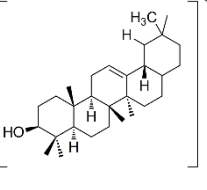


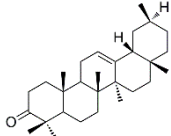
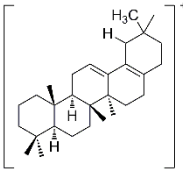
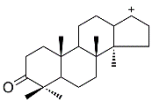
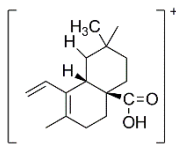
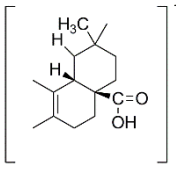
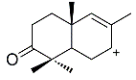
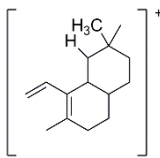
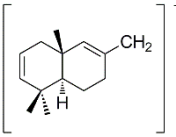
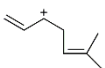
**Figure A3.** Positive ToF-SIMS spectrum of dammar resin: m/z 1 - 225 (A), m/z 225 – 350 (B) and m/z 350 – 500 (C).



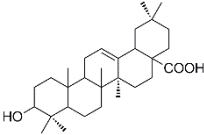
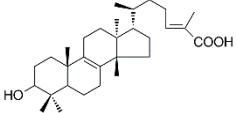
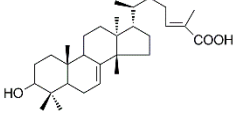
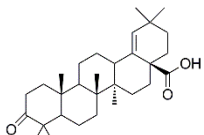
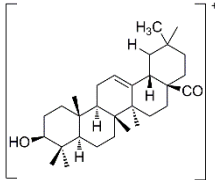
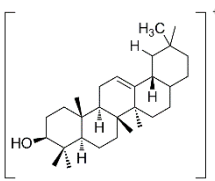
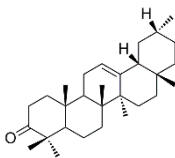
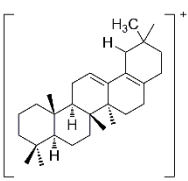
**Figure A4.** Positive ToF-SIMS spectrum of mastic resin: m/z 1 - 225 (A), m/z 225 – 350 (B) and m/z 350 – 500 (C).

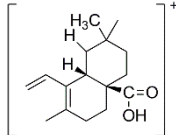
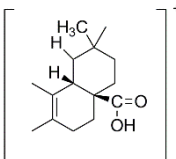
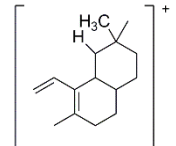
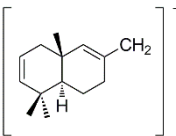
**Table A2** Characteristic fragments of dammar resin obtained during ToF-SIMS investigation.

| <b>m/z</b> | <b>Formula</b>   | <b>Assignment</b>           | <b>Structure</b>   | <b>Reference</b> |
|------------|--|-----------------------------|--|------------------|
| 456.34     | (C <sub>30</sub> H <sub>48</sub> O <sub>3</sub> <sup>+</sup> ) | Ursolic acid                |    | [1-4]            |
|            |  | Oleanolic acid              |    | [1-4]            |
| 442.37     | (C <sub>30</sub> H <sub>50</sub> O <sub>2</sub> <sup>+</sup> ) | Hydroxydammaranone          |    | [1-2-4-19-20]    |
| 439.34     | (C <sub>30</sub> H <sub>47</sub> O <sub>2</sub> <sup>+</sup> ) | oleanane-type fragment      |   |                  |
| 426.37     | (C <sub>30</sub> H <sub>50</sub> O <sup>+</sup> )              | Dammaradienol               |  | [4-7-19-20]      |
| 424.37     | (C <sub>30</sub> H <sub>48</sub> O <sup>+</sup> )              | Dammaradienone              |  | [2-4-7-19-20]    |
|            |  | Hydroxydammaranone fragment |  | [19-20]          |
| 411.35     | (C <sub>29</sub> H <sub>47</sub> O <sup>+</sup> )              | oleanane-type fragment      |  |                  |

|        |  |                           |   |          |
|--------|--|---------------------------|---|----------|
| 410.36 | (C <sub>29</sub> H <sub>46</sub> O <sup>+</sup> )              | Nor-amyrone               |     | [1-4-19] |
| 393.35 | (C <sub>29</sub> H <sub>45</sub> <sup>+</sup> )                | oleanane-type fragment    |     |          |
| 315.27 | (C <sub>22</sub> H <sub>35</sub> O <sup>+</sup> )              | Hydroxydammarone fragment |     | [19-20]  |
| 248.17 | (C <sub>16</sub> H <sub>24</sub> O <sub>2</sub> <sup>+</sup> ) | oleanane-type fragment    |     |          |
| 235.16 | (C <sub>15</sub> H <sub>23</sub> O <sub>2</sub> <sup>+</sup> ) | oleanane-type fragment    |    |          |
| 205.16 | (C <sub>14</sub> H <sub>21</sub> O <sup>+</sup> )              | Hydroxydammarone fragment |   | [19-20]  |
| 203.17 | (C <sub>15</sub> H <sub>23</sub> <sup>+</sup> )                | oleanane-type fragment    |   |          |
| 189.16 | (C <sub>14</sub> H <sub>21</sub> <sup>+</sup> )                | oleanane-type fragment    |   |          |
| 109.10 | (C <sub>8</sub> H <sub>13</sub> <sup>+</sup> )                 | Hydroxydammarone fragment |  | [19-20]  |

**Table A3** Characteristic fragments of mastic resin obtained during ToF-SIMS analysis.

| m/z    | Formula  | Assignment              | Structure  | Reference       |
|--------|--|-------------------------|--|-----------------|
| 456.34 | (C <sub>30</sub> H <sub>48</sub> O <sub>3</sub> <sup>+</sup> ) | Oleanolic acid          |    | [1-4-21]        |
|        |  | Masticadienolic acid    |    | [19-21-22]      |
|        |  | Isomasticadienolic acid |    | [3-19-20-21-22] |
| 454.34 | (C <sub>30</sub> H <sub>46</sub> O <sub>3</sub> <sup>+</sup> ) | Moronic acid            |   | [1-3-20-21]     |
| 439.34 | (C <sub>30</sub> H <sub>47</sub> O <sub>2</sub> <sup>+</sup> ) | oleanane-type fragment  |  |                 |
| 411.35 | (C <sub>29</sub> H <sub>47</sub> O <sup>+</sup> )              | oleanane-type fragment  |  |                 |
| 410.36 | (C <sub>29</sub> H <sub>46</sub> O <sup>+</sup> )              | Nor- amyrone            |  | [1-4-19]        |
| 393.35 | (C <sub>29</sub> H <sub>45</sub> <sup>+</sup> )                | oleanane-type fragment  |  |                 |

|        |  |                        |  |
|--------|--|------------------------|--|
| 248.17 | (C <sub>16</sub> H <sub>24</sub> O <sub>2</sub> <sup>+</sup> ) | oleanane-type fragment |  |
| 235.16 | (C <sub>15</sub> H <sub>23</sub> O <sub>2</sub> <sup>+</sup> ) | oleanane-type fragment |  |
| 203.17 | (C <sub>15</sub> H <sub>23</sub> <sup>+</sup> )                | oleanane-type fragment |  |
| 189.16 | (C <sub>14</sub> H <sub>21</sub> <sup>+</sup> )                | oleanane-type fragment |  |

**Table A4** Positive ions selected for PCA analysis.

| <i>m/z</i> | <i>Proposed Assignment</i>                   | <i>m/z</i> | <i>Proposed Assignment</i>                                  |
|------------|--|------------|---|
| 26.02      | C <sub>2</sub> H <sub>2</sub> <sup>+</sup>   | 73.07      | C <sub>4</sub> H <sub>9</sub> O <sup>+</sup>                |
| 27.03      | C <sub>2</sub> H <sub>3</sub> <sup>+</sup>   | 75.03      | C <sub>6</sub> H <sub>3</sub> <sup>+</sup>                  |
| 29.01      | CHO <sup>+</sup>                             | 77.04      | C <sub>6</sub> H <sub>5</sub> <sup>+</sup>                  |
| 29.05      | C <sub>2</sub> H <sub>5</sub> <sup>+</sup>   | 79.06      | C <sub>6</sub> H <sub>7</sub> <sup>+</sup>                  |
| 30.05      | C <sub>2</sub> H <sub>6</sub> <sup>+</sup>   | 81.08      | C <sub>6</sub> H <sub>9</sub> <sup>+</sup>                  |
| 31.03      | CH <sub>3</sub> O <sup>+</sup>               | 83.10      | C <sub>6</sub> H <sub>11</sub> <sup>+</sup>                 |
| 39.03      | C <sub>3</sub> H <sub>3</sub> <sup>+</sup>   | 85.07      | C <sub>5</sub> H <sub>9</sub> O <sup>+</sup>                |
| 40.04      | C <sub>3</sub> H <sub>4</sub> <sup>+</sup>   | 91.06      | C <sub>7</sub> H <sub>7</sub> <sup>+</sup>                  |
| 41.05      | C <sub>3</sub> H <sub>5</sub> <sup>+</sup>   | 95.09      | C <sub>7</sub> H <sub>11</sub> <sup>+</sup>                 |
| 42.04      | C <sub>3</sub> H <sub>6</sub> <sup>+</sup>   | 97.10      | C <sub>7</sub> H <sub>13</sub> <sup>+</sup>                 |
| 43.03      | C <sub>2</sub> H <sub>3</sub> O <sup>+</sup> | 105.06     | C <sub>8</sub> H <sub>9</sub> <sup>+</sup>                  |
| 43.07      | C <sub>3</sub> H <sub>7</sub> <sup>+</sup>   | 107.09     | C <sub>8</sub> H <sub>11</sub> <sup>+</sup>                 |
| 44.02      | C <sub>2</sub> H <sub>4</sub> O <sup>+</sup> | 109.10     | C <sub>8</sub> H <sub>13</sub> <sup>+</sup>                 |
| 44.07      | C <sub>3</sub> H <sub>8</sub> <sup>+</sup>   | 111.09     | C <sub>7</sub> H <sub>11</sub> O <sup>+</sup>               |
| 44.99      | CHO <sub>2</sub> <sup>+</sup>                | 123.12     | C <sub>9</sub> H <sub>15</sub> <sup>+</sup>                 |
| 45.04      | C <sub>2</sub> H <sub>5</sub> O <sup>+</sup> | 137.12     | C <sub>10</sub> H <sub>17</sub> <sup>+</sup>                |
| 50.03      | C <sub>4</sub> H <sub>2</sub> <sup>+</sup>   | 149.14     | C <sub>11</sub> H <sub>17</sub> <sup>+</sup>                |
| 51.03      | C <sub>4</sub> H <sub>3</sub> <sup>+</sup>   | 155.08     | C <sub>12</sub> H <sub>11</sub> <sup>+</sup>                |
| 52.03      | C <sub>4</sub> H <sub>4</sub> <sup>+</sup>   | 187.14     | C <sub>13</sub> H <sub>15</sub> O <sup>+</sup>              |
| 53.05      | C <sub>4</sub> H <sub>5</sub> <sup>+</sup>   | 189.16     | C <sub>14</sub> H <sub>21</sub> <sup>+</sup>                |
| 54.04      | C <sub>4</sub> H <sub>6</sub> <sup>+</sup>   | 191.18     | C <sub>14</sub> H <sub>23</sub> <sup>+</sup>                |
| 55.03      | C <sub>3</sub> H <sub>3</sub> O <sup>+</sup> | 201.17     | C <sub>15</sub> H <sub>21</sub> <sup>+</sup>                |
| 55.07      | C <sub>4</sub> H <sub>7</sub> <sup>+</sup>   | 203.17     | C <sub>15</sub> H <sub>23</sub> <sup>+</sup>                |
| 57.04      | C <sub>3</sub> H <sub>5</sub> O <sup>+</sup> | 207.16     | C <sub>14</sub> H <sub>27</sub> O <sup>+</sup>              |
| 57.08      | C <sub>4</sub> H <sub>9</sub> <sup>+</sup>   | 235.16     | C <sub>15</sub> H <sub>23</sub> O <sub>2</sub> <sup>+</sup> |
| 59.06      | C <sub>3</sub> H <sub>7</sub> O <sup>+</sup> | 248.17     | C <sub>16</sub> H <sub>24</sub> O <sub>2</sub> <sup>+</sup> |
| 65.05      | C <sub>5</sub> H <sub>5</sub> <sup>+</sup>   | 393.35     | C <sub>29</sub> H <sub>45</sub> <sup>+</sup>                |
| 66.04      | C <sub>5</sub> H <sub>6</sub> <sup>+</sup>   | 411.35     | C <sub>29</sub> H <sub>47</sub> O <sup>+</sup>              |
| 67.05      | C <sub>5</sub> H <sub>7</sub> <sup>+</sup>   | 439.34     | C <sub>30</sub> H <sub>47</sub> O <sub>2</sub> <sup>+</sup> |
| 69.08      | C <sub>5</sub> H <sub>9</sub> <sup>+</sup>   | 456.34     | C <sub>30</sub> H <sub>48</sub> O <sub>3</sub> <sup>+</sup> |
| 70.07      | C <sub>5</sub> H <sub>10</sub> <sup>+</sup>  |            |   |

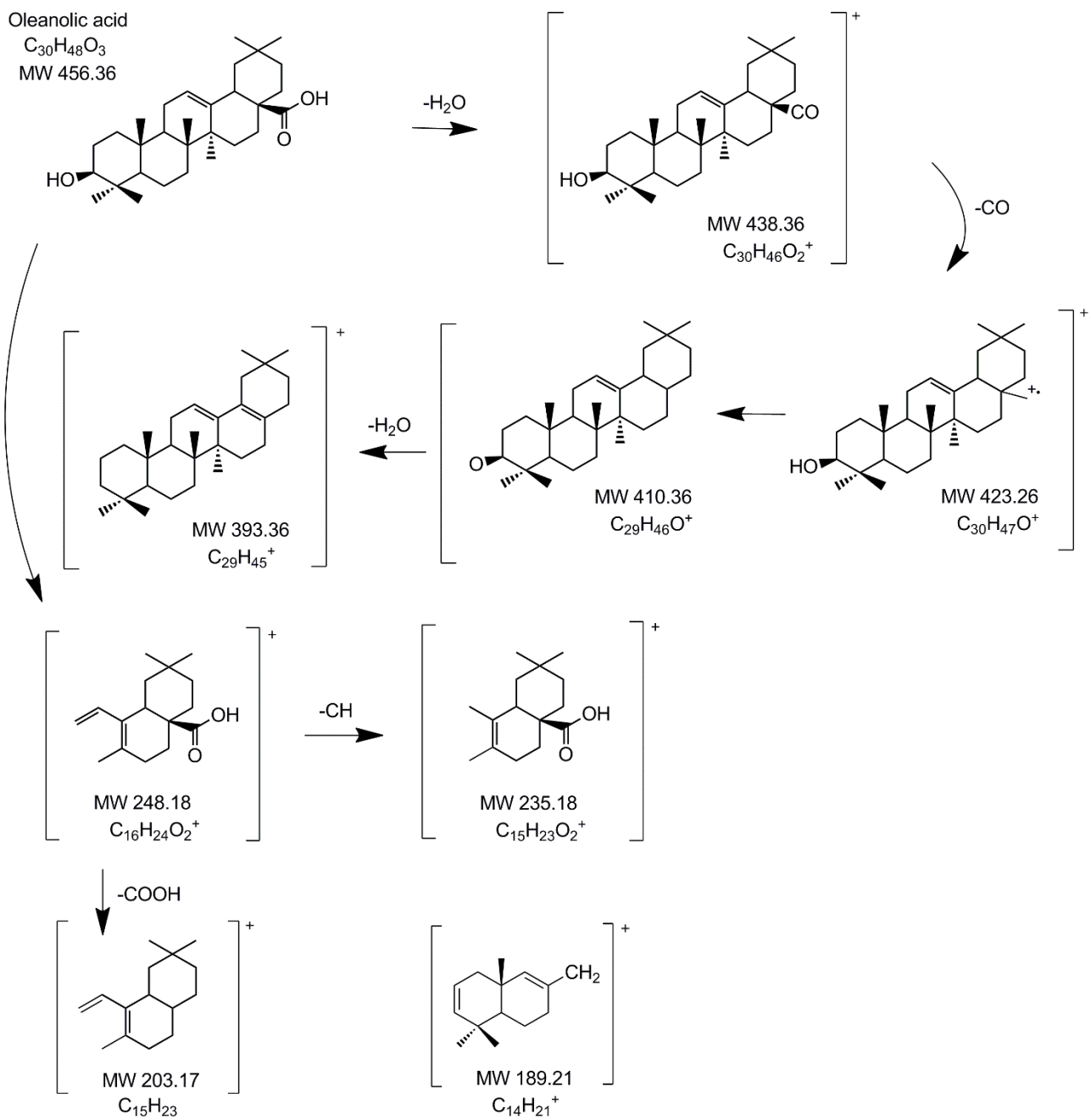


**Figure A5.** Proposed fragmentation pathway of oleanolic acid

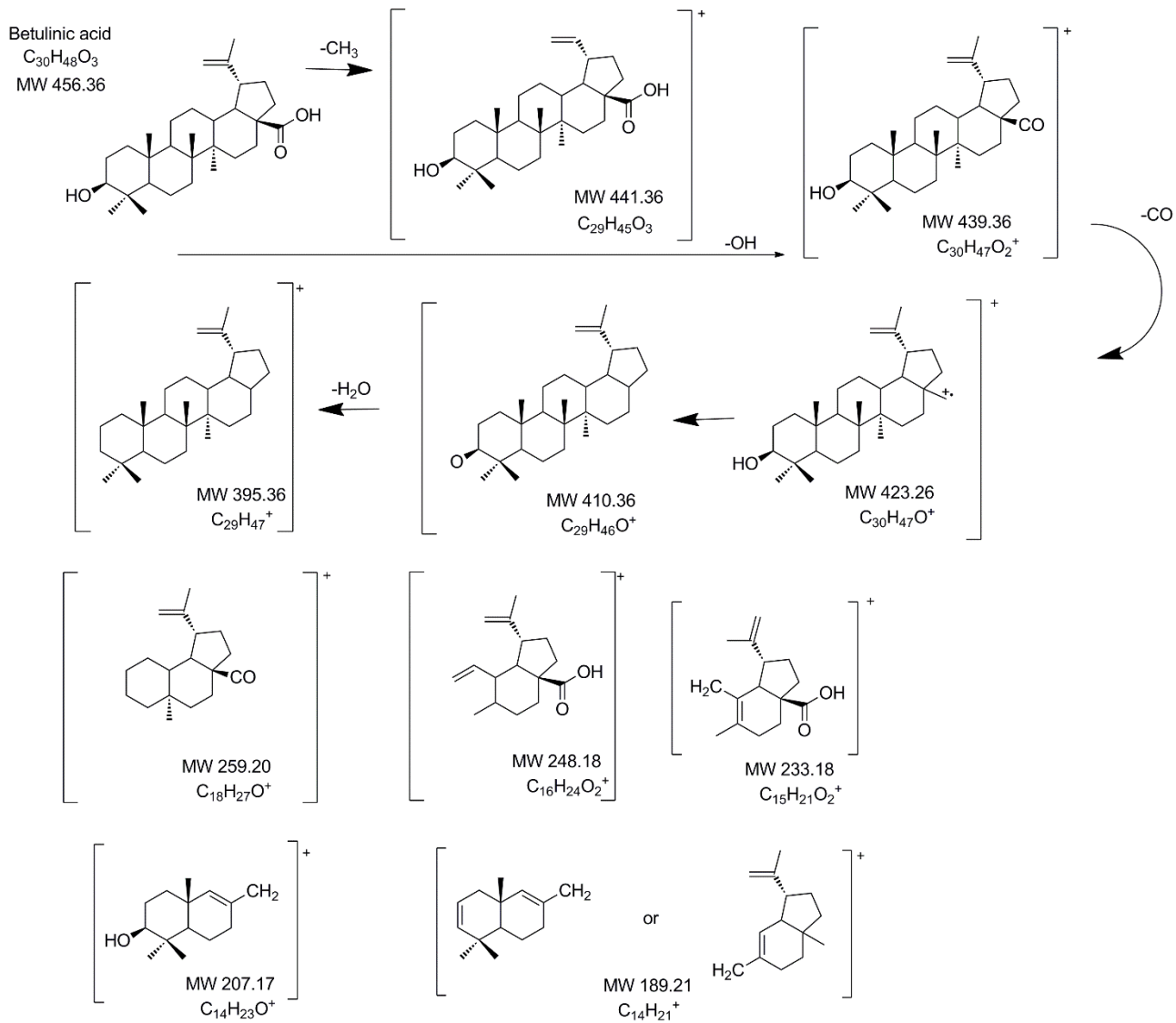


**Figure A6.** Proposed fragmentation pathway of betulinic acid

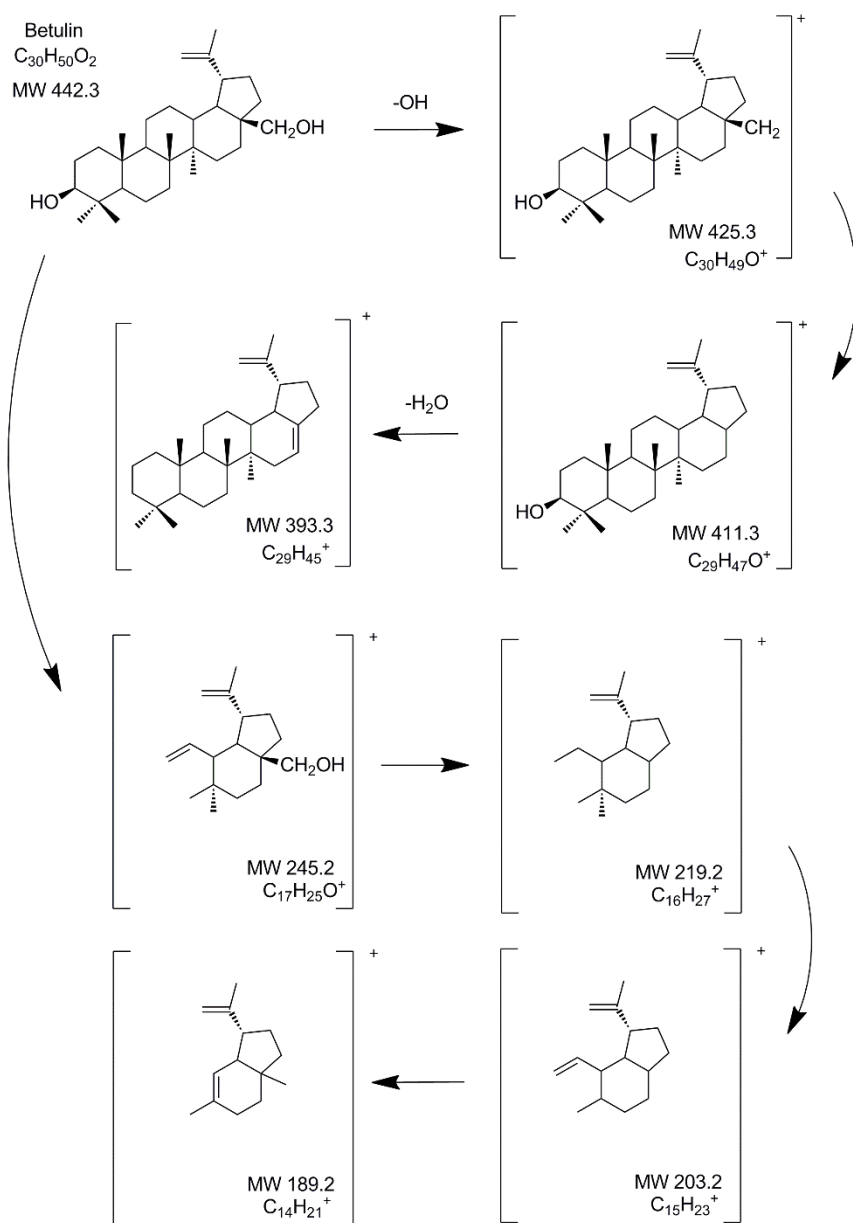


**Figure A7.** Proposed fragmentation pathway of betulin

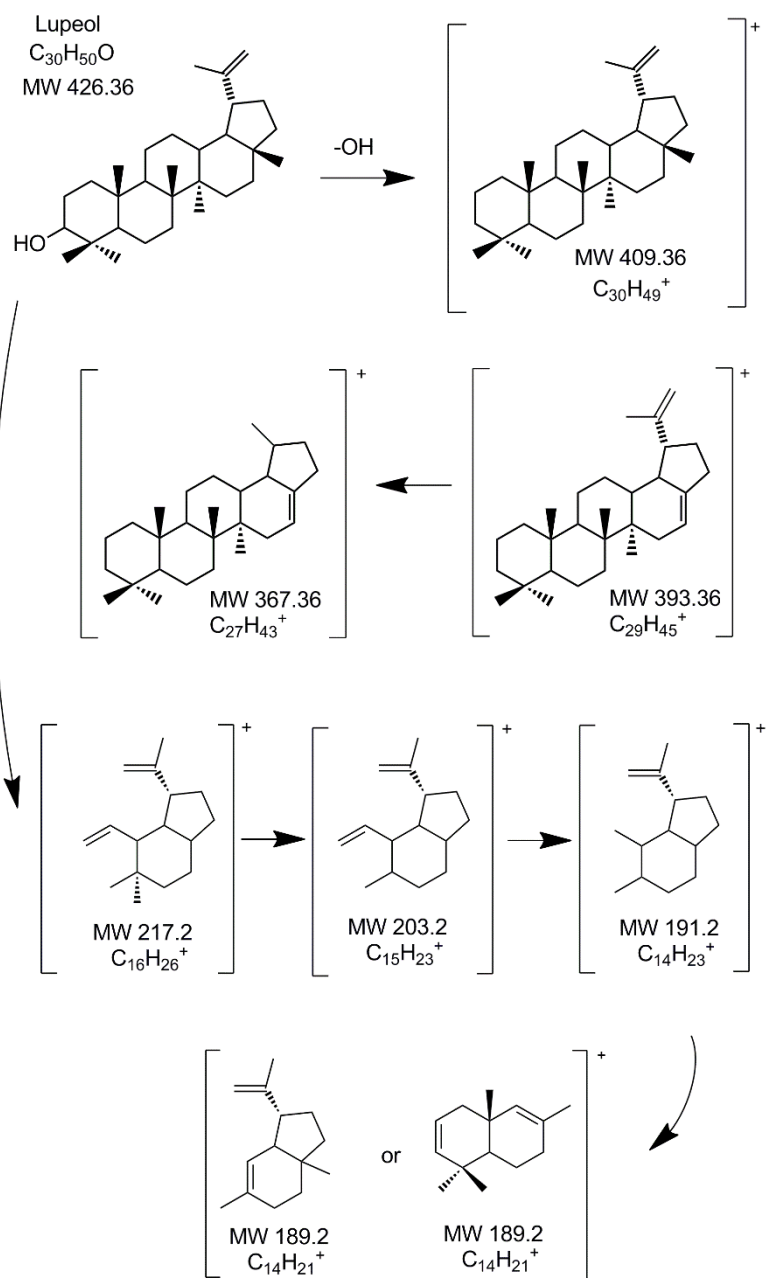


**Figure A8.** Proposed fragmentation pathway of lupeol

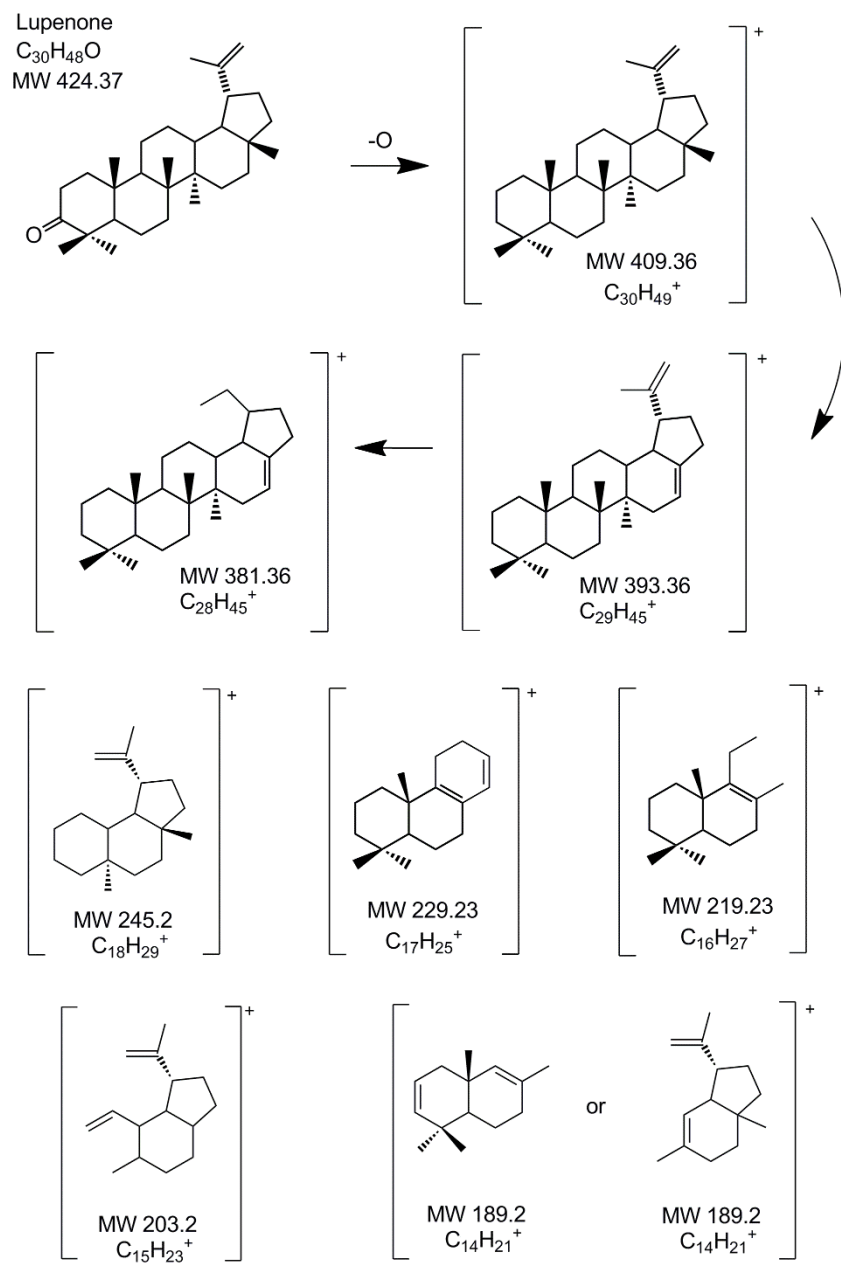


**Figure A9.** Proposed fragmentation pathway of lupenone